Structural and Dynamic Properties of

MHCII-Peptide Complexes

Dissertation zur Erlangung des akademischen Grades des Doktors der Naturwissenschaften (Dr. rer. nat.)

eingereicht im Fachbereich Biologie, Chemie, Pharmazie der Freien Universität Berlin

vorgelegt von
Diplom-Biochemiker Andreas Schlundt
aus Berlin
im Oktober 2011

Diese Arbeit entstand im Zeitraum von März 2007 bis Oktober 2011 am Leibniz-Institut für Molekulare Pharmakologie (FMP), Berlin und der Freien Universität Berlin unter Anleitung von Prof. Dr. Christian Freund.

Erstgutachter: Prof. Dr. Christian Freund

Protein Engineering Group

Leibniz-Institut für Molekulare Pharmakologie (FMP) und

Freie Universität Berlin

Robert-Rössle-Str. 10

13125 Berlin

Zweitgutachter: Prof. Dr. Volker Haucke

Freie Universität Berlin

Institut für Chemie und Biochemie

Membranbiochemie & Molekulare Zellbiologie

Takustr. 6

14195 Berlin

Disputation am: 05.01.2012

Meiner Familie

„Wer die Wahrheit nicht weiß, der ist bloß ein Dummkopf.

Aber wer sie weiß und sie eine Lüge nennt, der ist ein Verbrecher!“

- Bertolt Brecht -

(Leben des Galilei)

Content

Table of figures

Summary

The proteins of the Major Histocompatibility Complex (MHC) present peptidic antigens to T lymphocytes. Antigens of extracellular origin are thereby displayed by class II MHC molecules. In order to present these antigens a universal placeholder peptide, CLIP, has to be replaced. However this exchange process is not yet understood at atomic detail, despite the existence of numerous MHC-peptide crystal structures.

Nuclear magnetic resonance (NMR) is the most comprehensive method to investigate molecules at the atomic level in solution. The strict requirement for relatively large amounts of highly homogeneous protein has so far hampered NMR investigations of MHC molecules.

In the presented work the human MHCII protein HLA-DR1 was broadly investigated by NMR-spectroscopic methods for the first time. The incorporation of stable NMR isotopes, protein purification and refolding from bacterial *inclusion bodies* were optimized. An assignment of resonances to atoms of the protein backbone was achieved with high resolution-multi-dimensional spectra. This enabled the delineation of residues that are affected by the exchange of CLIP for a viral peptide *in vitro*. Moreover, characteristic differences between empty and loaded MHCII as well as its domain organization and stability were confirmed at the atomic level. The combined use of NMR data and crystal structures revealed a bipartite orientation of CLIP peptides when bound to HLA-DR1. Their thermodynamic equilibrium was governed by several H-bonds close to the P1 pocket of the MHC-peptide complex. Peptide reorientation from canonical to inverted binding was monitored by NMR and showed this process to be accelerated by the natural peptide exchange catalyst HLA-DM.

In the second part of the thesis, xenon-detection by NMR was invoked to observe the binding of the viral peptide HA to HLA-DR1. The functionalization of HA peptide with cryptophane allowed its detection by characteristic resonances from caged xenon-129 atoms. This process set the stage for the indirect detection of Cage-HA by saturation transfer during the exchange of xenon with cryptophane. The characterization of Cage-HA revealed a high comparability to wild-type HA. The peptide was administered to mice and was shown to evoke an HLA-DR1/HA-restricted T lymphocyte response. These results lay the foundation for the use of xenon-based MR-imaging of inflammation.

Zusammenfassung

Proteine des Haupthistokompatibilitätskomplexes (MHC) präsentieren peptidische Antigene gegenüber T-Lymphozyten. Antigene extrazellulärer Herkunft werden dabei durch MHCII-Moleküle ausgewiesen. Als Voraussetzung für Antigenpräsentation muss das universelle Platzhalterpeptid CLIP ersetzt werden. Dieser Prozess ist trotz zahlreicher MHC-Peptid-Kristallstrukturen im molekularen Detail nicht verstanden.

Kernmagnetresonanzspektroskopie (NMR) ist die umfassendste Methode zur atomar-aufgelösten Untersuchung von Molekülen in Lösung. Die Notwendigkeit großer Mengen homogenen Proteins hat NMR-Untersuchungen an MHC-Molekülen bisher erschwert.

In der vorliegenden Arbeit wurde das humane MHCII-Protein HLA-DR1 erstmalig umfassend NMR-spektroskopisch untersucht. Der Einbau stabiler NMR-Isotope, die Proteinreinigung und Rückfaltung aus bakteriellen *inclusion bodies* wurden optimiert. Es wurde eine Zuordnung von Resonanzen des Proteinrückgrats über hochaufgelöste, mehrdimensionale Spektren erreicht. Dies ermöglichte die Bestimmung von sensiblen Resten während des Austauschs von CLIP durch ein virales Peptid *in vitro*. Zudem konnten charakteristische Unterschiede zwischen unbeladenem und beladenem Protein und dessen Domänenstruktur/-stabilität auf atomarer Ebene bestätigt werden. Die Kombination aus NMR-Daten und Kristallstrukturen ergab einen neuartigen Bindungsmodus einer CLIP-Variante an HLA-DR1, was durch das Fehlen von essentiellen Wasserstoffbrücken im kanonischen Bindungsmodus von CLIP erklärt wurde. Mittels NMR konnte die Umlagerung aus der kanonischen Peptid-Orientierung in eine invertierte verfolgt werden, was zudem durch den natürlichen Peptidaustauscher HLA-DM katalysiert wurde.

Im zweiten Teil der Arbeit wurde Xenon-detektierte NMR zur Beobachtung der Bindung des viralen Peptids HA an HLA-DR1 verwendet. Die Funktionalisierung des Peptids mit Kryptophan erlaubte seine Detektion durch die charakteristische NMR-Resonanz eingeschlossener Xenon-129-Atome. Dies war Grundlage für die indirekte Detektion von Kryptophan-HA mittels Sättigungstransfer bei Austausch von Xenon mit Kryptophan. Die Charakterisierung von Kryptophan-HA ergab eine hohe Vergleichbarkeit mit HA. Das Peptid konnte als applikabel an Mäuse und immunogen für HLA-DR1/HA-restrizierte T-Lymphozyten eingestuft werden. Die Ergebnisse sind als Grundlage zur Verwendung von Xenon in der Magnetresonanz-tomographischen Visualisierung von Entzündungen zu sehen.

1 Introduction

1.1 The immune system

The Latin translation of '*immunis*' is best given by '*untouched*'. The immune system of an organism comprises its physiological and biochemical defense to causative organisms or compounds. While early immunology targeted the matter of infection, consequences and defeat options, biological sciences nowadays enable us to decipher genetic backgrounds of immunodeficiency, the molecular susceptibility to allergies and autoimmunity.

The most fundamental requirement of an immune system is the ability to distinguish between self and non-self. The detection, neutralization and destruction of pathogens are well developed throughout the animate world[1]. Simple unicellular organisms comprise enzymatic mechanisms to fight viral attacks. Plants and insects possess antimicrobial mechanisms based on peptidic defensins, phagocytosis and an ancient type of complement system. More sophisticated, mammals have developed a complex network of multiple organs, specialized tissues, cells and hundreds of protein classes. The human immune system involves physiological barriers like skin or mucosa as first mechanical outpost supported by cellular components and soluble factors such as antibodies. Communication between immune cells is mediated by cytokines and hormones.

The response to a pathogen is structured hierarchically. Upon invasion the organism activates the innate immune response within minutes to hours. In case of escape by the pathogen adaptive immunity is launched. It culminates in memory of pathogen recognition. This ability to ‘learn’ is one of the most sophisticated features in evolution and the greatest achievement of our immunological advance.

1.1.1 Mechanisms of innate immunity

Innate immunity is conceived as a broad, relatively non-specific response against pathogen. Vertebrates are capable of recognizing pathogenic structures like double-stranded RNA, particular nucleotide sequences, lipopolysaccharides, and formylated methionine. Macrophages or neutrophils recognize these structures leading to release of cytokines which affect other cells of the immune system at later stages. Histamine, secreted by neutrophilic mast cells, instead, promotes the inflammatory response.

The neutralization or destruction of parasites is mediated via different mechanisms. Opsonization marks invaders, activates the complement system and attracts immune effector cells. Phagocytosing cells are capable of directly ingesting and destroying intracellular bacteria. Secretion of cell-wall-lysing substances like lysozyme or the generation of reactive oxygen species efficiently harms bacteria. Once somatic cells are infected, Natural Killer cells provoke their apoptosis by the injury of cell membranes. This process sets up the synthesis of prostaglandin which causes pain, thrombocyte aggregation and vasodilatation.

1.1.2 Mechanisms of adaptive immunity

In contrast to a rapid innate response the adaptive immune system is capable of raising a strong and specific reaction against pathogen upon prolonged exposure. Antigen specificity includes the recognition of re-invading bacteria or viruses. Unique to vertebrates, the adaptive immune response is divided into the humoral and cellular arms[2]. To both arms the presentation of fragments from pathogens to T cells is underlying.

The humoral part describes the neutralization and labeling of pathogens with soluble antibodies secreted by plasma cells. Plasma cells have undergone maturation from B cells, a subtype of lymphocytes, which bind pathogenic protein sequences with surface B cell receptors (BCR). BCRs can occur in high variety based on somatic recombination of the corresponding gene segments. Antibodies, also named immunoglobulins (Ig), are the soluble pendant to membrane anchored BCRs. They are classified into IgA, IgD, IgG, IgE and IgM with additional sub-grouping standing for different functions like neutralization of pathogens, opsonization or complement activation.

The cellular immune response comprises the recognition of antigenic fragments by T lymphocytes (T cells) followed by activation and clonal expansion. T cells are characterized by their membrane spanning T cell receptor (TCR) restricted to one epitope presented by antigen presenting cells (APC). Similar to BCRs, TCRs show broad combinatorial variations leading to highly specific T cells which are sub-divided into cytotoxic or effector (T helper) cells. The surface protein CD8 defines cytotoxic T cells which provoke the apoptosis of infected cells. T helper cells are classified by CD4 and do not directly extinguish infected APCs. T helper cells are moreover divided into Th1 cells activating macrophages and Th2 cells

accounting for activation of B cells. Recently, a third class has been found named Th17[3] which seems to play a critical role in peripheral tolerance and the development of autoimmunity.

T cell as much as B cell stimulation by a cognate antigen leads to clonal expansion. In particular for B cells the long term survival of clones in form of memory cells is well described[4]. Upon re-exposure to the antigen a rapid immune response can be mounted by fast clonal expansion and ultimately provides high titers of cognate antibodies against pathogen. Memory B cells can be stored over several years and are essential for active vaccination. Figure 1.1 sketches the basics of cellular immune response opposing the humoral arm of adaptive immunity.

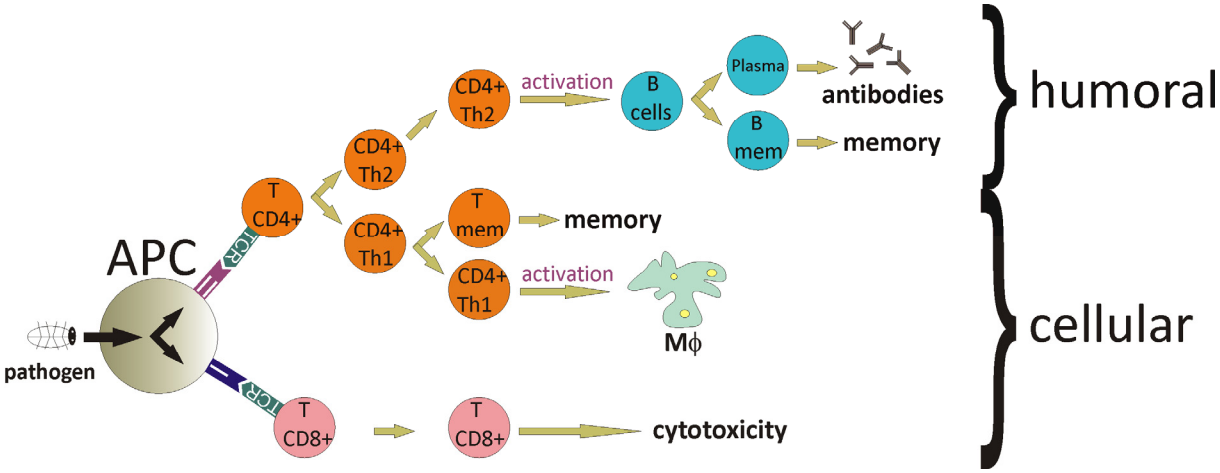

Figure 1.1: Simplified scheme of lymphocyte maturation upon contact with an antigen presenting cell (APC). "T" indicates a T cell, either CD4+ or CD8+. Th1 and Th2 indicate CD4+ T cell main subtypes. "Mϕ" is an abbreviation for macrophages which are activated by Th1 type CD4+ cells. "mem" indicates memory cells.

1.1.2.1 The immunological synapse

The central event of adaptive immunity is the engagement of an APC and a cognate T cell in a specialized cell-cell junction, sometimes referred to as the immunological synapse. The formation of the immunological synapse shows a comprehensive re-organization of proteins within the SMAC (supramolecular activation cluster)[5]. A cluster of adhesion molecules embeds the TCR/MHC/peptide trimeric complex in the center of the synapse (cSMAC) while surrounding molecules acting as co-receptors.

SMAC induced T cell activation is followed by signaling cascades, the details of which are still under intense investigation[6]. Indisputably, activation of T cells by APCs leads to clonal

expansion, which provides the T cell clone in higher quantity. Another effect of T cell stimulation is the clustering and activation of integrins (inside-out-signaling). This serves to stabilize interactions with cells like APCs or during migration of lymphocytes[7].

1.1.2.2 Antigen processing and presentation by class I MHC

The Major Histocompatibility Complex I (MHCI) pathway serves to display peptidic sequences from the cytoplasm. Therefore pathogenic and self-proteins are chopped into fragments within the proteasome. Peptides are then translocated into the endoplasmic reticulum (ER) by the transporter TAP (transporter associated with antigen processing) and loaded onto the folding chains of MHCI by help of enzymatic action from a multiprotein complex which includes tapasin (TPN), the thiol-disulfide oxidoreductase ERp57, and the chaperone calreticulin (CRT)[8]. MHCI-peptide complexes are taking the secretory pathway to be displayed on almost any cell type and eventually activating CD8+ T cells. The process is summarized schematically in the left panel of figure 1.2.

1.1.2.3 Antigen processing and presentation by class II MHC

Proteins of the class II Major Histocompatibility Complexes (MHCII) present antigenic peptide fragments derived from the extracellular space. This is exclusively accomplished by professional antigen presenting cells like macrophages, dendritic cells or B cells. Fragments are obtained after uptake of pathogens by the action of proteases such as cathepsins[9] in a late-endosome-like compartment[10], also named MIIC. Binding of linear sequences can also precede subsequent proteolytic action of cathepsins[11]. As depicted in the right panel of figure 1.2, fragments are loaded onto MHCII which at this point is pre-occupied by the placeholder peptide CLIP (class II associated invariant chain-derived peptide). CLIP is a product of cathepsin action on a protein named invariant chain (Ii). It is replaced by higher affine peptide through the enzymatic action of HLA-DM, a degenerate class II MHC without known peptide binding capability[12]. HLA-DM is potent in screening MHCII-peptide (pMHCII) complexes for their stability and acts catalytic towards selective presentation of long-lived pMHCII species[13]. Both pMHCII and HLA-DM persistently cycle between the MIIC and the cell surface. However, acidic conditions and the presence of cathepsins as much as thioreductive enzymes like GILT (γ-interferon inducible lysosomal thioreductase) were found to be crucial

for HLA-DM mediated antigen presentation (see Busch *et al.*[14] for further reading). HLA-DM is opposed by HLA-DO in its performance[15] depending on cell type and developmental stage. The roles of pMHCII-stability and half-life as determinants for immunodominance were found some years ago[16]. However, the availability of peptide is a central determinant for the occurrence of particular pMHC complexes and thus can be tissue-specific or -restricted. The identification of immunodominant peptides, e.g. in organ-specific autoimmunity, is therefore critical for the identification of harmful or autoreactive T cells.

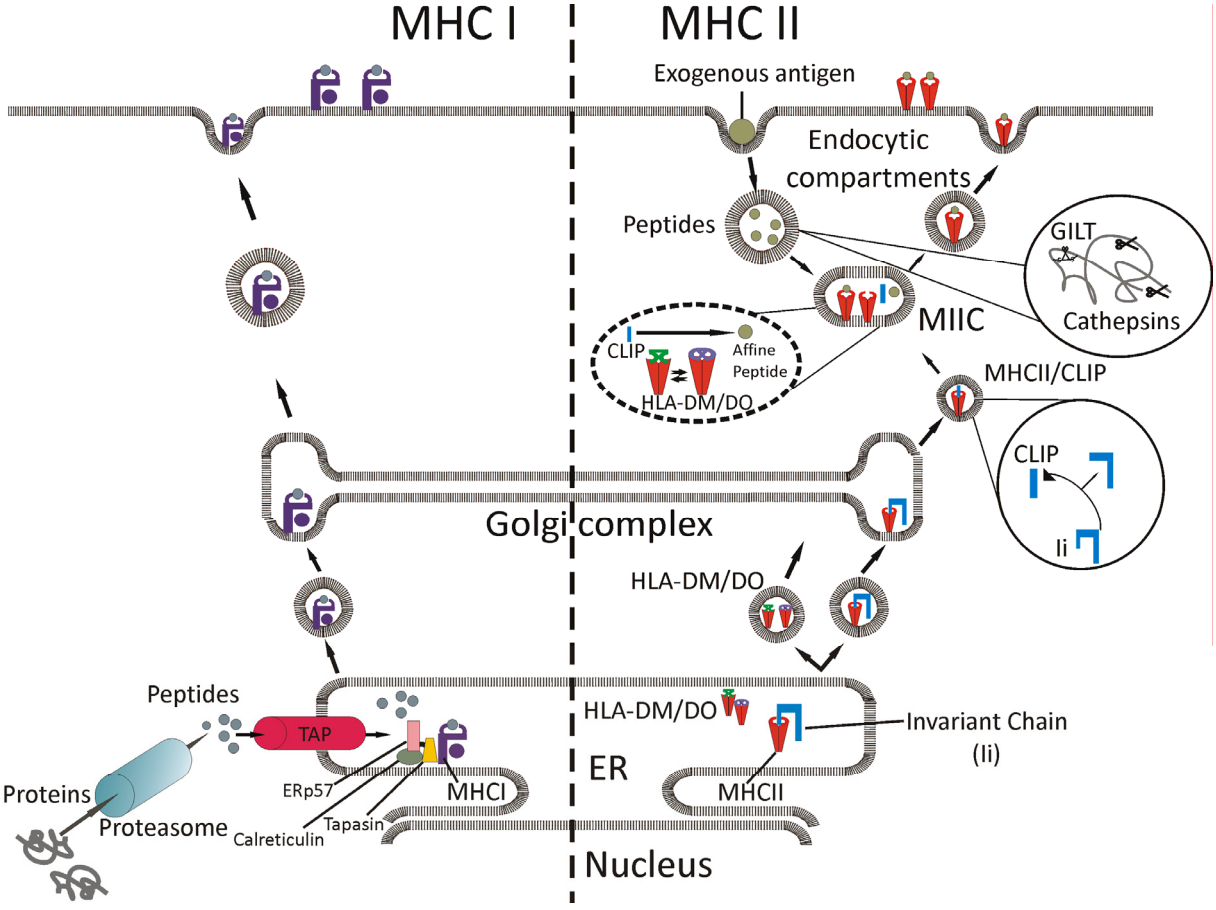

Figure 1.2: Scheme of human MHC class I and II pathways during maturation and antigen loading. Abbreviations are: ER, endoplasmic reticulum; MHC, major histocompatibility complex; TAP, transporter associated with antigen processing; CLIP, class II-associated invariant chain peptide; GILT, γ-interferon inducible lysosomal thioreductase; MIIC, MHCII containing compartment; HLA-DM, Human Leukocyte Antigen DM.

1.1.4 Discrimination of self and non-self peptides

Immunological defense is supposed to act predominantly towards antigens derived from pathogens or tumors. Presentation of self peptides by MHCI and MHCII molecules, however, is not suppressed actively. To avoid stimulation of T cells by self peptides (tolerance) the

adaptive immune system invokes a developmental program in the thymus: thymocyte maturation.

In the thymus, cells mature into different T-lymphocytes each of them carrying one unique clonal antigen receptor (TCR). Maturation encounters three important steps[17]. During β-selection only T cells with a functional TCR β-chain will pass the checkpoint. This serves to guarantee structural integrity together with the pre-TCRα complex. In the second step positive selection is undergone where lymphocytes are selected by sufficient affinity to MHC, which yields CD4+ or CD8+ T cells. Thymic epithelial cells express an unusually large number of tissue-specific host proteins, controlled by the transcription factor 'autoimmune regulator' (AIRE)[18]. Only clones with low affinity for thymus-presented MHC-peptide complexes are allowed to exit the thymus (negative selection of strongly interacting T cells). However, some autoreactive T cells can escape selection and are released into the periphery. There, additional mechanisms of tolerance exist as for example the induction of anergy, a non-responsive state of T cells in the periphery. Moreover, regulatory T cells (suppressor T cells[19]) counteract the function of typical effector T cells and maintain tolerance to self. Similarly, clonal deletion exists for B cells in the bone marrow. Autoimmunity is often mediated via self-reactive antibodies while no auto-reactive T cell response is measurable[20]. Properly described autoimmune or autoimmune-like diseases are related to few MHCI or MHCII alleles[21].

1.1.3 MHC molecules

MHC proteins form three classes from which only class I and II are directly involved in antigen presentation. All classes of human MHCs co-localize on chromosome 6 [22]. Human MHC molecules are termed HLA (human leukocyte antigen), which points to their early defined role in rejection of organs after transplantation[23]. The set of MHC molecules is unique to any individual. Human alleles are sub-divided into the types A, B and C forming the classical class I isotypes. HLA-D represents class II MHC and is further divided into the isotypes DR, DP and DQ. HLA-DM and HLA-DO are class II–like MHCs with special functions. Little is known about the alleles HLA-E, -F and -G. The MHC gene locus is known to show the highest polymorphism of all genetic loci. One chromosome contains a haplotype of MHCs. In a diploidic set of chromosomes the genotype is characterized by a pair of each HLA-A, B, C, DP, and DQ and is complemented by 1-2 pairs of HLA-DR. The diversity of MHCs is moreover

given by large genetic variations within chains of allelic isotype variants, defined as polymorphism. For example there are more than 800 known versions of DR, which has led to a DR sub-classification. In MHCI there are more than 1000 variations of HLA-A and -B, respectively whereas only few polymorphisms are known for HLA-C or HLA-DP. The appearance of non-silent point mutations, deletions and insertions is mainly restricted to the peptide binding domains with drastic effects on antigen specificity.

With this, millions of possible permutations lead to individual MHC content and display making up one decisive part of the adaptive immune system. Recently, there has been experimental support that MHC genotypes are selection criteria in sexual attraction between individuals[24] explaining their long-reaching impact in evolution.

1.1.3.1 MHC class I molecules

Class I MHCs are constructed from two chains as shown in figure 1.3, panel A. The α-chain (44 kDa, including the non-crystallizing transmembrane region) is made up of three domains, α1-α3, two of which, α1 and α2 are forming the peptide binding groove. α3 is proximal to the membrane and protrudes into a membrane spanning sequence followed by a short cytoplasmic C-terminal tail. The shorter chain is termed β2-microglobulin (β2m, 12 kDa) and complements the α-trinity by stabilizing it laterally without membrane contact. α3 and β2m are pure Ig folds, rich in β-sheet structures, whereas α1 and α2 contain helical stretches surrounding a β-sheet plateau. This arrangement forms the peptide binding groove which is characterized by its closed ends confining antigenic peptide length to 8-10 amino acids (see panel B). Thereby peptides are aligned in a biased orientation due to polar interactions at both their positively N- and negatively charged C-termini within the protein binding cleft[25]. The molecule comprises two essential disulfides in α and one in β2m as depicted in A.

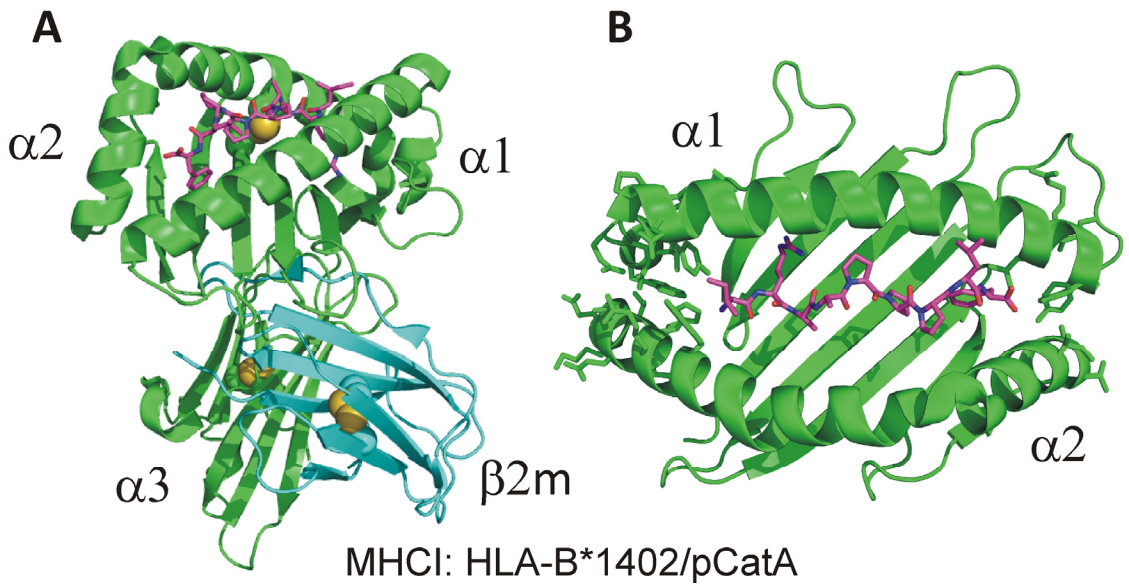

Figure 1.3 Structure of a classical MHC class I molecule. A) Shown are the ectodomains of HLA-B*1402 as cartoon in complex with the endogenous cathepsin A signal sequence peptide pCatA (shown as sticks in magenta). The heavy and light chains are colored green (α1 - α3) and light blue (β2microglobulin). Individual Ig-domains are denoted and disulfides shown as spheres. B) Top view onto the cartoon presentation of α1α2, which yield the peptide binding cleft. Side chains of residues close to the peptide termini are displayed and do not allow antigen extension outside the cleft. The pdb code of this structure is 3bxn[26].

1.1.3.2 MHC class II molecules

Class II MHCs consist of two equally shaped subunits, α (33 kDa) and β (28 kDa). Both comprise two extracellular domains. The α2/β2 domains are membrane-proximal immunoglobulin (Ig) domains whereas the distal α1/β1 domains also comprise α-helices. Both subunits contain a C-terminal transmembrane sequence and a small cytoplasmic chain which functions regulatory in MHCII surface abundance[27]. Essential disulfides are part of both chains, two of them in β and one in α. The MHCII upper domains α1 and β1 form the antigen binding groove, a β-sheet plateau which is embedded in two helices (see figure 1.4, panel A). The β1-helix is characterized by a significant kink central to the groove while the α1-helix protrudes into a short unfolded stretch at its N-terminus. Another small helical part appends to that with a rough twist of 90°. Although MHCII is structurally very similar to MHCI, figure 1.4 proves that class II binding clefts bear open ends allowing the capture of peptides longer than those for MHCI. Analogous to MHCI, the binding cleft is composed of 9 pockets numbered P1 - P9 (relative to the peptide position) which harbor peptide side chains (see panel B, top). A putative 10th pocket has been claimed by Zavala-Ruiz *et al.* in 2004[28]. In addition, peptide-MHC interactions are mediated via H-bonds. A set of 10-16 hydrogen

bonds is formed from MHCII side chains to the peptide backbone with the exception of three H-bonds contacting α1 residues' backbones at the N-terminal end of the helix (see panel B, bottom). Both pocket occupation and individual formation of H-bonds were found to act cooperatively in determining complex stability[29,30]. However, these features are very allele-specific. The impact of pocket 1 (P1) is most prominently expressed in DR alleles but in general pockets P1, P4, P6 and P9 are assumed to account for pMHCII stability. The allele-specific shape of the pockets leads to preferred residues to host in them. This explains the immunological power of MHC diversity with very distinct propensities in antigen presentation. In contrast to MHCI no fixed polar interactions at the peptide termini confines the alignment to one direction. However, as no alternative binding has been experimentally observed the dogma of canonical binding refers to the N-terminus positioned close to pocket P1. In accordance with a possible occupation of pockets the open ends enable the peptide to be positioned in more than one register (peptide isomerism)[31] if long enough. This feature is considered to promote immunodominance of particular peptide stretches or lead to altered immune responses due to tissue-specific presentation. The affinities of peptides to particular alleles are predicted by databases like SYFPEITHI based on empirical findings that deliver scores to individual peptide registers[32].

MHCII proteins are co-translationally sequestered into the endoplasmic reticulum (ER). Supported by the action of the chaperone calnexin the two subunits fold into a heterodimer stabilized by a third component, the invariant chain (Ii) which occupies the newly formed antigenic binding cleft. Delivery of MHCII-Ii to the late-endosomal loading compartment occurs in a nonameric complex where three MHCII heterodimers are transported by a triple bundle of invariant chain.

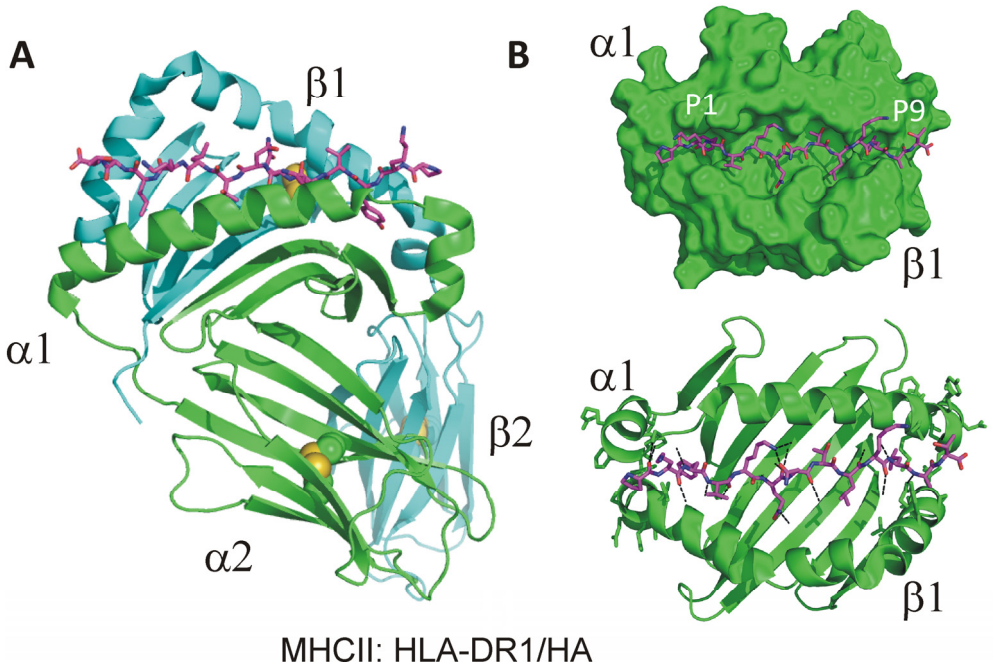

Figure 1.4: Structure of a classical MHC class II molecule. A) Ectodomains of HLA-DR1 as cartoon presentation in complex with the Influenza hemagglutinin peptide $HA_{306-318}$ (shown as sticks in magenta). The α-subunit is colored in green, the β-chain given in light blue. Individual Ig-domains are denoted. Disulfides are indicated as spheres. B) Top: Top view onto surface presentation of HLA-DR1/$HA_{306-318}$ with only α1β1 presented. The peptide binding groove reveals surface depressions to harbor antigenic side chains. For HLA-DR1 the most prominent ones, P1 and P9, are denoted. Bottom: Top view onto the same as in top figure in B when presented as cartoon. The side chains of HLA-DR1 amino acids close to the peptide termini are shown and reveal no interference. Polar contacts from the peptide to protein are drawn from peptide side to mark H-bonds. The pdb code is 1dlh[33].

1.2 Structural investigations of MHC molecules

The first crystal structures from the central components of any immunological synapse (IS), the pMHC-TCR, were published in the late 1980s/early 1990s starting from MHC class I and later on class II[34,35]. The group of Wiley accomplished pioneering work during that time and in 1996 the first ternary complex with a T cell receptor was deposited[36]. From then numerous crystal structures of pMHC and TCR complexes were revealed and interestingly, both MHCs and TCRs almost fully superimpose in all determined structures. However, these crystal structures all fail to reveal dynamic information at particular sites relevant for biological function. They can be prone to artifacts from crystal packaging and reliability depends on atomic resolution. At this point NMR methods can complement the lack of information. However, due to size limitations and the need of homogeneity at high concentrations it has successfully been applied only to structure determination of parts of CD4[37], the CD3-homodimer[38] and β2microglobulin[39] concerning central IS components .

1.2.1 Conformational flexibility of pMHCII complexes

Besides a wealth of static structural information from crystallography pMHC complexes are known to be highly dynamic. Heterogeneous sub-states had been described very early[40]. When empty, the binding cleft collapses into an unreceptive form. Re-binding of peptides depends on the catalytic action of HLA-DM or previously described MHC loading enhancers (MLE)[41]. Both can restore the protein's receptive state. A transiently opened binding cleft can then be re-occupied leading to a stable pMHCII. Whereas MLE functioning has been ascribed to the transient occupation of pocket 1, the principle of HLA-DM function is still unknown despite several attempts to target the mechanism[13]. Conformational heterogeneity is differently pronounced among MHC alleles and is thought to be guiding the editing process of HLA-DM[42].

The undefined conformation of empty MHCII did not allow determining its structure and still causes challenges in sample preparation. Also, pMHCII dynamics during peptide loading and exchange as well as the interaction between MHCII and HLA-DM are insufficiently explained by the combination of crystallography and mutational analysis. Thus, despite the size limitations, research has cautiously tried to address MHC molecules also by NMR techniques in the past years. In 1997, Jablonsky *et al.* determined the solution structure of the superantigen-binding site in a murine MHCII[43]. Later, mentionable progress has only been made for MHCI-attached β2microglobulin[44]. In 2007, the group of Garcia first published backbone assignments of a single-chain murine α1α2-MHCI complex with application to atomically resolved TCR-docking in solution[45]. No comparable studies have been published for any MHCII allele.

Clearly more attempts have targeted MHC-bound peptides. In the 1990s, Driscoll *et al.* analyzed an isotope-labeled cytochrome C peptide by two-dimensional NMR[46] proving the principal possibility to record magnetization transfer between MHC and peptide. However, the observation of peptides was complicated due to adopted relaxation behavior of the protein. Some years later Schmitt *et al.* confirmed class II MHC-conformational isomers by fluorine-19-NMR applied to a modified peptide. The study was a first solution-structural proof for MHC heterogeneity.

Peptide labeling with ^{19}F or ^{129}Xe have also been in the focus of MR-based imaging. They bear great potency in probing target molecules *in vitro* or *in vivo*. This potential has not been tested in MHC-related studies before.

1.3 Magnetic resonance techniques

Structures obtained by NMR still represent the minor portion of the fast growing number of structures deposited in the protein data bank (PDB)[47] within the last 25 years. Their information is complementary to crystal structures as it reflects a protein in its native state in solution. NMR techniques thereby allow observing binding events, transitions, (de)folding, and other processes at an atomic level.

NMR spectroscopy detects individual atoms, precisely nuclei, of a molecule. Nuclei are characterized by their magnetic interplay with adjacent atoms. To be detectable they have to carry a magnetic moment which, as for example for ^{1}H, arises from an odd number of protons and/or neutrons. As proteins, besides ^{1}H, mainly consist of NMR inadequate carbon (^{12}C) and nitrogen (^{14}N), stable isotope labeling with spin-1⁄2 ^{13}C and ^{15}N nuclei was a big achievement for protein NMR.

In addition to spectroscopy, magnetic resonance is also applied to the imaging of objects (MRI). Information on morphological changes based on tumors, ruptures, fractures or inflammations can be gained from locally varying relaxation properties of one nucleus, mainly the protons in water molecules. Its non-invasiveness favors MRI over x-ray-based computer tomography, radio-isotopic scintigraphy or open-histological imaging methods.

1.3.1 The basic principles of nuclear magnetic resonance

Nuclei are NMR active when they possess a quantum mechanical property called *spin* described by a spin quantum number I different from zero. The spin is conceived as a precision movement. Its quantum mechanical description is beyond the scope of this introduction[48]. Nuclei with a spin have a magnetic moment and allow for at least two distinct energy levels. Outside an external magnetic field both spin states hold the same energy and thus atoms will be equally occupying these levels. If - as inside the spectrometer - an external magnetic field B_0 is applied, the lower energy state will be occupied with slightly higher probability dependent on the field strength and the nucleus' gyromagnetic ratio γ (listed in table 1.1 for typical nuclei in biological NMR). Although protons show highest sensitivity amongst nuclei in a protein, spin state differences will be only in the range of a few in a million. Thus, the intrinsic insensitivity of NMR spectroscopy requires relatively large amounts of substance and is advantageously measured at high magnetic fields.

Table 1.1: List of nuclei used in biological NMR with spin quantum number and gyromagnetic ratio

Nucleus	I	$\gamma/2\pi^*$ in MHz T^{-1}
^{1}H	1/2	42.576
^{2}H	1	6.536
^{3}He	1/2	-32.434
^{13}C	1/2	10.705
^{14}N	1	3.077
^{15}N	1/2	-4.316
^{17}O	5/2	-5.772
^{19}F	1/2	40.053
^{31}P	1/2	17.235
^{129}Xe	1/2	-11.777

*The gyromagnetic ratio is given as divided by 2π here to illustrate the correlation of Larmor frequency (in MHz) and external field strength (in T).

The resulting net magnetization of a sample along the z-axis of the field B_0 can be described as a vector and is the sum of all spins. To deduce information from individual nuclei, a perpendicular field B_1 is applied (pulse) matching the so called Larmor frequency of the nucleus of interest. This tilts the net magnetization into the xy-plane with respect to the outer field as shown in figure 1.5, panel A. A receiver coil along x can detect the magnetization. Spins will start to re-equilibrate back to z when the B_1-pulse stops. This process is called relaxation and forms the basic event of detecting a resonating nucleus. The recorded net magnetization in xy will show a dampened trigonometric curve (Free Induction Decay: FID, see panel B). For a single spin the variation in signal intensity with time is described by

$$I(t) = I_0 \cos(\omega t+\theta) \exp(Rt).$$

The function reflects the spin precession yielding a distinct frequency ω depending on the specific atom's chemical environment. The signal amplitude I_0 is proportional to the amount of spins (nuclei) and thus the concentration of the sample. θ indicates a putatively shifted phase of the function and the signal's decay rate R shapes the exponential factor. As this is not a very convenient visual interpretation, time-domain data are Fourier transformed (FT)[49] into the frequency domain with a peak height corresponding to I_0 (see panel B of figure 1.5). R is directly proportional to the signal line width (LW) after FT. R largely affects signals as it increases with the molecular weight and the number of interfering nuclei in a protein.

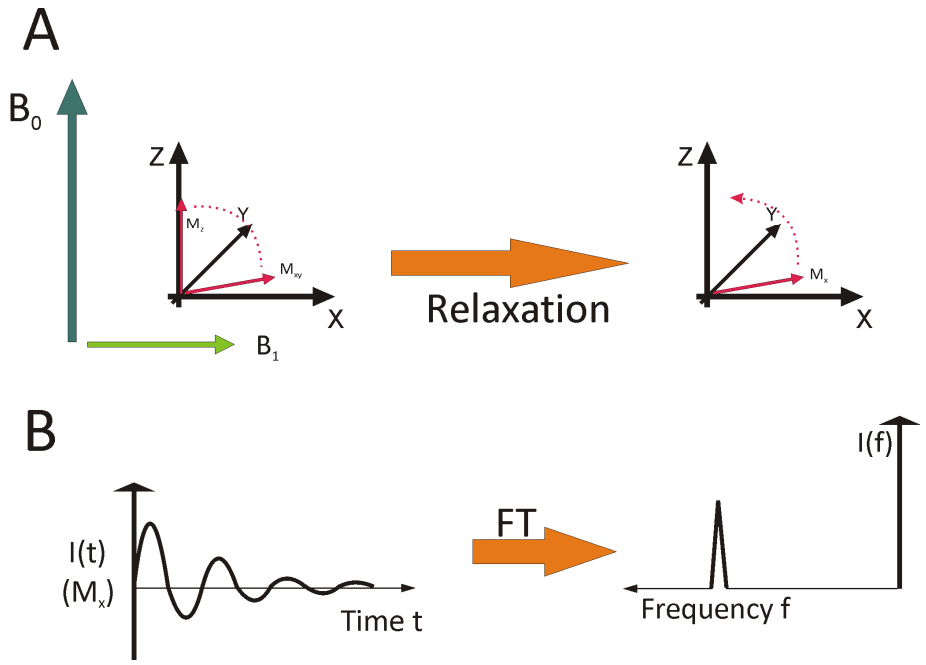

Figure 1.5: Simplified scheme of resonance detection in a one-spin NMR experiment. In A the spin is tilted from equilibrium magnetization along with static B_0 into the detectable xy-plane by the perpendicular field B_1 (left). The back-relaxation to z (right) produces a Free Induction Decay (FID) of the form as in B (left). This is then Fourier transformed (FT) into a frequency-based spectrum. 'I' stands for intensity corresponding to the net magnetization 'M'.

For a large molecule the FID will be a complex mixture of dampened trigonometric functions. Computer power is able to deconvolute the individual spin contributions yielding a spectrum of frequencies with respective line widths and amplitudes. As the variation of the observed resonances from the characteristic Larmor frequency is very small, the relative difference δ is used to normalize shifts from different spectrometers as it is

$$10^6\,\delta = (\nu - \nu_{Ref})/\nu_{Ref}, \text{ given in parts per million (ppm)},$$

where δ is the chemical shift and thus independent of the external field strength. The chemical shift of a nucleus is influenced by bound atoms (through-bond- or J-coupling) or through space (dipole-dipole-couplings, DD). Couplings are used to transfer magnetization to correlate nuclei and to retrieve information on inter-nuclear distances and torsion angles[50]. In large molecules a high number of dipoles surround a nucleus of question. In combination with a higher rotational correlation time T_c - which is a function of molecular weight[51] - this leads to decreased line sharpness and the need for novel labeling schemes and NMR experiments suppressing particular nuclear couplings (see 1.3.3).

1.3.2 Acquisition and processing of NMR data

1.3.2.1 The NMR spectrometer

The spectrometer's most space-consuming part is the magnet creating the stable field B_0. It needs to be shielded from external influences. It acts in a persistent superconducting fashion and is cooled to less than 6K with helium. Another layer of liquid nitrogen avoids permanent vaporization of the noble gas. Current magnets for biological NMR are in the range of 10 to more than 20 T, corresponding to proton Larmor frequencies of 400 MHz to 1 GHz.

The radiofrequency (RF) exciting coil is simultaneously fulfilling the function of the receiver coil presupposing a complex electronic. A second set of coils ('shim coils') functions to adjust for B_0 field inhomogeneities. Measurements take part in the temperature-controlled probe head where coils and sample tube are held in close proximity. The RF transmitter delivers pulses for selective excitation. The RF receiver sensitively captures resonances and amplifies incoming signals. Often a pre-amplifying device is put in between the probe and receiver. An Analog-to-Digital Converter (ADC) converts the signal into binary code as to be stored by the connected computer, usually in 16- or 32 bit style. Modern spectrometers contain a separate pulse-programmer which uses an interface with the spectrometer software.

The inherent insensitivity of NMR spectroscopy has long been complicated by intense electronic noise caused by long wires, cables and heat development within the system. The invention of cryo-probe platforms with minimized impedance has revolutionized modern NMR as the actively cooled data transfer leads to a several-fold gain in sensitivity.

1.3.2.2 Data acquisition

The process of NMR spectroscopic investigations is divided into distinct steps. First, one has to produce a sample with adequate properties in regard to labeling, concentration and homogeneity. This may be the limiting step whereas spectroscopic settings are rather optimized for standard experiments nowadays. The acquisition of NMR raw data describes the procedure of storing FIDs after a complex series of pulses and delays. The simplest one-dimensional proton spectrum is acquired involving three periods. Figure 1.6, panel A, shows a pre-scan delay in period p1 leading to equilibrium magnetization along z. In p2 a 90° pulse of optimized length is applied to tilt vectors into the xy-plane where then in period p3 magnetization is monitored during ^{1}H chemical shift evolution and the FID is stored. The process usually is repeated for a certain number of scans increasing the signal-to-noise (S/N).

Proteins contain too many hydrogen atoms to deduce relevant information from one-dimensional hydrogen spectra. By specifically observing protons bound to nitrogen, spectral complexity is reduced. Information on amino acids is gained as the protein backbone comprises one amide per residue. This 'finger-print' type spectrum is called ^{1}H-^{15}N-HSQC (heteronuclear single quantum correlation) spectrum. It forms the basis of many protein-related NMR experiment as it easily gives site-specific information. The HSQC experiment comprises a number of ordered pulses interspersed by delays of defined duration. During the pulse scheme magnetization is transferred from protons to nitrogen where chemical shift evolution takes place during t1 (see figure 1.6, panel B). It is then transferred back to protons before FIDs are recorded for proton chemical shift evolution in t2. t1 is incremented between repetitive experiments and by that the directly measured FIDs of protons also encode the chemical shift for nitrogen. Magnetization transfer is possible because of scalar coupling between both nuclei which is in the range of 92 Hz, i.e. the transfer takes approx. 5.4 ms for one direction. This is implemented in the INEPT (insensitive nucleus enhanced polarization transfer) sequence which describes the indirect detection of heteronuclei rather than their direct observation, which is less sensitive[52].

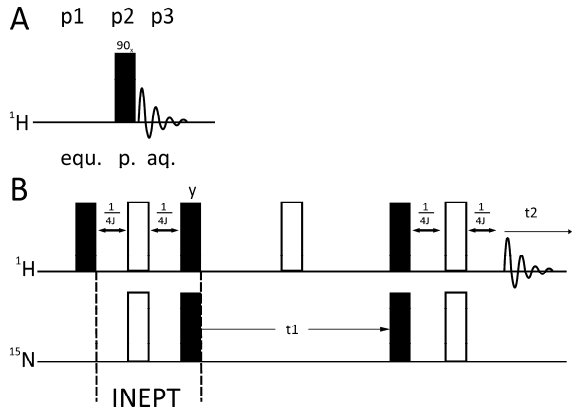

Figure 1.6: Pulse schemes of one-dimensional proton NMR (A) and two-dimensional proton-nitrogen-HSQC (B) experiments. Black bars indicate 90° pulses along x if not denoted differently. Open bars mark 180° pulses. In A, abbreviations are equ., formation of equilibrium magnetization; p., pulse; aq., acquisition forming one of the periods p1, p2 or p3, respectively. In B, INEPT stands for 'Insensitive Nucleus Enhanced Polarization Transfer'. J is the coupling constant (see main text). The sequence in B is simplified and no phase cycles and gradients for decoupling are shown. Parts of the sequences encoding water-suppression are not included.

A third dimension has to be implemented to correlate NH groups with Cα carbons or carbonyls or through space with other protons (^{15}N filtered NOESY or ^{15}N-NOESY-HSQC). Here, the HSQC pulse scheme is interrupted by another transfer step similar to INEPT. By this, a second incrementation creates one more indirect domain (not shown). The overall

time needed for 3D-NMR is a limitation to the investigation of large proteins. Rapidly relaxing nuclei will not leave much of the net magnetization by the end of the pulse sequence. Figure 1.7 shows the 3D-NMR experiments most commonly used for protein backbone assignments. The strong coupling of amides with Cα leads to possible transfer of magnetization to both the own and preceding carbons. This can be overcome by including the carbonyl as a filter to only allow for the preceding Cα. The pair-wise acquisition of HNCA/HNcoCA, HNCACB/HNcoCACB and HNCO/HNcaCO facilitates the deciphering of self-resonances and preceding amino acids, mandatory for an assignment of protein backbone. Any of these experiments will lead to thousands of FIDs containing information on all nuclei targeted by the pulse sequence.

The insensitivity of NMR rapidly accumulates spectrometer time for three-dimensional experiments, which requires balancing the number of scans for good S/N and indirect time-points for resolution. Each factor will linearly contribute to the increase of the acquisition time.

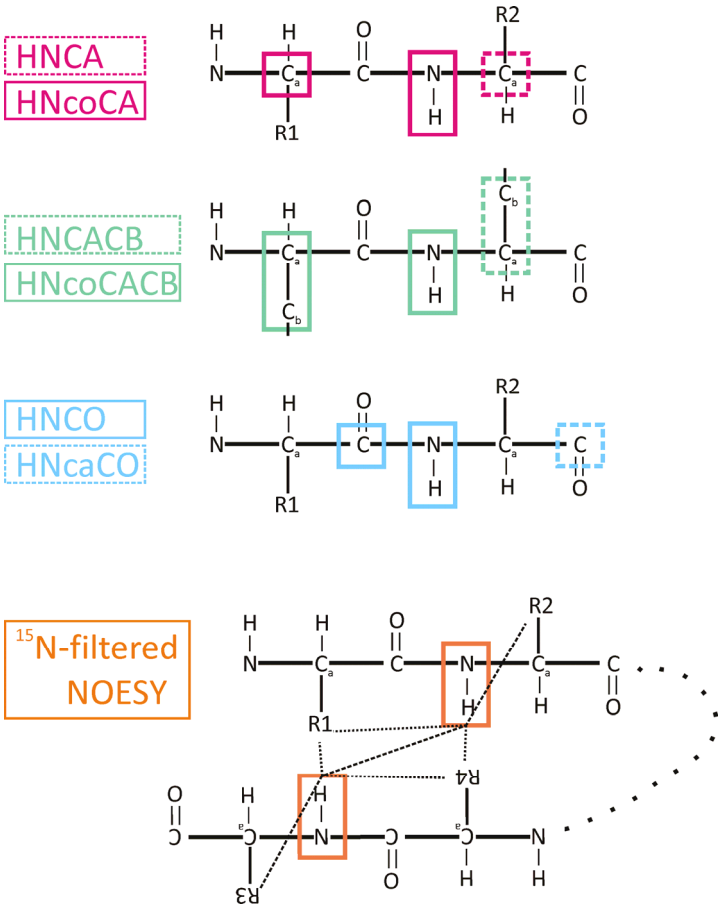

Figure 1.7: Schemes for spin systems in standard triple resonance experiments and nitrogen-filtered NOESY. Marked atoms are part of the spin system; broken rectangles indicate groups that are facultative. Magnetization transfer to both Cα (i and i-1) only occurs when no CO-filter is implemented. The NOESY gives putative cross signals to protons closer than ~5 Å to an amide.

1.3.2.3 Processing of NMR raw data

NMR raw data are processed into spectral plots extracting the chemical shift and line-width for every resonance by Fourier transformation (FT) of the FIDs. Mathematical modifications can be included in order to improve results. E.g. the number of FIDs used for FT can be chosen which mainly serves to minimize noise. Moreover, parts of the FIDs can be weighted by multiplication with a window (weighting) function. Obviously, the first part of an FID rather determines S/N as it encodes the maximum amplitude. In contrast, a weighting of the FID back part leads to sharpened line widths of peaks which are defined by the relaxation component of the FID. The effect of window function multiplication of FID has well been described by Ernst *et al.* (1987)[53]. Similarly, the artificial prediction of FIDs - either forward (prolonged) or backwards - is used to enhance resolution by mimicking additionally sampled data points.

1.3.3 Achievements and current possibilities in protein NMR spectroscopy

A major breakthrough of protein NMR can be ascribed to the development of triple resonance pulse schemes[54]. The size limit of proteins investigated by NMR became less relevant when spectral overlap was decreased by deuteration[55] and selective labeling approaches[56]. Cell-free protein bio-synthesis supports the recombinant production of proteins difficult to obtain from *E.coli*.

Line-broadening in large molecules has been addressed by the development of TROSY-NMR in 1997 [57]. *Transverse Relaxation Optimized Spectroscopy* takes advantage of the coupling between nitrogen and hydrogen in amides which leads to split resonances of differently relaxing components. While in standard HSQCs splittings are decoupled and intensities averaged, TROSY selectively extracts the slowly relaxing component leading to a narrower line width and stronger S/N. This finding has led to the standard implementation of TROSY in pulse sequences applied to large molecules[58], ideally combined with deuteration of proteins. The group of Lewis E. Kay established selective labeling of protonated hydrophobic side-chains on a deuterated background allowing measurements of proteins with hundreds of kDa[59]. This has been combined with the expansion of TROSY to methyl groups in amino acid side-chains[60]. Their relaxation properties were estimated with CPMG (Carr, Purcell, Meiboom, Gill[61])-sequences which allows the targeting of sparsely populated protein states.

Measurement of relaxation has been also proven useful in paramagnetic relaxation enhancement (PRE)-NMR. Paramagnetism occurs from unpaired electrons as present in copper, iron or nitroxides. Functional paramagnets incorporated into proteins lead to enhanced relaxation of NMR-active nuclei within a radius of more than 20 Å. They are used for long-range distance restraints and for monitoring transient interactions between proteins and ligands[62].

Another technique to obtain information about the folding and stability of secondary structure elements utilizes hydrogen-to-deuterium (H/D) exchange in combination with NMR techniques. H/D exchange in amides is a measure of dynamics based on formation or disruption of H-bonds or the shielding of NH-groups and has more recently been applied to larger proteins[63]. Figure 1.8 indicates the effect of exchange from visible NH to invisible ND for different rates within one molecule. The technique is only applied reliably for rates in the second-to-hours frame despite the development of pulse sequences for faster acquisition[64].

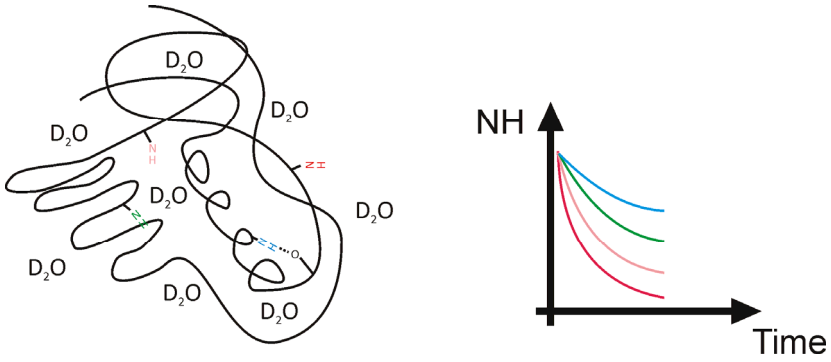

Figure 1.8: Hydrogen-to-deuterium exchange experiment. In a hypothetical protein amides are differently shielded against deuteron-replacement. Rates are determined by measuring NH intensities over time.

1.3.4 Magnetic resonance of xenon-129

Recent advances in MR also concern nuclei that are not contained in natural proteins. For example noble gases are used in MR imaging to display void spaces (lung) and other organs or tissue accessible through blood flow (brain)[65,66].

1.3.4.1 Xenon-129 and its spin hyperpolarization

The element xenon (Xe) appears in more than 50 different natural isotopes, nine of which are stable. Besides the quadrupolar isotope 131 only xenon-129 is NMR-active with a spin-1/2. Xenon was first subjected to NMR by Ito and Fraissard (1980) for the study of porous

materials[67]. They identified xenon to be inert and very sensitive to its environment, in particular to the morphology of adsorption sites. Early studies of interactions with proteins go back to the 1980s[68]. ^{129}Xe shows a broad chemical shift range of approximately 200 ppm in aqueous solution, its natural abundance of 26 %, however, ideally requires its enrichment for sensitive NMR studies. While the thermal spin polarization of xenon-129 is comparable to carbon-13 because of a similar gyromagnetic ratio, so-called hyperpolarization may be employed for polarization enhancement by a factor of almost 10^5.

Hyperpolarization of xenon-129 (hp ^{129}Xe) is achieved through spin-exchange optical pumping in a collision cell[69]. Firstly, as shown in Fig. 1.9, the angular momentum of circularly polarized photons is transferred to spins of rubidium (Rb) electrons by light absorption, and secondly, this Rb electron spin polarization is subsequently transferred to the nuclear spin of xenon atoms during collisions in the gas phase through Fermi contact interaction.

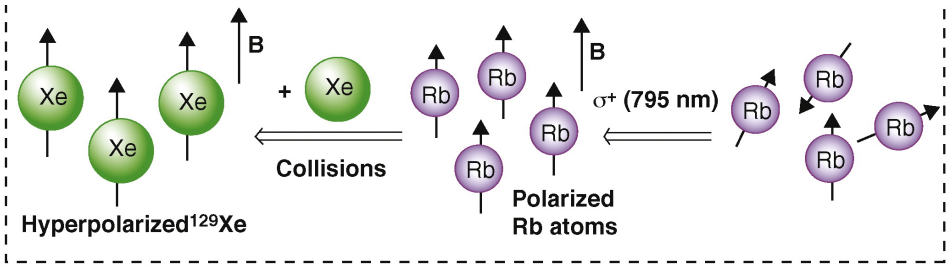

Figure 1.9: Principle of hyperpolarization in a collision cell. Laser-irradiated rubidium (Rb) is getting polarized in a magnetic field B. Subsequent collision with xenon (Xe) via Fermi contacts hyperpolarizes ^{129}Xe. The figure is adapted from Taratula and Dmochowski[70].

The high gain in sensitivity of hp ^{129}Xe may facilitate NMR studies that were not possible so far, or be interchanged to notable savings in acquisition time. Also, the huge magnetization of hp ^{129}Xe may be flipped with fast repetitive excitation pulses of very small angles. The resulting shortened repetition times are necessary for fast imaging or spectroscopy. Since xenon is not present in biological and most inorganic samples there is usually no background signal that requires active suppression.

Consequently, time-resolved spectroscopy and MR imaging became practical applications of hyperpolarized xenon[71]; in particular for the imaging of lungs[72]. The application of xenon to whole-body imaging has been rapidly optimized in rodents. Nowadays, pathologies in the pulmonary tract and gas transport are studied with intravenous injection of hp xenon-129[73]. Promising results for humans were recently published by the group of B. Driehuys[74].

1.3.4.2 Achievements with functionalized hp xenon-129

The use of hyperpolarized xenon has shifted from observing the bare atoms in solutions or gaseous phases towards specifically functionalized ^{129}Xe. This became possible with the findings of xenon to be trapped in cryptophane moieties ('caging'). A measurable affinity for xenon to hydrophobic cavities[75] and a modest capability of being caged[76] had been known before. However, the most favorable steric conditions were found with cryptophanes whose career started in 1981 with the synthesis of type A, also known as cryptophane-2,2,2 [77]. Cryptophanes are made up of two cyclotriveratrylene cups which are linked by three carbon spacers reaching from methylenes to longer alkyl chains (see figure 1.10). Water-soluble cages were introduced in the upcoming 21st century with partially higher xenon affinities compared to those in organic solvents. In parallel, cryptophanes were linked to biological scaffolds, which similarly helped to overcome its hydrophobic character. Its practical application as a sensor to image a binding event has been shown by Spence *et al.* in 2001 [78]. The method takes advantage of the characteristic, isolated chemical shift (CS) for caged xenon in aqueous buffers. Xenon NMR has been applied to the analysis of the avidin/biotin interaction, to diastereomeric binding[79] or DNA-DNA hybrids[80]. Wei *et al.* succeeded in detecting distinct resonances for intact and processed protease substrates[81].

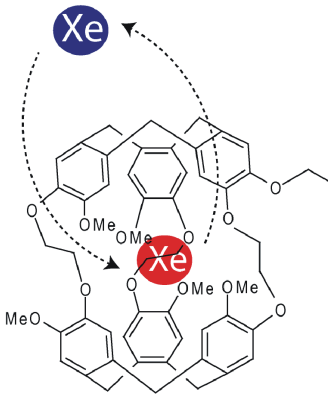

Figure 1.10: Structure of the cage compound cryptophane A (2,2,2). The potential exchange of xenon atoms with the cage is indicated. The moiety can be functionalized by replacing or derivatizing the free alkoxyl chain.

The concept of chemical exchange between bulk and caged xenon to indirectly detect the cryptophane-bound noble gas has paved the way to imaging-based applications. In the initial study by Schröder *et al*. in 2006 [82] saturation transfer with hyperpolarized xenon (HYPER-CEST) was used to two-dimensionally image an agarose phantom. The principle includes the decrease of excess bulk xenon magnetization whose depolarization is achieved by repetitively saturating caged xenon which is in exchange with the solution. This leads to a

3000-fold increased sensitivity compared to direct detection of caged xenon. However, an application of this principle to cells, tissues or organisms has not been reported before this thesis.

1.4 The objective of this study

This thesis aimed at approaching the human class II major histocompatibility complex molecule HLA-DR1 to investigations based on nuclear magnetic resonance (NMR) spectroscopy. The refolding protocol was to be optimized from bacterial *inclusion bodies* for obtaining soluble, homogeneous and isotope-labeled protein. Multi-dimensional high-resolution NMR spectra were to yield atomically resolved information on MHC-peptide complexes in solution. Questions of protein stability and folding, in particular targeting the difference between unloaded and loaded MHCII, were to be addressed by NMR experiments.

With this, one goal was to observe HLA-DR1/peptide complexes during catalyzed peptide exchange in the binding groove of HLA-DR1. Complementary information from crystal structures was to allow the correlation with dynamics in solution. The complex of HLA-DR1 with the placeholder peptide CLIP was to be investigated to examine the particular chaperoning role of CLIP.

In a second sub-project a functional peptidic probe for HLA-DR1 should be developed that would be amenable to xenon-NMR and to magnetic resonance imaging *in vivo* in the future. The system was to be established for detection of MHC-peptide binding and identification of the probe at low concentrations as would be necessary *in vivo*. The bio-tolerance of the probe was to be validated.

2 Materials and Methods

2.1 Standard methods in molecular biology

2.1.1 Bacterial strains and cells

- *E. coli* BL21 (DE3) (Novagen, Merck Biosciences, Germany): for protein expression,
  E. coli B, F-, dcm, ompT, hsdS (r_B^- m_B^-), gal λ (DE3) with a chromosomal copy of the galactose-inducible T7-polymerase gene regulated by the lacUV5 promoter

- *E. coli* XL1- Blue MRF' (Stratagene, La Jolla, CA, USA): for cloning,
  Δ(mcrA)183, Δ(mcrCB-hsdSMR mrr)173, endA1, supE44, thi-1, recA1, gyrA96, relA1, lac, [F', proAB, lacIqZΔM15, Tn10,(Tetr)], deficient in recombination and devoid of restriction systems/endonucleases

- *E. coli* DL39 (DE3) (provided by Prof. Dr. Volker Dötsch, University of Frankfurt, Germany):
  for protein expression, F-, LAM-, aspC13, fnr-25, rph- 1, ilvE12, tyrB507, gal λ (DE3), with chromosomal copy of galactose inducible T7-polymerase generegulated by the lacUV5 promoter and depleted in transaminases yielding auxotrophy for phenylalanine, tyrosine, aspartic acid, leucine, isoleucine, and valine[55]; intrinsic kanamycine resistance

- *E. coli* BL21 (DE3)Xpress (provided by Dr. Phillip Selenko, FMP Berlin, Germany):
  for cloning and protein expression, F- , ompT, hsdSB (rB- mB-), gal, dcm (DE3), for higher recovery rates of plasmid than from standard BL21 (DE3)

- D. *melanogaster* Schneider (S2) cells (provided by Dr. Olaf Rötzschke, MDC Berlin):
  stably SV40-transfected with HLA-DM originally encoded on Drosophila expression vector pRmHa, expression inducible with Cu^{2+} as described originally in[83]

2.1.2 Preparation of electrocompetent cells

Competent cells were produced from a single clone of a freshly streaked culture. 50 ml of LB-medium were inoculated and incubated overnight at 37°C. From this 25 ml were diluted into 500 ml LB and the culture was grown to an OD_{600} of 0.4. At this point the entire suspension

was chilled on ice for 30 min before cells were harvested (15 min, 1000 x g, 4°C). The bacterial pellet was re-suspended in 500 ml of ice-cold water and centrifuged again before transfer into 10 ml of 10 % glycerol in water. After a third step of spinning cells were mixed into 3 ml of GYT medium (0.125 % w/v yeast extract, 0.25 % tryptone w/v and 10 % v/v glycerol) split into aliquots of 50 µl, snap frozen in liquid nitrogen and stored at -80°C.

2.1.3 Preparation of plasmid DNA

Plasmid DNA was isolated from bacterial strains XL-1 blue or BL21Xpress carrying the vector-construct of interest. Small cultures (4-8 ml) or medium size cultures (to 50 ml) of LB were inoculated overnight with a single clone from ligation or retransformation or with a dip of cells from a glycerol stock and incubated at 30 - 37°C. Depending on plasmid copy number 2 - 6 ml (Miniprep) or 25 - 50 ml (Midiprep) of the culture were spun down for 10 min, 4000 g. Plasmids were isolated by utilization of commercial kits from Qiagen®, Novagen or Fermentas as suggested in the instruction. All plasmids were dissolved and stored in pure sterile water.

2.1.4 Polymerase chain reactions (PCR)

All PCRs were performed by standard methods or adapted from instructions given by the polymerase manufacturing company. I used *Kod Hot Start* DNA polymerase for cloning of the gross of HLA-DR1 constructs. *Taq* polymerase was applied in some cases. Standard PCR protocols required volumes of typically 50 - 150 µl. Template DNA was used in concentrations of 0.05 ng/µl from vector stocks or linear fragments. For *Kod Hot Start* polymerase-based PCRs amounts of all other components were used as follows: 2 % of total volume polymerase (1 U/µl), 2.5 mM $MgSO_4$, 2.5 mM dNTPs, and 0.3 µM forward and reverse primer each in sterile water. For *Taq*-based protocols the same components were used except for the enzyme (1 % of reaction volume with 1 U/µl) and 1.5 mM $MgCl_2$ instead of $MgSO_4$.

Colony PCRs were carried out with the *Taq*-based protocol. The template was added in 5 µl of the boiled colony supernatant as the last step.

A typical cycling procedure consisted of 30 s DNA strand denaturation at 94°C, 30 s primer annealing at 50 - 60°C and 1 min/kbp (*Taq*) or 45 s/kbp (*Kod*) polymerase driven elongation at 72°C. Primer annealing temperatures were adjusted to the particular sequence and length

of the DNA oligomers used. Steps were repeated 34 times for cloning and 30 - 32 times for colony-PCRs. An initial denaturation step of two minutes was applied. The last cycle was followed by a terminal 7-minute elongation step.

2.1.5 Gel-electrophoretic separation of DNA

DNA was separated in horizontally running agarose gels. Agarose was used in concentrations of 0.7 % (for vectors) to 1.2 % (w/v) (DNA fragments smaller than 400 bp) re-suspended in 1xTAE with 0.5 µg/ml ethidium bromide. Samples of DNA were loaded after mixing into sample buffer and gels run at a constant voltage of 80 - 200 V over a duration of 15 - 45 min. DNA bands were visualized with UV light irradiation provided by a gel documentation system.

- 50x TAE buffer, pH 8.0:	2 M tris(hydroxymethyl)aminomethane (Tris)
	50 mM ethylenediaminetetraacetic acid (EDTA)
	1 M glacial acetic acid
- 10x DNA sample buffer:	3 mg/ml bromophenol blue
	50 % glycerol
	33.3 mM EDTA, pH 8.0

2.1.6 Extraction of PCR fragments

PCR fragments were purified by gel-extraction for subsequent cloning. The reaction was separated in agarose gels. The gel band of interest - as indicated by the right size - was excised under minimum illumination with UV light. The gel slice was weighted and directly dissolved and processed with the Qiagen® gel-extraction kit according to the manual. The DNA was eluted and stored in sterile water. Concentrations were determined via photometrical measurements (extinction at 260 nm) or by comparison to bands of standard amounts in a DNA gel.

2.1.7 Enzymatic DNA restriction

Digestion of double-stranded DNA in PCR fragments or plasmid DNA was accomplished with nucleases from NEB®. All restriction enzymes were used according to the instructions in the

manual. I used standard enzymes in an exemplary protocol as follows: In a total volume of 60 µl 2.5 µl from a stock of one or two enzymes (simultaneous double digestion) were present. DNA was used in total from gel-extraction of PCR fragments or in 5 - 20 µg scales for cutting of vectors. Reactions were incubated at 37°C for 2 - 5 h and vectors were incubated another 30 min with 1 µl of Calf Intestine Phosphatase (CIP 1 U/µl) to dephosphorylate 3'-ends of the strands and suppress re-ligation. Digested vectors were purified and isolated via gel-extraction as described before. Restricted PCR fragments were purified with the PCR purification kit from Qiagen®.

2.1.8 Ligation of digested vectors and inserts

All ligations were made with purified components and using T4 ligase from NEB® in a total volume of 20 µl. 1 unit of enzyme was used in combination with T4 ligase buffer. I used a three-fold stoichiometric excess of insert with a tendency to higher excess for small inserts (less than 300 bp). The total amounts of DNA were 0.2 - 1.5 µg for the vector DNA and typically 0.1 - 0.4 µg for inserts depending on size.

Ligations were carried out for 12 - 20 hours at 16°C. The ligation reaction was desalted before transformation of *E.coli* strains XL1-blue or BL21Xpress. For this, BioRad® microspin columns were buffer exchanged for water as described in the instruction. The DNA was subjected to the columns followed by centrifugation for 4 min at 1000 x g.

2.1.9 Transformation of ligated constructs

10 - 15 µl of desalted ligation were used to transform *E.coli*. The solution was added to a re-thawed aliquot of cells and transferred to chilled transformation cuvettes from BioRad®. Immediately cuvettes were subjected to the BioRad Gene Pulser X cell™ and electroporation enforced by applying a pulse of 2.5 kV, 200 Ω and 25 µF. Cells were transferred into 1 ml of SOC medium and incubated for one hour at 37°C while shaking. The whole of the reaction was streaked to LB-agar plates supplemented with the antibiotic(s) to select for positively transformed clones. Plates were grown overnight or longer at 37°C.

2.1.10 Determination of positive clones after ligation and transformation

Ligation and subsequent transformation into the *E.coli* strain XL1-blue was testified by colony-PCRs. For that, 4 - 20 clones were picked to be analyzed for the presence of insert.

Single colonies were picked with a tip, dipped onto a replica plate and put into 10 µl of sterile water in a tube. Tubes were boiled for 5 - 10 min and centrifuged 2 min at maximum speed (16000 x g, 4°C). After removing the tip another 5-minute centrifugation step was carried out. Five microliters of the supernatant were pipetted to the prepared master mixes of PCR reactions as described before.

Alternatively, clones from transformation into BL21Xpress were tested for protein expression. For that, single clones were used for inoculation of a 4 - 5 ml culture of LB containing the relevant antibiotic. Cells were grown to an OD_{600} of 0.4 and protein expression induced with addition of 1 mM IPTG for the duration of 1 - 3 h. Aliquots representing 0.075 OD/ml were removed before and after induction, centrifuged (3 min, 16000 x g) and pellets solubilized in 12 µl of 3 x SDS (sodium dodecylsulfate) sample buffer. The reaction was boiled and separated in a 12 - 15 % SDS gel.

Clones yielding a DNA fragment of fitting size or showing significant expression of a correctly-sized protein were used to inoculate a culture of LB for growth overnight to isolate plasmid in a preparative scale for a sequence analysis. Sequences were analyzed by Seqlab GmbH in Göttingen, Germany, and aligned to the expected sequences with the WWW resource ClustalW[84] after optical inspection of the sequencing chromatogram with the software Chromas (www.technelysium.com.au).

2.2 Cloning, expression and refolding of HLA-DR1 subunits

2.2.1 Plasmids, vectors and constructs

All bacterial expressions were carried out with the IPTG inducible T7-polymerase-based pET vector system. HLA-DR1 subunits and their modified-chain-versions were cloned into pET vectors from Novagen (Merck Biosciences, Darmstadt, Germany) as summarized in table 2.1. (HLA-)DRα and (HLA-)DRβ ectodomains were subcloned from pRMHa and pRMHb, respectively, provided by the group of Dr. Olaf Rötzschke and Dr. Kirsten Falk at the MDC Berlin.

Table 2.1: List of expression constructs appearing in this study

construct ID	vector	resistance	restriction sites	remarks
DRα WT	pET 11a	ampicillin	NdeI, BamHI	DRA*01:01 ectodomains including amino acids 1 - 192[1]
DRβ WT	pET 24d	kanamycin	NcoI, XhoI	DRB1*01:01ectodomains including amino acids 1 - 198[1]
DRβ WTsel[3]	pET 11a	ampicillin	XbaI, blunt end via XhoI	DRβ WT from 24d via XbaI and XhoI/BamHI (Klenow filled)[2]
DRβ G86V	pET 24d	kanamycin	NcoI, XhoI	DRβ WT with glycine to valine mutation at position 86
DRβ G86Y	pET 24d	kanamycin	NcoI, XhoI	DRβ WT with glycine to tyrosine mutation at position 86
CLIP106-DRα	pET 11a	ampicillin	NdeI, BamHI	DRα WT with N-terminal Met-$CLIP_{106\text{-}120}$-$(Gly_4Ser)_3$ extension instead of Met1
CLIP106-DRβ	pET 21a	ampicillin	NdeI, XhoI	DRβ WT with N-terminal Met-$CLIP_{106\text{-}120}$-$(Gly_4Ser)_3$ extension instead of Met1

[1]numbers refer to the processed protein form after cleavage of the signal peptide
[2]see subsection of cloning in *Methods*
[3]subcloned version of DRβ WT, transformation into auxotroph strain DL39 required change in resistance marker

2.2.2 Cloning of MHCII subunits

2.2.2.1 Primers

Oligomers for cloning of expression constructs and their variations were synthesized by Eurofins MWG Operon GmbH, Germany. Short primers (< 40 bases) were ordered as salt-free, simply lyophilized oligomers. Primers with higher numbers of bases (up to 80 bases) were requested as HPLC- or SDS gel-purified versions in lowest possible scales including a quality certificate. All primers utilized during this study are listed in table 2.2.

Table 2.2: List of primers appearing in this study

primer	name	remark	sequence 5' - 3'
T7fwd	T7promfwd	binding T7 promoter, forward	TAATACGACTCACTATAGG
T7rev	T7termrev	binding T7 terminator, reverse	GCTAGTTATTGCTCAGCGGT
JS1	JSa1Ndefwd	start of DRα, forward adding NdeI site	GTTCCAGCATATGATCAAAGAAGAACATGTGATCATC
JS2	JSb1Ncofwd	start of DRβ, forward adding NcoI site	ATTACGCCATGGGGGACACCCGACCACG
AS5	ASa2bamrev	end of DRα, reverse adding BamHI site	TGGAACGGATCCTTAGTTCTCTGTAGTCTCTGGGAGAGGGCTTGGAGC
AS6	ASb2xhorev	end of DRβ, reverse adding XhoI site	CGTAATCTCGAGTTACTTGCTCTGTGCAGATTCAGACCGTGCTCTCC
AS7	ASDR1betaGly86Tyrfwd	glycine to tyrosine mutation in DRβ, forward	CACAACTACGGGGTTTACGAGAGCTTCACAGTGCAG
AS8	ASDR1betaGly86Tyrrev	glycine to tyrosine mutation in DRβ, reverse	CTGCACTGTGAAGCTCTCGTAAACCCCGTAGTTGTG
AS19	ASDRbeta86Vfwd	glycine to valine mutation in DRβ, forward	CACAACTACGGGGTTGTGGAGAGCTTCACAGTGCAG
AS20	ASDRbeta86Vrev	glycine to valine mutation in DRβ, reverse	CTGCACTGTGAAGCTCTCCACAACCCCGTAGTTGTG
AS34	1Alphalinkclip106fwd	N-terminal extension of DRα with $(Gly_4Ser)_3$-linker and overlap to $CLIP_{106-120}$, forward	GCAAGCACTCCCCATGGGAGGTGGAGGTTCAGGAGGTGGAGGTTCAGGAGGTGGAGGTTCAATCAAAGAAGAACATGTGATC
AS35	2Alphalinkclip106fwd	extension of products from AS34/36 to full $CLIP_{106-120}$ sequence and NdeI, forward	GTTCCAGCATATGAAGATGCGCATGGCAACACCTCTTCTCATGCAAGCACTCCCCATG-GGAGGTGGAGGTTCA
AS36	Betalinkclip106fwd	N-terminal extension of DRβ with $(Gly_4Ser)_3$-linker and overlap to $CLIP_{106-120}$, forward	GCAAGCACTCCCCATGGGAGGTGGAGGTTCAGGAGGTGGAGGTTCAGGAGGTGGAGGTTCAGGGGACACCCGACCACGTTTC
AS37	DRalphaintfwd	internal binding site in DRα, forward	CGAACAGCCCTGTGGAACTGAGAGAGCCCAACG
AS38	DRalphaintrev	internal binding site in DRα, reverse	CGTTGGGCTCTCTCAGTTCCACAGGGCTGTTCG

2.2.2.2 Cloning procedure for HLA-DR1 subunits and their genetic variations

HLA-DRα and HLA-DRβ expression constructs were chosen to exclusively contain protein ectodomains. Template constructs for the chains DRA*01:01 (DRα) and DRB1*01:01 yielding HLA-DR1 in complex were gifted from the collaborating group of Dr. Olaf Rötzschke and Dr. Kirsten Falk at the MDC Berlin as full length constructs.

Primers for the sub-cloning of HLA-DR1 domains were designed to cover sequences from amino acids 1 - 192 (DRα) and 1 - 198 (DRβ) from the processed forms (see UniProt entries DRA_HUMAN for DRα and 2B11_HUMAN for DRβ), respectively. An additional methionine

was set prior to the sequences being amino acid 0 in the expression constructs as it does not represent the native sequence and might be cleaved off in some cases[85].

DRα wild-type (WT) was amplified using the primers JS1 and AS5 (see table 2.2) thereby adding restriction sites NdeI (N-terminally) - including the start methionine - and BamHI (C-terminally). The purified amplificate was digested with the corresponding enzymes and ligated into vector pET 11a. After transformation into *E.coli* XL1-Blue, clones were tested for successful ligation with colony-PCR using the pair of primers T7promfwd/T7termrev and amplified in 50 ml cultures. DNA was prepped and sent for commercial sequencing with primers T7fwd and T7rev. Positive clones were stored as DNA constructs at -20°C.

DRβ WT was amplified with oligomers JS2 and AS6 yielding an N-terminal NcoI- and C-terminal XhoI-site. NcoI was chosen for incorporating the initial methionine in frame. The target vector was pET 24d and restriction/ligation was analogous to DRα.

The DRβ mutant G86Y was introduced into the wild-type DRβ sequence by PCR mutagenisis using AS7/AS6 and AS8/JS1 primer pairs, respectively. The two fragments were purified and 60 % of them used as stoichiometric templates in an assembly-PCR step with the flanking primers JS1 and AS6. The product was processed as before. For DRβ G86V, in a first step two fragments were amplified with primer pairs AS19/AS6 and AS20/JS1. Both products were inserted into pET 24d.

$CLIP_{106\text{-}120}$-linked DR1 subunits were designed with a 15mer linker comprising a triple motif of ($glycine_4serine$) put in between amino acid 1 of the protein subunit and CLIP amino acid 120. A methionine was put in front of CLIP amino acid 106 giving $CLIP_{106}$-DRα or $CLIP_{106}$-DRβ. $CLIP_{106}$-DRα was cloned by utilizing primers AS34 and AS5 in a first step. This intermediate was purified and used as a template for PCR step 2 with primers AS5 and AS35. The fragment was purified and cloned into vector pET 11a via NdeI and BamHI. The $CLIP_{106}$-DRβ construct was produced by amplification of DRβ WT with primers AS6 and AS36. This intermediate was used as template for a second PCR with oligomers AS6 and AS35. The resulting DNA was ligated with pET 21a after both components had been digested with NdeI and XhoI. All newly designed and produced constructs were sequenced with T7 primers and additionally with primers AS37/38 in case of $CLIP_{106}$-DRα.

2.2.3 Expression

2.2.3.1 Standard media, plates and antibiotics

- LB (Luria Bertani): 25 g/l (10 g tryptone, 10 g sodium chloride, 5 g yeast extract, Sigma Aldrich, MO, USA) in bidest water, autoclaved

- LB-agar plates: 15 g agar (Carl Roth GmbH + Co. KG, Germany) per liter of LB, autoclaved, antibiotics were added before preparation of plates

- Sf900 insect cell medium: Sf900 (Gibco®, Invitrogen, Germany), 1 % Antibiotic-Antimycotic™ (Invitrogen), 5 % heat inactivated fetal calf serum (Biochrom, Germany)

- M9 minimal medium for 1 l:
  100 ml 10xM9
  10 ml trace elements solutions
  1 ml 1 M magnesium sulfate ($MgSO_4$)
  0.3 ml 1 M calcium chloride ($CaCl_2$)
  0.2 - 0.4 % glucose
  1.5 ml thiamine (1 mg/ml)
  1.5 ml biotin (1 mg/ml)
  0.5 - 1 g ammonium chloride (NH_4Cl)
  1 ml of 1000x kanamycin/ampillicin
  ad 1 l H_2O, D_2O

- Trace elements solution for 500 ml:
  2.5 g EDTA
  0.25 g iron sulfate ($FeSO_4$)
  0.025 g zinc chloride ($ZnCl_2$)
  0.005 g copper sulfate ($CuSO_4$)
  ad 500 ml H_2O, pH 7.6

- 10x stock M9 solution for 1 l:	80 g disodium hydrogen phosphate (Na_2HPO_4)
	20 g potassium dihydrogen phosphate (KH_2PO_4)
	5 g sodium chloride (NaCl)
- Antibiotics as 1000x stocks:	kanamycin 35 mg/ml
	ampicillin 100 mg/ml

Anorganic salts were purchased from one of the companies: Carl Roth GmbH + Co. KG; Germany, Merck Biosciences, Germany; Sigma Aldrich, MO, USA or AppliChem GmbH, Germany. Antibiotics were obtained from Carl Roth GmbH + Co. KG, Germany. Organic solvents and acetic acid were provided by in-house supply. The enzymes Lysozyme and DnaseI were from AppliChem GmbH, Germany and Roche Diagnostics Deutschland GmbH, respectively.

2.2.3.2 Chromatography columns and purification systems

- MonoQ HR 10/10 (GE Healthcare, USA)
- Superdex 200 10/300 (GE Healthcare, USA)
- Superdex 200 PC (Pharmacia, Sweden)
- Home-built anti-FLAG sepharose column (murine monoclonal antibody clone M2, Sigma Aldrich, MO, USA)
- in-house coupled LB3.1 agarose/sepharose column (murine monoclonal antibody LB3.1 provided from hybridoma cultured at the MDC Berlin, preactivated agarose resin obtained from Novagen Merck Biosciences)
- ÄKTA purifier (Year 2002, GE Healthcare, actuated by software Unicorn 5.11)
- ÄKTA FPLC (Year 2007, GE Healthcare, actuated by software Unicorn 5.11)
- Pharmacia SMART micro-purification system (Pharmacia, Sweden, run by software SMART manager)
- 4-channel peristaltic tubing pump (Ismatec, IDEX Health & Science GmbH, Germany)

2.2.3.3 Expression of HLA-DR1 subunits

The protocol for production of functional HLA-DR1 wild-type and derivatives from bacterial expression and refolding was based on a previously published study by Stern and

colleagues[85]. In all cases extracellular DRα and DRβ chains of the human MHCII HLA-DR1 were expressed separately in T7-based expression vectors.

After re-transformation of vectors (typically 10 - 100 ng from a stock in water given to a re-thawed aliquot of cells) into the electrocompetent bacterial strains BL21 (DE3) or DL39 (DE3) cells were gently shaken for one hour at 37°C in SOC or LB media. Afterwards a small aliquot was transferred onto an agar plate with the corresponding antibiotic to select for positively transformed cells over night at 37°C.

For standard protein production yielding unlabeled or solely ^{15}N-labeled subunits a single clone was picked to inoculate a starting culture of LB (25 - 50 ml including the relevant antibiotic) for either several hours or overnight at 37°C. From that an expression culture of 0.5 – 2 l was inoculated by diluting the starting culture to an OD_{600} of maximum 0.01 in LB (unlabeled) or M9-medium for nitrogen labeling. Cells were grown under antibiotic restriction to an OD_{600} of 0.6 - 0.9 before induction of protein expression with 1 mM IPTG (Carl Roth GmbH). Expression was carried out for times of 4 hours (unlabeled protein) at 37°C to overnight-periods at 30°C for nitrogen-labeling. For better yields cells were given an additional aliquot of antibiotics before induction.

2.2.3.4 Expression of selective amino acid labeled HLA-DR1 subunits

For expressing proteins with selectively ^{15}N-labeled amino acids I used M9-based media supplemented with all amino acids. The particular amounts were i) rooted by suggestions from literature[86] and ii) calculated from the average abundance in *E.coli*. The relative amounts were downscaled to the assumed need of 2 g NH_4Cl for growth overnight. This corresponds to approximately 0.5 g of total elementary nitrogen. The contribution of nitrogen to the total mass in each amino acid was used to define mass values which yield the input given in table 2.3. All amino acids were added to the medium in an undissolved form. Media were shaken for 30 min to achieve complete dissolving before proceeding with cell growth.

The labeling of phenylalanine, leucine and valine was achieved via the transaminases-depleted DL39 strain, which simply required addition of any amino acid for growth. I added the relevant amino acids of interest in a labeled form from the very beginning. No scrambling of isotopes was expected due to the auxotrophy. Proteins were expressed overnight at 30°C. In the case of glycine I exclusively used a high excess of water-dissolved

^{15}N-labeled glycine shortly before induction. By that isotope dilution and scrambling were supposed to be kept in an appropriate balance. For reasons of minimized cross labeling, protein expression was carried for 6 hours at 37°C.

Table 2.3: Input amounts of individual amino acids for selective labeling

amino acid	amount used for 2 litres of expression culture in g
alanine	0.5
cysteine	0.1
aspartic acid	0.6
glutamic acid	0.2
phenylalanine	0.2
glycine	0.25
histidine	0.1
isoleucine	0.2
lysine	0.4
leucine	0.35
methionine	0.1
asparagine	0.7
proline	0.25
glutamine	0.4
arginine	0.5
serine	0.4
threonine	1.5
valine	0.3
tryptophan	0.1
tyrosine	0.2

All amino acids in unlabeled form were bought from Sigma Aldrich, MO, USA, Carl Roth GmbH + Co. KG or Roche Diagnostics Deutschland GmbH.

2.2.3.5 Deuteration of HLA-DR1 subunits

To achieve deuteration cells were grown on M9 that contained 1 mg/ml ^{15}N-ND_4Cl, 2 mg/ml ^{13}C-D_7-glucose and > 99.8 % of D_2O for expression of the chain designated for assignment. To minimize spin diffusion the invisible subunit was raised in M9 supplemented with 1 mg/ml ^{14}N-ND_4Cl, 2 mg/ml ^{12}C-D_7-glucose and > 99.8 % of D_2O. Cell growth was adapted to severed conditions in steps of low-glucose-M9 (50 ml), 50 % D_2O (300 ml, starting at OD_{600} of 0.2), and finally fully deuterated medium (2 l, starting at OD_{600} 0.2 - 0.4). Each step required growth overnight at 37°C. All M9 components were D_2O-washed before use or used as additives devoid of crystal water, kept in an evacuated atmosphere. Trace elements were

deuterated by double lyophilizing an equivalent volume of protonated solution followed by re-dissolving in D_2O. Ammonium chloride was dissolved in D_2O, lyophilized and dissolved in D_2O again. M9 stock was generated based on water-free salts obtained from Sigma™ with additional sterile filtering instead of autoclaving. Culture flasks were dried from residual water under sterile conditions. All stock components that were necessary (IPTG, antibiotics, vitamins, DTT) have been used in protonated form, but as stock solutions in D_2O.

Cells obtained from the half-deuterated, medium-size-cultures were washed with the fully deuterated medium before the last step of adaptation. Typical yields from these expressions were about 50 % of the standard amounts in single labeling.

Partial deuteration of subunits was achieved by growing cells on M9 as before but dissolving any of the components in D_2O instead of water. A medium size pre-expression-culture with 50 % D_2O to was implemented to adopt cells. Partial deuteration was insufficient for triple-resonance NMR but remarkably helpful for the acquisition of 3D-NOESYs.

2.2.4 Purification of *inclusion bodies*

- Buffer F1:
  - 25 % sucrose
  - 20 mM Tris pH 8.0
  - 15 mM sodium azide (NaN_3)
  - 0.5 mM EDTA
  - 10 mM dithiothreitol (DTT)

- Buffer F2:
  - 50 mM Tris pH 7.5
  - 1 % (w/v) sodiumdeoxycholate
  - 1 % (w/v) TritonX-100
  - 15 mM NaN_3
  - 100 mM sodium chloride (NaCl)
  - 0.5 mM magnesium chloride (MgCl2)
  - 10 mM DTT
  - 0.3 mg/ml lysozyme
  - 20 µg/ml DnaseI

- Buffer F3:	50 mM Tris, pH 8.0 100 mM NaCl 0.5 % TritonX-100 0.5 mM EDTA 15 mM NaN3 10 mM DTT
- Buffer F4:	as buffer F3, without TritonX-100
- Buffer F5:	20 mM Tris, pH 8.5 8 M urea 0.5 mM EDTA 10 mM DTT
- MonoQ running buffer A:	20 mM Tris, pH 8.0 or 9.0 8 M urea 2 mM DTT degassed and sterile filtrated
- MonoQ running buffer B:	as buffer A, complemented by 1 M NaCl

After expression individual chains were present as *inclusion bodies* which were isolated and prepared using a multistep-detergent-based protocol[87]. Cells were harvested by centrifugation (20 min, 4000 x g) and either stored at -80°C or preferably processed subsequently. Pellets were re-suspended in buffer F1 in a volume of 100 ml per liter of growth culture and transferred to an autoclaved Schott bottle. The homogeneous cell suspension was mixed with 2.5-fold volume of buffer F2 and stirred for 15 min until the cell suspension gained viscosity. At this point 0.5 mM $MgCl_2$ and 20 µg/ml DnaseI were added to the suspension and the mixture was stirred for another 15 min. Cells were frozen to -20 or -80°C in the bottle for at least one night.

The bottle was thawed at room temperature. The content was transferred to centrifuge beakers and spun for 30 min at 4°C and 15000 x g. Immediately, the supernatant was

discarded yielding the crude *inclusion bodies* (IBs). IBs were transferred to a 50 ml falcon tube by suspending them in 40 ml of buffer F3. The mixture was 3 - 4 times sonicated to powder IBs followed by 15 min of centrifugation at 4°C, 15000 x g and re-suspension in F3. Finally, one step of sonification with buffer F4 was performed to get rid of excess detergent.

The pellet was re-solubilized in buffer F5 (25 ml per liter of culture) by rotation for 2 - 12 hours at 8°C. The solution was centrifuged for 30 min at 12°C and 50000 x g and the supernatant transferred to a new tube after passing it through a 0.5 µM sterile filter. The protein solution was snap-frozen and stock-stored at -80°C or directly subjected to the ion exchange column.

The solubilized subunits were purified under denaturing conditions in 8 M urea, 20 mM Tris and 1 mM DTT (buffer A) at pH 8 (DRα and derivatives) or pH 9 (DRβ and derivatives) via an anion exchange column (MonoQ, HR 10/10) using the ÄKTA-FPLC system. Proteins were loaded to the pre-equilibrated (10 volumes of running buffer A) column with a flow of 1 - 2 ml/minute and a maximum pressure of 3 MPa by connecting a 10 or 20 ml Superloop. After restoring equilibrated conditions proteins were eluted by gradually mixing in running buffer B (1 M NaCl in buffer A) with a flow of 1.5 ml/min.

DRα was eluted in a linear gradient ranging from 0 to 50 % B over 10 volumes of column (70 ml). DRβ was re-collected in a non-linear gradient of buffer B. Best results were obtained with a maximum loading of 100 mg and stepwise elution as follows: 0 - 10 % buffer B over 25 ml, 10 - 20 % over 30 - 35 ml, 35 % over 15 - 20 ml and 50 % until drop of absorption beneath 0.4 AU_{280}. All fractions were collected in 2 ml steps and aliquots of 2 - 5 µl were tested for protein existence and purity on 12 – 15 % SDS gels. Fractions were pooled, concentrations determined photometrically and the protein frozen to -80°C in aliquots after adding 0.5 mM EDTA.

The detergents sodium dodecylsulfate, sodium deoxycholate and TritonX-100, urea, dithiothreitol DTT, sucrose and Tris were acquired from Carl Roth GmbH + Co. KG, Germany. Ethylenediaminetetraacetic acid (EDTA) was purchased from Sigma Aldrich, MO, USA.

2.2.5 Refolding of HLA-DR1 from solubilized *inclusion bodies*

For obtaining native heterodimeric HLA-DR1 both subunit chains were refolded in a 1:1 stoichiometry with or without 5 - 10-fold stoichiometric peptide excess by rapid dilution.

Other than in previous studies the protein was diluted to a concentration of 10 µg/ml for each subunit into 20 mM Tris, 25 % Glycerol, 0.5 mM EDTA, 3 mM GSH (reduced glutathione) and 0.3 mM GSSG (oxidized glutathione), pH 8.5. Typical refolding volumes were in the range of 1 - 15 liters. The refolding buffer had been prepared the day before and deoxygenized by bubbling gaseous nitrogen into the stirring solution. The glutathione (GSH/GSSG) redox system and potential peptides had been given to the buffer prior to refolding.

The dilution was carried out in 8 - 16 steps with a 30 - 60 minute period of gentle constant stirring in between. After minimum 72 hours proteins were concentrated with a Vivaflow ultrafiltration system at 4°C to ~1/30 of the refolding volume by continuous circular flow of 50 - 200 ml/minute dissecting the filtrate devoid of protein. The concentrated protein solution was filtrated into an autoclaved Schott bottle on ice, dialyzed to PBS at pH 7.4 overnight, filtered again and immuno-affinity-purified on an antibody-column carrying LB3.1 antibody immobilized to agarose or sepharose. The protein solution was repetitively run over the matrix in a half-automatic way, followed by washing with several column volumes (3 - 7 ml) of 10 mM phosphate buffer, pH 7.0. Elution was achieved with ~4 ml of 50 mM CAPS (pH 11.5) per ml of column volume directly into prepared 250 mM phosphate-buffer, pH 6.2 for neutralization (approx. 1/5 of total elution volume). These steps were repeated until no mentionable fraction was eluted anymore. Columns were neutralized with 10 mM phosphate buffer, pH 7.0 after each round and stored in PBS, 0.02 % sodium azide.

The preparation was applied to a superdex-200 column (Pharmacia) for buffer exchange in preparation of crystallography or dialyzed to the conditions required for NMR studies. In all other cases proteins were dialyzed to PBS pH 7.4 and stored with azide at 4°C. Typically, the fraction of successfully refolded protein was between 1 and 5 % of the total input protein.

- Refolding buffer:	20 mM Tris, pH 8.5
	25 % glycerol
	0.5 mM EDTA
	2 mM NaN_3
	0.3 mM oxidized glutathione (GSSG)
	3 mM reduced glutathione (GSH)
	+/- peptides 4 - 8 mg/l
	Degassed and/or rinsed with N_2 before use

- 1x PBS:	140 mM NaCl
	2.7 mM potassium chloride (KCl)
	10 mM Na_2HPO_4
	1.8 mM KH_2PO_4, pH 7.4 or 5.8

All chemicals were purchased from Carl Roth GmbH, Germany or Sigma Aldrich, USA.

2.2.6 Immobilization of LB3.1

Monoclonal mouse antibody LB3.1 was obtained from the group of Dr. Olaf Rötzschke/Dr. Kirsten Falk (MDC Berlin and IMMUNOS, Singapore). It was kindly provided by Maria Hofstätter, produced in hybridoma cells and extracted from the supernatant. The antibody was isolated with ProteinG-coupled sepharose and could be produced in high mg-amounts. Immobilization was carried out on PreAct agarose or sepharose resin from Novagen as suggested by the manufacturer. Incomplete coupling was compensated with incubation in Tris buffer to saturate any free aldehyde group. Coupling was 70 - 80 % efficient and columns were set up in volumes of 3 - 10 ml with an approximate capacity for HLA-DR1 of 0.5 - 1 mg/ml resin when freshly prepared. Columns were stored in PBS pH 7.4 supplemented with 0.02 % sodium azide. Typically, columns were set up *de novo* once a year.

2.3 Assessment of protein quality after refolding

2.3.1 SDS-stable dimers as indicator of MHC-peptide complexes

All preparations were tested for protein quality by optical inspection in SDS gels. Empty proteins were quality-assessed by rapid peptide binding offering a simple evaluation method by formation of characteristic SDS-resistant dimers[85]. For this, 0.5 - 5 µg of DR1 was incubated with a 10 - 100-fold excess of affine peptides (usually $HA_{306-318}$ or $CLIP_{106-120}$) for 2 - 18 hours at 37°C. The sample was shortly centrifuged at 15000 x g and the supernatant mixed with SDS sample buffer. The sample was then loaded onto 12 - 15 % SDS gels without prior boiling. Gels were stained with Coomassie and agitated in destainer to visualize bands.

- SDS running buffer, pH 8.6:	25 mM Tris
	200 mM glycine
	1 g/l SDS
- 5x SDS sample buffer:	156 mM Tris-HCl, pH 6.8
	62.5 % glycerol
	5 % SDS
	0.025 % bromophenol blue
	+/- 250 mM DTT
- Coomassie staining solution:	50 % (v/v) methanol
	10 % (v/v) acetic acid
	0.25 % (w/v) Coomassie Brilliant Blue R250
- SDS gel destaining solution:	30 % (v/v) methanol
	10 % (v/v) acetic acid

2.3.2 Analytical gel-filtration

Analytical or semi-analytical gel-filtrations on a Superdex200 were performed to verify the presence of monomodal heterodimeric populations. Analytical gel-filtrations on HLA-DR1 were performed in neutral (pH 7.4) or acidic (pH 5.8) PBS on a Superdex200 PC column (2.4 ml column volume run with a Biorad system) with a total of 25 - 50 µl from a 0.2 - 0.5 mg/ml solution. The flow rate was 0.04 ml/min and fractions were collected for further characterization in silver-stained SDS gels if necessary.

Half-analytical gel-filtrations were performed on a Superdex200 with a column volume of 24 ml connected to an ÄKTA-purifier. Samples were injected in a volume of 500 µl with a minimum concentration of 0.5 mg/ml at a flow of 0.5 ml/min.

2.3.3 Determination of particle size with Dynamic Light Scattering (DLS)

To ensure a homogeneous sample state for subsequent experiments dynamic light scattering was applied. The particle size is a measure of the oligomerization state of the sample and was determined for unloaded or peptide-loaded HLA-DR1 assuming a roughly globular shape

of MHCII. All samples were measured at 1 - 15 µM in a volume of 20 µl at room temperature on a Zeta Nanosizer ZS (Malvern, UK) using a low volume glass cuvette. Empty HLA-DR1 was measured directly after gel-filtration. Each result represented the average of ten repetitive runs of one minute duration to receive an internally averaged value for the masses. Derived complex masses were recalculated from the peak maximum for the main fraction using the internal calibration by the Zeta Nanosizer software (Malvern, UK). The recalculation from scattered light is based on the Stokes-Einstein relationship[88].

2.3.4 Peptide loading ELISA

ELISA studies were carried out by Shashank Gupta and Sebastian Günther at the MDC Berlin and the procedure is in detail described in reference[41]. Briefly, the peptide binding was read out by the detection of biotin synthesized to the peptide. Biotin was probed with europium labeled streptavidin. Eu^{3+} in support of an enhancer solution was excited at 340 nm showing fluorescence at 614 nm. The method was also used to indirectly determine binding of unlabeled peptide (Cage-HA) in competition with biotinylated HA (competition ELISA). Therefore a stable concentration of biotinylated HA was premixed with a growing concentration of Cage-HA. Each mixture was subjected to empty HLA-DR1 and the reaction carried out as before. By using unlabeled HA as a reference with known affinity to HLA-DR1 the apparent affinity for Cage-HA was estimated.

2.4 Purification of HLA-DM

Expression of FLAG-tagged HLA-DM under the influence of a copper-inducible promotor was performed in stably transfected Drosophila Schneider (S2) cells as described before[83]. These cells were kindly gifted by the group of Dr. Olaf Rötzschke and Dr. Kirsten Falk at the MDC Berlin. Cells were thawed in 6-well plates placing approx. 10^7 cells into 2 ml of Sf900 medium (supplemented with 1 % Antibiotic-Antimycotic and 5 % heat FCS) and incubated at 27°C. The medium was exchanged once after 6 - 12 hours to rinse off residual DMSO from the freezing solution. For conditioning the adhesive cells were expanded in larger T-flasks maintaining their density higher than 3 x 10^6/ml. After two weeks cells were transferred to a 250 ml Spinner flask in a volume of maximum 50 ml. This served as a permanent stock.

From the stock expression cultures with a density of 4 × 10^6/ml were set up either in 2 l - Schott flasks or 1 l - Spinner flasks to a maximal volume of ¼ of the bottle. After 2 - 3 hours

expression was induced with 1 mM cupric sulfate and cells were grown for five days at 27°C under gentle stirring (75 rpm for Spinner flasks) or shaking (65 rpm for Schott bottles). Culture supernatants were collected by centrifugation and filtrated by passing through a bottle top filter. Sterile filtrates were loaded onto anti-Flag–coupled sepharose repetitively followed by washing the columns with PBS pH 7.4. Elution was achieved with either 0.15 mg/ml Flag peptide or using 100 mM glycine (pH 3.0, Carl Roth GmbH) with immediate neutralization by 1 M Tris, pH 8.5 (corresponding to a 20-fold stock). The chromatographic steps were carried out in a half-automatic way using a peristaltic pump and self-packed columns from batch material. The protein elute was subsequently buffer exchanged to the required conditions by dialysis or gel-filtration (Superdex 200; GE Healthcare), its concentration was determined photometrically and aliquots were stored at 4°C after adding sodium azide to a final concentration of 0.02 %.

2.5 Nuclear magnetic resonance (NMR)

2.5.1 NMR accessories

NMR samples were transferred to and measured in 5 mm/4.2 mm (outer/inner diameter) 7-inch tubes optimized for 500 MHz produced by Norell™, NJ, USA. D_2O for protein labeling and as sample additive during measurements was obtained from Eurisotop™, France or Deutero GmbH, Germany, in a purity of more than 99.8 % for labeling and >99.9 % for sample additive. ^{15}N-ammoniumchloride and all types of labeled glucose were purchased from Eurisotop™, France. Single ^{15}N-labelled amino acids were ordered from Cambridge Isotope Laboratories Inc., MA, USA or Campro Scientific GmbH, Germany, with an isotope purity >98 %.

pH measurements of small volumes as NMR samples or peptide stocks for NMR designated loading of HLA-DR1 were performed with pH-meters and electrodes (type U402-M3-S7/200) from Mettler Toledo GmbH, Germany.

2.5.2 NMR spectrometers

All NMR spectrometers used in this study were 52 - 54 mm bore Bruker® originated machines of 600, 700, 750 or 900 MHz maximum (proton-based) frequency. With exception of the DRX600 machine all of them (Avance machines) were equipped with 5 mm triple-

resonance-cryoprobes of types TXI or TCI providing xyz- or z-gradients. The DRX600 was equipped with a non-cryogenic triple-resonance probe with z-gradient. Connected hardware was equipped with four detection channels (^{1}H, ^{2}H, ^{13}C, and ^{15}N) and 4 - 5 amplifiers. Actuating software XWIN-NMR and Topspin 2.1 was provided by Bruker® and run on Linux systems.

2.5.3 Acquisition of one- and multidimensional high field NMR spectra

Samples were prepared in neutral (pH 7.4) or acidic (pH 5.8) PBS, supplemented with 0.02 % sodium azide if designated for longer recordings at 37°C. 10 % of D_2O were added prior to measurement.

As all spectra were recorded with Bruker® NMR machines any abbreviation for commands, pulses, power levels etc. is referring to the Bruker® internal encryption. All pulse sequences were run from templates provided by the in-house NMR facilities, in parts modified or adapted. These sequences were set up by Monika Beerbaum and Dr. Peter Schmieder from the FMP Berlin. Individual setup of NMR experiments required the loading of latest standard pulse values for the nuclei ^{1}H, ^{13}C, ^{15}N and ^{2}H, for gradients and the current exact external magnetic field frequency (prosol).

After insertion into the probe head of the machine samples were locked, temperature equilibrated and tuned/matched (wobbled) for optimum resonance conditions of the receiver coils/channels for all measured nuclei with pre-written pulse programs.

Samples were shimmed for homogenization of the applied field either via gradient shimming (gradshim or topshim) in an iterative way. Additional manual shimming was applied for x and y for three-dimensional experiments.

One-dimensional ^{1}H-spectra were recorded in a water-presaturation mode for the optimization of proton excitation pulse (P1) length and power (PL1). The residual resonant water was used to determine the exact spectral proton offset (O1) by minimizing the signal integral. Spectral width (SW) was set to 12 - 16 ppm to cover the complete range of proteinogenic proton chemical shifts. P1, PL1 and O1 were found to be different in optimum in dependence of the machine used.

Proton and ^{1}H-^{15}N correlation spectra were recorded with a pulse program comprising a double watergate sequence to suppress water resonances by gradient mediated dephasing[89]. For maximum resolution dispersion in signal intensities the receiver gain value

was determined prior to acquisition by the actuating software. The resolution of proton spectra was defined by the directly detected complex data points given by *td* (time domain) which in most cases was set to 8192 or 16384.

For any two- or three-dimensional spectra with indirect detection of the heteronucleus (X) – namely ^{13}C and ^{15}N- via protons (^{1}H) the O1, P1 and PL1 were copied from the corresponding watergate proton spectrum.

Spectral resolution of heteronuclei ^{13}C and ^{15}N was determined by the number of indirectly measured data points. In ^{1}H-^{15}N-HSQC (Heteronuclear single quantum correlation) spectra to visualize protein amides values were set to 96 - 128, in rare cases 256 or more for ^{15}N. When implementing a third domain either for triple resonance spectra (^{13}C) or ^{15}N-filtered NOESY (NOESY-HSQC) spectra both indirect domains were recorded with 80 - 128 data points. The direct ^{1}H-dimension was acquired with 1024 points in multi-dimensional experiments. Increments were around 280 µsec for nitrogen, 85 µsec for the second proton and 170 µsec for alpha-carbons or 340 µsec for carbonyls. The number of scans reached from 4 for HSQCs of highly concentrated samples to more than 200 in case of low (< 100 µM) concentrations or for spectra with desired high signal-to-noise like PRE experiments. Comparison of HSQC and TROSY-HSQC spectra was achieved from recording 800 indirect points with 32 scans, respectively. Three-dimensional spectra were recorded using 16 - 36 scans.

All triple resonance experiments used for assigning HLA-DR1 subunit backbones were TROSY-connected. For TROSY (transverse relaxation optimized spectroscopy)-HSQCs and TROSY-based triple resonance spectra settings and procedures were as for standard HSQCs. ^{1}H-^{15}N coupling based transfer time (INEPT) was set to 5.4 ms in HSQC sequences. Broadband decoupling was applied to all indirect dimensions and to ^{2}H in TROSY-based 3D sequences with crush-pulses designed in-house.

After initial tests on temperatures all spectra with HLA-DR1 were measured at room temperature or 37°C as later on optimized for better signal-to-noise and resolution.

2.5.4 Spectral processing of high field NMR spectroscopic data

Processing of recorded NMR raw data was performed with the Topspin 2.1 or XWIN-NMR software packages provided by Bruker®.

Before Fourier transformation all dimensions were multiplied with the weighting function QSINE. A gain of resolution could be achieved by using a sine bell shift (SSB) of 4 in the direct

and 3 in all indirect dimensions. All indirect dimensions were linearly predicted to a maximum of twice the recorded data points. For nitrogen a complex linear prediction forward with a coefficient set to 16 was chosen. Carbon-13 was back-predicted to additional 2 preceding complex points at a coefficient of 16. The first FID was weighted with 1 for nitrogen points and 0.5 for direct and carbon points. Baselines were corrected automatically. NOESY-HSQC projections were processed from 3D spectra of protonated or deuterated samples with 112 x 128 and 100 x 102 indirect proton/nitrogen points, respectively. 256 nitrogen points were generated from FT whereof the central 245 were used for projection.
All spectra were phase corrected, if necessary, in each dimension. To compare spectra that had been recorded with different machines, they were referenced to each other with known and defined chemical shifts.

2.5.5 Plotting of spectra

Processed spectra were plotted to graphically improved images with the software SPARKY (T.D.Goddard and D.G.Kneller, 2002, University of California, San Francisco, USA) for optical reasons. Data analysis concerning chemical shift perturbations, signal intensities or assignment of resonances was performed with the CCPNMR analysis software package[90]. In few cases direct graphical export was performed from here.

2.6 Assignments of HLA-DR1 subunits

Initial residue types were obtained from selective labeling of the full protein in complex with $HA_{306\text{-}318}$ with ^{15}N-labeled glycine, valine, phenylalanine or leucine and recording HSQC spectra at concentrations of 50 - 100 µM at neutral pH and room temperature. Based on that DRβ backbone resonances of HLA-DR1/HA were assigned using ^{2}H-^{13}C-^{15}N-labeled DRβ in complex with ^{2}H-labeled DRα. I started from a 125 µM-sample which was very stable over time, recording the following spectra at 290 K and at neutral pH: HNCA, HNcoCA, HNCO, HNcaCO, HNCACB, HNcoCACB, and a ^{15}N-filtered NOESY. Assignments for HLA-DR1/HA could subsequently be transferred to the conditions used for HLA-DR1/CLIP complexes.
For HLA-DR1/$CLIP_{106–120}$ and $CLIP_{102–120}$ β-chain assignments, samples were measured at pH 5.8 and concentrations of 360 µM and 280 µM, respectively. For $CLIP_{102–120}$ HNCA, HNcoCa, HNCO, and HNcaCO and ^{15}N-filtered NOESY spectra were recorded at 310 K. For HLA-

DR1/CLIP$_{106–120}$ I recorded HNCA and HNcoCA spectra at 310 K yielding approximately 80 % assignments of the flipped orientation, whereas the spectra for the canonical orientation were almost identical to those of HLA-DR1/CLIP$_{102–120}$. The latter assignment was transferred to HLA-DR1/TEMPO-CLIP$_{106–120}$. Missing HLA-DR1/CLIP β-chain assignments were caused either by proline residues or the few cases of spectral overlap. The region of β102 - 115 could not be assigned unambiguously, presumably owing to line-broadening of these resonances.

Assignments of triple-labeled DRα were achieved in complex with deuterated β-chain and the help of HNCA/HNcoCA and HNCO/HNcaCO for both HLA-DR1/HA and /CLIP$_{102-120}$ at 310 K in PBS pH 5.8 at concentrations of 280 and 330 µM, respectively. For the HA-complexed sample a ^{15}N-filtered NOESY was recorded, too. Selective amino acid labeling was used for initial resonance filtering as for the β-chain. Assignment was successful at a level of approximately 85 % for CLIP$_{102-120}$ and almost 90 % for HA showing some gaps in loop regions. No individual assignment has been made for the flipped version of CLIP$_{106-120}$ or the flipped fraction of CLIP$_{102-120}$ although parts of the canonical assignments could be transferred by means of optical estimation.

Spectra were launched in the CCPNMR analysis software package[90] and sequential assignments of resonances performed by semiautomatic resonance search and manual linkage of pre-assigned stretches as described exemplarily in the *Results* chapter (see paragraph 3.3.2.3). All assignments are listed in table 3.2. Chemical shifts will be deposited online in the near future. Major parts of the theoretical assignment have been contributed by Dr. Jana Sticht, FMP Berlin.

2.7 NMR experiments and data analysis

2.7.1 Procedure of peptide loading and exchange monitored by NMR

To monitor exchange of HLA-DR1/CLIP to HA ^{1}H-^{15}N-HSQCs from HLA-DR1/CLIP were measured and samples were peptide exchanged with 0.5-fold to 20-fold HA peptide in presence of the dipeptidic MLE FR (50- to 100-fold). To follow sequential exchange identical spectra were measured repetitively in a row with constant conditions as for the untreated reference. A control with exclusive addition of FR was included allowing for unambiguous identification of FR-related peaks from natural abundance.

Peptide loading was observed starting from a sample containing subunit labeled empty HLA-DR1. Afterwards peptide was added in excess (as denoted in particular experiments) in presence of 100-fold MLE or stoichiometric HLA-DM and spectra were recorded at different time points with identical settings. Control spectra with FR or HLA-DM alone were recorded for potential unspecific appearance of new peaks. *A posteriori* loading of peptides $CLIP_{106-120}$, $CLIP_{102-120}$ and peptides I-XII was performed overnight with 5 - 20-fold excess over HLA-DR1 in presence of 100-fold FR or stoichiometric HLA-DM. Samples were centrifuged 5 min at 15000 x g and 4°C before subjecting them to NMR tubes. HLA-DR1, *a posteriori* loaded with TEMPO-$CLIP_{106-120}$, was gel-filtrated on a semi-analytical Superdex200 column to get rid of excess spin label. Here, the control sample of HLA-DR1/$CLIP_{106-120}$ was treated identically.
In all cases peptides and HLA-DM were NMR-invisible.

2.7.2 Measurement of chemical shifts and intensity changes

All chemical shift differences were calculated using the formula $\Delta\delta = (6(\delta H)^2 + (\delta N)^2)^{0.5}$. The usage of peak heights presupposed the adjustment and correction of Bruker® internal signal intensity scaling via the *nc_proc* command. Relaxation enhancement in the TEMPO-$CLIP_{106-120}$ experiments was measured by determining the ratio of peak heights to equally recorded wild-type $CLIP_{106-120}$ corrected for deviations based on minimal concentration differences. All epitope mappings were made for residues showing significant chemical shift perturbation or from large changes in intensity ratios. Significance was defined as a value above (chemical shift) or below (relaxation) the mean value ± standard deviation. Mappings were graphically visualized on crystal structures enabled by the Program PyMOL (De Lano Scientific). Determination of inversion rates for $CLIP_{106-120}$ from canonical to flipped alignment was done from measuring intensity decrease at the time points 155, 466, 777, 1088, 1399, 1710, 2021, 2332, 2643, 2954, 3265, 3576 and 17435 min after starting acquisition of ^{1}H-^{15}N-HSQC spectra with ^{15}N-labeled DRβ each in a resolution of 1024 x 110 point and 124 scans. Sample concentration was 100 µM. Intensities of peaks were normalized for residues given in paragraph 3.4.2.3 and plotted to time points. Curves were fit to the equation for single-exponential decay expressed by the formula $I(t) = I_0+I(0)e^{-Rt}$ where I(t) is the intensity at time point t, I_0 is residual intensity, I(0) is starting intensity (1) and R is the decay rate. The decay rate R was then converted to half-life values $T_{1/2}$ with the mathematical relation $T_{1/2} = \ln 2R$. Errors based on fitting were added to the plot. All coefficients of determination (1 - RMSD)

were clearly bigger than 0.9 indicating consistence. Secondary Cα-chemical shifts for the validation of secondary structure elements were obtained as described in reference[114].

2.7.3 Hydrogen-to-deuteron exchange (H/D experiments)

All H/D experiments were performed by maintaining buffer conditions of PBS pH 5.8. Samples of HLA-DR1 co-refolded with either $HA_{306-318}$ or $CLIP_{106-120}$ were lyophilized in protonated states by snap-freezing inside the NMR tube and overnight vacuum-freeze-drying using a Christ® double chamber system (Martin Christ GmbH, Osterode, Germany). The tube was placed inside an accessory-glass beaker equipped with cellulose filter membranes and no NMR tube lid. Lyophilized samples were stored at -20°C with sealing.

Sample powders were re-dissolved in 550 µl of pure D_2O and immediately subjected to NMR measurements with pre-adjusted settings to minimize dead time of the experiments. For semi-quantitative rate determination of HLA-DR1/$CLIP_{106-120}$ the sample was measured in repetitive ^{1}H-^{15}N-HSQC spectra with 96 indirect points and 16 scans yielding ~35 min of acquisition per time point. All spectra were processed identically and analysis of intensities carried out as described in the previous paragraph. The assignment of DRβ in complex with inverted short $CLIP_{106-120}$ was applied here.

2.8 Cage-HA and xenon-129-NMR studies

2.8.1 MR machine

All measurements with hyperpolarized ^{129}Xe were performed on a whole-body MR-imager (Bruker MedSpec 30/100) located at the Physikalisch-Technische Bundesanstalt (PTB) in Berlin with a field strength of 2.94 T using a home built double resonant ^{1}H- ^{129}Xe- transmit-receive-3-turn solenoid coil with an inner diameter of 18 mm and a length of 30 mm. The imager was administered by a console connected to a Linux system housing XWIN-NMR for acquisition and processing. All measurements were performed by or under supervision of Dr. Lorenz Mitschang and Dr. Wolfgang Kilian (PTB Berlin).

2.8.2 Preparation of hyperpolarized ^{129}Xe and ^{129}Xe NMR-spectroscopy

Generation of hyperpolarized ^{129}Xe was performed by Dr. Wolfgang Kilian at the Physikalisch-Technische Bundesanstalt (PTB) in Berlin. In detail the procedure is described in

reference[91]. All samples had volumes of 2 ml containing either solvent (PBS pH 7.4, water or organic solvents) alone, Cage-HA, HLA-DR1/Cage-HA (in PBS pH 7.4) or both species combined in concentrations as denoted. The xenon gas-pressure within the NMR-tube was 2.2 ± 0.1 bar with a hyperpolarization degree of 12 - 22 %. For direct xenon detection FIDs were usually acquired after a 0.2 ms Gaussian excitation 60 ppm downfield of the ^{129}Xe gas resonance, i.e. at the characteristic chemical shift of the cage. Detection band widths were ranging from 3 kHz to 21 kHz, depending on the desired resolution and inclusion of gaseous and bulk xenon resonances. To improve signal-to-noise FIDs were acquired in repetitive scans with manual shaking of the sample in between to support dissolution of hyperpolarized ^{129}Xe from the gas reservoir above the solution.

Data were filtered with a window function performing exponential multiplying (em) with additional line-broadening of 4 Hz, Fourier transformed, and manually phase- and baseline corrected with the Bruker XWinNMR software.

2.8.2 CEST

CEST pulse sequences have been designed by Dr. Wolfgang Kilian at the PTB Berlin and are explained in more detail elsewhere[82,92]. The pulse scheme is shown in figure 3.41. Chemical exchange saturation transfer of hyperpolarized xenon in bulk solution (HYPER-CEST or XCEST) was carried out by selective slice-excitation at 194 ppm, the characteristic chemical shift resonance of dissolved xenon to avoid susceptibility artifacts. The caged xenon polarization was destroyed by 150 repetitions of selective radio frequency excitations at around 60 ppm. Integration of the bulk xenon signal before and after selective destruction gave the ratio of magnetization loss due to exchange with the cryptophane moiety. The pulse sequence was applied 10 times with 15 s intervals. During these intervals the samples were manually agitated to drive the exchange of hyperpolarized gaseous ^{129}Xe in the reservoir above the liquid sample with dissolved ^{129}Xe. Saturation was performed either on-resonance (60 ppm) of Cage-HA or off-resonance as negative control at the mirror frequency to bulk xenon. The CEST experiment has been performed with a 2 ml sample in a home-built glass tube with PBS pH 7.4 as reference to determine background loss of hyperpolarization due to excitation and relaxation. Binding of Cage-HA to HLA-DR1 was examined by using 10 µM of Cage-HA alone, 10 µM preformed HLA-DR1/Cage-HA alone or both components at each 10 µM in PBS pH 7.4.

2.8.3 T cell assays with Cage-HA

Assays for antigenic peptide binding to professional antigen presenting cells (APC) for detection by restricted T cell populations were performed as duplicate together with and under supervision of Dr. Sabine Höpner at the MDC Berlin.

5 x 10^4 HLA-DRB1*0101 expressing fibroblast cells (L57.23)[93] per well were loaded with titrated amounts (10^{-10} - 10^{-5} M) of either HA or Cage-HA peptide. 5 x 10^4 mouse T cell hybridoma cells were added, using the HLA-DR1-restricted, HA-specific EvHA/X5 or the HLA-DR1-restricted, hAbl908-923-specific SaABL/G2[94]. Cells were incubated for 24 h in DMEM/5 % fetal calf serum (FCS) in 96-U-bottom plates. The T cell response was determined in a secondary assay encountering IL-2 production as described in reference[95]. Briefly, measurements were carried out by incubating 5x10^4 CTL-L cells with supernatant collected from the first incubation. 12 hours later ^{3}H-thymidine was added for further 12 h and cells were incubated at 37°C in DMEM / 5 % FCS before harvest. Proliferation was measured with the ^{3}H-thymidin-reader 1450 Microbeta from Wallac.

2.8.4 Elispot experiments with isolated mouse cells

Experiments dealing with mouse immunization and re-challenging of isolated spleen and lymph node cells were performed by or under supervision of Dr. Sabine Höpner at the MDC Berlin. The procedure has been described in more detail before[94]. Briefly, five HLA-DR1 transgenic mice (B10M/J background) were each primed with 10 µg/mouse (HA) or 20 µg/mouse (Cage-HA) peptide in Incomplete Freund's adjuvant (Sigma) supplemented with 50 µg CpG OND 1826 (Biotez GmbH) subcutaneously. After 12 days 1×10^6 freshly isolated Lymph node or spleen cells per well were incubated for 48 h (37°C, 5 % CO_2, RPMI 5 % FCS) with titrated amounts of HA or Cage-HA peptides in Elispot plates (Multiscreen plates HTS 96 well Filtration plate; Millipore) previously coated with α-IFNγ capture antibody (clone AN18.1724). Detection was carried out according to the manufacturer's recommendations, using a biotinylated α-IFNγ detection antibody (clone R4-6A2) followed by an avidine-HRP enzyme conjugate (Sigma) and 3,3- diaminobenzidine tablets (Sigma). Spots were counted using the 'ImmunoSpot' reader (C.T.L. Europe GmbH). Samples were set up in duplicates and experiments were carried out twice.

2.9 Peptides and spot membranes

2.9.1 Peptides

All peptides used in this study were synthesized either in-house (group of Dr. Michael Beyermann) or by EMC microcollections Tübingen, Germany, by standard Fmoc-protected solid-phase coupling. Standard peptides $HA_{306-318}$, $CLIP_{106-120}$, $CLIP_{102-120}$ and the dipeptidic MHC loading enhancer (MLE) Ac-FR-NH_2 were obtained in amounts of hundreds milligrams with different fractions of purity. Other peptides were obtained in a 1 - 30 mg scale in dependence of their application. Peptides I - XII for screening orientations were produced in 5 - 10 mg scales by EMC.

Cage-HA was synthesized by the group of Dr. Michael Beyermann from a commercially available prebuilt Cryptophane A block coupled to the peptide N-terminus with either amino acids GEEG and the amino-polyethyleneglycole-acid plus an additional acetate (Cage-HAI) or RKR and 6-aminohexanoic acid (Cage-HAII) as linker in between.

The FLAG peptide (sequence: N-DYKDDDDK-C) for elution of HLA-DM, FR, the TEMPO-$CLIP_{106-120}$, Abl peptide, biotinylated $HA_{306-318}$ and substitution mutants of $HA_{306-318}$ were produced by EMC microcollections in Tübingen under supervision of Prof. Dr. Karl-Heinz Wiesmüller. The 2,2,6,6-tetramethylpiperidine-1-oxyl (TEMPO)-labelled $CLIP_{106–120}$ was synthesized from a TEMPO-4-carboxylic acid forming an amide bond to 2,3-diamino-propionic acid (DAPA), which itself replaces Lys106 in the natural CLIP sequence. The identity of all peptides after HPLC runs was confirmed by HPLC-ESI mass spectrometry. All peptides with masses, sequences and additional remarks used in this study are summarized in table 2.4.

2.9.2 SPOT membrane: Sequence selection, synthesis and development

To define antigenic sequences with potency of inversion the IEDB database (ImmuneEpitopeDataBase: http://www.immuneepitope.org)[96] was screened for deposited epitopes for HLA-DR1. Peptides were required to have been appeared in one of the assays “B cell response”, “T cell response”, “MHC binding” or “Elution from MHC”. This resulted in more than 2000 entries with high redundancy. These were manually validated for potential pocket occupation after inversion as suggested in the SYFPEITHI database (http://www.syfpeithi.de)[32]. Length restriction was set to 20 amino acids for optimal synthesis, which yielded 41 candidate peptides. Sequences were spotted in both N- to C-

terminal direction and with inverted backbone together with a control set of HA-derived sequences, HA wild-type and both CLIP versions. All sequences are listed in appendix table X. Peptides were synthesised in a solid-phase mode onto a Whatman50 cellulose membrane by an automated SPOT method[97]. For incubation with HLA-DR1, membranes were shortly rinsed with ethanol and several times with TBS buffer. After a blocking step of 2 h at room temperature with 5 % bovine serum albumin in TBS spots were incubated with 30 µg/ml of protein in blocking buffer overnight at 4°C. To detect binding, membranes were treated for 1 h at room temperature with mouse-derived anti-HLA-DR1 L243 primary antibody (produced by Maria Hofstätter at the MDC Berlin) at a concentration of 3 µg/ml. After extensive washing with TBS membranes were incubated for 1 h with goat anti-mouse secondary antibody (1:1000, coupled to horseradish peroxidase, Rockland Immunochemicals), contained in blocking buffer. An enhanced chemiluminescence substrate (ECL, Enhanced Luminol, Perkin Elmer) in a total volume of 500 µl was used for detection on a LumiImagerTM (Boehringer Ingelheim). An optimal ratio of spot intensities and background was seen with 200 s illumination time.

- 1x TBS: 50 mM Tris-HCl, pH 7.4, 150 mM NaCl
- 1x blocking buffer: 5 % bovine serum albumin (BSA) in 1x TBS

2.9.3 Selection of peptides for orientational screens by NMR and crystallography

Peptides I - XII were selected for determining their orientation when bound to HLA-DR1 by crystallography and NMR. Ten of them were derived from the SPOT membrane and are listed in table 2.4. Those were chosen in a way also including negative spots as potential controls. Two additional peptides (XI and IX) were suggested from an in-house *in silico* prediction for antigen inversion performed by Dr. Bernd Rupp in the group of Dr. Ronald Kühne (FMP Berlin). The underlying algorithm is not explained here in detail but implemented a scoring function for each peptide side chain position to fill pockets of HLA-DR1 in either of the directions. Sequences with the highest calculated ratio when opposing backward and forward scores were considered and two of them appeared to be restrictive enough for one orientation when using $CLIP_{106-120}$ as the threshold.

2.10 Crystal structures

All crystal structures provided in this study have been determined and refined by Sebastian Günther (FMP, MDC Berlin) using the prepared proteins produced in collaboration. For crystallization MHC-peptide complexes were prepared as described in[98]. Consistently, proteins were concentrated to 10 mg/ml and subjected to the crystallization facility of the MDC Berlin headed by Prof. Dr. Udo Heinemann and under supervision of Dr. Yvette Roske. All subsequent steps were carried out by Sebastian Günther as in the reference[98]. All figures showing structural magnifications were generated using PyMOL (DeLano Scientific).

Table 2.4: List of peptides appearing in this study

peptide name	sequence N to C	MW in g/mol	remarks
$HA_{306-318}$	PKYVKQNTLKLAT	1502.8	sequence 306-318 from Influenza hemagluttinin
$bHA_{306-318}$	Biotin-6Ahx-SGSG-PKYVKQNTLKLAT	2131.0	Biotin linked to sequence 306-318 from Influenza hemagluttinin via a linker comprising aminohexyl and amino acids SGSG
Cage-HAI	CryptA-6Ahx-RKR-PKYVKQNTLKLAT	2975.2	$HA_{306-318}$ coupled to cryptophane A via basic linker
Cage-HAII	CryptA-Ac-NH_2-PEG-GEEG-PKYVKQNTLKLAT	2942.0	$HA_{306-318}$ coupled to cryptophane A via acidic linker, refers to Cage-Ha if not denoted differently
$CLIP_{106-120}$ WT	KMRMATPLLMQALPM	1730.9	sequence 106-120 from human Invariant chain splice form p35
$CLIP_{102-120}$ WT	KPVSKMRMATPLLMQALPM	2142.1	sequence 102-120 from human Invariant chain splice form p35
TEMPO-$CLIP_{106-120}$	X-DAPA-MRMATPLLMQALPM	1873.0	$CLIP_{106-120}$ coupled to PRE moiety 2,2,6,6-tetramethylpiperidine-1-oxyl and diaminopropionic acid as linker replacing lysine 106
HA_{Y308A}	PKAVKQNTLKLAT	1410.7	$HA_{306-318}$, P1-position tyrosine mutated to alanine
$HA_{anchorless}$	PKAVKANALKAAT	1281.5	$HA_{306-318}$ with all anchor residues mutated to alanine
hABL	KGKLSRLKPAPPPPP	1583	sequence from human tyrosine kinase ABL*, known for oncogenic activity
FR	Ac-FR-NH_2	362.0	dipeptidic MHC loading enhancer targeting the P1-pocket**
Potential canditates for inversion:			
tetX ($TT_{234-246}$)	ELIHVLHGLYGMQ	1509.9	Tetanus toxin from Clostridium tetani, peptide I
$SMU.616_{33-43}$	SILGGVATYGA	1008.4	uncharacterized protein from Streptococcus mutans, peptide II
MAGEA3	GDNQIMPKAGLLIIV	1582.2	Human Melanoma associated antigen 3, peptide III
pstS1 86-101	TGSGAGIAQAAAGTVNI	1458.9	phosphate binding protein from Bacterium tubercolosis, peptide IV
HA1 255-270	RGYFKMRTGKSSIMRS	1905.6	Hem-agglutinin, Influenza A virus H3N8, peptide V
TT 1147-1159	DYMYLTNAPSYTN	1553	Tetanus toxin from Clostridium tetani, peptide VI
P4a 293-307	SMRYQSLIPRLVEFF	1886.4	Major core protein from vaccinia virus (Pox), peptide VII
MBP 278-297	VDAQGTLSKIFKLGGRDSRS	2135.8	Human Myelin basic protein, peptide VIII
Bapa 360-381	NANIRYVNTGTAPIYNVLPT	2191	protective antigen from B. anthracic, peptide IX
TT 830-843	QYIKANSKFIGITE	1612.1	Tetanus toxin from Clostridium tetani, peptide X
lqpH 1-15	EHRVKRGLTVAVAGA	1563.9	19 kDa lipoprotein antigen from B. tubercolosis, peptide XI
Phl p5b 68-86	DKFKTFEAAFTSSSKAAAA	1978.5	Pollen allergen from Phleum pratense, peptide XII

*ABL = Abelson Murine Leukemia Viral Oncogene Homolog, see reference[94]

**see reference[99]

3 Results

3.1 Optimization of HLA-DR1 expression, purification and refolding

The present study aimed at addressing characteristics of different MHC-peptide complexes at an atomic level both by solution NMR and X-ray crystallography. Foremost, HLA-DR1 protein had to be prepared in sufficient amount and to high homogeneity. In order to pursue the NMR-based approach isotope labeling had to be achieved either by uniform nitrogen-/carbon-/deuterium-labeling or by amino acid selective labeling in *E.coli*. While HLA-DR1 had been obtained in sufficient quantities for certain biophysical measurements before, an optimized refolding procedure had to be developed to meet the stringency criteria of my approach.

3.1.1 Protein production

Protein expression constructs were successfully cloned and correct sequences verified for either protein used in this study. The integrity of all wild-type and modified HLA-DR1 subunits on protein level was tested by small-scale expressions. Exemplarily, figure 3.1 shows the appearance of a prominent new band for DRα and DRβ wild-type proteins after induction with 1 mM of IPTG, respectively. Both subunits were completely insoluble as expected for an extracellular eukaryotic protein containing disulfide bonds and as expected from previously published studies[85,100,101].

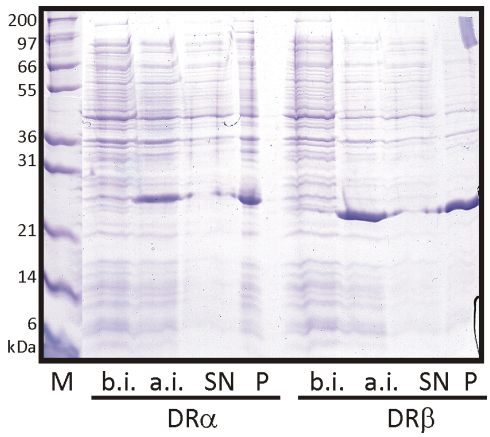

Figure 3.1: Expression and solubility test of HLA-DR1 ectodomains of DRα and DRβ. Coomassie-stained SDS-PAGE of IPTG induced expression of subunits in *E.coli*. The gel is Coomassie stained for protein visualization. M = molecular weight standard Mark12®, b.i. = before induction, a.i. = after induction, SN = supernatant after cell lysis, P = pellet after cell lysis

Neither the introduction of mutations G86V or G86Y into the DRβ wild-type (WT) sequence nor the extension of the construct by a genetically linked peptide had an effect on solubility. Expression yields were similar to WT for point mutants but appeared to be lower for the fusion proteins. The attachment of linked $CLIP_{106\text{-}102}$ to either of the subunits is exemplified for DRα in figure 3.2 with the protein chain running slightly higher in comparison to the wild-type subunit.

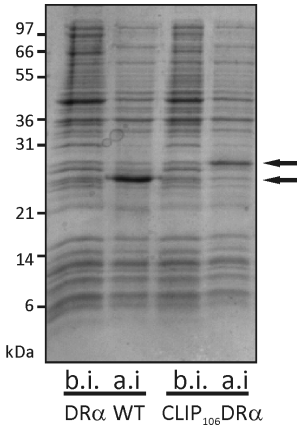

Figure 3.2: Expression of $CLIP_{106\text{-}120}$-linked DRα in comparison to DRα WT. Coomassie stained SDS-PAGE of IPTG induced expression in *E.coli*. Arrows indicate the difference in size. Protein molecular weight standards are indicated on the left. b.i. = before induction, a.i. = after induction

3.1.2 Expression of amino acid-selectively labeled proteins

Selective amino acid labeling was used to incorporate particular backbone amides which were labeled on an otherwise unlabeled background. I used *E.coli* strains DL39 (DE3), auxotroph for two aromatic and hydrophobic amino acids and the standard non-auxotroph BL21 (DE3) strain to obtain selective labeling.

To examine the suitability of *E.coli* strain DL39 (DE3) for selective labeling of amino acids leucine, valine and phenylalanine test cultures were set up under different conditions of amino acid composition. As depicted in figure 3.3 the aforementioned amino acids were essential for proper bacterial growth. Metabolically more promiscuous amino acids as the end-standing glycine or histidine could be omitted from the media without any influence on growth when compared to a full set of amino acids. Given that result it was decided to perform selective labeling of leucine, valine and phenylalanine in DL39 in contrast to glycine which was labeled in BL21.

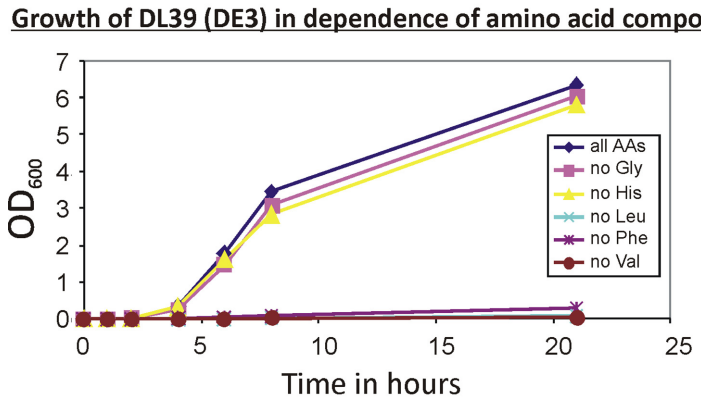

Figure 3.3: Growth of *E.coli* strain DL39 (DE3) in dependence of amino acid composition. Densities of growth cultures were determined measuring absorption at 600 nm at the indicated time points. All media were M9-based with individual amino acids (AAs) depleted as denoted in the inset legend.

The amounts of protein recovered from defined minimal media were similar to those obtained in complete media and is not discussed here in particular. Amino acid selective labeling was used at later stages with growth conditions as applied for figure 3.3.

3.1.3 Deuteration of HLA-DR1 subunits for NMR experiments

In order to minimize proton relaxation and as a consequence line-broadening of HLA-DR1 NMR signals protein subunits were individually deuterated. Adaptation of bacterial growth to conditions of low glucose and fully deuterated components is the most time-limiting step in expressing deuterated proteins. Three different ways were tested to obtain maximum yield in cell densities and protein expression in the minimum demand of time. Figure 3.4 is giving an overview of cultures when growing cells (i) *ab initio* in D_2O by direct inoculation with a single clone, (ii) by initially including 1.5 % of LB medium or (iii) by stepwise adaptation to increasing D_2O concentrations (see legend for details).

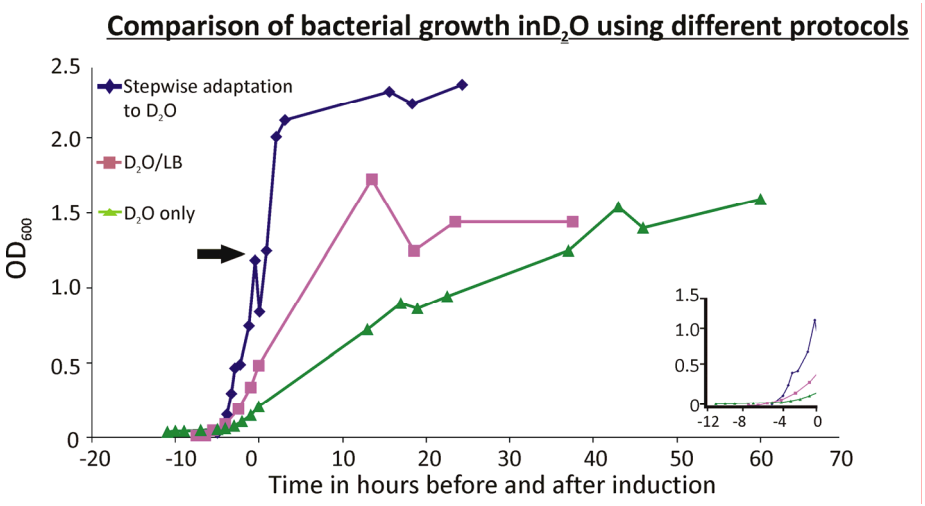

Figure 3.4: Bacterial growth in different conditions of deuterated media before and after induction of protein synthesis by IPTG. Densities of growing cultures were determined measuring absorption at 600 nm at indicated time points. The inset magnifies the time range before induction. The arrow indicates the time point of back-dilution before induction in the blue curve.

The best results in terms of growth rate were obtained under conditions of stepwise D_2O increase. While conceivably compromising slightly on the completeness of deuteration compared to *ab initio* growth in D_2O the convenience and larger absolute cell mass argue for the stepwise adaptation approach. Not only did cultures reach a proper density for induction much faster (see inset comparing 5 hours to 11) but they also continued growth undisturbed after induction at higher OD values (compare final OD_{600} values of 2.5 for blue rhombs and 1.5 in green triangle curves). This result was transferred to a *de novo* designed deuteration protocol as described in the *Methods* chapter. The expression yields were about 50 % compared to growth in protonated minimal medium, which is likely be caused by the input of only half the amount of deuterated, thus cost-intensive, glucose. Favorably, almost no residual protonation was observed in subsequent NMR experiments (see paragraph 3.3.2.2).

3.1.4 Refolding and optimization of subsequent steps in HLA-DR1 production

The most critical step in obtaining functional protein was to find conditions that yield refolded protein amounts of sufficient quality and quantity in a reproducible manner. The effort for obtaining the protein needed to be balanced to the prompt accumulation of data that justify a particular level of costs or material and time.

HLA-DR1 production was established based on a published protocol[85] as outlined in figure 3.5 summarizing the most important steps from protein expression to obtaining fully folded molecules. The first step for up-scaling the procedure to mg-amounts was to handle the

larger refolding volumes. The rapid-dilution-procedure requires low local protein concentrations to allow the formation of the native fold in the presence of incorrectly folded but initially soluble and aggregation-prone intermediates.

Initially the protein was concentrated via addition and swelling of sepharose G-25 as suggested in one protocol[85]. The swollen sepharose was filtered and bound protein eluted under high-salt conditions. However, only small amounts of protein were obtained from larger refolding volumes, most likely caused by inefficient mixing of the viscous refolding buffer and sepharose. In addition, larger volumes of sepharose were not easy to handle and subsequent elution did not reduce the volume to a large enough degree.

In the second approach the refolding reaction was concentrated under gaseous nitrogen pressure of 2-3 MPa across a polyether sulfone membrane with a molecular weight cutoff of 10 kDa. This low-volume device was actuated at room temperature for logistic reasons. Despite the visible loss of most of the protein a correctly folded fraction of < 0.5 % was recovered. However, considering the time that was needed to re-concentrate several liters this method did not qualify as applicable when concomitantly the major part of HLA-DR1 precipitated.

As a third option in-row-connected crossflow-filtration cells were utilized in an adjustable number for re-concentration under moderate pressure and at low temperatures. Cells could be reused when treated with care and volumes were reduced by a factor of 30-40-fold within half a day. The more, no solution transfer was necessary and the process could be interrupted at any time without the need for permanent observation. As the concentrating process worked in a reflux mode the apparent protein concentration only increased slowly but consistently disallowing the formation of local aggregation/precipitation nuclei. The applied volumes were possible to scale up to 15 liters - re-concentrated to 300-800 ml in a day - which was sufficient for the recovery of multiple parallel NMR sample. The loss of protein during the process was negligible as judged by no visible precipitation and only small reductions in flow rates across the membranes.

The subsequent step of immuno-affinity purification has been implemented after recovering high amounts of soluble but non-functional protein. Milligrams of native HLA-DR1 were obtained by binding to the native-fold-selective antibody LB3.1. The sequential elution of bound protein revealed decreasing affinity to LB3.1 related to the degree of native folding (see *Methods* chapter). The total yield, however, relative to the total amount of HLA-DR1 in

the refolding buffer was still in the range of 1-10 % depending on the age of the column and the actual species to be purified. It was found that remarkably more protein could be eluted via LB3.1 when HLA-DR1 was refolded in its empty, unloaded state, consistent with results published earlier[85]. Introducing an additional dialysis step to PBS pH 7.4 after re-concentrating the refolding reaction further improved the recovery of functional protein. Exclusion of the redox-active glutathione as it was present in the refolding buffer probably increased the integrity of antibodies immobilized on the column. In addition, antibody columns served as an ideal pre-concentration step for the samples before further use in any application.

A higher throughput of protein production was also supported by increasing refolding concentrations of the protein. Apart from previous protocols I successfully used 10 mg/l and subunit for refolding and even higher concentrations were still unproblematic in terms of precipitation. However, no higher yield of functional protein was obtained after all steps with higher input than 10 mg/l.

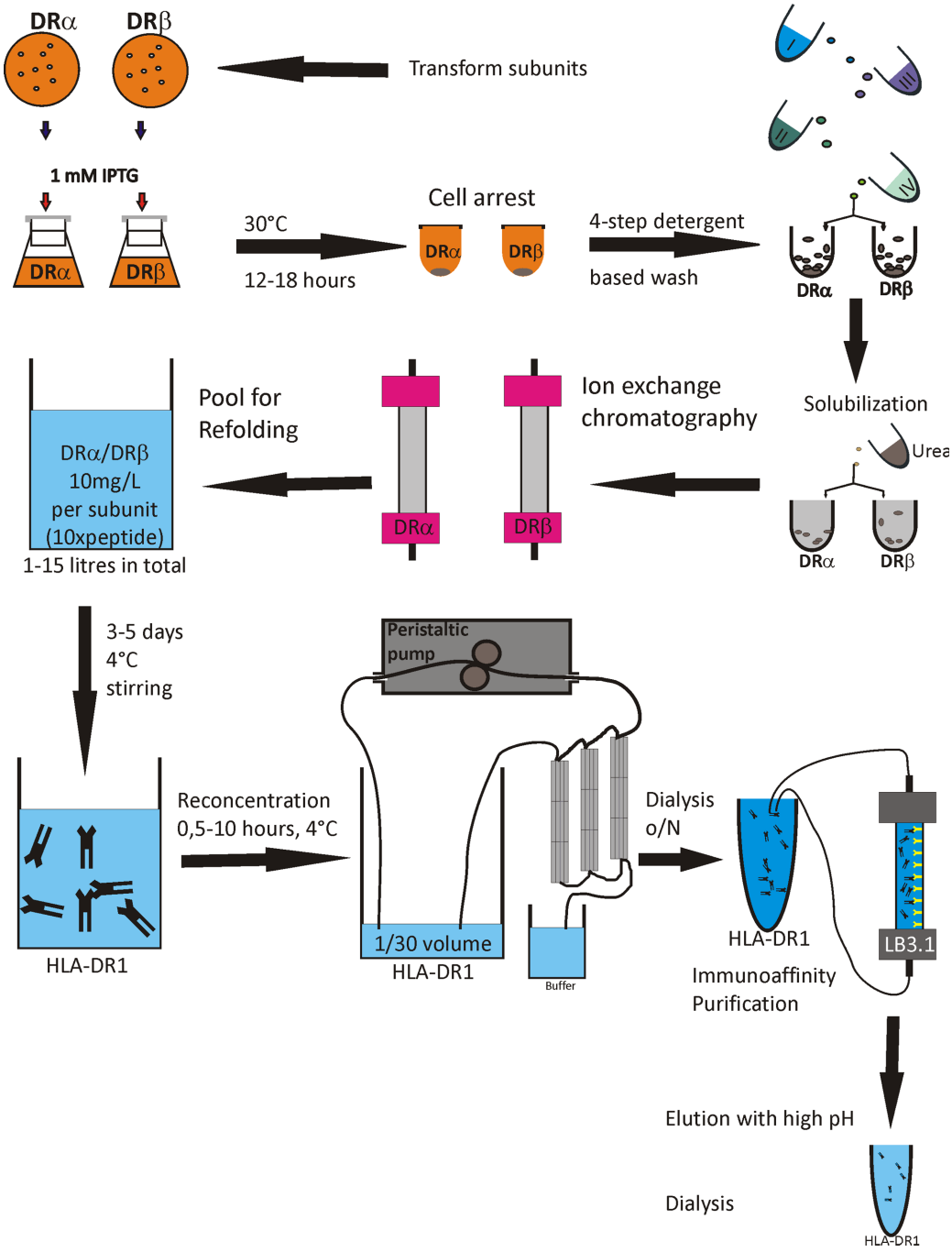

Figure 3.5: Schematic outline of producing HLA-DR1 from bacterial *inclusion bodies* which were obtained after detergent-based cell lysis. The figure only sketches central steps of the procedure. The complete and detailed protocol is given in the *Methods* chapter.

3.2 Examination of protein quality and functionality

On the basis of an efficient protocol to produce milligrams of native HLA-DR1 from bacterial expression it appeared necessary to probe protein folding and the formation of functional protein by simple and rapid biophysical methods. NMR-spectroscopic investigations for a comparatively large protein like HLA-DR1 have stringent requirements in regard to its molecular properties: the correct disulfide bonds have to be formed, the protein has to be capable to capture differently affine peptides (loading), and the protein has to be stable and monodisperse over longer periods of time. Furthermore, spectral quality of functional protein had to be improved by introducing single subunit labeling and deuteration.

3.2.1 SDS-PAGE-based evaluation of protein folding and peptide loading

As described before[85,102], refolded HLA-DR1 was tested under reducing or oxidizing conditions in an SDS-PAGE. As to be seen in figure 3.6 (panel A) both subunits showed slightly reduced mobility in an SDS-PAGE when reducing β-mercaptoethanol was present in the sample buffer. The altered mobility of the protein under non-reducing conditions is an indication of disulfide bond formation and is independent from additional denaturation of the sample by boiling.

Another simple readout for HLA-DR1 functionality is its ability to form SDS-resistant heterodimers when bound to particular antigenic peptides and under conditions where samples are not boiled (so called “gentle SDS-PAGE” [103,104]). In part B of figure 3.6 a third band occurs at the approximate MW of 50 kDa after loading HLA-DR1 with an excess of viral HA peptide. A mutant of HLA-DR1 (βG86Y) that cannot accommodate aromatic residues in pocket 1, instead, failed to form SDS-resistant dimers with this peptide. This does not qualify the mutant as unfolded but rather proves the more stable antigen binding of the protein wild-type. Interestingly, the mutant protein was capable of forming stable dimers with a version of the HA peptide ($HA_{anchorless}$) that does not provide any bulky side chains. Influenza-derived peptides, where all pocket positions are alanines, had been reported to maintain stably associated with both MHCI[105] and MHCII[106] before.

In panel C the different apparent molecular weight of complexes in dependence of the bound peptide are probed by SDS-PAGE. The characteristic shift of bands between 40 and 55 kDa highlights the strong influence of antigenic peptides to the migration behavior of HLA-DR1 because the total mass is comparable in all complexes (compare lanes with HA, $CLIP_{102}$,

$CLIP_{106}$ and HA_{Y308A} with alanine instead of tyrosine at the corresponding P1 position as negative control). Importantly, the same migration behavior was observed for a complex where peptide loading was performed *a posteriori* and a complex that resulted from the co-refolding of components (compare last outer right lanes in C).

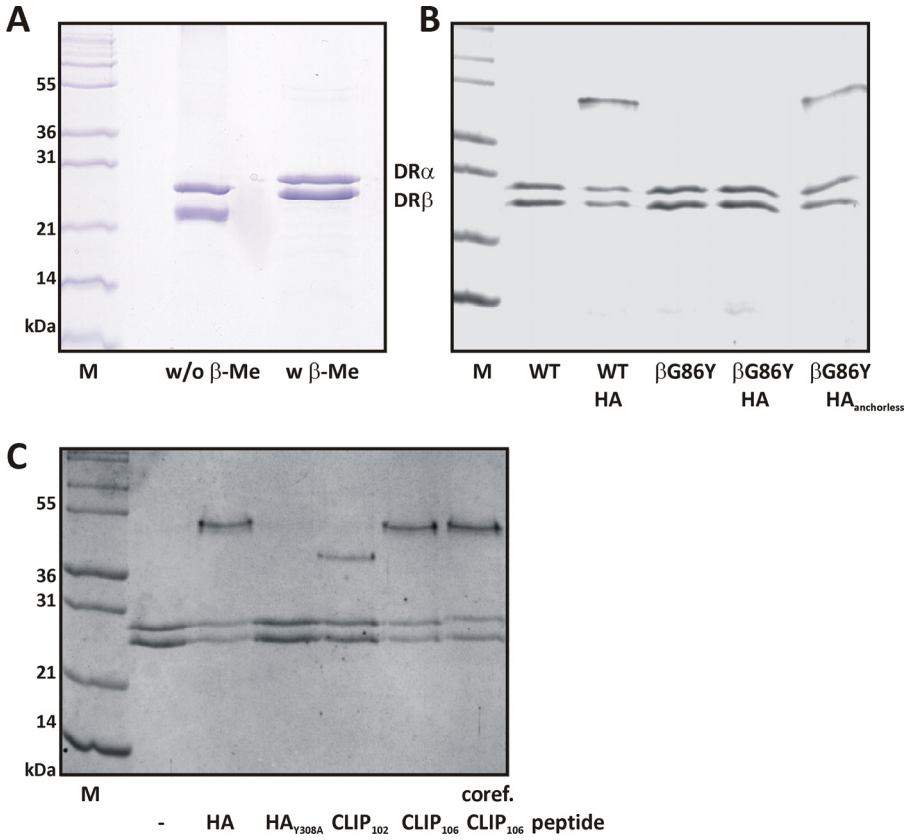

Figure 3.6: Functionality of refolded HLA-DR1 probed by SDS-PAGE-based experiments. A) Redox conditions influence migration behavior of HLA-DR1 subunits. Samples were loaded in presence or absence of 250 mM β-mercaptoethanol. B) Formation of SDS-resistant complexes upon peptide binding. Empty wild-type or mutant HLA-DR1 was loaded with peptides as indicated. Samples were not boiled prior loading to SDS gels. C) Loading of wild-type HLA-DR1 with different peptides under conditions as described in B. In the right lane co-refolded HLA-DR1/$CLIP_{106}$ is shown in comparison to the posterior loaded samples.

In summary, it was verified that either co-refolded or empty HLA-DR1 loaded *a posteriori* was able to form SDS-resistant heterodimers which are stably bound to antigenic (HA) or self-peptide (CLIP). Mutations in both HLA-DR1 and the peptides impaired heterodimer-stability giving rise to specific behavior of functional protein.

3.2.2 Peptide loading probed by enzyme linked immunosorbent assays (ELISA)

To examine the efficiency of peptide loading for HLA-DR1 and its control mutants ELISA experiments were performed in the group of Dr. Olaf Rötzschke at the MDC Berlin under supervision of Shashank Gupta and Sebastian Günther. This served to answer three

questions: i) will the protein complex be captured by the conformational HLA-DR1 antibody L243, ii) is peptide loading concentration-dependent and iii) how do HLA-DR1 mutants modulate peptide binding and exchange? For this, biotinylated peptides were loaded onto wild-type or mutant HLA-DR1 and complexes were transferred to L243-antibody-precoated plates where the amount of bound biotinylated peptide was detected via $Eu3^{+}$-coupled streptavidin.

As depicted in figure 3.7 HLA-DR1 wild-type (β86G) could be loaded with the cancer-related ABL, the $CLIP_{106}$ or the viral HA peptide in a concentration dependent manner. The mutation β86V does not severely abolish binding but a lower apparent affinity was observable for ABL and HA. Binding was significantly impaired in the βG86Y mutant indicating that the filling of the P1 pocket by tyrosine leads to steric occlusion of HA's tyrosine or CLIP's methionine at this position. In contrast, the capability of ABL loading is not affected, indicating a binding register with a relatively small residue in P1 in both wild-type and mutant HLA-DR1.

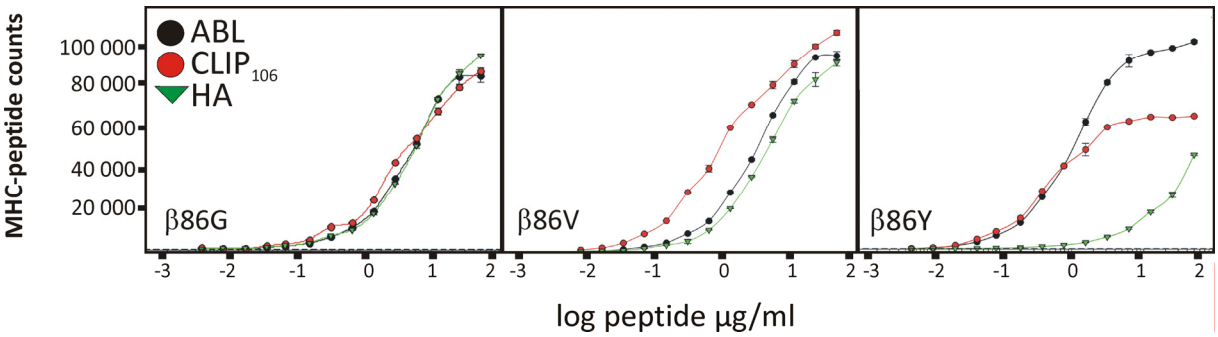

Figure 3.7: ELISA-probed concentration-dependent peptide binding to HLA-DR1 and two mutants thereof. Biotinylated peptides were detected with Eu^{3+}-labeled streptavidin after transfer of the loading reaction to L243-coated plates. β86G represents the wild-type protein.

The results altogether confirm that refolded HLA-DR1 can be loaded with peptides. The comparison of mutant proteins and peptides shows the importance of the P1 pocket for ligand binding.

3.2.3 Dynamic light scattering (DLS) analyses

Both crystallization and NMR spectroscopy require homogeneous, monomodal sample states. A method to examine the existence of oligomers in samples is Dynamic Light Scattering (DLS) where three-dimensional shapes of molecules are related to their size based on assumptions of a globular molecular shape. A continuous measurement of scattered light during a defined time period allows separate detection of different states of oligomerization,

given that their distinctions are large enough to be discriminated by the wavelength of the light source.

I probed empty HLA-DR1, HLA-DR1 loaded *a posteriori* and co-refolded HLA-DR1/HA or HLA-DR1/Cage-HA (a modification of wild-type HA which will be further discussed in section 3.5) by DLS as demonstrated in figure 3.8. The relative distribution of particle sizes clearly shows that empty protein comprises a broader range of protein species than complexed protein (compare outer left panel to all others). HLA-DR1 loaded *a posteriori* (second panel from left) still contains a higher molecular weight fraction in contrast to co-refolded samples from either HLA-DR1/HA or HLA-DR1/Cage-HA (right panels). For all samples the recalculated molecular weight marking the main fraction convincingly fits the expected size as summarized in table 3.1.

Hence, the presence of distinct populations within samples of HLA-DR1 can be unscrambled by DLS and confirms results from a similar study on HLA-DR1[107].

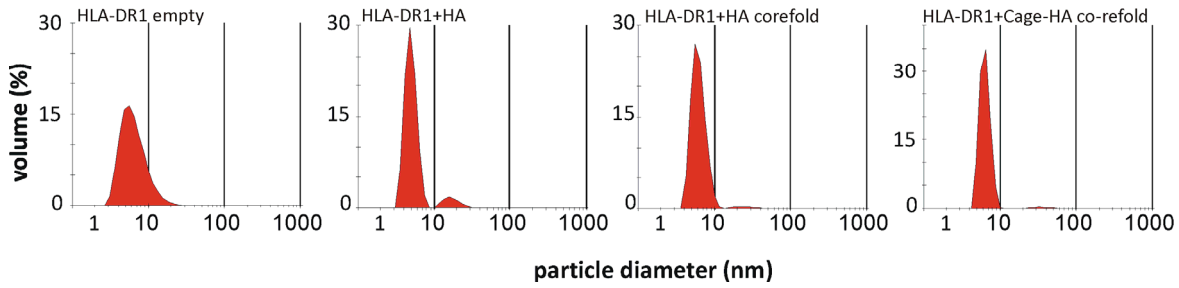

Figure 3.8: Analysis of sample modality for HLA-DR1 alone or in complex with peptide as probed by dynamic light scattering. Shown is the size distribution of molecular weight species within each sample. The calculated, model-dependent molecular weight (see *Methods* chapter) is given in Table 3.1. Note that empty samples could only be interpreted when measured instantly after gel-filtration.

Table 3.1: Determination of particle size and molecular weight recalculation from the data shown in figure 3.8 as performed for a single representative measurement by the Zeta Nanosizer ZS software (Malvern, UK)

	Main particle size in nm	**Molecular weight in kDa**
HLA-DR1 empty*	5.6	57
HLA-DR1+HA	4.8	46
HLA-DR1/HA co-refold	6.2	50
HLA-DR1/Cage-HA co-refold	6.4	53

*determined instantly after gel-filtration only

3.2.4 NMR spectral quality of empty and loaded HLA-DR1

Having optimized refolding to proper amounts of isotope-labeled HLA-DR1/peptide complexes one-dimensional proton- (^{1}H-1D) and two-dimensional proton-nitrogen correlation spectra (^{1}H-^{15}N-HSQC) were recorded for different preparations. The most obvious limitations in NMR for proteins of the given size were well reflected by the class II MHC HLA-DR1 in figure 3.9. Spectral overlap in combination with broadened line shapes leads to spectra that lack a significant number of resonances, in particular in empty HLA-DR1 as shown in panel A, and therefore do not allow the assignment of individual resonances to the protein sequence. For HLA-DR1 the stabilizing influence of antigenic peptide as prerequisite for a single monodisperse population is manifested in the drastic spectral improvement of the spectra of empty HLA-DR1 after subsequent loading of excess $CLIP_{106}$ in the presence of HLA-DM as natural catalyst (compare A and B). This indicates that - in line with results from DLS and gel-filtration profiles (also see paragraph 3.5.4) - loading with high-affine peptide leads to the formation of a homogeneous fraction with improved spectral properties compared to remaining unloaded, heterogeneous and/or oligomeric protein. However, spectral quality was even better for samples derived from co-refolding. Although spectra were almost identical the effective concentration of properly loaded HLA-DR1 was comparably higher, which was reflected in signal-to-noise and resolution (see panel C and inset).

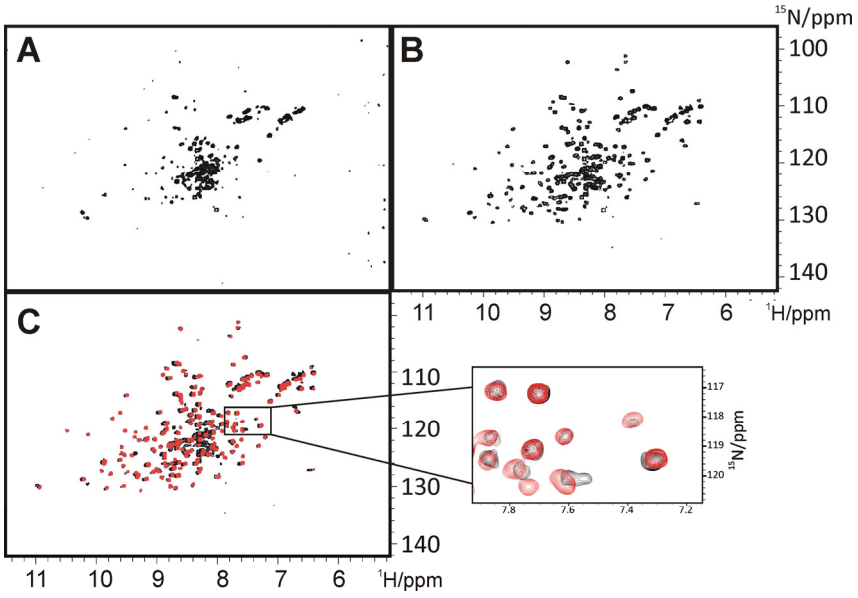

Figure 3.9: Peptide-loading of MHCII followed by NMR. ^{1}H-^{15}N HSQC spectra of HLA-DR1 in empty form (A), loaded with 10-fold excess of $CLIP_{106}$ in presence of HLA-DM measured after one hour at 37°C (B) and spectrum from B (black) compared to a co-refolded reference (red) (C). The inset shows a magnification from panel C. Only DRβ is ^{15}N-labeled and therefore visible (see next paragraph for details).

It was concluded that resonance assignments of multidimensional NMR spectra could only be obtained from pMHCII complexes whereas the spectra of empty HLA-DR1 were of insufficient quality. Complexes of pMHCII showed a peak dispersion as it is characteristic of folded protein, suggesting that resonance assignments could be successful for chain-specifically labeled, deuterated protein.

3.2.5 Deuteration and single subunit labeling in HLA-DR1 two-dimensional NMR

To reduce spectral overlap single subunit labeling was introduced exploiting the fact that HLA-DR1 is a heterodimer with roughly identically sized chains. This was accomplished by refolding ^{15}N-labeled subunits with unlabeled complementary chains. By this, spectral crowding was reduced by a factor of two enabling the recording of non-overlapping peaks even in the spectral center of a chain-specifically labeled sample. The need to record twice as many experiments was clearly outbalanced by the possibility to gain atomic resolution spectra. Figure 3.10 compares spectra recorded from uniformly labeled HLA-DR1 (panel A) and selectively α-labeled (panel B, red) or β-labeled (blue) samples co-refolded with viral HA peptide. As expected, spectral overlap is significantly reduced in B for both individually labeled chains. Since samples in B are deuterated, decreased line-width also contributes to the superior spectral quality. Therefore, ^{15}N/^{13}C-chain-specific labeling in combination with deuteration was set as the gold standard for the acquisition of triple resonance experiments.

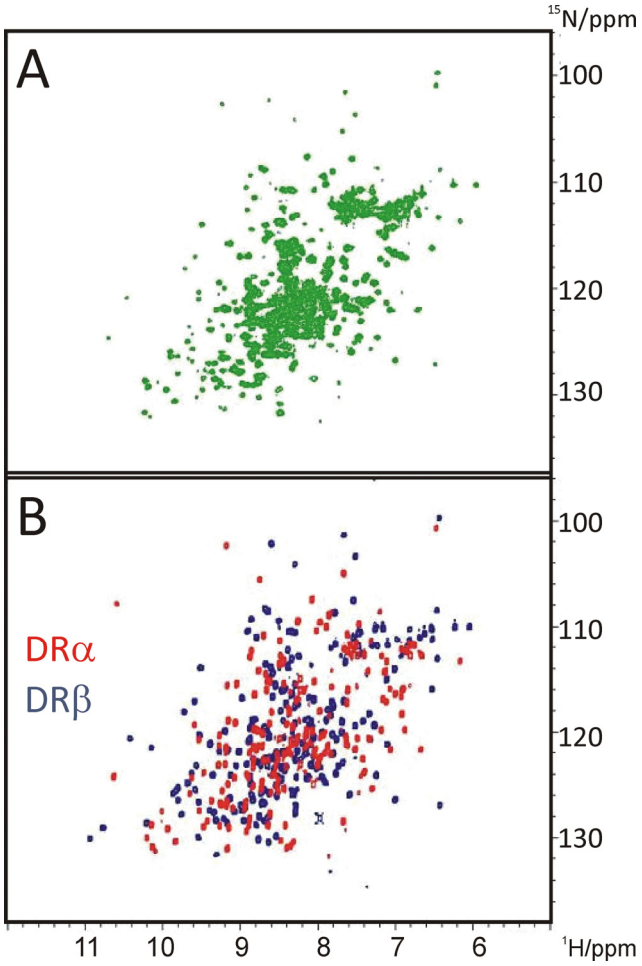

Figure 3.10: Subunit-labeling of HLA-DR1. ^{1}H-^{15}N HSQCs from HLA-DR1 in complex with co-refolded HA peptide when either uniformly ^{15}N-labeled (A) or with individually labeled subunits from two different samples (B). In B samples were additionally deuterated, which contributes to the appearance of numerous peaks under these conditions.

3.3 HLA-DR1 in NMR: assignments, peptide exchange and chemical shift perturbations

To gain mechanistic and structural insights into HLA-DR1/peptide structure and dynamics one prerequisite was to be able to differentiate by multi-dimensional NMR methods pMHCII complexes that contained different peptides. Changes in individual pocket occupations of the MHCII by peptide should be detectable by NMR and allow atomic resolution interpretations once the assignment for one of the complexes could be obtained. A successfully assigned protein domain would also be expected to assess secondary structure elements of pMHCII as predicted by the crystal structures.

3.3.1 Fingerprint spectra of HLA-DR1 in complex with different antigenic peptides

A typical starting point for NMR-based analysis of protein structure and dynamics is the acquisition of ^{1}H-^{15}N-HSQC spectra, also termed backbone fingerprint spectra. The high sensitivity of the chemical shift in regard to different chemical environments of a given NH group should give rise to distinct changes in NH resonances within the binding groove. For enhanced resolution I compared spectra from co-refolding with viral HA or $CLIP_{106-120}$ for either subunit separately. As shown in figure 3.11 ^{1}H-^{15}N-HSQC spectra for the two complexes were identical in major parts in both subunits independent of bound peptide. I expected these residues to belong to residues further apart from the peptide binding site, as for example the subunits' lower domains α2 and β2. In contrast, approximately half the peaks that are visible occur with singly defined chemical shifts indicating useful significant perturbations when comparing pMHCII species. Both samples appear as correctly folded proteins as judged by the large peak dispersion for both subunits.

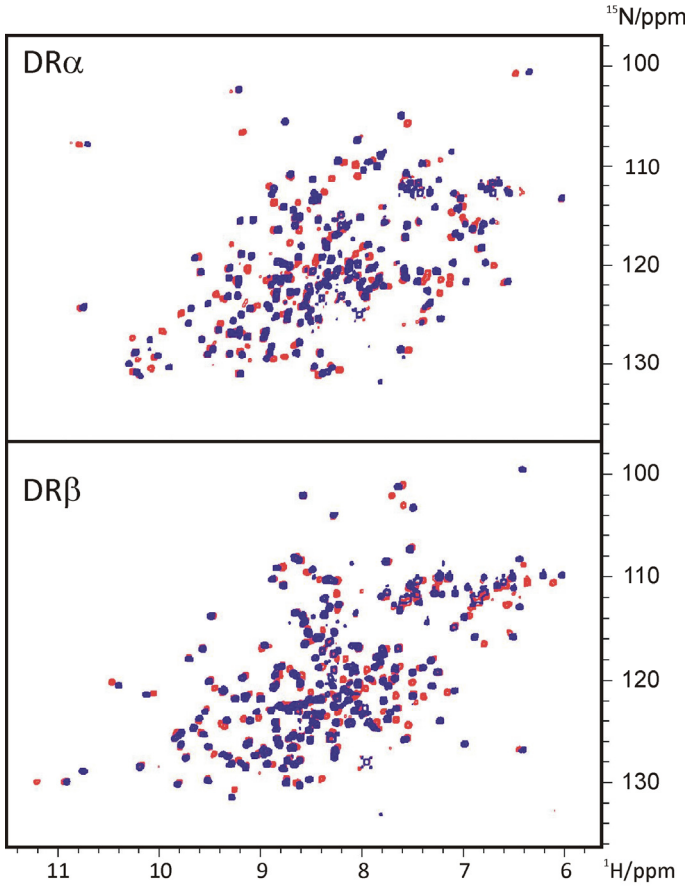

Figure 3.11: HLA-DR1/peptide complexes and their different 2D-NMR spectra. Shown are overlays of ^{1}H-^{15}N-HSQC spectra from ^{15}N-labeled HLA-DR1 in complex with $CLIP_{106-120}$ (red) and HA (blue). Top: Comparison of samples with exclusive DRα-labeling. Bottom: Samples with exclusive DRβ labeling.

3.3.2 Assignments of HLA-DR1

To monitor peptide exchange at the level of single residues HLA-DR1 subunits were assigned for the backbone. As discussed above it appeared reasonable to assign the protein backbone resonances subunit-wise (see figure 3.10). Starting with the HLA-DR1/HA complex I then proceeded to assign CLIP-bound HLA-DR1.

3.3.2.1 Amino acid selective labeling of HLA-DR1/HA

With amino acid type selective labeling I created starting points for subsequent sequential walks through the sequence by standard triple resonance experiments. Selective labeling with glycine, valine, leucine or phenylalanine was performed in both subunits simultaneously as described in paragraph 3.1.2. Resonances derived from the spectra of these individually labeled samples were utilized to identify the corresponding peaks in the uniformly labeled spectrum.

Figure 3.12 summarizes the results from individually selectively labeled samples with glycine, valine, leucine or phenylalanine. As expected, glycine resonances mostly appeared at ^{15}N frequencies below 115 ppm as was later confirmed by characteristic Cα chemical shifts in triple resonance spectra. As visible in the overlay in Figure 3.12, most of the resonances clearly correlated to a given peak in the uniformly labeled samples. Phenylalanine peaks did not merge with all peaks in the uniformly labeled samples (28 peaks instead of 24), probably caused by both degradation (see region around 7.4 and 127 ppm proton and nitrogen chemical shifts) and different acquisition and sample conditions. The glycine sample also showed more signals than expected (27 instead of 20) as expected from the number of amino acids in the protein, indicating significant scrambling into serine and threonine residues. Leucine and valine gave exactly the expected number of resonances (30 and 38, respectively).

Taken together, selective labeling was successful and set the stage for a complete backbone assignment of HLA-DR1 in complex with HA.

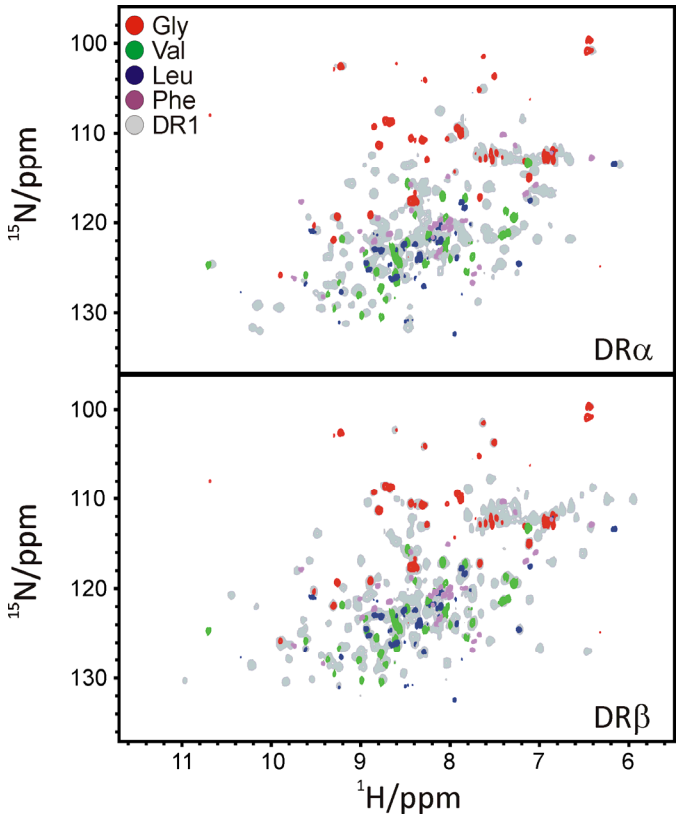

Figure 3.12: Selective labeling of amino acids as starting points for initial assignments. HLA-DR1/HA was co-refolded from subunits each of which was selectively labeled with one of the indicated amino acids (inset). Individual ^{1}H-^{15}N-HSQC spectra (see color code) were recorded and overlaid with spectra from samples uniformly labeled in one of the two subunits (in grey).

3.3.2.2 Subunit deuteration and TROSY-NMR

It was expected that deuteration would be of absolute necessity for acquisition of backbone-correlations in three-dimensional spectra. Obtaining relatively sharp lines for amides in two-dimensional HSQCs was not a guarantee for more pronounced line-broadening in triple-resonance spectra with their extended pulse schemes.

A good assessment of deuteration is the comparison of ^{15}N-NOESY-HSQCs, where the exchangeable amide protons couple through space with any close proton (< 5 Å), which were supposed to experience the effect of deuteration. In the triple-resonance spectra two effects were expected: i) any proton signal other than back-exchanged amides should vanish and ii) remaining resonances should be decreased in line-widths because of the lower spin relaxivity of deuterium.

Protonated or deuterated HLA-DR1 (^{15}Nβ) was co-refolded with HA peptide and samples measured with the same spectrometer settings. In figure 3.13 all useful proton-proton planes from a ^{15}N-NOESY-HSQC were projected into a single plane. An almost complete loss

of resonances in the region between 0 and 4 ppm indicates that DRβ grown on D_2O lacks detectable protons. In contrast many NOEs can be observed in the protonated sample in the left panel. These resonances are caused by protons bound to a carbon, except for aromatic CH resonances which would appear around 7 ppm. The only NOEs that are also visible in the deuterated sample are derived from direct NH-NH contacts that carry back-exchanged protons from standard NMR buffers. Furthermore, it is obvious that resonances mapping to amide groups (diagonal peaks between 6.5 and 11.5 ppm) are much more intense in the deuterated sample. This shows that reduced spin diffusion indeed leads to sharper signals (spectral resolution) and a better signal-to-noise. The significantly higher number of amide-amide NOEs is thus a valuable readout to measure the effect of deuteration on spectral quality.

Thus, deuteration was indispensable for any three-dimensional experiment originating from NH protons.

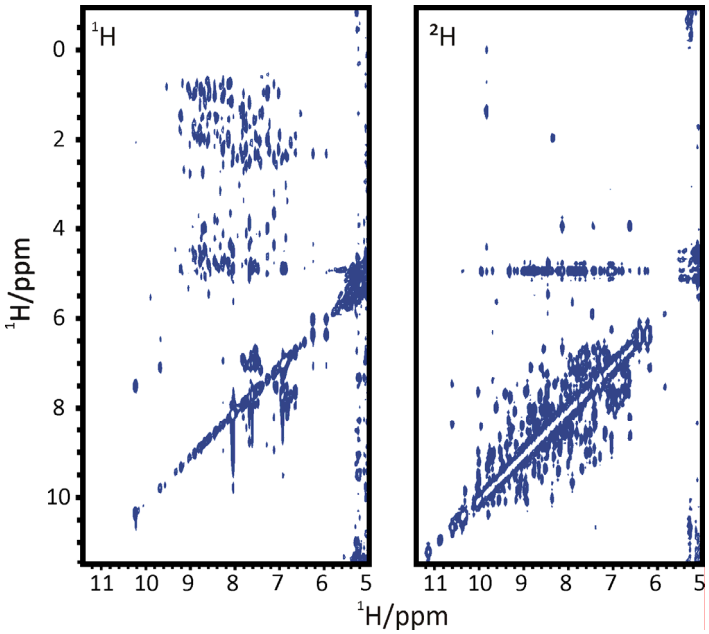

Figure 3.13: Effect of subunit deuteration on proton detection as measured by nitrogen-filtered proton-proton NOESYs. NOESY-HSQCs of HLA-DR1/HA, labeled in DRβ and either grown in water (^{1}H, left panel) or D_2O (^{2}H, right panel), were recorded as 3D spectra. Planes along the nitrogen frequency in the three-dimensional spectra were summed up in a projection yielding a quasi ^{1}H-^{1}H-2D-NOESY.

In combination with improving 3D-spectral quality from deuteration all triple resonance experiments were based on TROSY-^{1}H-^{15}N-HSQC approaches. The usefulness of *Transverse Relaxation Optimized Spectroscopy* relies on the increased line-sharpening of resonances by selecting the most intense component of amide-coupled correlations. The gain in line-width reduction is most pronounced when dipole-dipole-couplings and chemical shift anisotropy

cancel out for the respective component at high field strengths[57]. The decrease in amide line width was then transferred to a third dimension in the corresponding triple resonance experiments. The effect is demonstrated in figure 3.14 where a clear reduction of line width is visible for HLA-DR1 in complex with Ha peptide.

On the basis of this finding TROSY was applied to all amide correlated three-dimensional triple-resonance spectra.

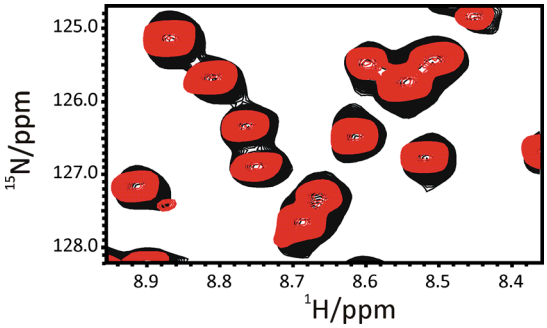

Figure 3.14: Effect of the TROSY-based acquisition mode. Zoom into an overlay of ^{1}H-^{15}N-HSQC spectra recorded from a sample containing HLA-DR1 in complex with HA peptide when either measured as standard HSQC (black) or in the TROSY-based mode (red).

3.3.2.3 Assignments of HLA-DR1 in complex with CLIP peptides and HA

While the spectral quality of the two-dimensional ^{1}H-^{15}N-HSQC was excellent it remained doubtful if the implementation of a third (carbon-) dimension would not lead to pulse program lengths that exceed relaxation times, and thus hamper signal-to-noise ratios. To achieve the best spectral outcome the most stable high-affinity complex of HLA-DR1 in complex with the viral HA peptide[103] (T_M > 81°C)[85] was chosen for initial analysis. A high-resolution crystal structure for this complex is available[33].

Labeling of DRβ with ^{15}N/^{13}C and ^{2}H was essential for a sequential walk along the resonance lines of neighboring amino acids. Additional deuteration of DRα was performed to reduce spin diffusion at the interface of subunits. Pairs of spectra as described in the *Methods* chapter yielded the complimentary information needed to assign these resonances.

The choice of moderate temperature (here room temperature) and neutral phosphate buffer was initially guided by the high stability of the monodisperse protein under these conditions but could later be shown to extend to pH 5.8 and 37°C with resulting in further improved spectra.

HNCA/HNcoCA and HNCO/HNcaCO pairs were used as indicated in table 3.2. The spin system extension to Cβ in the HNCACB and HNcoCACB spectra as evaluated for DRβ-HA (referring to labeled subunit and peptide in the HLA-DR1/peptide complex) clearly led to a severe loss of signal and further assignments were limited to the two initially mentioned experiments. In addition, ^{15}N-filtered NOESY-HSQC spectra were acquired and the typical patterns of NOE's between NH groups were used to confirm α-helical secondary structures. The regular order of backbone amides in helices allowed correlation of i- and i+1- residues, casually i+2-residues, too. As an example of the assignment strategy Figure 3.15 is showing a composite of spectral magnifications recorded for the assignment of residues 54 to 59 of DRα when part of HLA-DR/HA. These residues are positioned at the beginning of the helical stretch flanking the peptide binding groove of DRα1 (see part A of figure 3.15). The motif of F-X-X-X-X-G contains both phenylalanine and glycine resonances which were part of the amino acid selective labeling. Moreover, glycine exhibits significantly upfield-shifted Cα resonances which allow unambiguous identification among other Cα peaks. With this all sequential paths from phenylalanines to glycines were entered and followed until concluding. Cross peaks to resonances from E55, A56 and Q57 were obtained from suggestions within a defined range of deviation in the *analysis* software (see *Methods*). Particular indications for F54 and subsequent amino acids were taken from the program *shiftx*[108], which was especially helpful in the ^{15}N-dimension. When correlating backbone amides (part B) from an HSQC with Cα in an HNCA/HNcoCA pair (panel C) a clear connectivity was defined for the mentioned residues underlining the correctness of their NH-assignments. In addition, panel D of figure 3.15 shows NH-H polar contacts recorded from a ^{15}N-filtered NOESY. Strips were chosen for the amides from A and indicate NH-NH contacts for both i to i+1 and i+2 backbone resonances with the exception of E55 and A56. This is characteristic for helical segments in proteins and is nicely in line with the crystal structure of the complex as it is shown in part A of the figure. Overall, eighty percent backbone assignment were obtained for HLA-DR1 in complex with HA peptide and further on the strategy outlined above was successfully used to assign most of the backbone resonances for HLA-DR1 in complex with short and longer versions of CLIPs (i.e. $CLIP_{106\text{-}120}$ and $CLIP_{102\text{-}120}$) in both the canonical and inverted binding mode for DRβ as well as in the canonical mode for DRα (table 3.2 and section 3.4). Details on spectral acquisition parameters and sample conditions such as temperature and pH value are given in the *Methods* chapter and together with assignment

completeness are listed in table 3.2 for all complexes used in this study. Assignments have been achieved with the help of Dr. Jana Sticht.

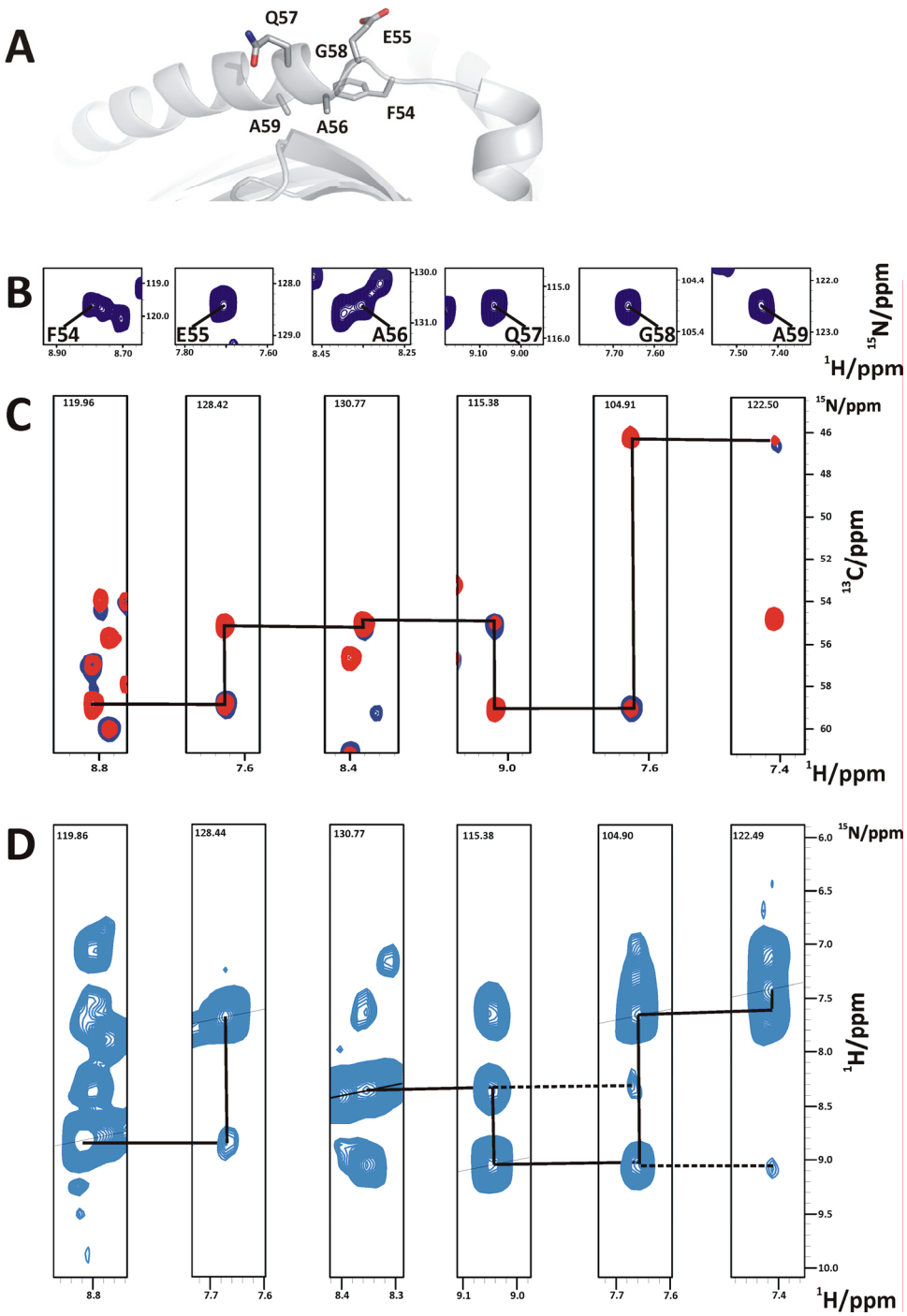

Figure 3.15: Backbone assignments of HLA-DR1 subunits in complex with peptide. Shown is the assignment of DRα from HLA-DR1/HA. A) Cartoon presentation of HLA-DR1 (pdb code 1dlh, HA peptide removed) zoomed into helix of DRα1, in particular residues phenylalanine 54 to alanine 59 which are shown with side chains as sticks. B) Sections of ^{1}H-^{15}N-HSQCs displaying the NH-resonances from A. C) Sequential walk through an HNCA/HNcoCA-pair along the stretch of residues belonging to backbone resonances in B. The HNCA is shown in red, the HNcoCA in blue. The strips were taken from slices with ^{15}N-chemical shifts as indicated at the upper end. D) Sequential walk through strips taken from a ^{15}N-filtered proton-proton NOESY. Displayed are cross peaks between NH groups of neighboring residues with nitrogen-filtered protons appearing horizontally and unfiltered protons on the vertical axis. The ^{15}N-slice position is indicated at the upper end of the strips, respectively. Diagonal peaks lie along the fine diagonal line within strips. Contacts of i, i+1-order are reflected by a straight line, i, i+2-contacts are marked by a dashed line.

Table 3.2: Overview of statistics of assigned HLA-DR1 subunits when in complex with HA or versions of CLIP

subunit/ peptide combination	concen-tration	T	pH	experiments recorded	approx. completeness (relative to number of assignable NH-groups)	remarks
DRβ/HA	125 µM	290 K*	7.5*	HNCA/HNcoCA HNCO/HNcaCO HNCACB/HNcoCACB ^{15}N-NOESY§	80 %	primarily lack of resonances from loop regions β102-115, β163-168 and N-terminus
DRβ/CLIP$_{106-120}$, inverted&	360 µM	310 K	5.8	HNCA/HNcoCA	80 %	primarily lack of resonances from loop regions β102-115, β163-168 and N-terminus, unambiguities from flipping (e.g. line-broadening during acquisition)
DRβ/CLIP$_{102-120}$, canonical#	280 µM	310 K	5.8	HNCA/HNcoCA HNCO/HNcaCO ^{15}N-NOESY	90 %	primarily lack of resonances from loop regions β102-115, β163-166 and single N-terminal residues
DRα/HA	280 µM	310 K	5.8	HNCA/HNcoCA HNCO/HncaCO ^{15}N-NOESY	90 %	almost exclusively lacks single assignments in termini
DRα/CLIP$_{102-120}$, canonical&	330 µM	310 K	5.8	HNCA/HNcoCA HNCO/HNcaCO ^{15}N-NOESY	85 %	almost exclusively lacks assignments in termini, e.g. C-terminus appears too flexible in DRα, loop region around α150

*assignments could be transferred to 310 K and pH 5.8; §measured at 310 K; $also applicable to the inverted fraction of DRβ/CLIP$_{102-120}$ (see figure 3.29) and to samples that were in complex with DRα-linked CLIP$_{106-120}$ (see figure 3.34); #was transferrable to canonical DRβ/CLIP$_{106-120}$, (see figure 3.28) and DRβ/TEMPO-CLIP$_{106-120}$ (see figure 3.26); &also applicable to samples that were in complex with DRβ-linked CLIP$_{106-120}$ (see figure 3.34)

3.3.3 Validation of assignments with Cα-secondary chemical shift analysis

The correlation of backbone chemical shifts with secondary structure in molecules has been a matter of debate since the beginning of routine-like protein assignments[109,110]. Recent progress has been claimed in predicting chemical shifts from pdb-coordinates but this approach is still of limited success for novel or more complex folds[111,112]. One easy opportunity to evaluate chemical shifts (in case when a high resolution crystal structure is available) is to subtract values of experimentally measured Cα chemical shifts from the standard random coil values of free amino acids. Differences of more than +2 indicate helical residues, whereas negative numbers (> -1) represent β-sheet residues. Since Cα-chemical shifts are a robust measure of secondary structure for stretches of amino acids greater than

three, this application also serves as indicator for conceivable discrepancies of secondary structure formation in solution compared to crystal structures.

For both HLA-DR1 subunits it became obvious that secondary structure elements, as they were previously observed in numerous crystal structures, are also maintained in solution. Figure 3.16 contains an exemplary plot of Cα-secondary chemical shifts for the subunits α1 and β1 in complex with HA or $CLIP_{102-120}$. Individual values fitted to their predicted values almost without exception (see indication of secondary structure elements below). Also, missing assignments related well with unstructured loops which show large variations in crystal structure B-factors[113].

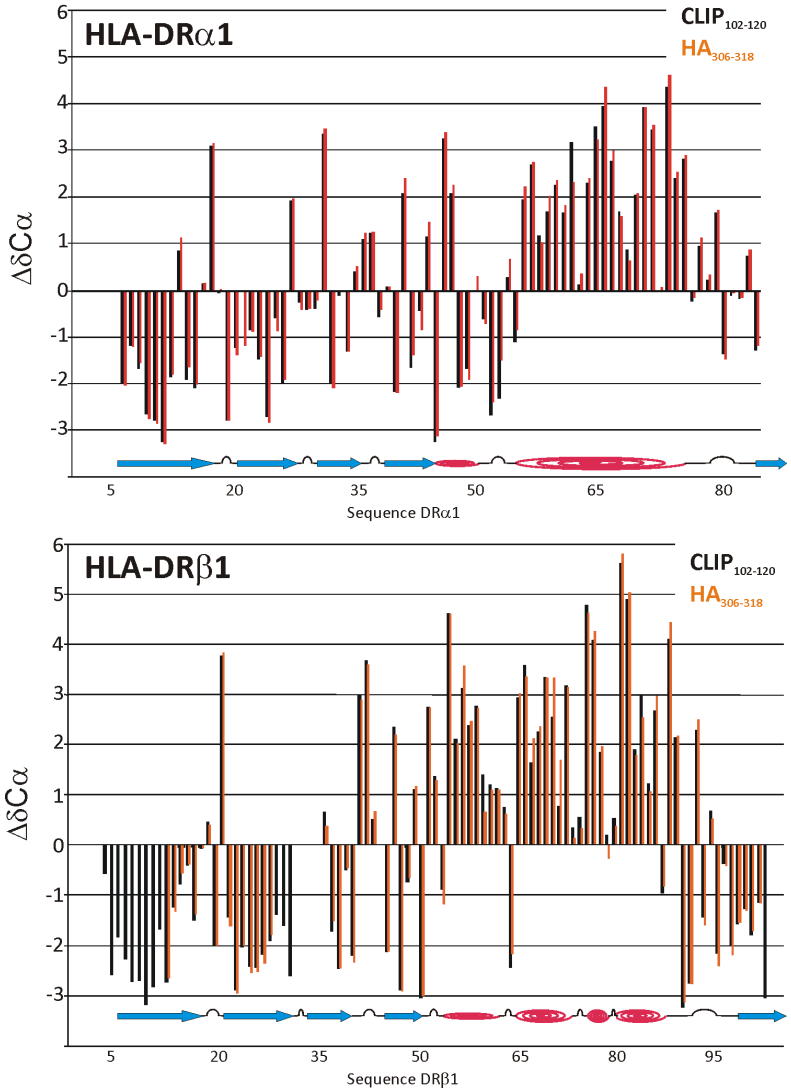

Figure 3.16: Cα-chemical shift analysis of HLA-DR1 subunits α1 (top) and β1 (bottom) when in complex with either HA or canonically bound $CLIP_{102-120}$. Plotted are the differences between Cα chemical shifts and empirically determined random coil values[114]. Clearly positive differences represent α-helices and negative values are indicative for residues in β-sheets. Below the plot secondary structure elements for α1 and β1 from crystal coordinates (pdb code 1dlh) are shown.

3.3.4 H/D exchange experiments

Having demonstrated secondary structure integrity in peptide-complexes of HLA-DR1 it was further asked if domain stabilities were reflected in experiments that probe the accessibility of amide protons to replacement by deuterons. The technique of H/D exchange is often used to study in particular folding processes and transitions in conformations[63,115] which occur on a time scale of several seconds to hours.

The following experiments were carried out for two reasons: i) to probe the applicability of recombinant pMHCII complexes in hydrogen-to-deuterium exchange studies and ii) to verify the presence and to determine the relative stability of secondary structure elements. It was expected that exchange would proceed to a smaller extent in stable immunoglobulin folds (marking the membrane proximal domains α2 and β2) with strong inter-sheet H-bonds than for helix-dominated α1 and β1 domains. Thereby a verification of the results described in section 3.3.3 would be obtained.

To replace protons with deuterium the protein had to be buffer exchanged. This was achieved by lyophilizing (freeze-drying) the sample from protonated buffers with subsequent re-dissolving in the same volume of D_2O. This had the advantage of small dead times since samples could be directly transferred to the spectrometer after dissolution. On the other hand, in certain cases freeze-drying destroys a protein's native fold.

It was therefore first tested if lyophilized HLA-DR1 in complex with viral HA was spectroscopically identical to its original state. A DRβ-^{15}N-labeled sample of HLA-DR1/HA was freeze-dried and dissolved in pure H_2O. The protein was completely soluble as judged by optical inspection. ^{1}H-^{15}N-HSQCs were measured before and after lyophyllization with identical settings. Panel A, left side, of figure 3.17 shows that the overlaid spectra display identical chemical shifts of respective residues. Thus, it was concluded that the freeze-dried protein could be completely restored as a prerequisite for exchange experiments.

Next, lyophilized HLA-DR1/HA was dissolved in D_2O to determine how many amide resonances of the β-chain were still present in an HSQC after exchange for ~25 minutes. If all amides were exchanged within minutes the determination of exchange rates would not have been possible. As shown in the right panel in part A of figure 3.17, approximately half of all resonances were still present when compared to the lyophilized reference sample dissolved in water. Almost no side chain amides were found in the spectrum and the average signal

intensity was decreased notably. However, the identification of particular amide resonances confirmed the general applicability of the approach.

To examine peak intensity changes over time individual resonances had to be re-assigned in D_2O. Small differences in pH (compare pD=pH+0.4)[116] were measurable although this effect had been compensated by pH-adjustment before lyophyllization. 67 of 170 assigned residues could be defined unambiguously after dissolving HLA-DR1/$CLIP_{106-120}$ in deuterium after 30 minutes. The sample was investigated for more than 1500 minutes with HSQC experiments recorded each ~30 minutes. Approximately half of all resonances had undergone full H/D exchange after the first spectrum. Identifiable peaks were mapped to the primary structure of HLA-DR1 as shown in panel B of figure 3.17. Obviously, the major fraction of exchange-resistant amides was located in DRβ2. This result was in line with expected higher stability of the pure Ig-fold of DRβ2 compared to the mixed α/β fold of DRβ1.

A robust determination of exchange rates was not possible because of large fitting errors. Instead, residues were sorted into four categories of exchange with residual protonation after at least 30 minutes, 100 minutes, 300 minutes and 1000 minutes (see color code in bar chart of panel B). Exemplarily, panel C of figure 3.17 shows a magnification of superimposed HSQCs from the four selected time points. Whereas T51 and S63 were not present more than 30 minutes after dissolving the sample in D_2O, T154 and F122 amides were still partially protonated after almost one day. The experiment is summarized in panel D where all re-assigned peaks are mapped onto the structure of HLA-DR1/$CLIP_{106-120}$ by exchange categories. Clearly, the majority of stable amides were found in the anti-paralleled β-sheets of DRβ2 in line with panel B. In sum, an average decline in amide-proton exchange between membrane-proximal DRβ2 and peptide-binding DRβ1 was found, indicating a higher overall stability of the β2 domain. Within DRβ1, β-sheet amides were significantly more stable than helical residues.

Results from H/D experiments show the applicability to pMHCII and are a starting point for addressing questions related to protein flexibility such as local unfolding events. Moreover, the H/D experiment has confirmed secondary structure elements.

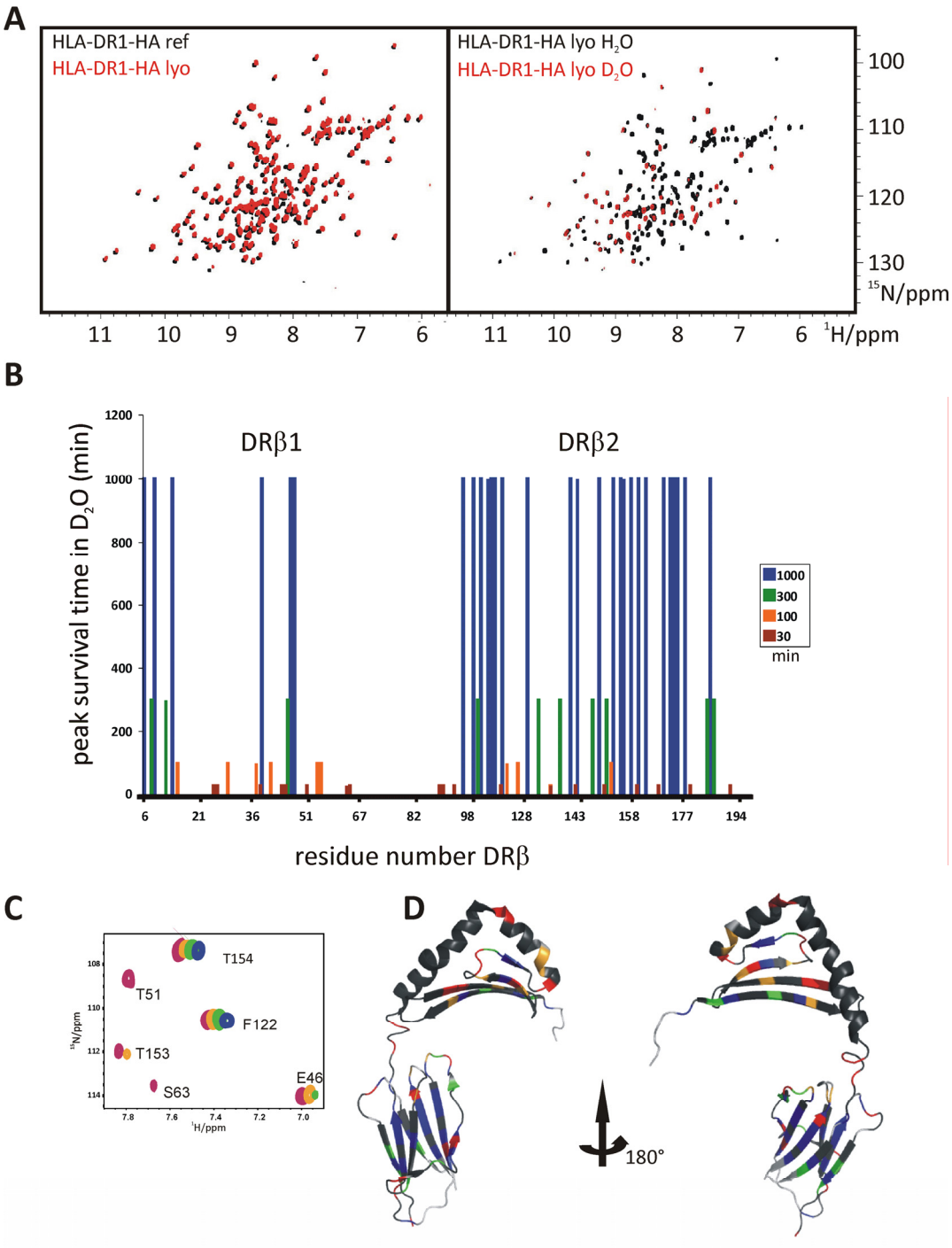

Figure 3.17: H/D exchange in HLA-DR1/peptide complexes. A) Integrity of pMHCII complexes after lyophyllization and re-dissolving in H_2O. Left, ^{1}H-^{15}N-HSQC overlay of HLA-DR/HA, labeled in DRβ, when either measured from a reference or after lyophyllization and re-dissolving in water. Spectra are shifted by 0.02 ppm in ^{1}H relative to each other for easier inspection. Right, Overlay of ^{1}H-^{15}N-HSQC spectra of lyophilized HLA-DR/HA when re-dissolved either in water (black) or D_2O (red). B) Semi-quantitative analysis of H/D exchange in HLA-DR/$CLIP_{106-120}$. Protonated HLA-DR1/ $CLIP_{106-120}$ was lyophilized and re-dissolved in D_2O with immediate acquisition of stacked ^{1}H-^{15}N-HSQC spectra, each of ~30 minutes recording time. Re-assignable residues were plotted against their amide group stability as denoted in the legend. C) Excerpt of ^{1}H-^{15}N-HSQC spectrum showing DRβ resonances from the sample in B. Different rates of proton-deuteron exchange for individual resonances are visible. Spectra are shifted in ^{1}H relative to each other for easier inspection. D) Mapping of all re-assignable resonances to the structure of HLA-DR1/$CLIP_{106-120}$ (only the DRβ subunit is shown) determined by Sebastian Günther (pdb code 3pgc). Individual survival times were color-coded as in B. Uncolored stretches could not be re-assigned or were not detectable after the experimental dead time due to fast exchange.

3.3.5 Peptide exchange observed by NMR spectroscopy in presence of HLA-DM

Resonance assignments for HLA-DR1 in complex with peptides allowed monitoring peptide exchange with site-specific resolution.

Figure 3.18 displays the exchange of $CLIP_{102-120}$ for viral HA in presence of equimolar amounts of HLA-DM. HA was added in steps of half-, equi- and 10-fold molar stoichiometries relative to HLA-DR1/$CLIP_{102-120}$ followed by immediate acquisition of ^{1}H-^{15}N-HSQC spectra containing resonances solely from ^{15}N-labeled DRβ. The spectral overlay reveals a slow-exchange regime relative to the NMR time scale displayed by two distinct populations at the half-molar titration point. Each of them refers to one of the complexes (HLA-DR1/$CLIP_{102-120}$ and HLA-DR1/HA, respectively). This was expected as stable pMHCII complexes show low off-rates. Higher affinity of HA compared to CLIP is expressed by almost exclusive presence of HA-related resonances at a HLA-DR1:CLIP:HA-stoichiometry of 1:1:1. No further change in peak intensity was found when HA was added in 10-fold excess. The figure shows two types of peaks: i) perturbed by peptide exchange or ii) unaffected.

The experiment demonstrates that exchange of bound antigens can be followed for individual residues. The NMR spectra proved the fast and complete replacement of CLIP in the presence of HLA-DM as happens within lysosomal compartments of professional APCs.

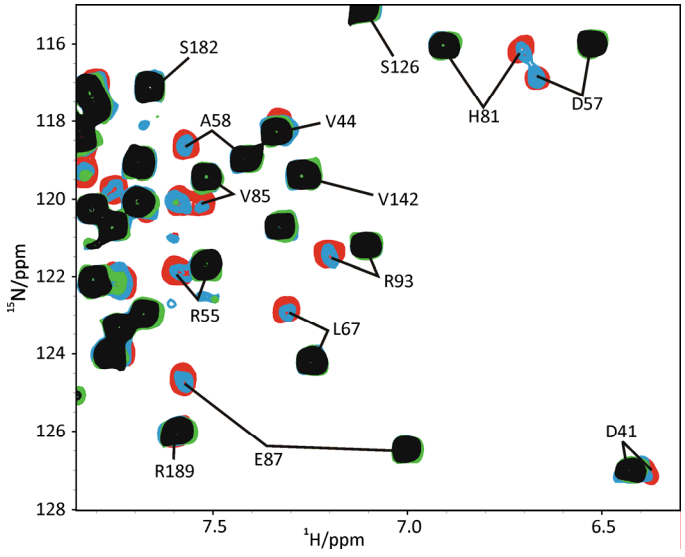

Figure 3.18: CLIP-to-HA peptide exchange observed in 2D-NMR. Overlay of ^{1}H-^{15}N-HSQCs showing DRβ-labeled HLA-DR1 in complex with $CLIP_{102-120}$ (red) in presence of equimolar HLA-DM and increasing amounts of HA peptide. CLIP: HA molar ratios are 2:1, blue; 1:1, green and 1:10, black. Selected known assignments are shown for respective pMHCII complexes.

Having verified or re-assigned spectral assignments of both pMHCII complexes combined chemical shift differences were calculated. Figure 3.19, panel A, shows a plot of differences for all NH-backbone resonances sorted by subunits. In panel B significant chemical shift differences were mapped to the surface of HLA-DR1 indicating “hotspots” of sensitivity. The structure in complex with canonical $CLIP_{102\text{-}120}$ (pdb code 3pdo) had been determined in collaboration with Sebastian Günther, Dr. Olaf Rötzschke, Yvette Roske and Udo Heinemann (see section 3.4).

Significant shifts exclusively mapped to the peptide binding domains α1 and β1 as was expected from a consistent HLA-DR1 architecture in known structures. They indicated binding-sensitive HLA-DR1 residues to be only in direct vicinity of the antigenic peptide. Notably, a structural proof for the integrity of membrane proximal domains in solution had been missing so far. Although a detailed structural mechanism of peptide substitution cannot be revealed by such an experiment, residues chemically involved were unambiguously defined for the exchange process.

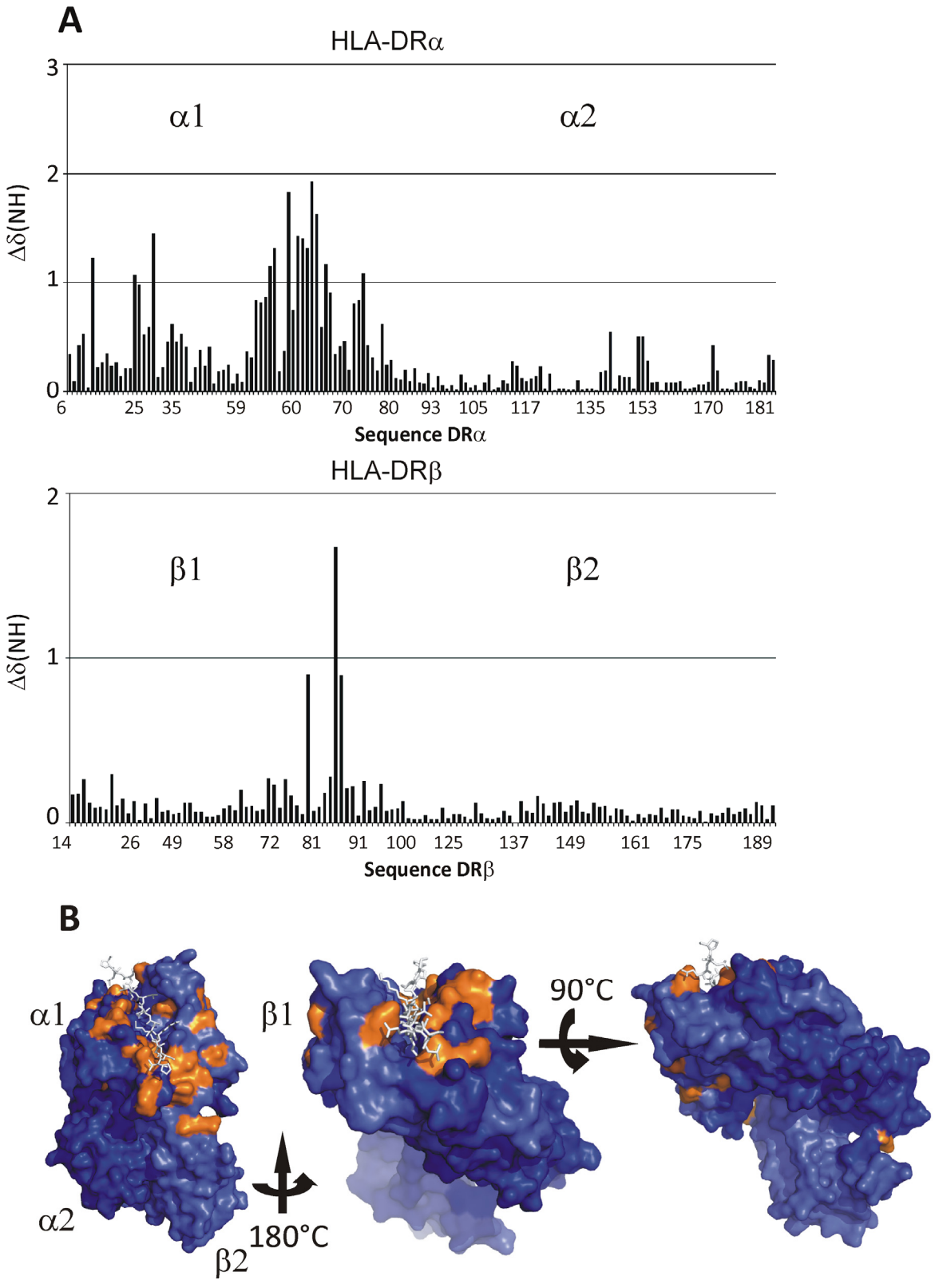

Figure 3.19: Chemical shift perturbations from CLIP-to-HA exchange mapped to the crystal structure of HLA-DR1 in complex with $CLIP_{102-120}$ (pdb code 3pdo). In A, all changes in chemical shifts are shown for residues that could be assigned unambiguously for both complexes in either DRα (top) or DRβ (bottom). B, significant chemical shift differences are mapped to HLA-DR1 providing an epitope map on the peptide binding domains α1 and β1. The peptide $CLIP_{102-120}$ is shown as white sticks.

3.4 Bivalent binding mode of CLIP peptides when bound to HLA-DR1

In parallel to high resolution multidimensional NMR the route of crystallizing HLA-DR1 has been followed. To this point the crystallization of bacterially produced human MHCII in complex with natural peptides had been achieved with the help of stabilizing proteins like superantigens[117] or in the presence of a T cell receptor[118]. This thesis successfully combined information from "pure" HLA-DR1 crystal structures and NMR experiments to unravel novel aspects of pMHCII complexes.

3.4.1 Crystal structures of CLIP length versions 106-120 and 102-120

In collaboration with Sebastian Günther (FMP, MDC Berlin) crystal structures of peptide-bound HLA-DR1 without stabilizers were obtained. All statistics on crystals and structures are summarized in[98] if not denoted differently.

To correlate data from NMR studies with coordinates from crystal structures HLA-DR1 was crystallized in complex with two versions of CLIP (see sequences in figure 3.20, part A). These two CLIP variants had been described before to be present in pools of peptides stripped from antigen presenting cells[119,120]. Presumably, both are a product of Invariant chain cleavage by cathepsins. No structure had been published from HLA-DR1/CLIP before. HLA-DR1 with CLIP version 106-120 was crystallized at room temperature from a co-refolded sample that had been used for NMR before. In the structure, surprisingly, the $CLIP_{106\text{-}120}$ was positioned in the opposite orientation to any other peptide observed before (see figure 3.20, panel B, left side). In fact, the inverted alignment of N-and C-terminus at the same time still provided a reasonable occupation of pockets (see panel C) and maintained almost all H-bonds between peptide and protein.

When crystallizing HLA-DR1 with co-refolded longer $CLIP_{102\text{-}120}$ immediately after purification the canonical peptide N-to C- orientation was found. Part B of figure 3.20 opposes both structures showing that the overall protein fold is identical and also fits previous structures of HLA-DR1. Both complexes were crystallized at room temperature and under similar conditions. The inverted alignment was likely to be enabled by the peptide symmetry relative to pocket position P5 in HLA-DR1 (see panel C of figure, where P5 is central to the distance between P1 and P9). In either orientation the crucial anchor positions P1 and P9 are occupied with methionines. Since pocket occupations in positions 4 and 6 are also possible in both orientations, the two major requirements of peptide binding - preservation of the H-

bond network and favorable pocket interactions - are met in both canonical and inverted complexes.

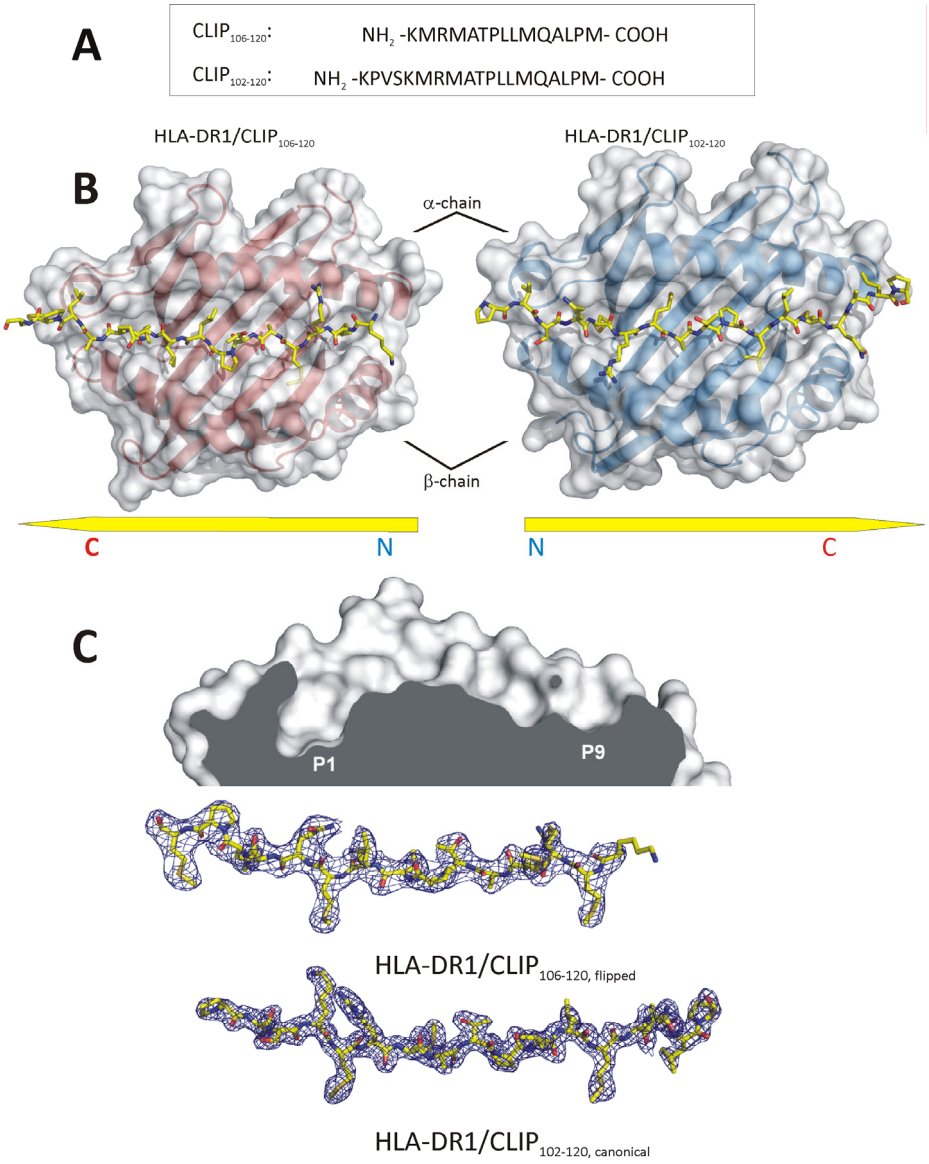

Figure 3.20: Crystal structures of HLA-DR1 bound to CLIP length variants when grown at room temperature. A) Amino acid sequences of CLIP variants used in this study. In B, the left panel shows the crystal structure of HLA-DR1 bound to $CLIP_{106–120}$. The right side shows the analogous view onto the structure of HLA-DR1/$CLIP_{102–120}$. The arrows indicate peptide orientations. Structures are shown as semitransparent surface top view (white) onto α1β1 domains, with the ribbon presentation embedded. The relative positions of the domains are indicated. Peptides are displayed as sticks. C) Upper: Lateral cut of the binding groove of HLA-DR1 (peptide removed), highlighting the antigen-binding pockets P1 and P9. Lower: Electron density maps of peptides derived from the crystal structures of HLA-DR1/$CLIP_{106–120}$ and HLA-DR1/$CLIP_{102–120}$ are shown from the same perspective inside the binding groove. Parts of the figure have been provided by Sebastian Günther.

It was further asked if the inverted orientation of $CLIP_{106-120}$ on the surface of HLA-DR1 was an artifact based on crystal packing. Freshly co-refolded HLA-DR1/ $CLIP_{106-120}$ was subjected to a second crystal screen at 4°C. Here the peptide was positioned in the canonical way

similar to $CLIP_{102-120}$ (see figure 3.21). Structures of canonical CLIPs were almost fully superimposable leaving an overhang of amino acids 102-105 which span the "left" terminal part of the HLA-DR1 binding cleft. In fact, exactly this site is unoccupied only when short CLIP (106-120) is orientated canonically (see figure 3.21), but not in the reverse orientation (see Figure 3.20). Possibly, crystallization of the canonical form was promoted when low temperatures did not allow excess mobility for inversion.

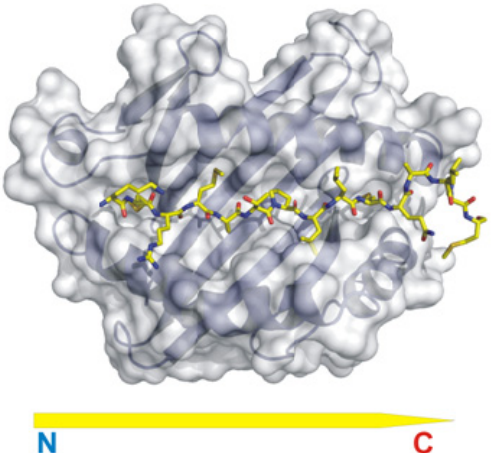

Figure 3.21: Crystal structure of canonical HLA-DR1/$CLIP_{106–120}$, when grown in a screen carried out at 277 K. The structure is shown as in the previous figure with the arrow indicating the peptide orientation. Parts of the figure have been provided by Sebastian Günther.

3.4.2 The dynamics of $CLIP_{106-120}$ reorientation assessed by NMR spectroscopy

I decided to further investigate peptide inversion by NMR in order to proof peptide re-orientation in solution and to unravel the kinetics of exchange.

3.4.2.1 Dynamic $CLIP_{106-120}$ peptide re-orientation

Presumably, the observed lack of contacts between the N-terminus of short canonical $CLIP_{106-120}$ and HLA-DR1 could determine peptide orientation. We therefore compared the atomic details between canonical and inverted $CLIP_{106-120}$ at the β1-chain helical end around residues 85-95 and at the opposing helical formation in α1 (residues 45-55). A lack of two possible H-bonds from canonical $CLIP_{106-120}$ to HLA-DR1 is visible (see figure 3.22, part A). While all contacts to the β1-helix were saturated, hydrogen bonds of the peptide backbone with α-chain helical residues phenylalanine 52 and serine 53 remained unsatisfied. Since these hydrogen bonds belong to the essential and conserved H-bonds in pMHCII complexes[121] this was assumed to be of relevance for thermodynamic stability.

NMR experiments on HLA-DR1/ $CLIP_{106-120}$ over time showed large spectral rearrangements when observed in ^{1}H-^{15}N-HSQC backbone spectra. As demonstrated in panel B of figure 3.22 the HSQC measured directly after co-refolding differed from the spectrum five days later. Several peaks showed significant differences in chemical shifts. Protein degradation and aggregation have been ruled out as neither peak broadening nor characteristic resonances of degraded fragments were visible. The oxidation of methionines in CLIP as cause of spectral changes was not supported by mass spectra obtained from NMR samples. A spontaneous release of CLIP was unlikely because in the following this particular sample was used to determine the inverted $CLIP_{106-120}$ structure with HLA-DR1. In the light of the crystallographic findings it was rather likely that within five days bound $CLIP_{106-120}$ changed its orientation relative to HLA-DR1. Presumably, a distinction between a kinetically trapped form (mediated by conditions from refolding) and a thermodynamically more stable conformation (additional H-bonds after inversion) had to be made for HLA-DR1/peptide complexes.

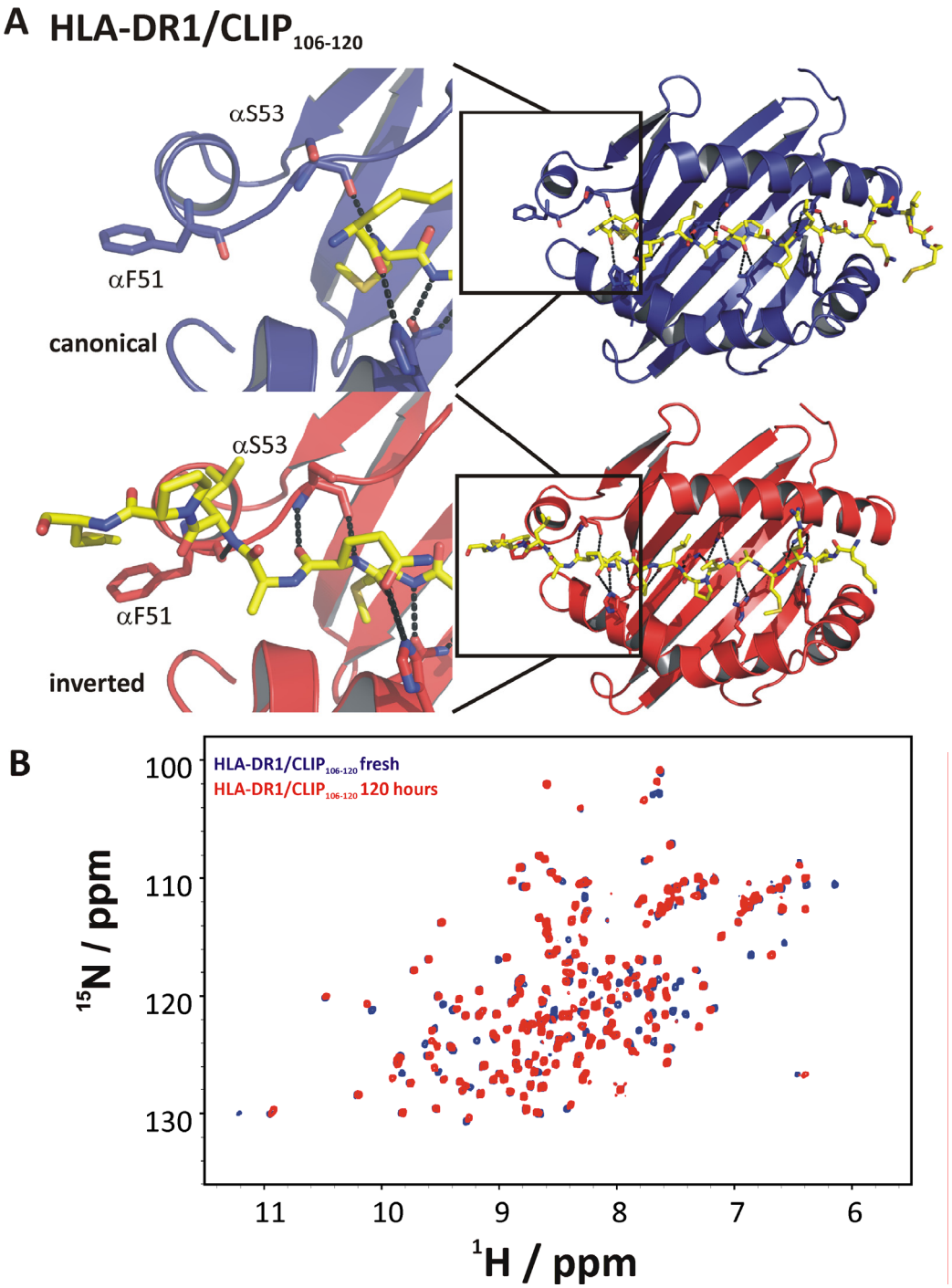

Figure 3.22: Structural proof of $CLIP_{106-120}$-inversion. A lack of hydrogen bonds is the likely driving force in $CLIP_{106–120}$ reorientation when bound to HLA-DR1. In A, right panel, is shown a comparison of ribbon-displayed structures of HLA-DR1 (only α1β1 displayed, top view) with canonical or inverted $CLIP_{106-120}$. The left side magnifies the binding cleft region harboring the canonical peptide's N terminus of HLA-DR1 crystal structures in complex with $CLIP_{106–120}$, color coded as in the right panel. The peptide ligand is shown in yellow. B shows a ^{1}H-^{15}N-HSQC overlay of β-chain labeled HLA-DR1 in complex with $CLIP_{106-120}$ either when measured directly after co-refolding (blue) or 5 days later with incubation at 310 K.

3.4.2.2 Mapping of chemical shift changes during CLIP$_{106-120}$ peptide flip

Changes in amide chemical shifts during the peptide inversion were expected to map to the α1/β1 domains. To examine affected residues peptide inversion was monitored in DRβ. Indeed, significant shift differences were found for β1- but not β2-residues. This is shown in figure 3.23, part A where a spectral zoom-in of figure 3.22, panel B is shown. Residue number 95 marks the transition from β1 to β2 domains. When plotting all assigned residues with their chemical shift changes during inversion (see part B in figure 3.23) the effect unambiguously mapped to β1 and was sensed by the entire domain. Peptide flipping was reminiscent to the exchange of CLIP to HA (see section 3.3.5) and likely included release and rebinding.

Altogether, the existence of two different peptide binding modes in solution was demonstrated, thereby underlining the results obtained by X-ray crystallography.

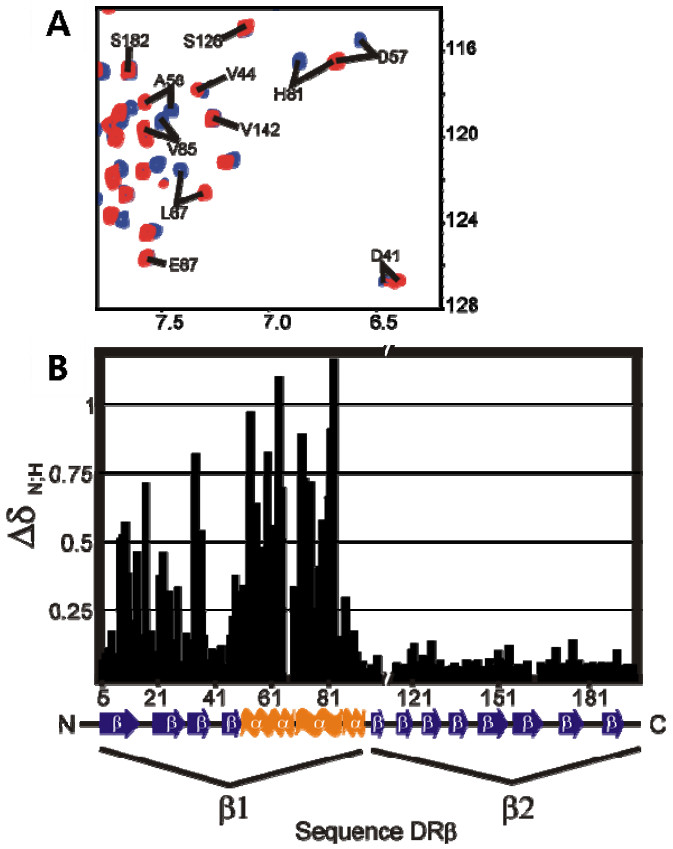

Figure 3.23: Chemical shift mapping of CLIP-inversion. ^{1}H-^{15}N-HSQC overlay of HLA-DR1/CLIP$_{106–120}$ when either measured freshly co-refolded (blue) or after 120 h at 37°C (red) as for figure 3.22. In A, an excerpt is shown with a set of residues. B shows all NH-chemical shift differences in HSQC spectra of co-refolded HLA-DR1/CLIP$_{106–120}$. Values are plotted as combined changes of ^{15}N and ^{1}H chemical shifts (Δδ) against the sequence for HLA-DR1 β-chain residues that are assigned unambiguously in both orientations. The unassigned loop region of β101–115 is not displayed proportionally.

3.4.2.3 Kinetic quantification of CLIP$_{106-120}$ peptide inversion

It was asked if a consistent quantification of the time course of peptide inversion could be deduced from affected resonances. For this, a series of ^{1}H-^{15}N-HSQC spectra was measured starting with a freshly co-refolded sample of HLA-DR1/CLIP$_{106-120}$, ^{15}N-labeled in DRβ. Signal intensities of canonical peaks were determined and fitted to an exponential decay. Panel A of figure 3.24 exemplifies the progressive loss of intensity for residue leucine 67. The half-life of selected residues is plotted in panel B of figure 3.24. In average, the half life of HLA-DR1 resonances with the MHCII bound to canonical CLIP$_{106-120}$ was determined to be about one day (23 ± 3 hours). That would have led to a theoretical loss of more than 95 % of signal intensity after 5 days, which was in line with the observations.

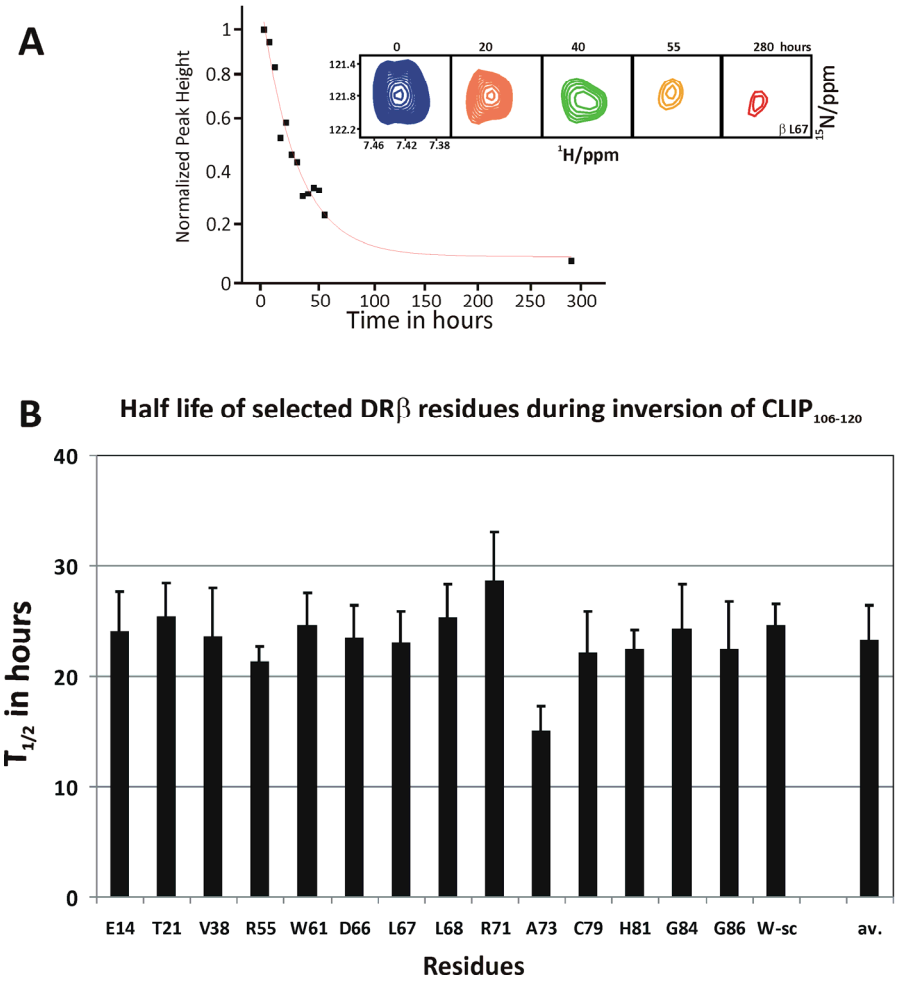

Figure 3.24: Quantitative analysis of the inversion of CLIP$_{106-120}$. The resonance intensities of selected residues from the HLA-DR1 subunit β1 were followed starting from a canonical sample of HLA-DR1/CLIP$_{106-120}$. A) The curve shows the NH-correlating resonance of residue L67 measured repetitively over 300 hours. The intensity loss is demonstrated for selected time points as shown in the ^{1}H-^{15}N-HSQC magnifications. Values were fitted to an exponential decay to deduce the half-life. B) The calculated half-lives are displayed for selected residues. Error bars indicate the uncertainty from curve fitting. W-sc stands for a tryptophan side chain; av. means the average (23.4 ± 3.1 h) with the error given as standard deviation of all plotted residues.

3.4.3 Co-refolding vs. posterior loading of HLA-DR1/CLIP$_{106-120}$ complexes

CLIP$_{106-120}$, when changing its orientation in complex with HLA-DR1, provoked the question if peptide inversion was also observed after posterior loading of CLIP$_{106-120}$ in presence of the MHC loading enhancer FR onto empty protein.

Spectra of *a posteriori* loaded HLA-DR1 were compared to a co-refolded reference which had undergone complete flipping. As depicted in figure 3.25 the loading of short CLIP$_{106-120}$ led to the detection of resonances corresponding to the inverted state of the complex and no changes in spectra were observed over time. Glycines 54 and 86 map to opposite ends of the binding cleft and prove the effect to be not just of local coincidence.

This result confirmed an immediate formation of the thermodynamically more stable inverted pMHCII when CLIP$_{106-120}$ peptide is added to unloaded HLA-DR1.

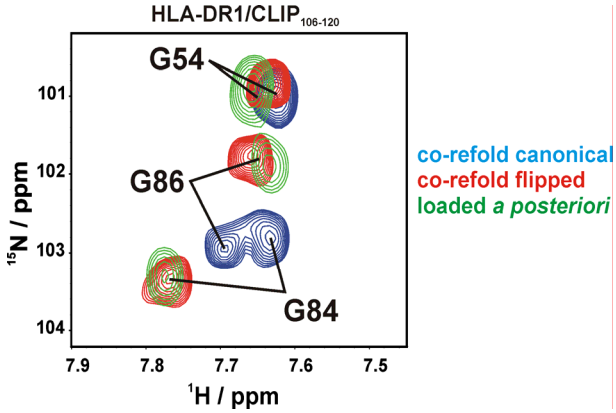

Figure 3.25: Co-refolding vs. posterior loading of HLA-DR1/CLIP$_{106-120}$ complexes. Superposition of overlaid of ^{1}H-^{15}N-HSQC spectra obtained from ^{15}N-DRβ-labeled samples of HLA-DR1 in complex with CLIP as indicated.

3.4.4 Paramagnetic spin-labeled CLIP$_{106-120}$

To more directly proof the inverted conformation of CLIP$_{106-120}$ - when bound to HLA-DR1 in solution - the method of paramagnetic relaxation enhancement (PRE) was applied. PRE restraints become useful for mapping effects to a more extended distance (> 25 Å) and are suited for proteins like MHCII which provide large interaction surfaces. I obtained a modified version of CLIP$_{106-120}$ synthesized by the group of Prof. Dr. Karl-Heinz Wiesmüller (EMC microcollections and University of Tübingen) in which the N-terminal methionine 105 was attached to the PRE-active TEMPO (2,2,5,5-tetramethyl-4-piperidin-1-oxyl) radical bridged by a diaminopropionic acid instead of lysine 106 (see part A of figure 3.26). The unpaired

electron of the radical acts paramagnetic and thereby line-broadens resonances within its vicinity.

To achieve a complete inverted alignment of $CLIP_{106-120}$ empty ^{15}N-DRβ-labeled HLA-DR1 was loaded *a posteriori* with CLIP peptides in presence of MLE. To suppress effects of excess PRE-peptide samples were gel-filtrated before data acquisition. Differences in chemical shifts were found between ^{1}H-^{15}N-HSQCs of both complexes for certain residues and map the the peptide binding cleft (as shown exemplarily in panel B of figure 3.26). Besides the majority of resonances not perturbed by TEMPO, a set of peaks showed notable line-broadening in the presence of the PRE group. Using the correlation between line width and peak height[122] intensity ratios were calculated for all assigned resonances. This is summarized in figure 3.26, part C. Significant deviations from the value for unaffected resonances (< 0.7) were used for surface mapping to the structure of HLA-DR1 (see panel D). The hotspot of PRE action is indicated by the red colored residues which center on P9. This confirmed the peptide N-terminus to be present at the opposite end relative to a canonical orientation.

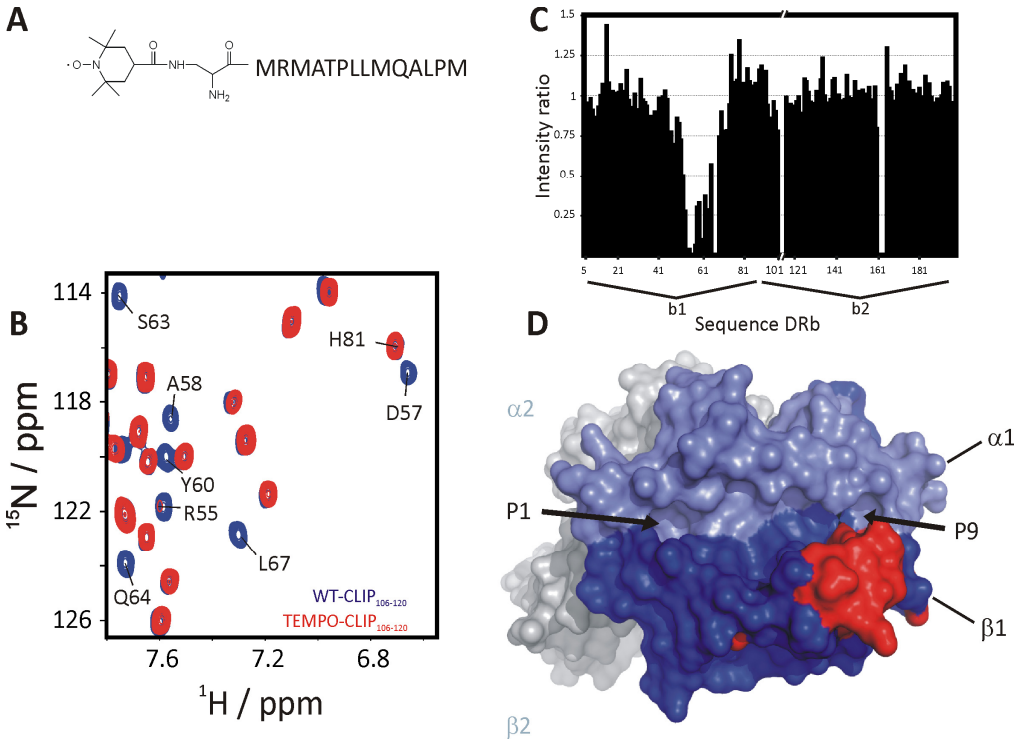

Figure 3.26: Spin-labeled $CLIP_{106–120}$ proves the inverted orientation in solution. A shows the primary sequence of $CLIP_{106–120}$ carrying an N-terminal TEMPO (2,2,6,6-tetramethylpiperidinyloxy) moiety. B displays superimposed ^{1}H-^{15}N-HSQC-NMR spectra showing HLA-DR1 loaded with wild-type $CLIP_{106–120}$ and TEMPO-$CLIP_{106–120}$ subsequently loaded to empty HLA-DR1 (^{15}Nβ). In C, intensity ratios of all unambiguously assigned resonances from both ^{1}H-^{15}N-HSQC spectra were plotted to the HLA-DRβ sequence. P indicates a proline invisible in the HSQC spectrum, and asterisks mark missing assignments. D) Epitope mapping of residues that show significantly reduced HSQC-peak intensities (ratio < 0.7) according to C. The pdb code is 3pgc.

A control experiment with co-refolded TEMPO-$CLIP_{106-120}$ was performed to determine paramagnetic relaxation enhancement around P1. However, the paramagnetic effect of TEMPO was only found for valine 85 (see upper bar chart in panel A of figure 3.27 and spectrum in B). Presumably, one of the harsh steps during purification of complexes (e.g. drastic changes in pH) caused the loss of paramagnetism as would occur from modification of the unpaired electron configuration in TEMPO. The presence of TEMPO-$CLIP_{106-120}$ was confirmed by mass spectrometry together with a mass peak lacking 16 Da in mass. This reflected the loss of oxygen harboring the unpaired electron. Next, chemical shift changes between canonical TEMPO- and wild-type $CLIP_{106-120}$ were investigated. As delineated in the bottom chart of panel A and the spectrum in panel B of figure 3.27, small perturbations mapped to a region around P1 (see panel C). This was possibly caused by the TEMPO moiety. It was concluded that TEMPO-modified $CLIP_{106-120}$ first adopts a canonical orientation when co-refolded with HLA-DR1 similar to wild-type $CLIP_{106-120}$.

The experiments confirm that posterior loading of $CLIP_{106-120}$ to HLA-DR1 yields the peptide in an inverted orientation. The application of PRE-labeling allowed a direct observation of peptide orientation in solution.

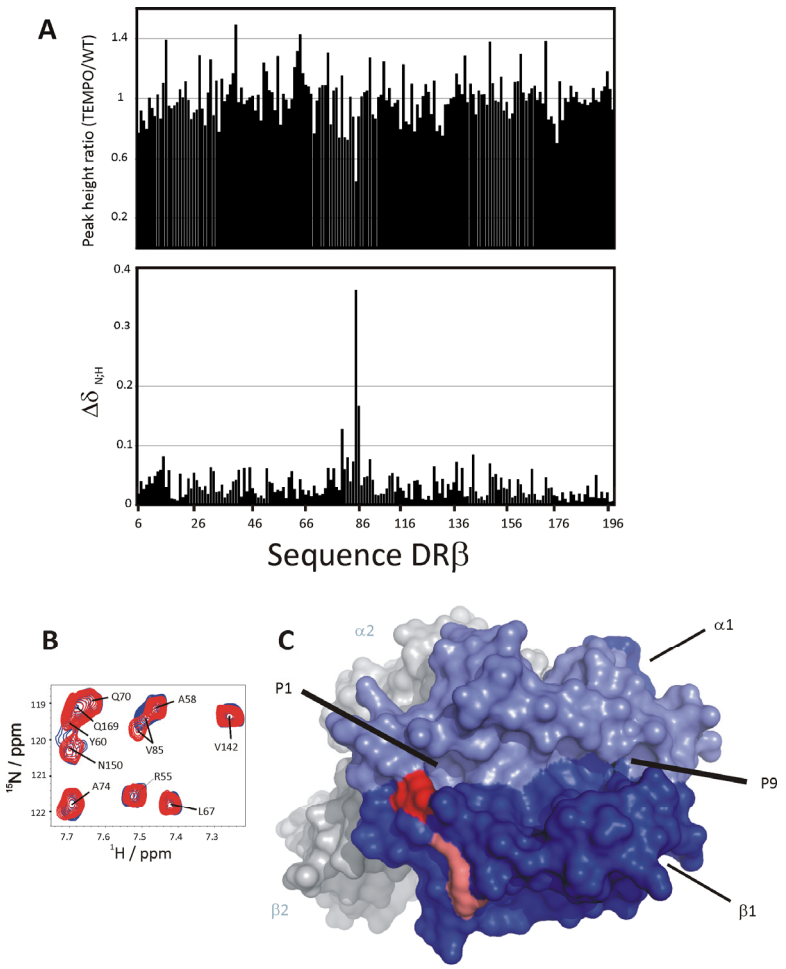

Figure 3.27: PRE-measurement of co-refolded TEMPO-CLIP$_{106-120}$. A) Top panel: Plot of relative HSQC peak intensities comparing HLA-DR1/ TEMPO-CLIP$_{106-120}$ and HLA-DR1/CLIP$_{106-120}$ after co-refolding. Bottom panel: Plot of combined chemical shift differences for all assigned backbone amides between spectra as denoted in the top panel. B) Spectral zoom-in showing overlaid ^{1}H-^{15}N-HSQC spectra for the aforementioned pMHCII complexes with color codes as in figure 3.26. C) Epitope mapping of PRE effect from TEMPO-CLIP$_{106-120}$ (dark red, only valine 85 is significantly affected) and of significant chemical shift perturbations (additional light red) from A.

3.4.5 HLA-DM induced peptide flip of CLIP$_{102-120}$

3.4.5.1 Comparison of canonical CLIP$_{102-120}$ and CLIP$_{106-120}$ in solution

So far the observation of peptide inversion was limited to the short CLIP$_{106-120}$. The N-terminally elongated CLIP$_{102-120}$ was thought to be resistant to inversion based on the existence of the saturated N-terminal H-bond network. However, a dynamic behavior of CLIP$_{102-120}$ was analyzed considering bidirectional orientation to be possible. Therefore, the transfer of NMR assignments from short CLIP$_{106-120}$ to long CLIP$_{102-120}$ was examined first.

Spectra of short CLIP$_{106-120}$ or the longer CLIP$_{102-120}$ co-refolded with ^{15}N-β-labeled HLA-DR1 were acquired. The overlay in figure 3.28 (inset) shows that resonances almost fully merged in their chemical shifts. All differences are summarized in a plot to the β-chain residues (part

A in figure 3.28). Significant peak shifts structurally mapped to the peptide's N-terminal elongation (yellow sticks) in HLA-DR1 (part B of figure 3.28, see color code for subunits). The analogous experiment was carried out with DRα and these shift differences were also considered for epitope mapping (no spectra and plots are shown for DRα).

Thus the small length difference between CLIPs is solely sensed by the adjacent protein surfaces. The involvement of β-residue Cys15, located beneath the binding cleft (see epitope mapping on the frontal, dark-blue β-subunit) is likely mediated via its sulfur bridge with β-Cys79 close to P1. The findings indicate an identical binding mode and register for both canonically aligned peptides.

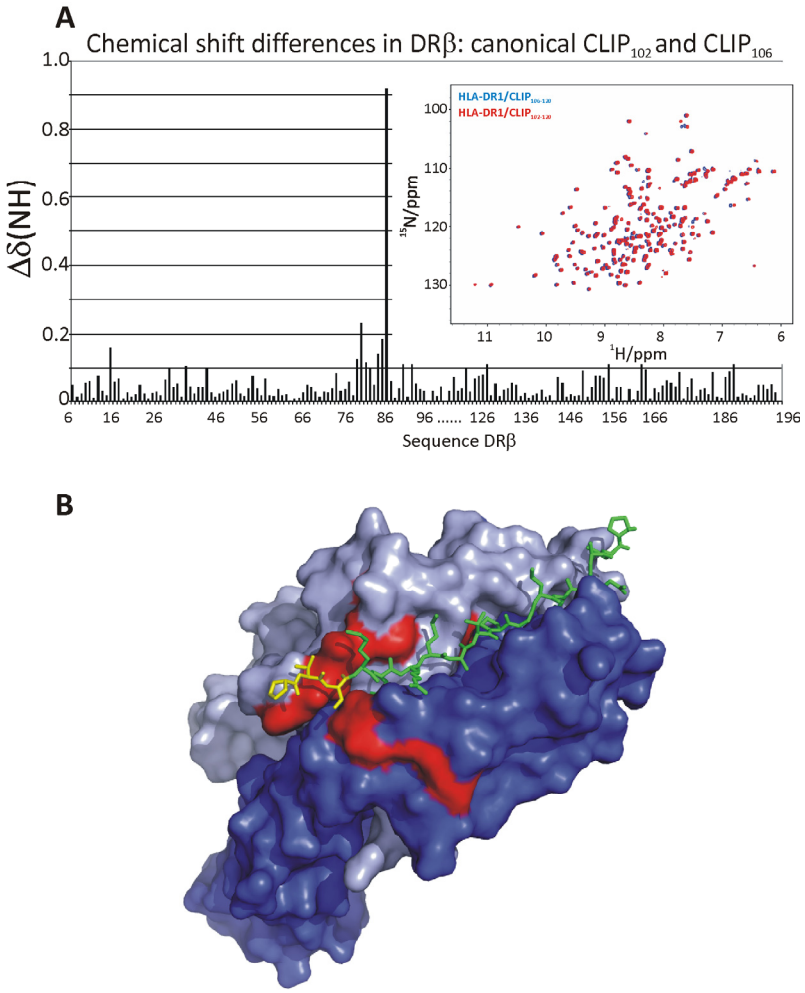

Figure 3.28: HLA-DR1 in complex with canonical versions of CLIP as compared by their fingerprint spectra. A) Plot of differences in combined chemical shifts from all assigned NH-resonances in DRβ when either bound to canonical $CLIP_{106-120}$ or $CLIP_{102-120}$. The inset shows the corresponding ^{1}H-^{15}N-HSQC. B) Mapping of residues (red) that were significantly affected by the difference between canonical CLIPs when bound to HLA-DR1 as sensed by both DRα and DRβ. No spectra and plots are shown for DRα. The structure - obtained from HLA-DR1/$CLIP_{102-120}$ and determined by Sebastian Günther (pdb code 3pdo) - is presented as surface display with DRα in light blue and DRβ in dark blue. $CLIP_{102-120}$ is shown as sticks with residues obtained from the electron density. In yellow are marked amino acids that represent the extension in comparison to the shorter $CLIP_{106-120}$.

3.4.5.2 HLA-DM induced flipping of $CLIP_{102-120}$ acts catalytic to the equilibrium

During long-time measurements of HLA-DR1 in complex with longer $CLIP_{102-120}$ conformational heterogeneity was also measurable by the emergence of a second set of resonances. The process was slow when observed over months in one sample. It was therefore the question if the sample showed degradation or if changes were caused by peptide flipping. In continuously acquired spectra from DRβ-labeled HLA-DR1/$CLIP_{102-120}$ an approximate intensity-leveling of original and new resonances was seen after 5 months.

To clarify if new resonances map to inverted short $CLIP_{106-120}$ a spectrum from equilibrated HLA-DR1/ $CLIP_{102-120}$ was overlaid with either of the spectra from HLA-DR1/$CLIP_{106-120}$. As shown in figure 3.29, panel A, a number of resonances appeared as doubled peaks in the equilibrated sample of longer CLIP indicating two populations. Interestingly, each of the resonances from $CLIP_{102-120}$ fitted a corresponding peak from either canonical or inverted $CLIP_{106-120}$. It was concluded that an equal mixture of canonical and inverted $CLIP_{102-120}$ was present. Thus, both CLIP complexes showed peptide reorientation in solution but with significantly different propensities for the final state. Judged by the similarity of chemical shifts, also flipped fractions of $CLIP_{106–120}$ and $CLIP_{102–120}$ shared structural homology.

Equilibrated complexes were expected to form immediately when loading long $CLIP_{102-120}$ posterior to empty MHCII. ^{15}N-DRβ-labeled HLA-DR1 was loaded with an excess of peptide. When comparing the resonances with an equilibrated sample spectra were almost identical. This is proven by the spectral overlay shown in figure 3.29, part B. In line with results from the short $CLIP_{106-120}$ it was concluded that posterior loading of peptides to MHCII leads to the lowest energy state for the complex.

Based on these findings, the effect of HLA-DM to samples with co-refolded CLIPs was examined. Considering a transient peptide release during peptide reorientation and exchange these processes were expected to be enhanced by HLA-DM as the chaperone interacts with MHCII and stabilizes its empty state[123]. Intrinsic peptide inversion of long $CLIP_{102-120}$ was compared to catalyzed exchange in the presence of stoichiometric amounts of HLA-DM. Part C of figure 3.29 shows the formation of equilibrated HLA-DR1/$CLIP_{102-102}$ in the presence of HLA-DM within the experimental dead time of 30 minutes. In contrast, spectral monitoring of progressive intrinsic inversion indicates equilibration over weeks. Catalysis was confirmed with short $CLIP_{106-120}$ which immediately was found fully inverted in the

presence of HLA-DM (not shown). Altogether, HLA-DM acted catalytic to the inversion of peptide and formation of binding equilibria for HLA-DR1/CLIP complexes.

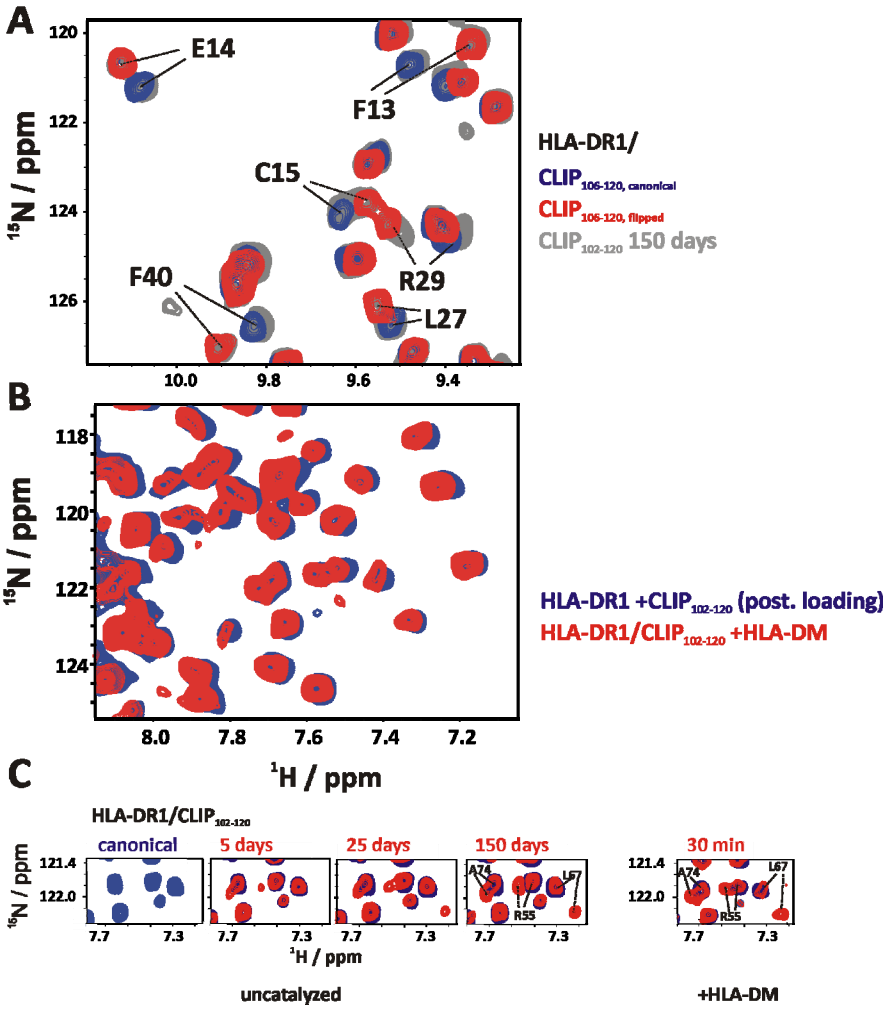

Figure 3.29: HLA-DM catalyzes CLIP peptide re-orientation. A) Magnified overlay of ^{1}H-^{15}N HSQC spectra acquired for co-refolded HLA-DR1/$CLIP_{102–120}$ after 150 d (gray) or for co-refolded $CLIP_{106–120}$ fresh (blue) or after 5 d (red). B) Spectral overlay of DRβ-labeled HLA-DR1, *a posteriori* loaded with $CLIP_{102-120}$ (blue) and HLA-DM edited co-refolded HLA-DR1/ $CLIP_{102-120}$. C) Left: superimposed region of ^{1}H-^{15}N HSQC spectra showing HLA-DR1/$CLIP_{102–120}$ when freshly co-refolded (blue) or at indicated time points (red). Right: Interconversion of the same resonances when equimolar amounts of HLA-DM were added before spectral acquisition. Representative resonances are indicated.

3.4.6 Exchange of bidirectional CLIP peptides by HA peptide

Considering that two CLIP orientations could be formed from MHC-peptide-editing in cells it was asked whether exchange by high affine antigenic peptides would occur for HLA-DR1-CLIP complexes independent of peptide directionality. The Influenza hemagglutinin-derived HA-peptide was used to investigate peptide exchange by HLA-DM. Figure 3.30 clearly shows identical HLA-DR1/HA complexes after exchange independent of the previous CLIP orientation by means of three resonances in DRβ1.

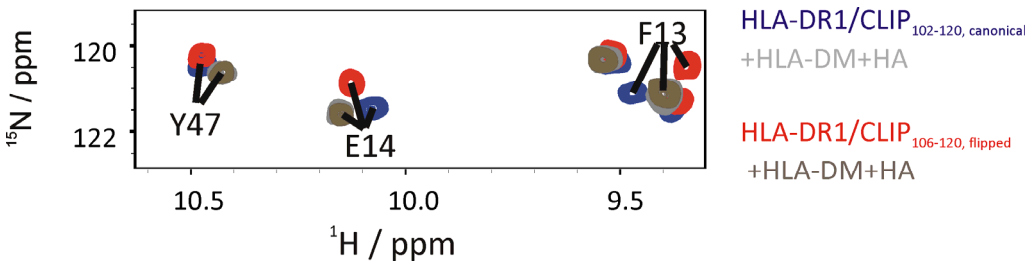

Figure 3.30: Exchange of bidirectional CLIP peptides by HA peptide. Shown are superimposed ^{1}H-^{15}N-HSQC spectra of HLA-DR1 /$CLIP_{102–120}$, representing canonical CLIP, HLA-DR1/$CLIP_{106–120}$ representing inverted CLIP, and spectra of these two samples after HLA-DM–catalyzed exchange against $HA_{306–318}$. The samples were labeled in DRβ.

Thus, both CLIP orientations were still susceptible to replacement by higher affine binders, which is a prerequisite for a conceivable intracellular function of inverted MHCII-peptide complexes. Hence, a simultaneous existence of both orientations *in vivo* is considerable.

3.4.7 Linked HLA-DR1/CLIP complexes for stable peptide orientation

3.4.7.1 Rational design of linker constructs

The existence of pMHCII complexes with an inverted binding mode has been shown *in vitro* here. While a potential intracellular presence of such complexes will be difficult to prove, their existence on cell surfaces would be easier to investigate. One option could be antibodies that are restricted to one orientation of the peptides. Therefore pMHCII complexes with one stable orientation for antibody generation were designed. It was asked if genetic linkage of peptides to either of the subunits would allow refolding of stable complexes with unidirectionally bound CLIP. Acquired NMR spectra were expected to be sufficiently similar to the spectra of either canonically or inversely bound non-linked CLIP peptide and to allow the rapid resonance assignments of the linked constructs.

Figure 3.31 outlines the strategy of my fusion construct design. Published studies[124] gave the rational for a 15mer linker comprising a triplet of $glycine_4serine$. This was linked to the N-termini of either the DRα or DRβ subunit, followed N-terminally by $CLIP_{106-120}$ with an additional starting methionine. While this approach has been used to link peptides to DRβ subunits, no experience for DRα-linkage was available at that time.

DRβ-linked CLIP was expected to yield the canonical alignment. In turn, inverted alignment of CLIP was expected when linked to DRα (see figure 3.31). During refolding fused chains were used with the complementary wild-type subunit.

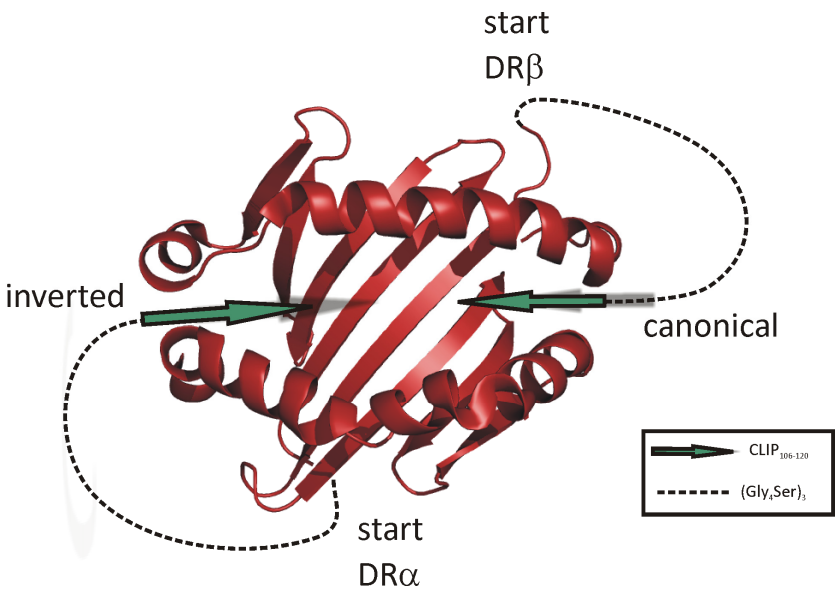

Figure 3.31: Principle of genetic linkage of $CLIP_{106-120}$ to HLA-DR1 subunits via N-termini. The peptide sequence was preceded by a starting methionine and prolonged by a $(Gly_4Ser)_3$ linker sequence. The picture shows a ribbon display of HLA-DR1 with α1β1 top view only. Refolding was carried out in presence of the unmodified complementary subunit.

3.4.7.2 Biochemical and spectroscopic characterization of linker constructs

HLA-DR1/$CLIP_{106-120}$ fusion proteins were successfully refolded by the same technique as unmodified proteins. As shown in part A of figure 3.32, proteins were soluble and pure. SDS-resistance of heterodimers and sensibility to reducing agents were found in DRα-linked HLA-DR1/CLIP. No SDS-resistant heterodimer was observed for DRβ-linked HLA-DR1/CLIP. Interestingly, the correlation of CLIP orientation and SDS-stability was confirmed by complexes with unlinked peptide (panel A of figure 3.32, compare lanes 3, 4, 6, 7, and 8). This indicated the presence of CLIP-orientations as intended by design.

A direct proof for designed CLIP-orientations in complexes was desirable. Therefore, HSQC spectra from HLA-DR1 samples with fused CLIP were compared to reference spectra with non-covalently attached CLIP. An inverse-labeling-strategy was used, in which the unmodified subunit was NMR-visible. First, this suppressed overlap with unassigned resonances from linker and peptide. Second, I expected chemical shift changes at the sites of linker-attachments in the respective subunits.

Spectral quality was similar to unlinked complexes confirming successful refolding. In ^{15}N-DRα-labled samples free canonical CLIP was compared to DRβ-linked $CLIP_{106-120}$. Convincingly, spectral fits (see figure 3.32, part B, left panel) indicate that the peptide was

canonical when fused to the β-chain. In contrast, peptide-fusion to DRα led to a good superposition with the reference spectrum of inverted $CLIP_{106-120}$ in ^{15}N-DRβ-labled samples. Small chemical shift perturbations were likely to be caused by the linker.

Thus, $CLIP_{106-120}$-linkage to HLA-DR1 subunits via a 15mer linker was successful in biasing one peptide orientation. The result was a prerequisite for reliable production of orientation-dependent antibodies.

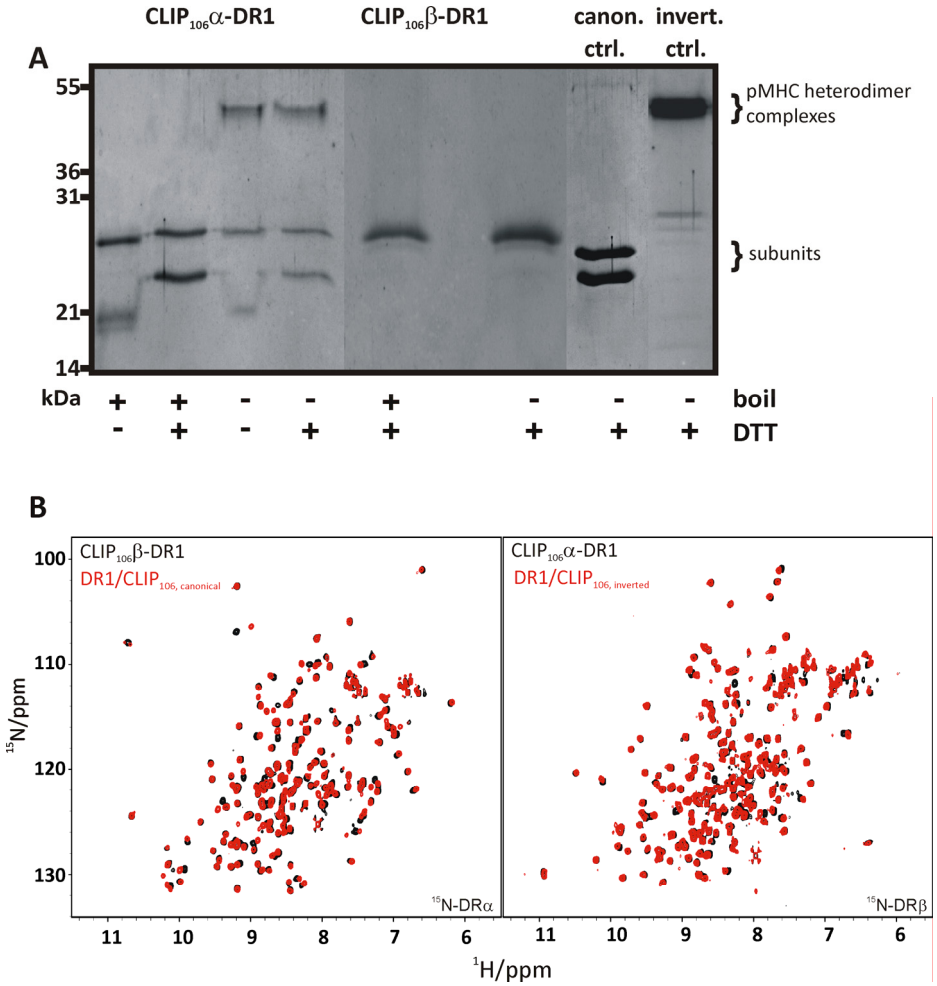

Figure 3.32: Characterization of $CLIP_{106-120}$-linked HLA-DR1 versions. A) HLA-DR1/CLIP complexes probed for SDS-resistance in dependence of peptide orientation. SDS-PAGE analysis of samples as indicated with or without prior boiling. In addition, DRα-linked $CLIP_{106-120}$ has been tested for the presence of disulfides by adding dithiothreitol (DTT). B) Left, Spectral overlay of ^{1}H-^{15}N-HSQCs recorded from samples of HLA-DR1, labeled in DRα, when either bound to fused $CLIP_{106-120}$ (black) or canonical non-linked $CLIP_{106-120}$ peptide. Right, spectral overlay of ^{1}H-^{15}N-HSQCs recorded from samples of HLA-DR1, labeled in DRβ, when either bound to fused $CLIP_{106-120}$ (black) or inverted free $CLIP_{106-120}$.

3.4.7.3 Crystal structure of $CLIP_{106-120}$α-DR1

To correlate NMR spectra with atomic coordinates CLIP-fused HLA-DR1 was subjected to crystallization. Whereas no crystals were grown for canonical DRβ-linked $CLIP_{106-120}$ a

structure for DRα-linked $CLIP_{106-120}$ was obtained (not deposited in pdb, yet). The fused peptide was found inverted with pocket occupation and H-bond network identical to non-linked $CLIP_{106-120}$ (see figure 3.33). No linker residues were identified with sufficient electron density. Likely, high linker flexibility also allowed co-refolding of $CLIP_{106-120}$ in the given register. A direct alignment of the structure with the one derived for non-linked inverted $CLIP_{106-120}$ showed the linker not to interfere with protein folding and did not alter side chain conformations of crucial MHCII residues.

Presumably, the lack of crystallization of DRβ-linked CLIP was caused by sample heterogeneity. A closer inspection of HSQC spectra revealed a fraction of ~10 % that neither mapped to "canonical" nor "inverted" peaks. Nevertheless, the structure of DRα-linked CLIP was in line with results from NMR studies confirming the rationale of the complex design in terms of intended peptide orientation.

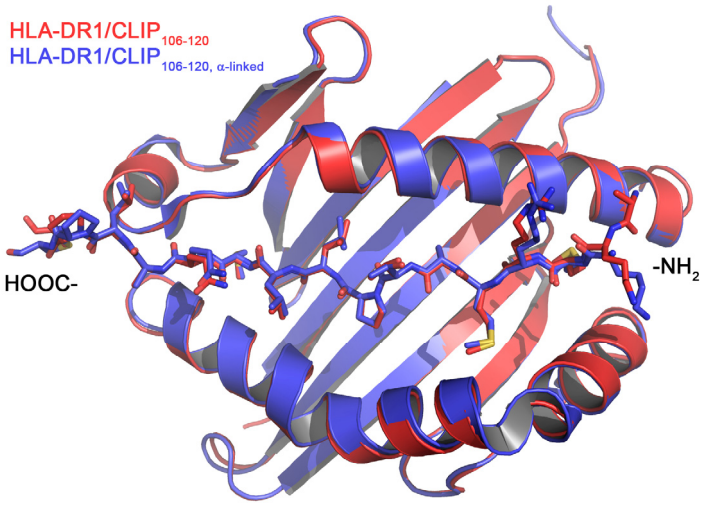

Figure 3.33: Crystal structure of $CLIP_{106-120}$ linked to the α-chain of HLA-DR1 aligned with HLA-DR1 in complex with non-linked flipped $CLIP_{106-120}$, (pdb code 3pgc). Only the α1/β1-domains are shown as ribbon presentation. The peptide is presented as sticks. The amino- and carboxy-termini are indicated.

3.4.7.4 Susceptibility of $CLIP_{106-120}$-DR1 fusion proteins to HLA-DM

For the generation of antibodies pMHCII complexes would have to remain stable in peptide orientation over longer periods of time. Also expression and secretion of MHC-fused peptides on surfaces of transfected cells would have to pass editing in the endosome. To investigate editing of HLA-DR1/$CLIP_{106-120}$ fusion proteins by HLA-DM, samples were mixed with stoichiometric amounts of the natural catalyst. This served to quickly unravel peptide isomerism which might form very slowly without HLA-DM. As demonstrated in spectra of

figure 3.34 both complexes showed no chemical shift perturbations after addition of HLA-DM. Thus, $CLIP_{106-120}$, linked to one of the subunits, was stabilized in one orientation and remained aligned in a trapped binding mode from the very time point of folding.

Altogether, linked complexes of HLA-DR1/$CLIP_{106-120}$ seemed suitable for producing CLIP-orientation-dependent antibodies for cell surface detection.

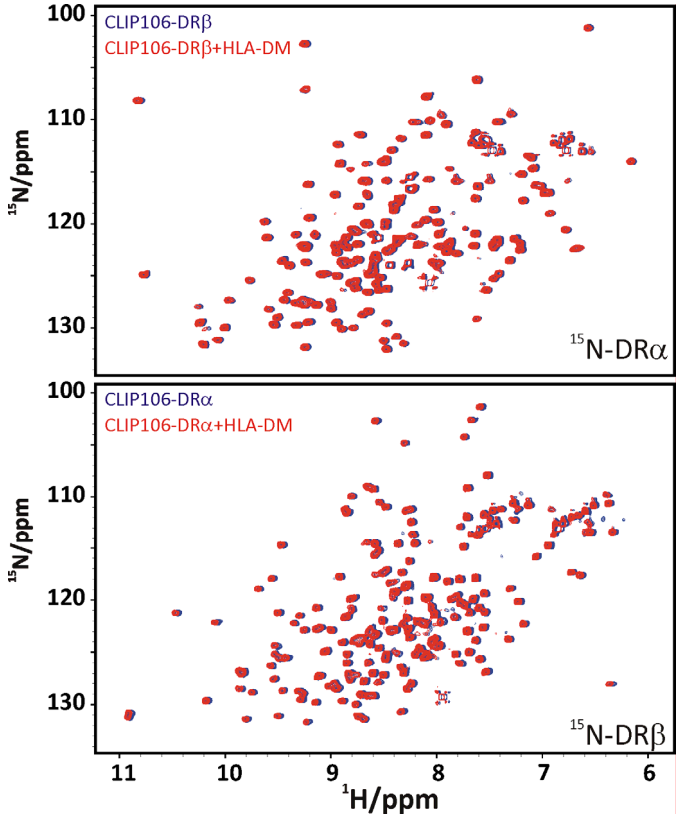

Figure 3.34: Susceptibility of HLA-DR1/CLIP fusion proteins to HLA-DM. $CLIP_{106}$-DRβ (top) or $CLIP_{106}$-DRα (bottom) - ^{15}N-labeled in the unmodified chain - were measured without or with stoichiometric amounts of HLA-DM in ^{1}H-^{15}N-HSQC experiments. Overlaid spectra were manually shifted by 0.01 ppm ^{1}H chemical shift relative to each other to enable comparison of resonances.

3.4.8 Other peptide ligands with potentially inverted presentation

3.4.8.1 Defining ligands for a screen of peptide orientation

As shown before peptides are principally not restricted to a single orientation when bound to MHCII. It was asked if peptides with a similar behavior as CLIP could be identified. Therefore, the structural features that govern peptide inversion would ideally be defined. From the two crystal structures determined in this study no general correlation between primary sequences and flipping probability was deducible.

I screened a set of peptides for HLA-DR1 binding that had been synthesized both in N-to C-terminal (odd numbers) and C- to N-terminal arrangement (following even numbers) to examine the impact of peptide backbones. The selection of sequences was guided by the restriction that inverted sequences (C-to N) potentially fit the HLA-DR1 pockets based on binding data derived from established databases (see *Methods* chapter). Only residues not leading to steric clashes were considered. Moreover, antigens had to be at least described once in the IEDB database (http://www.immuneepitope.org/)[96]. In collaboration with Sebastian Günther we selected 41 sequences. Together with CLIPs, HA and technical controls (see figure 3.35, panel A) they are summarized in the appendix table X.

Sequences were immobilized on a spot membrane and incubated with empty HLA-DR1, subsequently probed with antibody L243- and horseradish-peroxidase-coupled anti-mouse antibody. I expected peptides to bind HLA-DR1 in both N-C- and C-N - direction assuming that solely side chains were accounting for efficient interactions. If so, the backbone alignment would not have an effect on binding to the MHCII. Panel A of figure 3.35 shows the spot membrane after development. All sequence pairs were stained with a comparable intensity in either direction of synthesis. Some of the sequences (19/20; 45/46; 73/74) were not bound by HLA-DR1 at all. Hence, our rationales for peptide selections were not completely justified by this assay. Moreover, a positioning of HLA-DR1 relative to the peptides was not possible to determine.

Next, ten of the peptides with different affinity were selected (e.g. compare IV and VIII) for further investigation. Two additional peptides were included as suggested by Dr. Bernd Rupp who developed an *in silico* prediction for inverted peptides. The 12 peptides (in roman numerals) are shown in table 3.3. They were synthesized in mg-amounts in N-C orientation and used in loading assays to probe for SDS-resistant complexes with HLA-DR1 (panel B in figure 3.35). Half of the peptides showed stable heterodimeric bands in the gel (see panel B of figure 3.35).

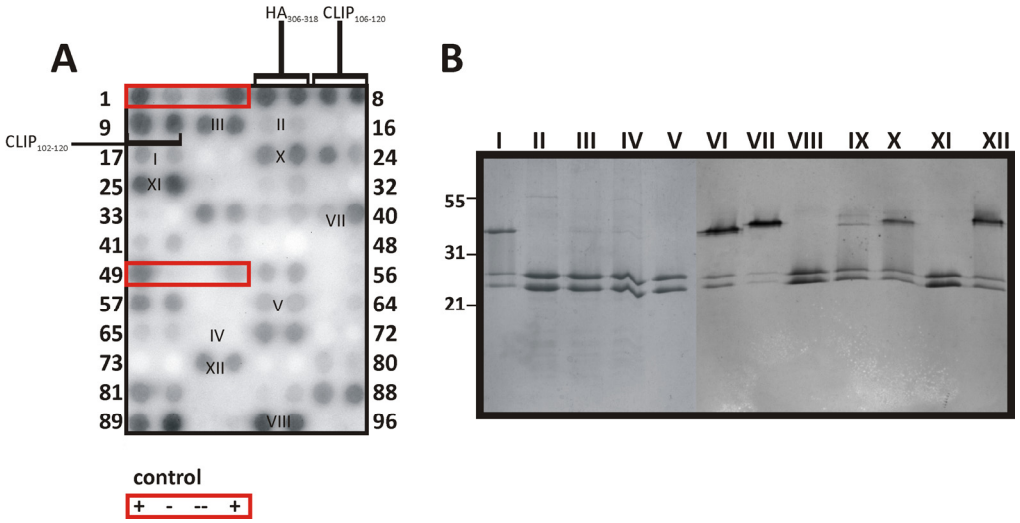

Figure 3.35: Screen for potentially inverted peptides. A) Peptide spot array of selected sequences that were probed for HLA-DR1-binding and detected with chemiluminescence. Roman numerals, centrally positioned to a spot pair, indicate sequences that were picked for further characterization. All sequences from panel A are summarized in table X in the appendix. B) SDS-PAGE analysis of HLA-DR1 when loaded with the peptides from panel A to determine SDS-resistance of the complex. Sequences VI and IX were derived from an *in silico* prediction (see main text). All sequences in panel B are listed in table 3.3.

Similar to canonical $CLIP_{106-120}$, a lack of SDS-resistance does not necessarily indicate an unstable pMHCII complex (see section 3.4.7.2) Thus, all peptides were loaded to ^{15}N-labeled HLA-DR1 for NMR studies. Except for peptide IX (no spectrum obtained) all complexes showed HSQC spectra characteristic for loaded protein (see appendix figures X1/X2 for all spectra). However, differences were found in signal-to-noise, spectral completeness, dispersion of amide resonances and peak shapes. No co-refolding experiments were possible because of limited peptide amounts. Apart from a reasonable number of resonances in the α2/β2 domains the assignments from HLA-DR1/HA or HLA-DR1/CLIP complexes could not be transferred. To derive peptide orientations from these spectra was therefore impossible.

It was then examined if HSQC spectra revealed more than one set of peaks indicating two parallel orientations similar to $CLIP_{102-120}$ (see section 3.4.5.2). None of the spectra displayed a reasonable number of additional peaks. As no information on peptide orientation was minable from NMR spectra crystallization of complexes was initiated. This was done by Sebastian Günther (MDC Berlin) who used buffer-exchanged NMR samples in crystallization screens.

Structures were obtained for HLA-DR1 with peptides VI, VII, IX, X and XII. All peptides were found in canonical orientations (not deposited in pdb, yet). All complementary biophysical

data obtained for HLA-DR1 in complex with peptides I-XII are summarized in table 3.3 including melting points (determined by Sebastian Günther).

Table 3.3: Selected antigenic peptide sequences with origin, biophysical data, spectra and crystals of complexes with HLA-DR1 (all spectra are to be found in the appendix figures X1/X2)

Peptide number	Peptide	Spots	Sequence	Antigen	Origin	SDS-resistant complex	Crystals	Spots	Spectral quality#	~T_M[§] (pH 5.5) in °C
I	tetX (TT 234-246)	17/18	ELIHVLHGLYG MQ	Tetanus toxin	Clostridium tetani	strong	no	ok	very good	79
II	SMU.616 33-43	13/14	SILGGVATYGA	uncharac-terized protein	Streptococcus mutans	no	no	weak	bad	74
III	MAGEA 3	11/12	GDNQIMPKA GLLIIV	Melanoma associated antigen 3	Homo sapiens	very weak	no	strong	very good	70
IV	pstS1 86-101	67/68	TGSGAGIAQA AAGTVNI	posphate binding protein	Myco-bacterium tuberculosis	very weak	no	none	good	72
V	HA1 255-270	61/62	RGYFKMRTGK SSIMRS	Hem-agglutinin	Influenza A virus H3N8	no	no	ok	very good	69
VI	TT 1147-1159	!	DYMYLTNAPS YTN	Tetanus toxin	Clostridium tetani	very strong	yes	!	good	77
VII	P4a 293-307	39/40	SMRYQSLIPRL VEFF	Major core protein	Vaccinia virus (Pox)	very strong	yes	good	good	82
VIII	MBP 278-297	93/94	VDAQGTLSKIF KLGGRDSRS	Myelin basic protein	Homo sapiens	no	no	strong	very good	73
IX	Bapa 360-381	!	NANIRYVNTG TAPIYNVLPT	protective antigen	B.anthracis	weak	yes	!	n.d.	70
X	TT 830-843	21/22	QYIKANSKFIGI TE	Tetanus toxin	Clostridium tetani	strong	yes	good	ok	71
XI	lqpH 1-15	25/26	EHRVKRGLTV AVAGA	19 kDa lipoprotein antigen	Myco-bacterium tuberculosis	no	no	strong	good	70
XII	Phl p 5b 68-86	75/76	DKFKTFEAAFT SSSKAAAA	Pollen allergen	Phleum pratense	very strong	yes	good	ok	75

#spectral quality was validated optically with respect to spectra of known, stable complexes with CLIPs or HA
!not on spot membrane
[§]melting point

3.5 Functionalized HA peptide as ^{129}Xe-MR-probe

In parallel with the MHC protein, peptide binding was addressed by NMR spectroscopy via detection of peptide resonances.

From assigning HLA-DR1 protein NMR resonances binding, exchange and inversion of peptide could be traced at atomic detail. Isotope labeled peptides would certainly complement NMR studies *in vitro.* In addition, they are potentially useful sensors in magnetic resonance (MR) techniques - in particular *in vivo* imaging - where labeling and detection of endogenous protein is not possible. A peptidic MR-probe, captured by MHCII, was conceived an alternative to current imaging methods in detecting site-specific binding.

An antigenic peptide was fused to cryptophane A which is MR-detectable by capturing the noble gas xenon-129. Xenon-129 was hyperpolarized thereby enhancing sensitivity and theoretically allowing the detection of the sensor at low µM- to nM-concentrations, similar to *in vivo* conditions.

3.5.1 Cryptophane A - HA

HA peptide was fused to Cryptophane A by chemical coupling. Successful amide coupling of the carboxylated cryptophane moiety with amino-PEGylated HA was carried out by the group of Dr. Michael Beyermann at the FMP Berlin. Coupling yields with HA peptide were optimized to 20 - 40 mg with 85 - 96 % purity, which was essential for using the peptide in co-refolding experiments. The hybrid compound was termed Cage-HA.

Two versions of Cage-HA (I and II) were investigated; both are shown in figure 3.36 consisting of an amino acid sequence and a cage-linking module. Their difference relates to the three additional amino acids N-terminal to HA and by different linkers, namely 6-amino-hexyl (I) or the more water-soluble polyethylene glycol (II).

Type I Cage-HA could be loaded onto HLA-DR1 but stock solutions did not exceed 1 mM in aqueous buffer. Enhanced protein precipitation during loading in NMR samples was observed with Cage-HA I. The hydrophobic aminohexyl-linker and basic amino acids were suspected to promote aggregation. Thus, type II Cage HA was designed with a PEG linker and acidic amino acids to optimize charge compositions and increase solubility.

Cage-HA II showed improved solubility and did not hamper protein quality when loaded onto HLA-DR1. Stock solutions of 5 - 10 mM were possible and the construct was used for xenon-129-spectroscopic studies.

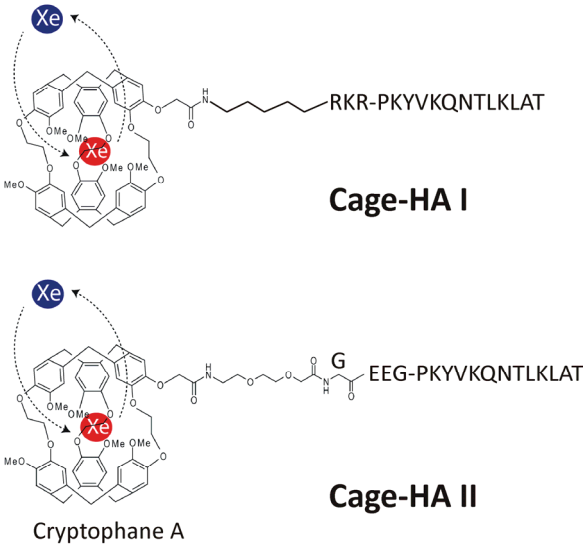

Figure 3.36: The two versions of Cage-HA used in this study. The viral peptide sequence is represented by PKYVKQNTLKLAT. Cage-HA I is given in the top of the figure whereas Cage-HA II is shown in the bottom panel. The capability of cryptophane to transiently host xenon atoms is indicated.

3.5.2 Xenon-129 NMR of Cage-HA

All xenon-NMR measurements were performed under guidance of Dr. Wolfgang Kilian and Dr. Lorenz Mitschang at the Physikalisch-Technische Bundesanstalt (PTB) Berlin. Cage-HA II was probed for displaying a resonance with the characteristic chemical shift of xenon caged by cryptophane A in ^{129}Xe-NMR. Figure 3.37 shows two prominent peaks with a defined chemical shift difference of ~200 ppm from a sample in PBS which was put under ^{129}Xe-pressure (see details on hyperpolarization in *Methods* chapter). The gas phase signal at 0 ppm was used as calibration point throughout the entire study. A third resonance at approximately 65 ppm represented ^{129}Xe when captured by HA-coupled cryptophane A. A control measurement with cryptophane A dissolved in DMSO was carried out and proved the signal at 64 ppm to be produced by the cage-moiety (not shown). Thus, Cage-HA was amenable to xenon-NMR studies as a sufficient signal-to-noise ratio was obtained with the utilized parameters (see inset and legend).

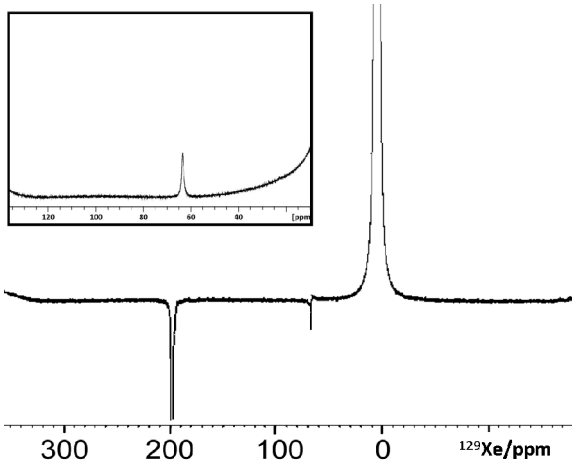

Figure 3.37: Xenon-129 NMR resonances from Cage-HA II in PBS pH 7.4. The spectrum is calibrated to gaseous xenon (0 ppm, truncated). Bulk xenon in solution at 194 ppm is peak-truncated, caged xenon is resonating at approx. 64 ppm. Phasing was adjusted to optimal baseline display. The inset shows up-phased caged xenon with a higher resolution as obtained in a separate acquisition with smaller band width.

3.5.3 Loading of empty HLA-DR1 with Cage-HA

The applicability of Cage-HA *in vivo* requires biophysical comparability to unmodified HA peptide *in vitro*. First, empty recombinant HLA-DR1 was loaded with either Cage-HA or wild-type HA(wt). In figure 3.38 a pronounced SDS-resistant heterodimeric band is shown for both Cage-HA- and HAwt-loaded protein (compare bands 3 and 5 from left) whereas empty HLA-DR1 fell apart into single subunits in the gel. Thus, Cage-HA was capable of binding to HLA-DR1 similar to unmodified HA.

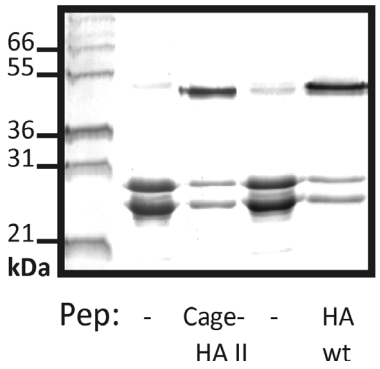

Figure 3.38: SDS-PAGE analysis of Cage-HA versus wild-type HA (HAwt) after complex formation with HLA-DR1. The gel shows a Coomassie Blue staining with the left lane as standard in kDa.

3.5.4 Characterization of HLA-DR1/Cage-HA

HLA-DR1/Cage-HA complex characterization was carried out together with Sebastian Günther from the MDC/FMP Berlin. HLA-DR1/Cage-HA was probed for complex stability in a competition-ELISA. Increasing concentrations of Cage-HA or HAwt competed with biotinylated HA (bHA) in binding to HLA-DR1. The remaining fraction of bHA bound to the MHCII was determined. Panel A of figure 3.39 shows normalized sigmoidal curves for the two peptides. Transition points indicated apparent affinities and revealed an approximate 30-fold higher K_D for Cage-HA compared to wild-type HA. Likely, this was caused by steric hindrances of the cage with regard to MHCII binding of HA.

Next, we tested if HLA-DR1/Cage-HA would comprise a compact complex similar to HLA-DR1/HAwt showing a single population in a gel-filtration (GF) run (figure 3.39, panel B). Complex shape is an important determinant for stability and compactness. Less compact folds of MHCII molecules are more prone to resume into the non-receptive state[104,107]. Both complexes were passed through an analytical GF column. We also included empty HLA-DR1 which is characterized by broadened peaks arising from multiple species (red curve, 1-2 ml) and *a posteriori* loaded protein with HAwt (green curve). The latter showed an unloaded fraction of oligomerized HLA-DR1 (non-receptive) at 0.9 ml and an HA-peptide peak at 2 ml. Together with co-refolded HLA-DR1/HAwt these two samples showed a peak at 1.5 ml elution volume indicating properly folded pMHCII complex. The co-refolded HLA-DR1/Cage-Ha sample showed one single peak confirming its purity (blue curve). However, the heterodimer was eluting at a later time point (~2 ml). Presumably, the bulky hydrophobic cage and the included linker retained the pMHCII complex through unspecific interaction with the matrix. Its presence was confirmed via SDS-PAGE within this fraction (not shown).

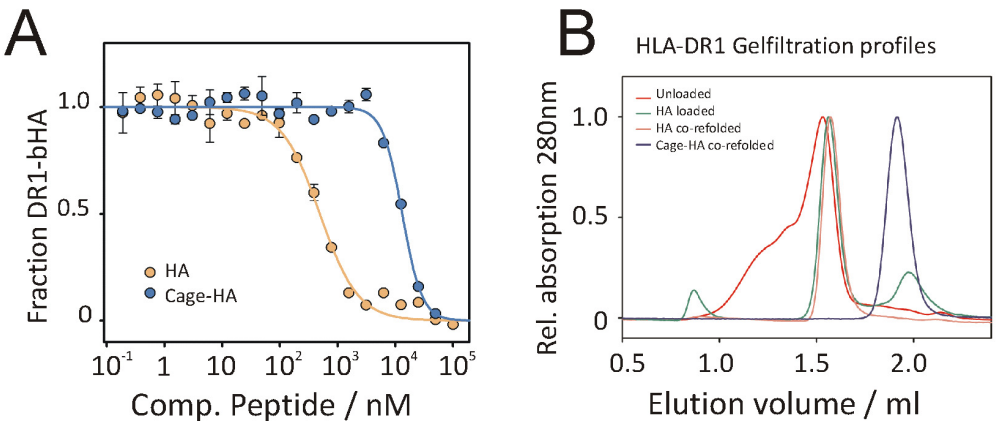

Figure 3.39: Biophysical characterization of Cage-HA with HLA-DR1. A) Representative competition ELISA experiment. Increasing amounts of HAwt or Cage-HA were added to an equimolar mixture of HLA-DR1 and biotinylated HA (bHA) for detection with Eu^{3+}-labelled streptavidin (n=2). Counts were normalized with the fitted curve origin to be 1. B) Gel-filtration profiles of empty HLA-DR1 in comparison with HA-bound or Cage-HA bound HLA-DR1. HLA-DR1 was either co-refolded with peptide or peptide was loaded afterwards (see legend). Parts of the figure were provided by Sebastian Günther.

Both Dynamic Light Scattering (DLS) and Thermal Shift Assays (TFA) were used to determine the heat stability of HLA-DR1/Cage-HA. Values were compared to HLA-DR1/HAwt and empty protein. As summarized in table 3.4 unloaded HLA-DR1 showed significantly reduced stability compared to peptide-loaded protein. The two methods yielded T_M values in similar ranges for all three samples. Cryptophane A, when attached to HA-peptide, slightly reduced the HLA-DR1/HA stability, which was in line with the results from ELISA.

DLS was used to recalculate particle sizes and both pMHCII complexes showed almost identical molecular weights (MW). This was expected as the cage only accounted for an additional mass of 1.5 kDa. The higher MW for empty HLA-DR1 was compatible with broadened peaks leading to uncertainties in the MW recalculation (see figure 3.8). With this, the biophysical integrity of HLA-DR1/Cage-HA was proven.

Table 3.4: Melting points and molecular weights of HLA-DR1/Ha and HLA-DR1/Cage-Ha

	MW / kDa*$^{+}$	Purity*	T_m / °C *	T_m / °C $^{\#}$
HLA-DR1	57	> 99 %	~65	68
HLA-DR1/Ha	50	> 99 %	~86	86
HLA-DR1/Cage-Ha	53	> 99 %	~78	81

*Determined by Dynamic Light Scattering, $^{+}$values recalculated from particle size, $^{\#}$determined by thermal shift assay

3.5.5 ^{129}Xe-chemical shift perturbation of Cage-Ha upon binding to HLA-DR1

In the following, the binding of Cage-HA to HLA-DR1 was probed by xenon-129 NMR methods. If the cage sensed binding to the MHCII, hyperpolarized xenon-129 would conceivably show a perturbed chemical shift for the cage-resonance. Two samples were measured to compare the exact chemical shift of caged xenon in either free Cage-HA or co-refolded HLA-DR1/Cage-HA (each sample at 10 µM in PBS). Measurements were performed with or under the supervision of Dr. Wolfgang Kilian and Dr. Lorenz Mitschang at the PTB Berlin in a home-built coil in a permanent magnetic field provided by a tomograph of approx. 2.94 T or 35 MHz Larmor frequency of xenon.

Figure 3.40 shows an overlay of cage-resonance peaks in panel A. Peak positions were found shifted by 1 ppm (63.3 and 64.3 ppm) when referencing spectra to their gas signals (see inset). The line width of bound cage was increased by 6 Hz (37 instead of 31 Hz). Although mechanisms of xenon relaxation inside the cage are still under investigation, this indicated enhanced relaxation as would be expected from a peptide when complexed to a large protein. Relaxation also caused a small loss of the signal-to-noise ratio. Combining both samples yielded an effective line width of 66 Hz, which convincingly compared to the theoretical peak shape from the sum of both samples when measured individually (see part B in figure 3.40). Thus, two different states of cage were present in the overlaid spectrum. We concluded that the ^{129}Xe chemical shift change was not caused by technical uncertainties but indicated the xenon-129 to sense the binding between Cage-HA and HLA-DR1. This was mandatory to qualify Cage-HA as a functioning MR probe for HLA-DR1.

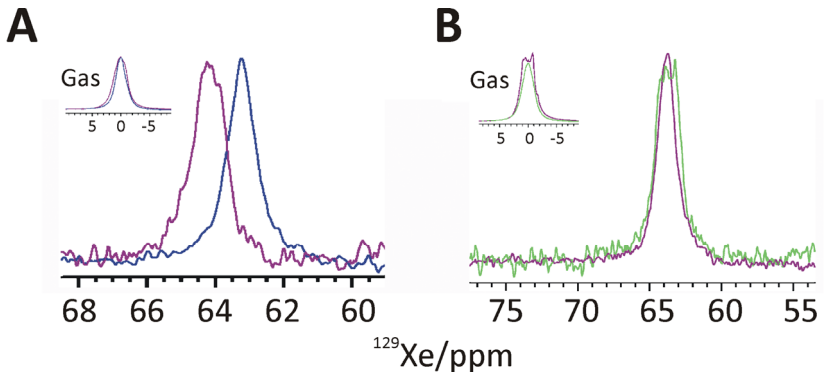

Figure 3.40: ^{129}Xe-NMR of pMHCII complex formation. A) ^{129}Xe signal of Cage-HA in the absence (blue) or presence (magenta) of equimolar amounts of HLA-DR1. B) Lines observed from a sample comprising the two mixed species from A (magenta) or from the calculated sum of the individual signals observed in A (green). Insets display ^{129}Xe gas signals of the corresponding spectra used as reference at 0 ppm.

3.5.6 ^{129}Xe-HYPER-CEST: Indirect detection of Cage-HA

MR-based imaging of cage-fused scaffolds would have to be carried out at lower concentrations compared to spectroscopic measurements. The method of HYPER-CEST[82] uses the rapid exchange between cryptophane-bound and bulk xenon to gain sensitivity. The successful xenon-based detection of HLA-DR1/Cage-HA therefore called for the indirect measurement of cage resonances.

A schematic pulse program (see figure 3.41, part A) was suggested by Dr. Wolfgang Kilian (PTB Berlin) which allowed the twofold acquisition of FIDs selectively from bulk xenon. The two FIDs were interrupted by selective pulses that saturated xenon localizing to the cage. By this, progressive depolarization of xenon, exchanging with the cage, was sensed by polarized bulk xenon. The entire sequence was repeated 10 times for statistical reasons. By this, also the background depolarization from applied pulses to bulk xenon was determined by saturation at a cage-non-related frequency or in a sample devoid of cage compound.

Part B of figure 3.41 exemplary shows the 10 FID pairs from a combined sample of 10 µM free Cage-HA and 10 µM co-refolded HLA-DR1/Cage-HA. Saturation was performed either at the characteristic cage frequency of 60 ppm (“on-resonance”) or 330 ppm (“off-resonance”). Latter represented the mirrored frequency relative to the bulk solvent pool of Xe. Both experiments are exemplified by magnified pairs of FIDs. The visible loss of intensity was more pronounced when saturation was done on-resonance.

Panel C shows the quantification of relative FID intensities before and after saturation on- and off-resonance, respectively. A stable loss of bulk magnetization was found in all four samples: Cage-HA alone, HLA-DR1/Cage-HA, HLA-DR1/Cage-HA+Cage-HA (equimolar) or buffer. The pulse flip angle caused 15 % signal damping which is represented by the loss of intensity in two consecutive FIDs, also including the buffer control.

Additional signal loss was found in samples with cage when saturation was carried out on resonance. Chemical exchange was expected to account for this finding. It was asked whether damping effects from individual samples correlated with the concentration of cage. As shown in part C of figure 3.41, specific depolarization of 18 % from free Cage-HA and 12 % from HLA-DR1/Cage-HA were found. The difference was most likely caused by unequal xenon exchange rates with cryptophanes based on steric hindrance by the MHCII where the cage is less mobile. A combined sample revealed 33 % of cage-related signal loss which is approximately the sum of the two individual samples.

Altogether, saturation of xenon could be applied to both the free and complexed Cage-HA similarly. This might allow using HYPER-CEST in probing for molecules *in vivo* at very low concentrations.

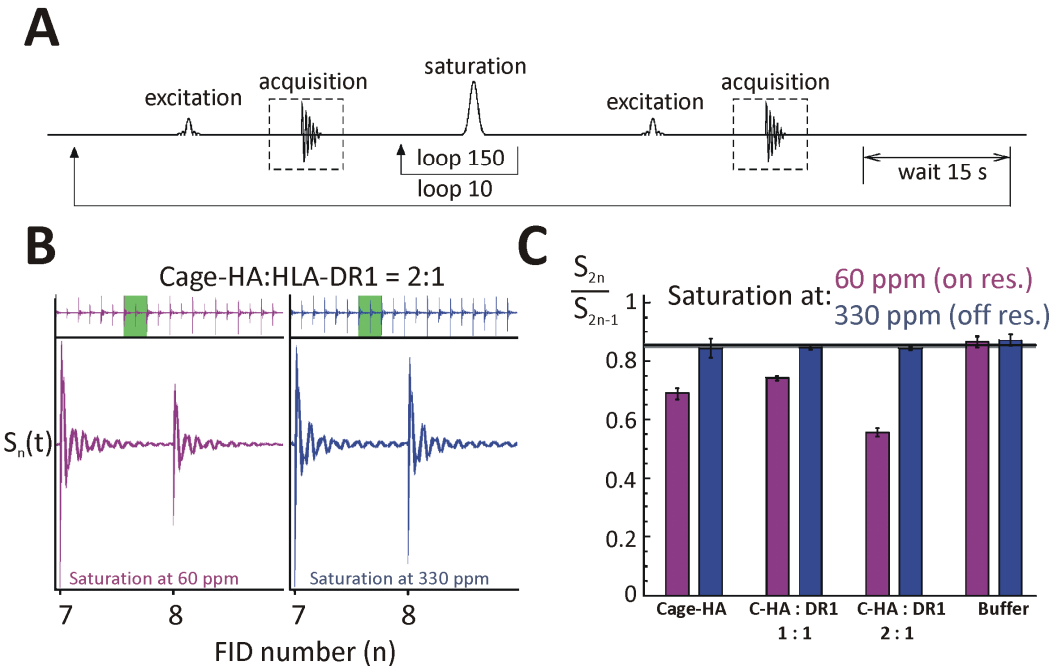

Figure 3.41: Cage-HA binding to HLA-DR1 probed by CEST (chemical exchange saturation transfer). A) Simplified scheme of the ^{129}Xe Hyper-CEST pulse sequence as described in the text and *Methods* chapter. The saturation was carried out either on-resonance (Cage-HA, 60 ppm) or off-resonance (330 ppm) as control. B) Plot of all 10 FID pairs from a stoichiometric, combined sample of Cage-HA and co-refolded HLA-DR1/Cage-HA when saturation was performed either on- or off-resonance (see A). One of ten pairs is plotted in magnification. C) Quantification of results from B. FID integral ratios were averaged (shown with standard deviation) for samples as indicated when either saturated on-resonance or off-resonance. C-HA is Cage-HA. The black line indicates background signal damping based on loss of polarization due to excitation and relaxation (~15 %).

3.5.7 Cage-HA in mouse-priming and stimulation of T-cells *in vitro*

The bio-availability of Cage-HA was assessed to examine immunogenicity when compared to unmodified HA-peptide. Therefore, Cage-HA was tested in two *in vivo* and cell studies. Mouse experiments including priming, sacrificing and the isolation of spleen and lymph node cells as much as all steps of the ELISPOT protocol have been carried out by, with or under the supervision of Sabine Höpner, MDC Berlin in accordance with the institutional guidelines of the MDC mouse facility (see also reference[125]).

It was then asked how T cells positive for HLA-DR1 would respond to Cage-HA compared to HA alone. Spleen or lymph nodes were isolated from HLA-DR1-transgenic mice primed either with HA or Cage-HA. Cells were *ex vivo* challenged with HA or Cage-HA in an ELISPOT (enzyme-linked immunosorbent SPOT) titration series to measure interferon-gamma

secretion. HLA-DR1/HA restricted cells were expected to respond to their antigen. It was questionable whether peptides were able to stimulate T cells from mice that had been primed with the other antigen.

As figure 3.42 depicts, both the Cage-HA and HA primed mice generated T cells that could be recalled *ex vivo* by their antigens. Panel A shows an example for isolated spleen cells of one mouse individual each. The titration led to decreasing numbers of stained spots each of which represented a stimulated T cell clone. Also cross-stimulation with HA or Cage-HA led to a visible response by T cells from the same individual. However, quantifying the number of spots at the highest concentration of Cage-HA, the latter was only half as potent in re-challenging HA-primed mice compared to wild-type Ha. In contrast, wild-type HA was fully potent in re-stimulating Cage-HA-primed mice. Nevertheless, these data show that HLA-DR/HA restricted T cells were capable in being stimulated by Cage-HA. Control peptides and DMSO did not show responses (not shown).

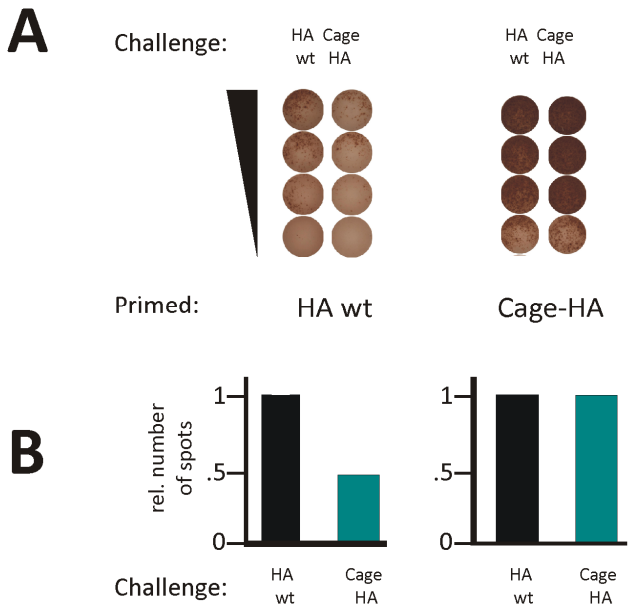

Figure 3.42: Immunogenicity of Cage-HA. A) ELISPOT analysis of T cell response to HA and Cage-HA after re-challenging isolated murine spleen cells. Mice had been primed with HA or Cage-HA *in vivo* before. Production of interferon-γ by T cells was visualized with cognate antibodies staining spots of cells. Rows show dilutions of re-challenging peptide. B) Relative quantification of results from A. At the highest concentrations spots were counted and normalized to HAwt and plotted. Experiments have been performed with at least five mice and assays were made in duplicates. One representative experiment is shown.

Next, Cage-HA was tested for presentation by professional antigen presenting cells when compared to wild-type HA-peptide. Stably HLA-DR1-transfected murine fibroblasts (L57.23) presenting Cage-HA or HAwt were used to stimulate HLA-DR1-restricted T cells. L57.23 cells were loaded with titrated amounts of peptides and cells incubated with either HA-specific

murine T cells EvHA/X5 or a control cell line (SaABL/G2), restricted to the ABL peptide (see section 3.2). Secretion of IL-2 (interleukin-2) was quantified by incubating unrelated T cells with the culture supernatant. Stimulation-induced proliferation was counted via incorporation of ^{3}H-labeled thymidine.

As shown in figure 3.43 the loading of wild-type HA led to concentration-dependent stimulation of EvHA/X5 but not the unrelated T cell line SaABL/G2. The same was found for Cage-HA but T cell responses were not as pronounced when compared to HAwt. The ~30-fold lower affinity for HLA-DR1 determined by ELISA (see figure 3.39) was presumably causing this effect.

Altogether, binding of Cage-HA to HLA-DR1 was confirmed in cell-cultures and *in* mice. Moreover, Cage-HA was potent in stimulating HLA-DR1/HA restricted T cells. Thus, this novel probe bears the potential to be used as MR-probe for MHCII dependent immunological activity.

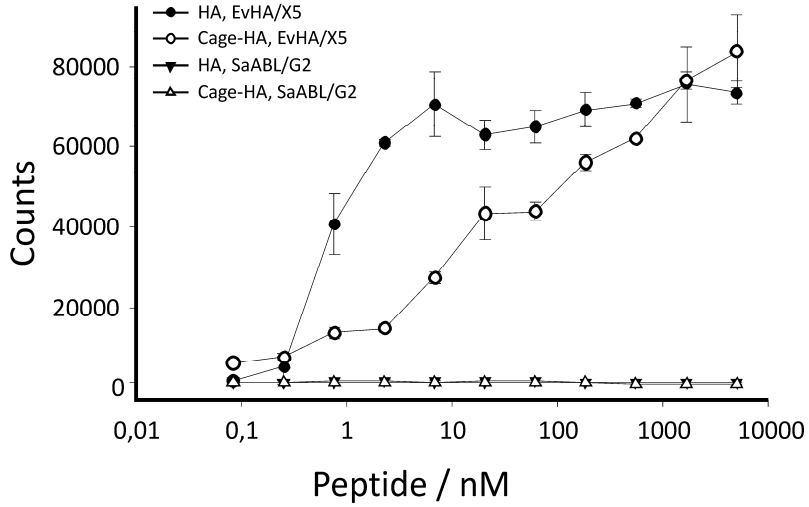

Figure 3.43: T cell response triggered by Cage-HA. HLA-DR1-expressing L cells (L57.23) were incubated with increasing amounts of HA (solid circles) or Cage-HA (open circles) in the presence of the HA-specific T cell hybridoma line EvHa/X5 (circles) or the control line SaABL/G2 (triangles). Counts reflect the stimulation-dependent production of IL-2 as determined in a secondary assay (see text and *Methods* chapter).

4 Discussion

This thesis was initiated in order to reassess MHCII-peptide interactions with the only technique capturing atomically-resolved comprehensive information in solution, nuclear magnetic resonance (NMR) spectroscopy. Although numerous well resolved MHCII-peptide crystal structures are available, they all merge in a static picture of these immunologically relevant molecules. A dynamic view onto the determinants of MHCII stability, peptide loading and exchange had been envisaged from the very beginning of MHC research. Recent approaches mainly allowed to draw conclusions about specific sites by mutational analysis[126,127]. Here, NMR spectroscopy was successfully applied to investigate MHCII-peptide dynamics with atomic resolution and to test the potential usage of antigenic peptides as magnetic resonance probes for *in vitro*/*in vivo* applications.

4.1 The production of HLA-DR1 from *E.coli*

The successful application of solution NMR is limited by protein size and the preparation of monomodal samples. These requirements certainly have hampered previous approaches to analyze class II MHC proteins by NMR. The need of isotope labeling excluded the option of eukaryotic protein production where correct folding is more easily achieved instead. Interestingly, first, surprisingly high-quality-two-dimensional NMR spectra of HLA-DR1 had been acquired in the group of L. J. Stern already in 2004 (as shown in the doctoral thesis of Z. Zavala-Ruiz[128]), but no experimental follow-up study has been published since then. Although initial assumptions on comparable structures of empty and loaded MHCII, as well as the effect of different peptides to spectra were made at this time, no assignments or indications on individual amino acids had been given. Moreover, spectra had only been obtained from fully-deuterated samples and the thesis does not give further comments on acquisition times and buffer conditions. Nevertheless, spectra were used to partially confirm results obtained with other experiments. Possibly, preliminary results have been validated as not worth the effort in sample preparation later on.

Here, the production of the human MHCII allele HLA-DR1 has been successfully adapted and up-scaled to amounts necessary for more comprehensive NMR studies based on an optimized refolding protocol of bacterial *inclusion bodies*. Immuno-affinity purification was

the most reliable way to isolate natively folded HLA-DR1 from the majority of non-native species. In contrast to previous assumptions[85] this step was also crucial for peptide-co-refolded MHC complexes to yield homogeneous samples. Although earlier studies report higher yields for the bacterial production of HLA-DR1[85,101] than obtained during my protein preparations, they were made on a 5 - 10-fold smaller basis and numbers only referred to the folded fraction of MHCII within the total soluble pool after purification. An earlier quantification of refolded HLA-DR1[129] was exceeded by a factor of almost 10 in the studies presented here. The additional steps introduced here have extended the purification time but were compensated by increased yields, reliability, and reproducibility and came at only moderate additional costs. It is questionable in how far experience is transferable to the production of other MHCII alleles. Different from HLA-DR1 they might still depend on structure-stabilizing tools as leucine zippers - e.g. applied to HLA-DR2[130] - to achieve stable heterodimers.

In section 3.2 it was shown that the refolded protein was capable of binding peptide implying the formation of functional protein. Moreover, recognition of both empty and loaded HLA-DR1 by two native conformer-specific antibodies[93], namely LB3.1 and L243, confirmed a well-folded species. However, dynamic light scattering (DLS) revealed the inhomogeneity of empty MHC protein. The tendency to aggregate is expressed through residing in a peptide-non-receptive state leading to intrinsic heterogeneity, which has already been described in earlier studies as by Stern and Wiley in 1992. They reported that only peptide binding stabilized the empty heterodimer against aggregation[104]. Inhomogeneity might interfere little with approaches that monitor a particular functional fraction (e.g. ELISA) but impairs averaging methods like NMR. Aggregation was prevented by storing protein complexed with an exchangeable peptide. Once loaded, complexes remained stable for years without obvious oligomerization as had also been reported before[131] (and personal communication with Dr. Olaf Rötzschke). Recently it was shown that HLA-DR1 is significantly more susceptible to digestion by cathepsins when not being loaded with peptide[132]. Thus, the difference in stability between empty and loaded MHCII *in vitro* underlines the relevance *in vivo*.

Oligomerization and heterogeneous conformations did not allow analyses of NMR spectra from unloaded HLA-DR1 in my work. Hence, the empty protein was not amenable to assignment strategies or the measurement of structurally relevant NOEs. This lack of a single

defined conformation might be a hallmark for concentrated empty MHCII preparations in general and explain the failure to crystallize such species. In contrast, two-dimensional spectra of excellent quality were obtained for peptide-loaded HLA-DR1 proving complex homogeneity. Almost any tested peptide - when loaded to HLA-DR1 - led to an acceptable HSQC spectrum. However, spectral quality was likely affected by individual pMHCII affinities. Recent studies have discussed the metamorphic behavior of MHCII in the light of a biological relevance[133,134]. The acquisition of heterogeneous, inactive forms upon peptide loss is hypothesized to take place on APCs and lead to MHCII non-receptiveness. Conceivably, this mechanism might avoid undesired loading of self-antigens.

In the future, NMR could directly prove the equilibrium-driven interplay between empty/multimodal and loaded/monomodal conformations.

4.2 The backbone resonance assignment of HLA-DR1/CLIP and -HA

Technical progresses of NMR spectrometers and novel labeling techniques have made NMR assignments accessible to larger proteins, although it is not yet a standard procedure. The assignment of fingerprint spectra from entire MHCII ectodomains was a prerequisite for successive experiments that relied on the interpretation of local effects in backbone amides. Here, direct site-specific information in solution for the first time could be extracted for MHCII molecules at this stage.

4.2.1 Selective labeling and deuteration from the perspective of acquired spectra

Selective labeling and deuteration were supposed to minimize spectral crowding and line-broadening of peaks, both hindering the assignment progresses.

Reducing spectral overlap by subunit-labeling has convincingly proven useful. Thus, it was not considered necessary to develop protocols to further restrict labeling to individual domains (segmental labeling) by means of chemical ligation[135] or intein-based approaches[136].

Selective labeling of amino acids (AASL) did not severely modify the protocol and was powerful in revealing certain types of amino acids. The observed glycine scrambling might be suppressed by varying the amount of glycine in the culture medium or by changing the time

point of supplementation to the medium. Finally, the knowledge about glycine catabolism was also helpful in considering additional peaks as being serine or threonine amides.

It did not seem necessary to incorporate 100 % of deuterium to obtain sharpened peaks in crowded spectral regions. However, for triple resonance experiments it is critical to overcome fast Cα proton (Hα) relaxation as signals deteriorate from strong couplings and relaxation[137]. While Cα is mainly deuterated by D_2O rather than D_7-glucose[138], additional protonation in side-chains will still promote spin diffusion. For triple-labeled samples almost all amides where found with full spin systems in 3D-experiments and the lack of NOEs between amides and carbon-bound protons was also indicative of successful hydrogen displacement. Thus, deuteration had been performed with nearby completeness and this set the stage for recording triple resonance spectra.

4.2.2 Proceedings in assigning the backbones

HLA-DR1 backbone assignments of more than 80 % in complex with peptides allowed a comprehensive interpretation of the experimental NMR data. The remaining non-assignable resonances were mainly located to the terminal extensions or residues DRβ102-115 which lack electron density or show increased B-values in crystal structures. This is likely caused by an increased flexibility of these regions, since dynamic behavior in certain time regimes enhances relaxation and hampers signal detection. In contrast, the unstructured stretch of β92-100 linking DRβ1 and β2 was assignable in all cases and is also well presented in structures with different resolutions (compare pdb entries 2fse[139] and 1klu[140]). Additionally, numerous amide resonances in the spectra remained unassigned as no connectivity to assigned peaks could be made. For certain residues a second set of satellite resonances were found, which might be caused by alternative conformations due to local unfolding of HLA-DR1 or partial disulfide breakage.

Chemical shifts of Cβ atoms are in principal very helpful to identify amino acid types[141] but they could rarely be detected. Likely, magnetization transfer pathways were too long for a protein of this size. The lack of Cβ resonances had been reported for a significantly smaller MHCI construct before[45] although this did not restrict the backbone assignment. While Cβs might still be detectable with higher concentrations and at even higher temperatures full side-chain assignments are often hindered by severe signal overlap in proteins as large as MHCII. Moreover, a strategy to correlate side-chains with amides is of moderate success,

which complicates an assignment. This is one limiting step for proteins to qualify for solution structure determination albeit alternative approaches are being discussed only based on backbone assignments, amide-amide-NOE's and amide-RDCs (residual dipolar couplings)[142]. Favorably, both NH-NH-NOEs and NH-vector RDCs are relatively unimpaired by an accelerated relaxation in larger proteins.

4.2.3 Secondary chemical shift analysis and H/D exchange

HLA-DR1 secondary structure as observed in crystals was confirmed by chemical shift analysis and H/D exchange. While in the majority of cases the occurrence of secondary structures is very similar for NMR and X-ray-derived structures, a number of cases suggest true differences between solution and crystal structures as for example reported by Gouda *et al*. in 1992 for a Staphyllococcal protein[143]. In particular the flexible helices of MHCII binding clefts are likely involved in determining complex stability and receptiveness to peptide loading or HLA-DM binding[121,144]. In line with dynamic differences of individual secondary structure elements results from H/D exchange experiments in this study reveal differential domain rigidity of HLA-DR1. Although exchange rates are influenced by the protein primary sequence[145], residues close to the peptide clearly experience higher flexibility (see figure 3.17). Intrinsic peptide release makes most of these residues solvent-accessible while in the bound state they are buried or trapped in H-bonds. With a set of experiments, a determination of intrinsic peptide release (off-) rates appears to be possible by comparing H/D exchange rates of these residues among pMHCII complexes. Exchange rates would be mainly determined by the off-rates as transiently empty MHC will experience rapid H/D exchange. In contrast to other studies[146,147] no rebinding of peptides after H/D exchange will influence the rate based on the high excess of deuterons which would not allow measurable re-protonation. However, subtle rate differences might not be accessible to H/D exchange. Very fast exchanging peaks will remain unconsidered due to experimental dead times. On the other hand novel, fast pulse schemes[64] might reduce dead times significantly.

4.2.4 The exchange of peptides at the atomic level

Having the HLA-DR1 backbone assignments at hand, chemical shift changes accompanying peptide replacement could be mapped onto the corresponding crystal structures. This is

exemplified for the paradigmatic CLIP-to-HA exchange shown in figure 3.18. While mutational analyses can only target few residues, the HSQC-based approach yields information on all assigned residues at once. Additional aspects highlight the benefit of high-field NMR spectroscopy: First, the unperturbed peaks from α2 and β2 domains support the rigidity of these modules as it was already indicated by close superposition of these regions in crystal structures of different pMHCII complexes. Second, the similar composition of secondary structure in both HLA-DR1/HA and -/CLIP α1β1 domains is supported by Cα chemical shift values in solution. Third, low peptide on-rates/off-rates[148,149] are confirmed by the peptide exchange experiments. The presence of distinct pMHCII resonances at equimolar peptide stoichiometries defines the exchange rate between CLIP and HA to be lower than differences in chemical shifts (in Hz). As a graded release and binding of peptides during exchange has been a matter of debate[147] the NMR-observable peptide substitution could potentially define the involvement of single residues at certain time points. Unfortunately, the slow-exchange regime complicates extracting exact rates from plotted NMR spectra[150]. Fourth, the exclusive existence of HLA-DR1/HA in a sample with twofold HA-excess over CLIP confirms CLIP to always be exchanged against higher-affine antigens *in vivo*. This is most likely driven by a notably higher intrinsic off-rate. Peaks showed higher intensity for HLA-DR1/HA compared to CLIP, which might be explained by less line-broadening from chemical exchange with sub-populations or less heterogeneity of this sample compared to HLA-DR1/CLIP. The assumptions are in line with i) values of HLA-DR1/HA thermal stability which were approximately 10 K higher than for HLA-DR1/CLIP and ii) particular CLIP-specific dynamics as shown in section 3.4 (see figure 3.22).

4.2.5 An outlook to the acquisition of more sophisticated spectra from HLA-DR1

In order to investigate different conformational states of HLA-DR1 the use of side-chain resonances from MHCII is very desirable for applications like methyl-TROSY for CPMG relaxation dispersion experiments[60]. Similarly, ^{13}C-NOESYs would help to examine local changes in structure as measurable sensors of protein-protein interactions. In particular atoms forming crucial or transient hydrogen bonds might give superior information for the disclosure of mechanisms or the transient binding of the catalyst HLA-DM. However, intelligent labeling will have to overcome spectral crowding and aid assignments.

Adjusting temperature, pH, and buffer might also improve spectral quality for a particular pMHCII complex. For example, for the gold standard HLA-DR1/HA temperatures higher than 40°C are not problematic in actual measurements over several days to weeks. Increased resolution and S/N would remarkably shorten the acquisition of spectra allowing the acquisition of more complex experiments that capture relaxation and chemical exchange. However, this also requires comparability to other samples. Although many affine pMHCII complexes show thermal stabilities above 70°C sample degradation will still be an issue in long-lasting NMR experiments measured over weeks. As for example HLA-DR1/CLIP complexes (T_M > 70°C) precipitated over time at 37°C, NMR acquisition was not performed at higher temperatures.

pMHC complexes comprise large protein surfaces and the intrinsic complex stability is ideally suited for the use of spin-label techniques. Paramagnetic relaxation enhancement (PRE) induced by the label could reveal mechanisms of peptide editing in the presence of multiple antigens for selective complex formation. A stable 1:1 stoichiometry, as it is obtained for the pMHC complexes after gel-filtration, also rules out solvent mediated relaxation enhancement as it might occur in solutions with excess of spin labeled ligand. Similarly, spin labels could be attached to the MHC via disulfide coupling[151] or sortase-mediated reactions[152]. Spin labeling has been used successfully to reveal protein structure restraints, folds and relative orientations of bound ligands in other studies[62,153,154] and might be used to determine interaction interfaces.

More recently, the power of NMR in trapping dynamics over a broad range of time scales has become evident. Figure 4.1 gives an overview of NMR techniques that are applied to investigate different time-scales of motion. On the right panel of the table a remark of anticipated applicability for HLA-DR1 based on experiences gained during this thesis is added. Some of these techniques bear great potency to address transient but central MHCII interactions during maturation and regulation of the antigen-presenting complex, as there are for example HLA-DM, invariant chain, peptides, and cathepsins in the late endosome and chaperones in the ER. In particular the transient interaction of MHCII with the natural peptide exchange catalyst HLA-DM has failed to become directly visible, e.g. by crystallography, until now[13]. The results shown here encourage further NMR-based investigations of this crucial interaction in the near future.

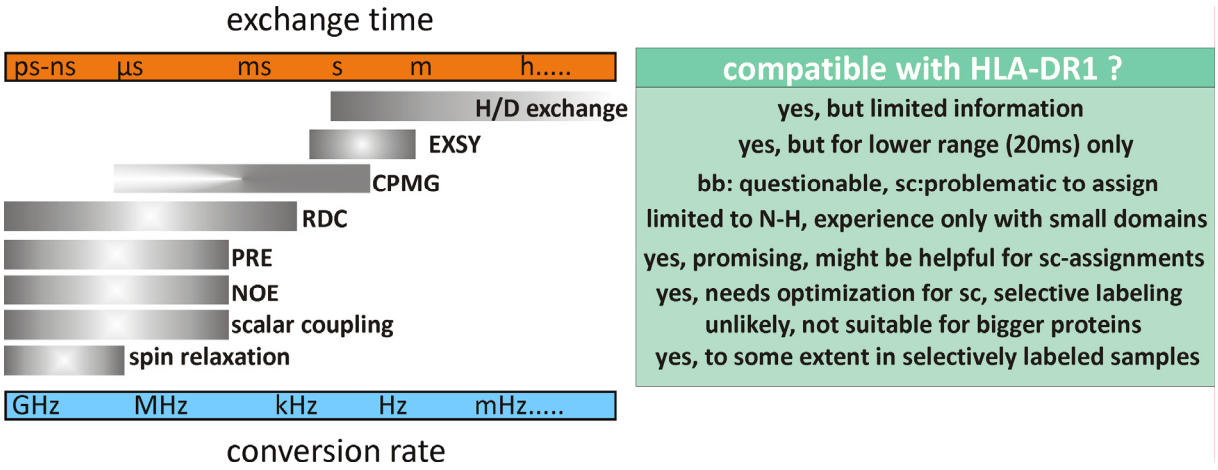

Figure 4.1: Overview of exchange time regimes as they can be addressed with NMR experiments. A non-linear plot of potential time ranges (orange bar on top) for exchange or molecular motions is given. The lower blue bar represents the respective frequency of interconversion between states occupied by a protein. Typical NMR techniques/experiments that serve to determine rates in the expected range are indicated. The right green panel gives a short comment concerning the applicability as anticipated for HLA-DR1 from the current perspective. The figure is based on reference[155]. Abbreviations are: H/D, hydrogen/deuterium; EXSY, exchange spectroscopy; CPMG, Carr-Purcell-Meiboom-Gill (relaxation-dispersion); RDC, residual dipolar coupling; PRE, paramagnetic relaxation enhancement; NOE, Nuclear Overhauser Effect (based spectroscopy); bb, backbone; sc, side-chains.

4.3 The bimodal binding of CLIPs to HLA-DR1

The canonical alignment of bound peptides has been a dogma since the beginning of structural access to MHC proteins. The lack of conserved residues contacting the peptide's C- and N-terminal main-chain like in MHCI structures[25] gave rise to a less confined peptide binding mode in the first MHCII structure by Brown *et al.* in 1993[35] where no single peptide could be resolved. However, a canonical N- to C-terminal alignment was assumed and confirmed in an MHCII structure by Stern *et al.* in 1994[33]. Despite theoretical assumptions on inverted peptide binding in both MHC classes[156,157] no experimental data had supported this before.

The herein presented findings show the dynamic re-orientation of pMHCII complexes. This unprecedented observation will have to be considered in antigen processing and presentation pathways. Its conceivable impact on the interpretation of autoimmune causalities or immunological deficiencies will contribute to current hypotheses about the molecular mechanisms underlying autoreactive T cell recognition.

4.3.1 HLA-DR/CLIP in crystal structures and NMR studies

The class II-associated invariant chain (Ii) peptide (CLIP) was found as placeholder peptide preceding stable formation of antigenic pMHCII complexes for cell surface presentation[12,158]. Although Ii is rather conserved a distinct binding sequence for human MHCII has not been defined consistently[158,159] in length. Structures of MHCII proteins with CLIP have remained rare cases[160,161] before this study. One was determined for HLA-DR3 complexed with an endogenous form of CLIP and a murine structure was solved with human CLIP linked to the MHC β-subunit. Besides, alternative CLIP recognition modes are suggested[162,163].

The novelty of CLIP peptide inversion relative to the binding site of HLA-DR1 was discovered and confirmed by the combined use of crystallography and NMR spectroscopy. Crystallization is conceived as separation process of one major species[164]. However, non-crystallizing "impurities" might be of relevance for the observation of sub-populations and distinct alternative conformations. They reflect transitions between dominating populations (canonical and inverted $CLIP_{106\text{-}120}$) and would allow an understanding of dynamic mechanisms. Facing conformational heterogeneity, crystallization might either be not successful, lead to badly resolved or only partially interpretable structures. NMR spectroscopy is complementary, since it allows observing dynamics, tracking transitions or defining flexible clusters which are invisible in crystals. On the other hand crystal growth is possible for proteins almost without size limit and exceeds the capabilities of NMR for larger proteins[165] like MHCs. Recent progress in combing the two techniques has improved both structure determination[166] and chemical shift prediction[167]. Our crystal structures of HLA-DR1 in complex with CLIP peptides mark the visible components of thermodynamic equilibria depending on temperature, peptide length and kinetic prerequisites during complex formation. They did not allow us to directly observe the peptide re-alignment as it was then proven by solution NMR. Assigned fingerprint spectra of HLA-DR1 allowed the mapping of inversion-sensitive residues to the peptide binding α1β1 domains. Flipping CLIP is categorized as peptide exchange process catalyzed by the chaperone HLA-DM and comparable to replacement of either CLIP by viral high-affine HA (see also figure 4.3). Complementary to traditional chemical shift mapping, observing the effects of PRE by the TEMPO spin label was powerful in unambiguously proving the present peptide orientation in solution. Examples of PRE labeling to map transient complexes[62] or the remodeling of intermediates[168] have been mentioned earlier in this thesis. In both cases crystal structures

were available. Clearly, these are prime examples for integrated structural-biology approaches to trap distinct states of protein complexes that mark biological key interactions. It will be of great interest to examine in how far the current studies can be transferred to MHC molecules of other alleles within this polymorphic gene locus (see also figure 4.1 in the previous section).

4.3.2 A new binding mode?

Based on results presented here the general assumption of peptides to bind in the canonical orientation appears no longer acceptable. It remains to be shown, however, that inverted peptide display is a more ubiquitous feature of pMHCII complexes. Alternatively, it is also conceivable that peptides derived from Ii exhibit a special case or the inherent properties of the HLA-DR1/CLIP complex lead to orientational artifacts.

4.3.2.1 Peptide inversion as explanation for elusive findings in the literature

Literature provides several studies with an extended role of CLIP apart from its placeholder function. On dendritic cells (DC) CLIP was up-regulated upon maturation and was suggested to play a role in suppressing type I T helper cell polarization[169]. Similarly, in absence of H2-DM (the murine homologue of HLA-DM) increased ratios of Th2/Th1 were measured defining a central role for CLIP in CD4+ T cell polarization. This process requires peripheral tolerance against the self-peptide CLIP, a still poorly understood immunological phenomenon. Exogenous application of CLIP led to MHCII down-regulation and also favored activation of B cells over Th1-polarization[170] while a murine study on an Ii-knockout background revealed a Th1 polarization of CD4+ T cells[171].

In the light of these findings the question of altered immune responses to exogenous peptide capture versus intracellularily-processed antigen arises. The group of Unanue found hen egg white lysozyme (HEL) to stimulate two distinct sets of T cells depending on the action of H2-DM[172]. An N-terminal flanking region of HEL was responsible for susceptibility to DM[173], which would not be of relevance for exogenously added peptides. Length variations of CLIP have also shown to differentially stimulate regulatory (Treg) or effector T cells by Hess and Thoburn in 2006 [174]. This was confirmed by active development of functional Treg cells upon addition of free antigenic peptide.

Does the modulation of antigen processing play a critical role in altered immune responses and might HLA-DM-inducible realignment of CLIP add another explanation for altering T cell responses? Is the proper functioning of the antigen processing machinery an important factor?

The impact of HLA-DM and cathepsin S was suggested to correlate with the allele-dependent stability of the pMHCII[175]. MHCII alleles with low affinity for CLIP are more likely to present affine exogenous antigen on the cell surface, even in the absence of the two components. Interestingly, it is exactly the low affine MHCII/CLIP complexes that were supposed to play a decisive role in autoimmunity[176,177]. In such a model, a certain pool of surface-presented self-peptide (e.g. CLIP) would then act towards enhanced tolerance. Although antigen processing is mediated by more than HLA-DM and one type of cathepsins, the critical role of these two might also imply a potential role of flipping CLIPs in autoimmunity. Ii degradation in complex with MHCII might initially not allow a non-canonical orientation of CLIP fragments. It is supposed that Ii aligns the CLIP core canonically based on structural and mutational studies[160,178,179]. The stepwise action of cathepsins will then mainly create fragments long enough to reside canonically as digestion motifs close to the core will be less accessible[180]. However, Chicz *et al.* found $CLIP_{106\text{-}120}$ to be the most prominent Ii fragment in a DM-depleted cell line[119] indicating that trimming to the core is possible without catalyzed peptide exchange. Similarly, in 2004 Röhn *et al.* found short CLIP fragments on a low-DM background in mature DCs[169]. Unfortunately, the definite peptide orientation cannot be concluded from this, since orientation-dependent antibodies are not available to date. Hypothetically, trimming of released, soluble fragments might generate a growing pool of short CLIP capable of inversion to restore H-bonds. Based on that canonical CLIP orientation presupposes a down-regulated functioning of cathepsins. Then inverted CLIP potentially acts autoimmunogenic if invariant chain processing in the periphery is different to the thymus. However, according to Bakke and Dobberstein (1990) affine CLIP-binding alleles require the general removal of an endosomal retaining motif in Ii by cathepsin S for pMHCII surface presentation[181].

HLA-DM will at least create a fraction of inverted CLIP based on the results presented here. In long $CLIP_{102\text{-}120}$ the orientational equilibrium indicated a similar thermodynamic stability of both complexes. H-bond networks were saturated in both orientations due to peptide length and the anchor symmetry of CLIP accounted for comparable pocket occupation.

Conformation-specific antibodies could help determining an orientational ratio in dependence of the maturation state of APCs or HLA-DM expression.

Inversion might explain the bimodal behavior of other peptides when presented to T cells. The findings for HEL[182] could be transferred to diabetes-related antigens where only a limited number of relevant epitopes has been elucidated. Recent studies focused on unexpected weak binders[183] or atypical binding modes[184]. The partial occupation of the I-A^{g7} binding cleft by a self-antigen was held responsible for low pMHCII stability, escape from negative selection and the onset of autoimmunity in a mouse model. In such a scenario, only a large local concentration of antigen would allow MHC occupation and the following immune response to be initiated. Realignment could explain findings (e.g. in reference[185]) in a way that exogenous peptide will bind inverted whereas longer fragments from processing will be trapped canonically or vice versa. This could be examined by investigating peptide inversion for diabetes-related alleles such as I-A^{g7} (mouse) or HLA-DQ8 (human).

The existence of separate pMHC pools provides another possible explanation for autoreactive T cells to escape selection. Register isomerism might account for co-existing HLA-DQ/CLIP isomers in a transfected B lymphoblastoid cell line[120]. Here, it remained questionable if thymic presentation could potentially be so different from peripheral processing. However, HLA-DQ was confirmed to be involved with both CLIP cohorts in the peripheral and central lymphoid organs[186]. A link to celiac disease was suggested for a register-shifted CLIP sequence and its binding to DQ2. Again, tissue-specific expression of HLA-DM and cathepsins together with antigen abundance might be a critical point to be looked at in future research since this might bias the formation of atypical peptide fragments.

The potential immunological relevance of inverted antigens is displayed in figure 4.2. Complete charge reversal of canonical and flipped CLIP would elicit two entirely different cohorts of T cell subsets, since the high specificity of the T cell receptor will sense this change in surface polarity. Even if autoreactive T cells are fully depleted in the thymus for the canonical self-peptide-orientation this will not prevent detection of inverted peptides in the periphery. Future work is of crucial necessity for the proof of inverted antigens to be present on cell surfaces and to induce T cell responses. A starting point to find such distinct T cell sets for the two different pMHCII orientations could be the design of genetically linked single-chain constructs that sterically allow for only a single orientation. Ideally, T cell

populations will be deciphered that do not cross-react with the respective second orientation. Immunization of probands with modified peptides would then lead to *in vivo* T cell stimulation and become detectable with the appropriate single-chain MHC-tetramers *ex vivo*[187]. By this a progressive discovery of autoimmune-epitopes might be possible. The focus, aside from proving the existence of such CLIP-orientation-dependent T cell clones, has to be on the identification of unknown epitopes displaying bimodal orientations. Studies with a similar setup like presented here will have to be extended to alleles with stronger impact for autoimmunity than HLA-DR1, in particular human HLA-DQ (diabetes) or HLA-DR2 (multiple sclerosis). Ideally this is complemented by mouse studies where profound experience with model diseases is available with non-obese diabetes (NOD)[188] and experimental autoimmune encephalomyelitis (EAE)[189].

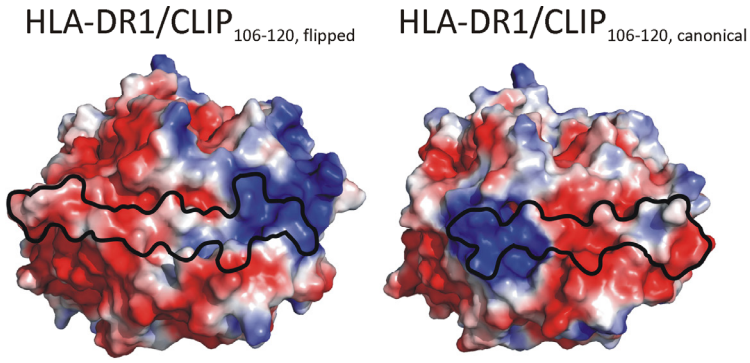

Figure 4.2: Electrostatic surfaces of HLA-DR1/CLIP$_{106-120}$-complexes as based on structures with pdb codes 3pgc (left) and 3pgd (right). Only the α1β1 domains of the MHCII are shown as top view, indicating the surface seen by the T-cell receptor. The peptide derived surface is indicated by a black line, emphasizing the drastic charge redistribution induced by CLIP inversion. Blue and red correspond to electrostatic surface potentials of ±2 kT/e. Surface potentials were calculated using the program APBS[190] by Sebastian Günther.

4.3.2.2 A unique chaperoning function of CLIP encoded by its sequence?

The degeneracy of CLIPs is reflected through their variable sequence length during presentation. However, despite of that a critical core motif was found to be crucial for MHCII stability and transport to endosomes[191]. The ability to act as a chaperone in maturation of almost any MHCII allelic subtype indicates promiscuous binding capability, albeit with affinities covering four orders of magnitude[192]. Increased recycling of MHCII after addition of CLIP to DCs has been observed[193] indicating a function in MHCII down-regulation. Besides, variable truncation points during digestion of Ii were explained by the action of multiple

cathepsins[180] such that independent of tissue or cell stage rapid degradation of Ii is possible. This explains the simultaneous occurrence of multiple length fragments in previous studies.

Possibly, the herein observed CLIP core sequence symmetry – with methionines, prolines and alanines as moderate anchors, favoring peptide inversion - also accounts for sufficient binding to different alleles. Bimodal binding of CLIP, in principle, could then enhance the probability that CLIP is bound tightly by a particular allele. It remains elusive why nature would set up such a redundant system to ensure proper CLIP function. One answer would be that rapid rebinding of CLIP will be possible in all types of MHCII if no affine antigenic peptide is available. It seems more economical to store MHCII rather than degrade it during underemployment. Protein inactivation would be prevented by CLIP rebinding. In fact, studies describe a storage pool retaining MHCII in resting APCs[194] or cells with improper CLIP functioning[195]. Instead of adapted mechanisms for individual alleles Ii fits the requirements of all haplotypes.

The hypothesis of generously chaperoning CLIP is supported by findings from herpes simplex virus which harbors comparable binding motifs in its protein fragments thereby escaping immune presentation[196]. This demonstrates the high biological risk of promiscuous regulatory mechanisms to be targeted by invaders. Invariant chain, however, might have found a way to equip its CLIPs with multiple features to maintain chaperoning function. Peptide inversion would be one option to ensure this safeguard mechanism.

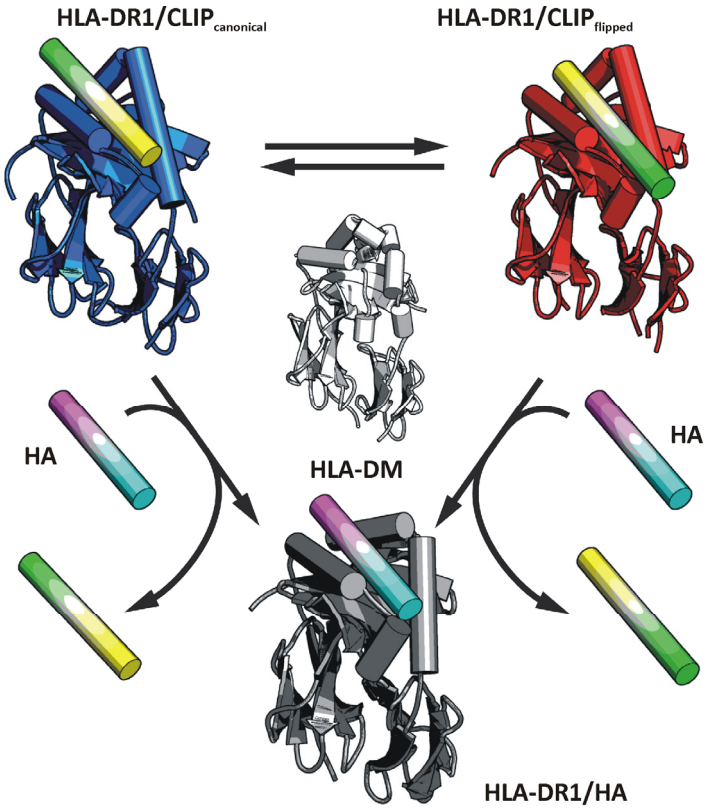

Figure 4.3: Simplified scheme of the extended chaperoning function of CLIPs (class II associated invariant chain-derived peptides) based on the experimental observations. HLA-DR1 is shown in complex with canonical (blue) or inverted (red) CLIP (as cylinder). The CLIP color code indicates the orientation. The inter-conversion is facilitated by HLA-DM (grey), enabling both CLIP-MHCII complexes to replace ligand for the viral antigen $HA_{306-318}$. Parts of the figure have been provided by Sebastian Günther.

4.3.2.3 The role of experimental bias: Co-refolding vs. loading

The chaperoning function of CLIP starts with the co-expression and sequestration of invariant chain (Ii) into the endoplasmic reticulum (ER). Ii has been assumed to act co-translational in the folding of MHCII[197]. Recent studies suggested an interaction between the α-chain and CLIP's N-terminus while residues forming pockets 6 to 9 bind the CLIP C-terminal half[198]. Although difficult to prove it is agreed on that Ii and MHCII fold simultaneously to guarantee an *ab initio* occupied binding cleft. Models, in which the preterm capture of peptides in the ER accounts for the presentation of self-peptides, have been discussed[199]. However, evidence is mounting that the cross-presentation of self-antigens rather involves peptide capture in downstream endo-/ lysosomal compartments (e.g. by autophagy)[200].

This work differentiates a dynamic behavior of CLIPs with regard to their time-point when encountering the MHCII, i.e. either during co-refolding with HLA-DR1 or during posterior loading to the protein. The lack of experimental data on the influence of different buffer

conditions during protein preparation - in particular folding - prohibits an assumption towards the role of pH, salt concentration etc. for peptide alignment. *In vivo,* the range of pH faced by a pMHC over the presentation pathway covers three orders of magnitude[201]*;* not including strong acidic conditions in lysosomal compartments of pMHCII degradation. Not only will this affect local protonation/folding of the protein, but in particular H-bond stabilization between MHC and antigen will be subject to change. The observation of apparently very different T cell responses to pMHCII either assembled in endosomes or on the cell surfaces has been made before[172]. An exemplary study describing pH-based preferences for particular residues at pockets 6 and 9 within the murine MHCII H2-A^{g7} can be found in literature[202]. Accordingly, mildly alkaline conditions during HLA-DR1 *in vitro* refolding might lead to a subordinate role of H-bonds which, in turn, will be a determinant of thermodynamic stability in more acidic conditions like NMR buffers. In line with this, regular antigen loading in acidic compartments would always provoke the formation of the most stable pMHCII from a thermodynamic point of view. Presumably, this process is not accidentally co-localized with the proteolytic digestion of antigen. In contrast, the optimal sequestration of peptide side-chains into MHC surface pockets will be of greater importance for folding as has been assumed for HLA-DR1 before[30]. Possibly, the stereo-chemically mirrored peptide backbone after inversion would be a non-preferred option for folding when a similar pocket occupation is possible in a canonical alignment. Presumably, the peptide backbone stereo-chemistry does play a role in kinetic stability as it is supported by the lack of success in crystallization of candidate peptides for inverted binding (see paragraph 3.4.8).

Three possible experimental approaches would shed light on this problem. First, to unravel a role for chirality in peptides D- instead of L-amino acids could be used. Second, a comprehensive investigation of pH-impact on flipping would help to clarify the role of H-bonds. Notably, no catalytic action of HLA-DM should be possible anymore at neutral pH. Third, selected peptides might rather reveal a CLIP-like dynamic behavior when studied directly after co-refolding. It still has to be considered that inversion could also appear from the flipped into the canonical orientation.

4.3.3 Identification and prediction of inverted peptides other than CLIPs

The question arises whether peptide inversion is a unique phenomenon of this very HLA-DR1-CLIP complex. The pseudo-symmetry of CLIP certainly facilitates bidirectional binding to HLA-DR1 but it seems rather unlikely that amongst hundreds to thousands of peptides in a cell no sequence is found that fulfills the criteria of reverse binding. The question why no inverted peptide was crystallized so far provokes two observations to be mentioned. First, guided by a canonical understanding of peptide alignment, roughly half of all structures have been solved with a peptide genetically linked to the β-subunit. The linker likely would prohibit peptide inversion for steric reasons. Second, a number of pMHC complexes designated for crystal screens were certainly chosen or designed based on optimized anchor residues. Again, this introduced a strong bias with respect to pocket occupation, e.g. P1 for HLA-DR-subtypes. Consequently, unilateral empirical data and resultant algorithms in epitope prediction prevented to consider other alignment possibilities.

A growing number of epitope prediction resources for MHCII is available[32,203,204] which differ in particular details. Their increasing reliability depends on the number of deposited structures. Nevertheless, none of these algorithms can compete with epitope prediction for MHCI alleles. This might be caused by enhanced isomerism for longer sequences, since they might bind in different registers - and potentially orientations - to the open binding groove of MHCII. Here, peptide inversion additionally might account for inefficient correlation of prediction and measured pMHC stability.

Allowing for alternative alignments in epitope prediction will have to coincide with structures providing determinants of peptide inversion. At this stage the dilemma of a reasonable starting point crops up. Obviously there is no simple predictable motif for inverted presentation by HLA-DR1. Our unsuccessful attempt to crystallize further inverted pMHCII complexes and rather obtaining the canonical forms in some cases (see table 3.3) were likely caused by several inadequacies. Only deposited motifs with a correlation to pathologies were selected. Those were based on sequences that had been described as bound to HLA-DR1 before. Presumably, the putative existence of a canonical motif still generates a biased alignment. Binding to the spot membrane was clearly driven by the succession of proper anchor residues neglecting the impact of orientation. The more, all selected sequences came with sufficient length such that they could have escaped incomplete saturation of the H-bond network in the canonical direction.

Sub-populated complexes with inverted alignments might have been both not visible in NMR and failed to crystallize. Clearly, multiple orientations with similar populations were not present in any of the 12 preparations based on HSQC spectra, displaying one resonance per amino acid. Theoretically, the non-crystallized samples could still harbor inverted peptides. A broader crystal screen would have been desirable to potentially find conditions that shift equilibria towards inverted complexes. However, small amounts of synthesized peptide and the inefficient loading of low-affine peptides hampered such an approach.

Information from structures of inverted peptides thus might have to be gained from an artificial setup which would still provide useful conformational determinants for peptide inversion. One option addresses the stepwise terminal truncation of selected peptides in order to isolate the core motif for inverted binding. Limited proteolysis of peptide overhangs might also facilitate crystallization[205]. Alternatively, the substitution of individual CLIP residues could shift populations of canonical/inverted complexes. Their influence on complex stability and changes in crystal structures would provide useful insights. This approach of modifying the CLIP sequence seems advantageous as NMR assignments would possibly be transferable and allow deducing peptide orientations when crystallization fails. Similar studies on single-residue-contributions to pMHCII kinetics have been carried out in HLA-DR1. Experiments in the group of Jack Gorski[30,206], where HA side-chains were substituted systematically, led to a fundamental understanding of H-bond- and anchor residue-cooperativity of MHC-peptide complexes. Another promising option is the genetic linking of peptides to the α-subunits of MHCII. As demonstrated here for $CLIP_{106\text{-}120}$, non-linked HLA-DR1/peptide in both solution studies and our crystal structure well compares to the linked form. The increase of locally available peptide during (re)folding favors larger yields of native-folded protein. The approach is less cost-intense than refolding in the presence of excess peptide. The concept of covalent linkage was also used for canonical structures[139,207]. The group of Kappler created an extensive library encoding canonical β-subunit-linked peptides[208] which are screened for motifs stimulating (autoreactive) T cells. In order to determine the potential role of inverted antigens it appears promising to expand this approach to α-subunit-linked peptides with inverted presentation to shed light on their putative impact for autoimmune diseases. Protease-cleavage sites within the linker would allow using non-linked peptide at later stages e.g. to determine susceptibility to HLA-DM. This was shown to be crucial in recent studies for overcoming increased stability of a

peptide-subunit-linked pMHCII complex[149]. Finally, computational methods might help to delineate the rules governing peptide alignment. *In silico* calculations could estimate the possibility of inverted peptides in pMHC complexes. However, molecular dynamics simulations will heavily rely on experimental restraints. In turn, latter might help to improve the quality of a calculation when implemented. Interestingly, in 1996 the group of Terry Lybrand performed a hypothetical docking and simulation of an inverted GAD (glutamic acid decarboxylase) peptide bound to HLA-DQ[157]. Despite the lack of experimental confirmation, no principal hindrance for flipped MHCII-peptides was already discussed then. Altogether, in combining these approaches an improved prediction of epitopes could precede a more successful selection of inverting motifs.

4.3.4 Tools to identify the peptide orientation *in vivo*

Rapid and unambiguous determination of peptide inversion is of particular interest if studies do not allow comprehensive structural analyses. Tools to probe peptide orientations would also validate a structure but proving peptide orientations on cell surfaces poses a challenge.

Ideally, orientation-dependent antibodies could be generated from phage/yeast-display libraries and screened against a pMHC with unambiguous orientation. The herein achieved concept of genetic α-linkage is a promising tool to select the orientation-specific antibodies during screening of the respective libraries. Similar to canonical alignment during refolding of β-linked pMHCII, the unstructured $(G_4S)_3$-linker did not interfere with binding of the peptide to HLA-DR1 in the α-linked pMHCII. Although the immediate inverted alignment of α-linked $CLIP_{106\text{-}120}$ seemed to contradict the canonical orientation of unlinked $CLIP_{106\text{-}120}$ directly after refolding, this underlines the bias that is introduced by the steric conditions of the linker to the α-subunit. This procedure bears great potential to compose inverted complexes that might otherwise be difficult to isolate from bidirectional mixtures of unlinked pMHCII complexes. The design should also be transferable to eukaryotic expression systems. Antibodies - functionalized with fluorophores for fluorescence activated cell sorting (FACS) - could be tested in transfected cells. Ideally, linked pMHCII complexes would be incorporated into tetramers[187] to identify/isolate cognate T cells *ex vivo*.

FRET (Förster resonance energy transfer) provides an alternative to define peptide orientation *in vitro*. Fluorophores, attached to both the protein and peptide, allow energy transfer in close proximity. However, fluorophores might change the peptide's orientational

equilibrium due to the introduction of H-bonds between the fluorophore and the protein. Also changes in hydrophobicity and steric rearrangements are to be considered to influence natural peptide orientations. Difficulties are met in applications based on chemical cross-linking and mass-spectrometric analysis. Cross-linking in presence of imidoesters or formaldehyde is difficult to interpret because of unspecific linkages. As pMHC will need to be present as an equimolar complex high throughput setups are disfavored because additional purification steps are required. In contrast, the site-specific usage of photo-sensitive cross-linkers such as para-Benzoyl-phenylalanine[209] requires a strict complex geometry which might be hindered by the intrinsic dynamics of the MHC complex.

For detailed investigations of complexes NMR is a suitable tool. Paramagnetic tags and intermolecular NOEs will unambiguously yield distances and orientations. Complete assignments are not necessarily required but in order to yield site-resolved information on peptide binding the identity of the resonances at this site needs to be known. Although challenging, peptide orientation will only be unambiguously proven with information at the level of individual amino acids.

4.4 Caged HA peptide for MHCII detection in hyp-Xe^{129}-NMR

In addition to investigating HLA-DR1 by NMR-spectroscopy, this study aimed at proving the applicability of peptide-functionalized cryptophane to sense binding of MHCII in ^{129}Xe-NMR. Indirect detection of the peptide-MHC binding event *in vitro* has been achieved through hyperpolarized ^{129}Xe, a fundamental prerequisite for *in vivo* applications at low concentrations.

4.4.1 Peptidic probes for MR imaging of cell surface MHC

Observing antigenic peptide rather than the MHC protein seems to be an alternative path to investigate pMHC complexes. Assignment procedures would be less time-consuming and peptides could be tested in higher throughput. However, isotope-labeled peptides still come at relatively high costs. Recombinant expression and *in vitro* binding of labeled peptide has recently been applied to MHCI[210]. In fact, peptides bear great potency as probes for *in vivo* studies. MHCII is a promising target for imaging as it accumulates at sites of inflammation. Using isotope-labeled proteins *in vivo* is impossible with the exception of few sophisticated

approaches from in-cell-NMR[211]. Thus, detection is mainly based on fluorescence methods which only allow for limited tissue penetration of the corresponding electromagnetic radiation in whole-body imaging[212]. Although recent attempts for directed evolution of fluorescent proteins are promising[213] penetration depth would not compare to magnetic resonance-based imaging (MRI). Here, probes normally use a gadolinium-complex moiety to locally enhance the relaxation of water[214]. So far no antigen-presenting cell has been imaged with MHC-targeted probes by gadolinium-based, proton-detected MR according to current literature.

Similarly, since the late 1980s relaxivity is achieved with iron oxide nanoparticles (IONs)[215]. They require a more adjusted chemistry but show advantageous half-life and bio-compatibility. In 2008 the group of Stephen O´Brien targeted the rat MHCII RT1 *in vivo* by antibodies functionalized with super-paramagnetic IONs (SPIONs)[216] to probe expression in the renal medulla. For the first time inflammation was detected with IONs not relying on unspecific moiety-uptake by macrophages.

Hyperpolarized noble gases - in particular xenon-129 - are a novel trend in biology benefiting from caging compounds with characteristic chemical shifts. The power in sensing binding or enzymatic reactions has recently been proven[78,217]. In this study the concept of hyperpolarized xenon-129 was successfully applied to HLA-DR1/HA and might represent an initial step to alternative imaging techniques.

4.4.2 (Bio-)applicability of Cage-HA

Bio-tolerance is mandatory to any MR-based biosensor and determined by toxicity and bio-transformability, i.e. the metabolizing and subsequent degradation of the biosensor. However, investigating tolerance will only pay off when functionality, specificity and sensitivity of the probe have been tested *in vitro* as was achieved to some extend for Cage-HA. Initial evidence for good bio-availability was taken from mouse experiments. No effect on animal health was notable when Cage-HA had been injected into mice (20 µg/mouse, see *Methods* chapter). To determine the potential toxicity of Cage-HA, nevertheless, would require intensive testing of tolerance to varying concentrations and times of application. The fusion peptide was capable of stimulating HLA-DR1/HA restricted T cells *in vivo* and *ex vivo* with some restriction compared to wild-type HA. Presumably, T cells positive for Cage-HA were more restrictively shaped during selection than those for HA alone. Thus, most of them

would also respond to wild-type HA *ex vivo*. In contrast, wild-type HA-primed cells would only partially respond to Cage-HA. However, this assumes a comparable antigen presentation by both HLA-DR1 complexes. Efficient antigen loading is pivotal for Cage-HA to function as *in vivo* probe. Unspecific binding will be of relevance in whole-body-imaging where the probe is supposed to exclusively 'stain' patches with specific targets enriched. Similarly, a control peptide not related to the HLA-DR1/HA - TCR system would have been of need, but limited amounts of substance did not allow the production of additional constructs at that time. Moreover, turnover of Cage-peptide might be different to wild-type HA and quantification of its metabolism over time would be required in future experiments.

4.4.3 The binding of Cage-HA to HLA-DR1: Direct and indirect detection

Cage-HA proved to capture ^{129}Xe for sufficient time to yield a characteristic cryptophane resonance *in vitro*. Binding of an antigen to MHC has been demonstrated here by xenon-NMR for the first time. The chemical shift difference of 1 ppm between free and MHC-bound Xe-cryptophane is in the lower range compared to results from previous studies utilizing targeted cage compounds[79,217]. To detect subtle changes in chemical environments between 'bound' and 'unbound' cage, flexibility was to be balanced with restrictiveness. If the cryptophane is kept too close to the binding site, this might lead to sterically induced, yet unwanted interactions with the protein surface. To the contrary, if the linker is too long, the binding site might be too remote to be sensed by the caged xenon. As our results already showed that binding of Cage-HA is slightly compromised compared to wild-type HA (see figure 3.39), it seems unlikely that the linker length could be further reduced without additional loss of affinity. For the particular case of HLA-DR1/HA figure 4.4 illustrates the assumed correlation between linker length and signal shapes of caged HA. Here, the interplay of linker length, favoring xenon exchange and sharp line shapes, and chemical shift sensitivity by shortened linkers is delineated. Decreased xenon exchange in HLA-DR1-bound Cage-HA was also found in our studies (see section 3.5.6). Probably, a less hydrophobic cryptophane, as for example type-1,1,1 introduced by Fairchild *et al.* in 2010[218] would allow attaching shorter linker constructs that could in turn lead to larger chemical shift differences of ^{129}Xe between free and bound Cage-HA. In addition to modifying cryptophane-A itself, the chemical composition of the linker was shown to influence chemical shift, line width and xenon on-rate of the moiety through diastereomers, flexibility and length[219,220]. Notably, loss

of cage-signal - as with yet shorter linkers - can also indicate binding[79] (see figure 4.4) but prohibits using exclusively the frequency of bound probes in appropriate pulse schemes.

Presumably, unspecific interactions of xenon with HLA-DR1 would not have been visible by resonances in the cryptophane chemical shift region. However, unspecific binding could additionally be ruled out with HYPER-CEST where linearity between cage concentration and loss of bulk xenon was demonstrated. Certainly, no additional unspecific binding would have been observable when excess Cage-HA was added to HLA-DR1/Cage-HA (see figure 3.41). Thus, the effect of CEST could be ascribed to the presence of cage-compound and confirms the specificity of the 1 ppm chemical shift difference between free and HLA-DR1-bound Cage-HA in figure 3.40.

Favorably, in the CEST experiment the high excess of bulk xenon was inert to significant losses of polarization (figure 3.41). Using solute bulk xenon for data interpretation in experimental setups of low concentrations appears to be a good choice as the potential application of cage-probes *in vivo* might lead to resonance line-broadening and rapid signal loss. However, concentrations of cages *in vivo* will have to be much lower. HYPER-CEST has been shown to work at nanomolar concentrations[82]. The group of Alex Pines detected a 1 µM sample with CEST whereas conventional averaging did not yield signals after 450 scans[221]. In contrast to the Pines group our work does not yet give evidence for the detection of Cage-HA exclusively by CEST but not by direct simple averaging. Nevertheless, a starting point to reduce concentrations is given by the applicability of HYPER-CEST to pMHC. So far, the method had only been tested in the biotin-streptavidin complex formation[82] which is of little impact to human biology.

Cage-HA measurements were performed in a weak magnetic field with improper shimming adjustments, manual sample agitation and a home-built coil. Very strong fields in combination with state-of-the-art probeheads allow the detection of thermally polarized xenon-129. Significant progress would be made in combining the sensitivity of hyperpolarization with the improved resolution from high-field NMR spectrometers. Then, a chemical shift difference of 1 ppm will be expressed by several hundred Hertz. This allows a distinction of free and bound populations more effectively.

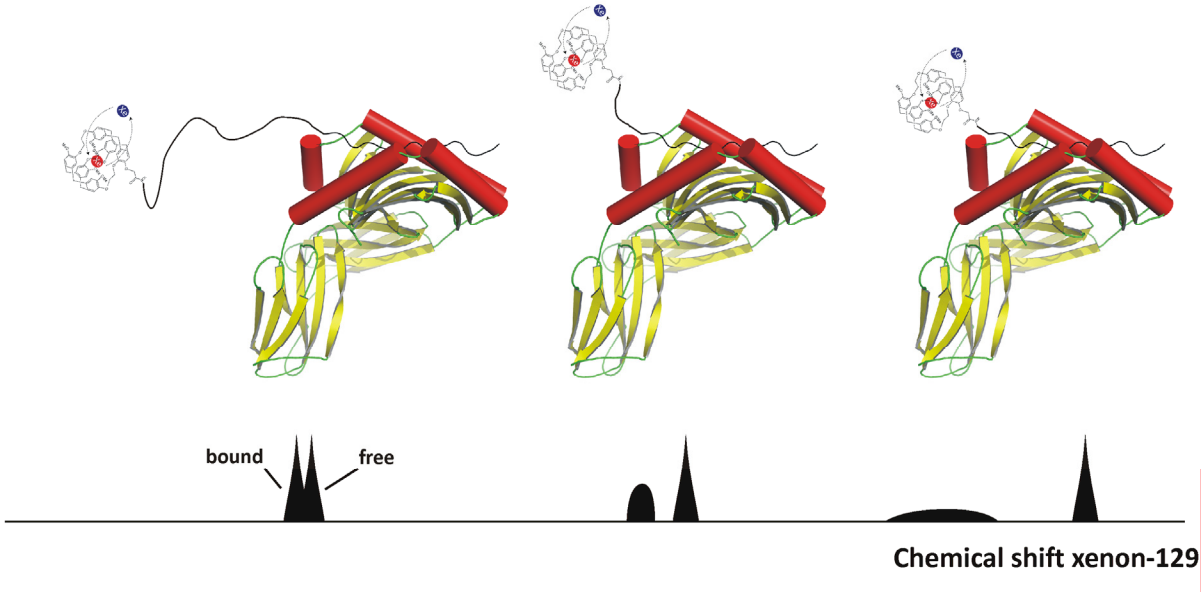

Figure 4.4: Correlation between linker modulation and line shape as anticipated for Cage-HA when bound to HLA-DR1. The right resonance represents the free Cage-HA and the left peak indicates MHCII-bound peptide. As sketched here, linker shortening will lead to enhanced sensitivity towards the target as displayed by a larger change in chemical shift. On the other hand confined linker flexibility might lead to inefficient xenon exchange and enhanced relaxation shown by lowered S/N and line-broadening. The structure used in the figure is pdb-encoded with 1dlh[33] and presented as cartoon with cylindrical helices. Note that cryptophane and xenon are shown out of scale in size.

4.4.4 Current limitations and perspectives for cryptophane-based MR probes

Application of caged-xenon-MR *in vivo* is critically dependent on three factors: i) toleration of the probe by the organism, ii) signal detection, and iii) sensitivity. Tolerance is only addressable by determining half-lethal concentrations in studies that are performed according to official guidelines. More importantly, information on cryptophane metabolism and pharmacokinetics is needed in the long term. Incomplete bio-transformation bears the danger of enrichment in the liver or the kidney. Mass spectrometric investigations of mice organs will have to precede studies in humans. Antibodies for cage-scaffolds could trace degradation or confirm their integrity during their applications *in vivo*. Likely, half-life is depending on the probe itself as target-binding might prevent its degradation.

Probing intracellular targets remains problematic with MR as has been discussed extensively for gadolinium-chelated compounds[222,223]. Cellular uptake was found to be dominated by endocytosis and did not allow unambiguously addressing targets in the cytoplasm or other compartments inside the cell. To study pathways of internalized MR probes several groups have used bi-functional ligands attached to fluorophores which facilitate their localization by

microscopic methods[224,225]. A first study on cage-fused peptide uptake was published in 2008[226]. Very recently, Boutin *et al*. successfully combined fluorescence data and xenon spectroscopy in the transferrin system[227].

The current design suggests that several of these experimental aspects could be optimized by surface markers like MHCII. Yet it remains challenging to examine how continuous supply with fresh hyperpolarized xenon can be achieved in a certain tissue[65]. Resorption via lungs might not provide sufficient partial pressure in the blood for efficient encapsulation and detection of ^{129}Xe. Certainly, accessibility to cells is also depending on tissue-specific factors. Detection is also limited by the local concentration of target protein in the body. Lymph nodes highly enriched in MHCII molecules might therefore be an advantageous locus. Broadly distributed proteins will be difficult to detect; in particular when the signal is additionally split as was found in lungs for gaseous xenon[74]. Significantly different MR parameters like T1/T2 times and xenon-cage exchange rates might require further experimental adjustments in case tissues are probed. Hyperpolarized xenon-129, for example, yields a T1 of few seconds in blood[228] compared to 141 s *in vitro* determined by Dr. Wolfgang Kilian (PTB Berlin) during this study[92].

Transition into living systems will have to pass cell culture stages. For spectroscopic detection equipment will have to allow the supply of media with xenon and the experimental setup has to fit with hardware requirements. Few studies have seriously addressed this bottleneck[229,230]. High cell densities were incompatible with prolonged survival as they are ideally required in xenon-NMR studies (data not shown and personal communication with Prof. Ivan Dmochowski, University of Pennsylvania). High-resolution spectroscopic imaging could only be carried out in wide-bore high-field spectrometers which are now available and allow the imaging of tissue at almost cellular scale[231]. Their applicability to imaging studies with xenon yet needs to be examined. Higher xenon-129 polarization would raise the observable magnetization. 20 % as by Dr. Wolfgang Kilian (PTB Berlin) are not regularly achieved by other groups or commercial polarizers. A recent paper, however, reported levels of more than 50 % for large scale production[232]. The HYPER-CEST pulse scheme is adjustable towards more repetitions and loops (see figure 3.41). However, saturation could lead to sample heating and continuous xenon supply poses some challenges to the experimental settings. Instead, the transfer of CEST to the gas signal after extraction from the solution would in principle allow to achieve higher sensitivity[233]. Increased

exchange would also be monitored in cage-dendrimers[234] although a steric confinement of the ligand could be problematic for target recognition. Analysis of multiple targets has been suggested by Spence *et al.* in 2006[78] using differently derivatized cryptophanes which resulted in separate chemical shifts in one experiment. Similarly, the modification or racemization of linkers might save resources and time for simultaneously probed targets[219].

References

1. Beck, G. & Gail, S.H. Immunity and the Invertebrates. *Scientific American* 275, 60-6 (1996).
2. Mayer, G. Microbiology and Immunology, Part 1, Immunology. in *On-Line Textbook* (USC School of Medicine).
3. Harrington, L.E. et al. Interleukin 17-producing CD4+ effector T cells develop via a lineage distinct from the T helper type 1 and 2 lineages. *Nat Immunol* 6, 1123-32 (2005).
4. McHeyzer-Williams, L.J. & McHeyzer-Williams, M.G. Antigen-specific memory B cell development. *Annu Rev Immunol* 23, 487-513 (2005).
5. Monks, C.R., Freiberg, B.A., Kupfer, H., Sciaky, N. & Kupfer, A. Three-dimensional segregation of supramolecular activation clusters in T cells. *Nature* 395, 82-6 (1998).
6. Smith-Garvin, J.E., Koretzky, G.A. & Jordan, M.S. T cell activation. *Annu Rev Immunol* 27, 591-619 (2009).
7. Hogg, N., Patzak, I. & Willenbrock, F. The insider's guide to leukocyte integrin signalling and function. *Nat Rev Immunol* 11, 416-26 (2011).
8. Sadegh-Nasseri, S., Chen, M., Narayan, K. & Bouvier, M. The convergent roles of tapasin and HLA-DM in antigen presentation. *Trends Immunol* 29, 141-7 (2008).
9. Chapman, H.A. Endosomal proteases in antigen presentation. *Curr Opin Immunol* 18, 78-84 (2006).
10. Harding, C.V. Intracellular organelles involved in antigen processing and the binding of peptides to class II MHC molecules. *Semin Immunol* 7, 355-60 (1995).
11. Turk, V., Turk, B. & Turk, D. Lysosomal cysteine proteases: facts and opportunities. *EMBO J* 20, 4629-33 (2001).
12. Denzin, L.K. & Cresswell, P. HLA-DM induces CLIP dissociation from MHC class II alpha beta dimers and facilitates peptide loading. *Cell* 82, 155-65 (1995).
13. Busch, R. et al. Achieving stability through editing and chaperoning: regulation of MHC class II peptide binding and expression. *Immunol Rev* 207, 242-60 (2005).
14. Busch, R., Doebele, R.C., Patil, N.S., Pashine, A. & Mellins, E.D. Accessory molecules for MHC class II peptide loading. *Curr Opin Immunol* 12, 99-106 (2000).
15. Denzin, L.K., Sant'Angelo, D.B., Hammond, C., Surman, M.J. & Cresswell, P. Negative regulation by HLA-DO of MHC class II-restricted antigen processing. *Science* 278, 106-9 (1997).
16. Lazarski, C.A. et al. The kinetic stability of MHC class II:peptide complexes is a key parameter that dictates immunodominance. *Immunity* 23, 29-40 (2005).
17. Starr, T.K., Jameson, S.C. & Hogquist, K.A. Positive and negative selection of T cells. *Annu Rev Immunol* 21, 139-76 (2003).
18. Anderson, M.S. et al. Projection of an immunological self shadow within the thymus by the aire protein. *Science* 298, 1395-401 (2002).
19. Sakaguchi, S. Naturally arising CD4+ regulatory t cells for immunologic self-tolerance and negative control of immune responses. *Annu Rev Immunol* 22, 531-62 (2004).
20. Edwards, J.C., Cambridge, G. & Abrahams, V.M. Do self-perpetuating B lymphocytes drive human autoimmune disease? *Immunology* 97, 188-96 (1999).
21. Jones, E.Y., Fugger, L., Strominger, J.L. & Siebold, C. MHC class II proteins and disease: a structural perspective. *Nat Rev Immunol* 6, 271-82 (2006).
22. Shiina, T., Hosomichi, K., Inoko, H. & Kulski, J.K. The HLA genomic loci map: expression, interaction, diversity and disease. *J Hum Genet* 54, 15-39 (2009).
23. Abbas, A.K. & Lichtman, A.H. Ch. 10 Immune responses against tumors and transplant. in *Basic Immunology. Functions and disorders of the immune system. 3rd.* (Saunders, 2009).

24. Jacob, S., McClintock, M.K., Zelano, B. & Ober, C. Paternally inherited HLA alleles are associated with women's choice of male odor. *Nat Genet* 30, 175-9 (2002).

25. Madden, D.R., Gorga, J.C., Strominger, J.L. & Wiley, D.C. The three-dimensional structure of HLA-B27 at 2.1 A resolution suggests a general mechanism for tight peptide binding to MHC. *Cell* 70, 1035-48 (1992).

26. Kumar, P. et al. Structural basis for T cell alloreactivity among three HLA-B14 and HLA-B27 antigens. *J Biol Chem* 284, 29784-97 (2009).

27. Matsuki, Y. et al. Novel regulation of MHC class II function in B cells. *EMBO J* 26, 846-54 (2007).

28. Zavala-Ruiz, Z., Strug, I., Anderson, M.W., Gorski, J. & Stern, L.J. A polymorphic pocket at the P10 position contributes to peptide binding specificity in class II MHC proteins. *Chem Biol* 11, 1395-402 (2004).

29. Anderson, M.W. & Gorski, J. Cooperativity during the formation of peptide/MHC class II complexes. *Biochemistry* 44, 5617-24 (2005).

30. Ferrante, A. & Gorski, J. Cooperativity of hydrophobic anchor interactions: evidence for epitope selection by MHC class II as a folding process. *J Immunol* 178, 7181-9 (2007).

31. Belmares, M.P., Busch, R., Mellins, E.D. & McConnell, H.M. Formation of two peptide/MHC II isomers is catalyzed differentially by HLA-DM. *Biochemistry* 42, 838-47 (2003).

32. Rammensee, H., Bachmann, J., Emmerich, N.P., Bachor, O.A. & Stevanovic, S. SYFPEITHI: database for MHC ligands and peptide motifs. *Immunogenetics* 50, 213-9 (1999).

33. Stern, L.J. et al. Crystal structure of the human class II MHC protein HLA-DR1 complexed with an influenza virus peptide. *Nature* 368, 215-21 (1994).

34. Bjorkman, P.J. et al. Structure of the human class I histocompatibility antigen, HLA-A2. *Nature* 329, 506-12 (1987).

35. Brown, J.H. et al. Three-dimensional structure of the human class II histocompatibility antigen HLA-DR1. *Nature* 364, 33-9 (1993).

36. Garboczi, D.N. et al. Structure of the complex between human T-cell receptor, viral peptide and HLA-A2. *Nature* 384, 134-41 (1996).

37. Wittlich, M., Thiagarajan, P., Koenig, B.W., Hartmann, R. & Willbold, D. NMR structure of the transmembrane and cytoplasmic domains of human CD4 in micelles. *Biochim Biophys Acta* 1798, 122-7 (2010).

38. Call, M.E. et al. The structure of the zetazeta transmembrane dimer reveals features essential for its assembly with the T cell receptor. *Cell* 127, 355-68 (2006).

39. Esposito, G. et al. Removal of the N-terminal hexapeptide from human beta2-microglobulin facilitates protein aggregation and fibril formation. *Protein Sci* 9, 831-45 (2000).

40. Sadegh-Nasseri, S. & McConnell, H.M. A kinetic intermediate in the reaction of an antigenic peptide and I-Ek. *Nature* 337, 274-6 (1989).

41. Marin-Esteban, V., Falk, K. & Rotzschke, O. "Chemical analogues" of HLA-DM can induce a peptide-receptive state in HLA-DR molecules. *J Biol Chem* 279, 50684-90 (2004).

42. Sadegh-Nasseri, S. et al. Conformational heterogeneity of MHC class II induced upon binding to different peptides is a key regulator in antigen presentation and epitope selection. *Immunol Res* 47, 56-64 (2010).

43. Jablonsky, M.J., Subramaniam, P.S., Johnson, H.M., Russell, J.K. & Krishna, N.R. The solution structure of a class II major histocompatibility complex superantigen binding domain. *Biochem Biophys Res Commun* 234, 660-5 (1997).

44. Hoshino, M. et al. Mapping the core of the beta(2)-microglobulin amyloid fibril by H/D exchange. *Nat Struct Biol* 9, 332-6 (2002).

45. Varani, L. et al. Solution mapping of T cell receptor docking footprints on peptide-MHC. *Proc Natl Acad Sci U S A* 104, 13080-5 (2007).

46. Driscoll, P.C. et al. Two-dimensional nuclear magnetic resonance analysis of a labeled peptide bound to a class II major histocompatibility complex molecule. *J Mol Biol* 232, 342-50 (1993).

47. Berman, H.M. et al. The Protein Data Bank. *Acta Crystallogr D Biol Crystallogr* 58, 899-907 (2002).

48. Keeler, J. *Understanding NMR spectroscopy*, (John Wiley & Sons; 1st edition, 2005).

49. Ernst, R.R. Nobel Lecture. Nuclear magnetic resonance Fourier transform spectroscopy. *Biosci Rep* 12, 143-87 (1992).

50. Karplus, M. Vicinal Proton Coupling in Nuclear Magnetic Resonance. *J. Am. Chem. Soc.* 85, 2870–1 (1963).

51. Wuthrich, K. NMR studies of structure and function of biological macromolecules (Nobel lecture). *Angew Chem Int Ed Engl* 42, 3340-63 (2003).

52. Morris, G.A. & Freeman, R. Enhancement of nuclear magnetic resonance signals by polarization transfer. *J. Am. Chem. Soc.* 101, 760–62 (1979).

53. Ernst, R.R., Bodenhausen, G. & Wokaun, A. Chapter 4: Fourier Transformation, weighting functions and sensitivity. in *Principles of Nuclear Magnetic Resonance in One and Two Dimensions* (Oxford, 1987).

54. Ikura, M., Kay, L.E. & Bax, A. A novel approach for sequential assignment of 1H, 13C, and 15N spectra of proteins: heteronuclear triple-resonance three-dimensional NMR spectroscopy. Application to calmodulin. *Biochemistry* 29, 4659-67 (1990).

55. LeMaster, D.M. & Richards, F.M. NMR sequential assignment of Escherichia coli thioredoxin utilizing random fractional deuteriation. *Biochemistry* 27, 142-50 (1988).

56. Tzakos, A.G., Grace, C.R., Lukavsky, P.J. & Riek, R. NMR techniques for very large proteins and rnas in solution. *Annu Rev Biophys Biomol Struct* 35, 319-42 (2006).

57. Pervushin, K., Riek, R., Wider, G. & Wuthrich, K. Attenuated T2 relaxation by mutual cancellation of dipole-dipole coupling and chemical shift anisotropy indicates an avenue to NMR structures of very large biological macromolecules in solution. *Proc Natl Acad Sci U S A* 94, 12366-71 (1997).

58. Foster, M.P., McElroy, C.A. & Amero, C.D. Solution NMR of large molecules and assemblies. *Biochemistry* 46, 331-40 (2007).

59. Religa, T.L. & Kay, L.E. Optimal methyl labeling for studies of supra-molecular systems. *J Biomol NMR* 47, 163-9 (2010).

60. Velyvis, A., Schachman, H.K. & Kay, L.E. Application of methyl-TROSY NMR to test allosteric models describing effects of nucleotide binding to aspartate transcarbamoylase. *J Mol Biol* 387, 540-7 (2009).

61. Loria, J.P., Rance, M. & Palmer, A.G., 3rd. A TROSY CPMG sequence for characterizing chemical exchange in large proteins. *J Biomol NMR* 15, 151-5 (1999).

62. Bashir, Q., Volkov, A.N., Ullmann, G.M. & Ubbink, M. Visualization of the encounter ensemble of the transient electron transfer complex of cytochrome c and cytochrome c peroxidase. *J Am Chem Soc* 132, 241-7 (2010).

63. Weininger, U. et al. A remote prolyl isomerization controls domain assembly via a hydrogen bonding network. *Proc Natl Acad Sci U S A* 106, 12335-40 (2009).

64. Schanda, P. & Brutscher, B. Very fast two-dimensional NMR spectroscopy for real-time investigation of dynamic events in proteins on the time scale of seconds. *J Am Chem Soc* 127, 8014-5 (2005).

65. Mugler, J.P., 3rd et al. MR imaging and spectroscopy using hyperpolarized 129Xe gas: preliminary human results. *Magn Reson Med* 37, 809-15 (1997).

66. Pavlovskaya, G.E., Cleveland, Z.I., Stupic, K.F., Basaraba, R.J. & Meersmann, T. Hyperpolarized krypton-83 as a contrast agent for magnetic resonance imaging. *Proc Natl Acad Sci U S A* 102, 18275-9 (2005).

67. Ito, T. & Fraissard, J. in *Proceedings of the 5th Int. Conf. on Zeolites* 510-15 (Naples, 1980(June)).

68. Tilton, R.F., Jr. & Kuntz, I.D., Jr. Nuclear magnetic resonance studies of xenon-129 with myoglobin and hemoglobin. *Biochemistry* 21, 6850-7 (1982).

69. Berthault, P., Huber, G. & Desvaux, H. Biosensing using laser-polarized xenon NMR/MRI. *Prog Nucl Magn Reson Spec* 55, 35-60 (2008).

70. Taratula, O. & Dmochowski, I.J. Functionalized 129Xe contrast agents for magnetic resonance imaging. *Curr Opin Chem Biol* 14, 97-104 (2010).

71. Goodson, B.M. Nuclear magnetic resonance of laser-polarized noble gases in molecules, materials, and organisms. *J Magn Reson* 155, 157-216 (2002).

72. Ruppert, K., Mata, J.F., Brookeman, J.R., Hagspiel, K.D. & Mugler, J.P., 3rd. Exploring lung function with hyperpolarized (129)Xe nuclear magnetic resonance. *Magn Reson Med* 51, 676-87 (2004).

73. Driehuys, B., Moller, H.E., Cleveland, Z.I., Pollaro, J. & Hedlund, L.W. Pulmonary perfusion and xenon gas exchange in rats: MR imaging with intravenous injection of hyperpolarized 129Xe. *Radiology* 252, 386-93 (2009).

74. Cleveland, Z.I. et al. Hyperpolarized Xe MR imaging of alveolar gas uptake in humans. *PLoS One* 5, e12192 (2010).

75. Bartik, K., Luhmer, M., Heyes, S.J., Ottinger, R. & Reisse, J. Probing molecular cavities in alpha-cyclodextrin solutions by xenon NMR. *J Magn Reson B* 109, 164–68 (1995).

76. Ripmeester, J.A., Ratcliffe, C.I. & Tse, J.S. The nuclear magnetic-resonance of Xe-129 trapped in clathrates and some other solids. *J Chem Soc-Faraday Trans I* 84, 3731–45 (1988).

77. Gabard, J. & Collet, A. Synthesis of a (D3)-Bis(cyclotriveratrylenyl) macrocage by stereospecific replication of a (C3)-subunit. *J Chem Soc Chem Commun*, 1137-39 (1981).

78. Spence, M.M. et al. Functionalized xenon as a biosensor. *Proc Natl Acad Sci U S A* 98, 10654-7 (2001).

79. Spence, M.M. et al. Development of a functionalized xenon biosensor. *J Am Chem Soc* 126, 15287-94 (2004).

80. Roy, V. et al. A cryptophane biosensor for the detection of specific nucleotide targets through xenon NMR spectroscopy. *Chemphyschem* 8, 2082-5 (2007).

81. Wei, Q. et al. Designing 129Xe NMR biosensors for matrix metalloproteinase detection. *J Am Chem Soc* 128, 13274-83 (2006).

82. Schroder, L., Lowery, T.J., Hilty, C., Wemmer, D.E. & Pines, A. Molecular imaging using a targeted magnetic resonance hyperpolarized biosensor. *Science* 314, 446-9 (2006).

83. Sloan, V.S. et al. Mediation by HLA-DM of dissociation of peptides from HLA-DR. *Nature* 375, 802-6 (1995).

84. Larkin, M.A. et al. Clustal W and Clustal X version 2.0. *Bioinformatics* 23, 2947-8 (2007).

85. Frayser, M., Sato, A.K., Xu, L. & Stern, L.J. Empty and peptide-loaded class II major histocompatibility complex proteins produced by expression in Escherichia coli and folding in vitro. *Protein Expr Purif* 15, 105-14 (1999).

86. Fiaux, J., Bertelsen, E.B., Horwich, A.L. & Wuthrich, K. Uniform and residue-specific 15N-labeling of proteins on a highly deuterated background. *J Biomol NMR* 29, 289-97 (2004).

87. Nagai, K. & Thogersen, H.C. Synthesis and sequence-specific proteolysis of hybrid proteins produced in Escherichia coli. *Methods Enzymol* 153, 461-81 (1987).

88. Einstein, A. Über die von der molekularkinetischen Theorie der Wärme geforderte Bewegung von in ruhenden Flüssigkeiten suspendierten Teilchen. *Annalen der Physik* 17, 549ff. (1905) (2005).

89. Piotto, M., Saudek, V. & Sklenar, V. Gradient-tailored excitation for single-quantum NMR spectroscopy of aqueous solutions. *J Biomol NMR* 2, 661-5 (1992).

90. Vranken, W.F. et al. The CCPN data model for NMR spectroscopy: development of a software pipeline. *Proteins* 59, 687-96 (2005).

91. Kilian, W., Seifert, F. & Rinneberg, H. Dynamic NMR spectroscopy of hyperpolarized (129)Xe in human brain analyzed by an uptake model. *Magn Reson Med* 51, 843-7 (2004).

92. Schlundt, A. et al. A xenon-129 biosensor for monitoring MHC-peptide interactions. *Angew Chem Int Ed Engl* 48, 4142-5 (2009).

93. Fu, X.T. & Karr, R.W. HLA-DR alpha chain residues located on the outer loops are involved in nonpolymorphic and polymorphic antibody-binding epitopes. *Hum Immunol* 39, 253-60 (1994).

94. Höpner, S. Charakterisierung einer hABL-spezifischen CD4+-T-Zellantwort und die Anwendung des AdEtOH als Katalysator der Peptidbeladung. *Doctoral Thesis, FU Berlin* (2008).

95. Falk, K. et al. Ligand exchange of major histocompatibility complex class II proteins is triggered by H-bond donor groups of small molecules. *J Biol Chem* 277, 2709-15 (2002).

96. Vita, R. et al. The immune epitope database 2.0. *Nucleic Acids Res* 38, D854-62 (2010).

97. Kramer, A. & Schneider-Mergener, J. Synthesis and screening of peptide libraries on continuous cellulose membrane supports. *Methods Mol Biol* 87, 25-39 (1998).

98. Gunther, S. et al. Bidirectional binding of invariant chain peptides to an MHC class II molecule. *Proc Natl Acad Sci U S A* 107, 22219-24 (2010).

99. Gupta, S. et al. Anchor side chains of short peptide fragments trigger ligand-exchange of class II MHC molecules. *PLoS One* 3, e1814 (2008).

100. Altman, J.D., Reay, P.A. & Davis, M.M. Formation of functional peptide complexes of class II major histocompatibility complex proteins from subunits produced in Escherichia coli. *Proc Natl Acad Sci U S A* 90, 10330-4 (1993).

101. Stockel, J. et al. Refolding of human class II major histocompatibility complex molecules isolated from Escherichia coli. Assembly of peptide-free heterodimers and increased refolding-yield in the presence of antigenic peptide. *J Biol Chem* 269, 29571-8 (1994).

102. Burrows, G.G., Bebo, B.F., Jr., Adlard, K.L., Vandenbark, A.A. & Offner, H. Two-domain MHC class II molecules form stable complexes with myelin basic protein 69-89 peptide that detect and inhibit rat encephalitogenic T cells and treat experimental autoimmune encephalomyelitis. *J Immunol* 161, 5987-96 (1998).

103. Roche, P.A. & Cresswell, P. High-affinity binding of an influenza hemagglutinin-derived peptide to purified HLA-DR. *J Immunol* 144, 1849-56 (1990).

104. Stern, L.J. & Wiley, D.C. The human class II MHC protein HLA-DR1 assembles as empty alpha beta heterodimers in the absence of antigenic peptide. *Cell* 68, 465-77 (1992).

105. Collins, E.J., Booth, B.L., Jr. & Cerundolo, V. Extensive alanine substitutions increase binding affinity of an influenza nucleoprotein peptide to HLA-Aw68 and do not abrogate peptide-specific CTL recognition. *J Immunol* 162, 331-7 (1999).

106. Verreck, F.A. et al. The generation of SDS-stable HLA DR dimers is independent of efficient peptide binding. *Int Immunol* 8, 397-404 (1996).

107. Zarutskie, J.A. et al. A conformational change in the human major histocompatibility complex protein HLA-DR1 induced by peptide binding. *Biochemistry* 38, 5878-87 (1999).

108. Neal, S., Nip, A.M., Zhang, H. & Wishart, D.S. Rapid and accurate calculation of protein 1H, 13C and 15N chemical shifts. *J Biomol NMR* 26, 215-40 (2003).

109. Le, H. & Oldfield, E. Correlation between 15N NMR chemical shifts in proteins and secondary structure. *J Biomol NMR* 4, 341-8 (1994).

110. Oldfield, E. Chemical shifts and three-dimensional protein structures. *J Biomol NMR* 5, 217-25 (1995).

111. Meiler, J. PROSHIFT: protein chemical shift prediction using artificial neural networks. *J Biomol NMR* 26, 25-37 (2003).

112. Shen, Y. & Bax, A. Protein backbone chemical shifts predicted from searching a database for torsion angle and sequence homology. *J Biomol NMR* 38, 289-302 (2007).

113. Powers, R., Clore, G.M., Garret, D.S. & Gronenborn, A.M. Relationships between the precision of high-resolution protein NMR structures, solution-order parameters and crystallographic B factors. *J. Magn. Reson. B* 101, 325-327 (1993).

114. Wishart, D.S. & Sykes, B.D. The 13C chemical-shift index: a simple method for the identification of protein secondary structure using 13C chemical-shift data. *J Biomol NMR* 4, 171-80 (1994).

115. Mandell, J.G., Baerga-Ortiz, A., Falick, A.M. & Komives, E.A. Measurement of solvent accessibility at protein-protein interfaces. *Methods Mol Biol* 305, 65-80 (2005).

116. Chang, W.T. & Douglas, K.T. Mechanistic studies of carboxypeptidase Y from Saccharomyces cerevisiae. pH and pD profiles and inactivation at low pH (pD) values. *Biochem J.* 187, 843-849 (1980).

117. Zavala-Ruiz, Z., Strug, I., Walker, B.D., Norris, P.J. & Stern, L.J. A hairpin turn in a class II MHC-bound peptide orients residues outside the binding groove for T cell recognition. *Proc Natl Acad Sci U S A* 101, 13279-84 (2004).

118. Wang, L. et al. Crystal structure of a complete ternary complex of TCR, superantigen and peptide-MHC. *Nat Struct Mol Biol* 14, 169-71 (2007).

119. Chicz, R.M. et al. Predominant naturally processed peptides bound to HLA-DR1 are derived from MHC-related molecules and are heterogeneous in size. *Nature* 358, 764-8 (1992).

120. Fallang, L.E. et al. Complexes of two cohorts of CLIP peptides and HLA-DQ2 of the autoimmune DR3-DQ2 haplotype are poor substrates for HLA-DM. *J Immunol* 181, 5451-61 (2008).

121. Stratikos, E., Wiley, D.C. & Stern, L.J. Enhanced catalytic action of HLA-DM on the exchange of peptides lacking backbone hydrogen bonds between their N-terminal region and the MHC class II alpha-chain. *J Immunol* 172, 1109-17 (2004).

122. Volkov, A.N., Bashir, Q., Worrall, J.A., Ullmann, G.M. & Ubbink, M. Shifting the equilibrium between the encounter state and the specific form of a protein complex by interfacial point mutations. *J Am Chem Soc* 132, 11487-95 (2010).

123. Denzin, L.K., Hammond, C. & Cresswell, P. HLA-DM interactions with intermediates in HLA-DR maturation and a role for HLA-DM in stabilizing empty HLA-DR molecules. *J Exp Med* 184, 2153-65 (1996).

124. Vollers, S.S. & Stern, L.J. Class II major histocompatibility complex tetramer staining: progress, problems, and prospects. *Immunology* 123, 305-13 (2008).

125. Dickhaut, K. et al. Enhancement of tumour-specific immune responses in vivo by 'MHC loading-enhancer' (MLE). *PLoS One* 4, e6811 (2009).

126. Wilson, N., Fremont, D., Marrack, P. & Kappler, J. Mutations changing the kinetics of class II MHC peptide exchange. *Immunity* 14, 513-22 (2001).

127. Doebele, R.C. et al. Point mutations in or near the antigen-binding groove of HLA-DR3 implicate class II-associated invariant chain peptide affinity as a constraint on MHC class II polymorphism. *J Immunol* 170, 4683-92 (2003).

128. Zavala-Ruiz, Z. (2004), Doctoral Thesis, Structural Studies of the Human Class II Major Histocompatibility Complex Protein HLA-DR1, MIT, Boston.

129. Cameron, T.O. et al. Labeling antigen-specific CD4(+) T cells with class II MHC oligomers. *J Immunol Methods* 268, 51-69 (2002).

130. Kalandadze, A., Galleno, M., Foncerrada, L., Strominger, J.L. & Wucherpfennig, K.W. Expression of recombinant HLA-DR2 molecules. Replacement of the hydrophobic transmembrane region by a leucine zipper dimerization motif allows the assembly and secretion of soluble DR alpha beta heterodimers. *J Biol Chem* 271, 20156-62 (1996).

131. Parra-Lopez, C. et al. Major histocompatibility complex and T cell interactions of a universal T cell epitope from Plasmodium falciparum circumsporozoite protein. *J Biol Chem* 281, 14907-17 (2006).

132. Hartman, I.Z. et al. A reductionist cell-free major histocompatibility complex class II antigen processing system identifies immunodominant epitopes. *Nat Med* 16, 1333-40 (2010).

133. Germain, R.N. & Rinker, A.G., Jr. Peptide binding inhibits protein aggregation of invariant-chain free class II dimers and promotes surface expression of occupied molecules. *Nature* 363, 725-8 (1993).

134. Santambrogio, L. et al. Extracellular antigen processing and presentation by immature dendritic cells. *Proc Natl Acad Sci U S A* 96, 15056-61 (1999).

135. Shekhtman, A. Protein chemical ligation as an invaluable tool for structural NMR. *Protein Pept Lett* 12, 765-8 (2005).

136. Liu, D., Xu, R. & Cowburn, D. Segmental isotopic labeling of proteins for nuclear magnetic resonance. *Methods Enzymol* 462, 151-75 (2009).

137. Kushlan, D.M. & LeMaster, D.M. Resolution and sensitivity enhancement of heteronuclear correlation for methylene resonances via 2H enrichment and decoupling. *J Biomol NMR* 3, 701-8 (1993).

138. Shekhtman, A., Ghose, R., Goger, M. & Cowburn, D. NMR structure determination and investigation using a reduced proton (REDPRO) labeling strategy for proteins. *FEBS Lett* 524, 177-82 (2002).

139. Rosloniec, E.F., Ivey, R.A., 3rd, Whittington, K.B., Kang, A.H. & Park, H.W. Crystallographic structure of a rheumatoid arthritis MHC susceptibility allele, HLA-DR1 (DRB1*0101), complexed with the immunodominant determinant of human type II collagen. *J Immunol* 177, 3884-92 (2006).

140. Sundberg, E.J. et al. Minor structural changes in a mutated human melanoma antigen correspond to dramatically enhanced stimulation of a CD4+ tumor-infiltrating lymphocyte line. *J Mol Biol* 319, 449-61 (2002).

141. Grzesiek, S. & Bax, A. Amino acid type determination in the sequential assignment procedure of uniformly 13C/15N-enriched proteins. *J Biomol NMR* 3, 185-204 (1993).

142. Raman, S. et al. NMR structure determination for larger proteins using backbone-only data. *Science* 327, 1014-8 (2010).

143. Gouda, H. et al. Three-dimensional solution structure of the B domain of staphylococcal protein A: comparisons of the solution and crystal structures. *Biochemistry* 31, 9665-72 (1992).

144. Carven, G.J. et al. Monoclonal antibodies specific for the empty conformation of HLA-DR1 reveal aspects of the conformational change associated with peptide binding. *J Biol Chem* 279, 16561-70 (2004).

145. Bai, Y., Milne, J.S., Mayne, L. & Englander, S.W. Primary structure effects on peptide group hydrogen exchange. *Proteins* 17, 75-86 (1993).

146. Hausmann, D.H., Yu, B., Hausmann, S. & Wucherpfennig, K.W. pH-dependent peptide binding properties of the type I diabetes-associated I-Ag7 molecule: rapid release of CLIP at an endosomal pH. *J Exp Med* 189, 1723-34 (1999).

147. Ferrante, A., Anderson, M.W., Klug, C.S. & Gorski, J. HLA-DM mediates epitope selection by a "compare-exchange" mechanism when a potential peptide pool is available. *PLoS One* 3, e3722 (2008).

148. Nag, B. et al. Antigenic peptide binding to MHC class II molecules at increased peptide concentrations. *Mol Immunol* 31, 1161-8 (1994).

149. Anders, A.K. et al. HLA-DM captures partially empty HLA-DR molecules for catalyzed removal of peptide. *Nat Immunol* 12, 54-61 (2011).

150. Fielding, L. NMR methods for the determination of protein-ligand dissociation constants. *Curr Top Med Chem* 3, 39-53 (2003).

151. Wu, K.P., Kim, S., Fela, D.A. & Baum, J. Characterization of conformational and dynamic properties of natively unfolded human and mouse alpha-synuclein ensembles by NMR: implication for aggregation. *J Mol Biol* 378, 1104-15 (2008).

152. Popp, M.W., Antos, J.M., Grotenbreg, G.M., Spooner, E. & Ploegh, H.L. Sortagging: a versatile method for protein labeling. *Nat Chem Biol* 3, 707-8 (2007).

153. Iwahara, J., Schwieters, C.D. & Clore, G.M. Ensemble approach for NMR structure refinement against (1)H paramagnetic relaxation enhancement data arising from a flexible paramagnetic group attached to a macromolecule. *J Am Chem Soc* 126, 5879-96 (2004).

154. Wu, K.P. & Baum, J. Detection of transient interchain interactions in the intrinsically disordered protein alpha-synuclein by NMR paramagnetic relaxation enhancement. *J Am Chem Soc* 132, 5546-7 (2010).

155. Mittermaier, A.K. & Kay, L.E. Observing biological dynamics at atomic resolution using NMR. *Trends Biochem Sci* 34, 601-11 (2009).

156. Gopalakrishnan, B. & Roques, B.P. Do antigenic peptides have a unique sense of direction inside the MHC binding groove? A molecular modelling study. *FEBS Lett* 303, 224-8 (1992).

157. DeWeese, C., Kwok, W.W., Nepom, G.T. & Lybrand, T.P. Characterization of a Novel Reverse-orientation Model for a Peptide/MHC Complex Putatively Associated with Type I Diabetes Mellitus. *J Mol Model.* 2, 205-216 (1996).

158. Riberdy, J.M., Newcomb, J.R., Surman, M.J., Barbosa, J.A. & Cresswell, P. HLA-DR molecules from an antigen-processing mutant cell line are associated with invariant chain peptides. *Nature* 360, 474-7 (1992).

159. Sette, A. et al. Invariant chain peptides in most HLA-DR molecules of an antigen-processing mutant. *Science* 258, 1801-4 (1992).

160. Ghosh, P., Amaya, M., Mellins, E. & Wiley, D.C. The structure of an intermediate in class II MHC maturation: CLIP bound to HLA-DR3. *Nature* 378, 457-62 (1995).

161. Zhu, Y., Rudensky, A.Y., Corper, A.L., Teyton, L. & Wilson, I.A. Crystal structure of MHC class II I-Ab in complex with a human CLIP peptide: prediction of an I-Ab peptide-binding motif. *J Mol Biol* 326, 1157-74 (2003).

162. Siebenkotten, I.M., Carstens, C. & Koch, N. Identification of a sequence that mediates promiscuous binding of invariant chain to MHC class II allotypes. *J Immunol* 160, 3355-62 (1998).

163. Neumann, J. & Koch, N. A novel domain on HLA-DRbeta chain regulates the chaperone role of the invariant chain. *J Cell Sci* 119, 4207-14 (2006).

164. Chernov, A.A. Protein crystals and their growth. *J Struct Biol* 142, 3-21 (2003).

165. Kwan, A.H., Mobli, M., Gooley, P.R., King, G.F. & Mackay, J.P. Macromolecular NMR spectroscopy for the non-spectroscopist. *FEBS J* 278, 687-703 (2011).

166. Chen, Y.W., Dodson, E.J. & Kleywegt, G.J. Does NMR mean "not for molecular replacement"? Using NMR-based search models to solve protein crystal structures. *Structure* 8, R213-20 (2000).

167. Shen, Y. & Bax, A. SPARTA+: a modest improvement in empirical NMR chemical shift prediction by means of an artificial neural network. *J Biomol NMR* 48, 13-22 (2010).

168. Korzhnev, D.M., Religa, T.L., Banachewicz, W., Fersht, A.R. & Kay, L.E. A transient and low-populated protein-folding intermediate at atomic resolution. *Science* 329, 1312-6 (2010).

169. Rohn, T.A. et al. Upregulation of the CLIP self peptide on mature dendritic cells antagonizes T helper type 1 polarization. *Nat Immunol* 5, 909-18 (2004).

170. Chaturvedi, P., Hengeveld, R., Zechel, M.A., Lee-Chan, E. & Singh, B. The functional role of class II-associated invariant chain peptide (CLIP) in its ability to variably modulate immune responses. *Int Immunol* 12, 757-65 (2000).

171. Topilski, I., Harmelin, A., Flavell, R.A., Levo, Y. & Shachar, I. Preferential Th1 immune response in invariant chain-deficient mice. *J Immunol* 168, 1610-7 (2002).

172. Pu, Z., Lovitch, S.B., Bikoff, E.K. & Unanue, E.R. T cells distinguish MHC-peptide complexes formed in separate vesicles and edited by H2-DM. *Immunity* 20, 467-76 (2004).

173. Lovitch, S.B., Pu, Z. & Unanue, E.R. Amino-terminal flanking residues determine the conformation of a peptide-class II MHC complex. *J Immunol* 176, 2958-68 (2006).

174. Hess, A.D. & Thoburn, C.J. Immune tolerance to self-major histocompatibility complex class II antigens after bone marrow transplantation: role of regulatory T cells. *Biol Blood Marrow Transplant* 12, 518-29 (2006).

175. Villadangos, J.A. Presentation of antigens by MHC class II molecules: getting the most out of them. *Mol Immunol* 38, 329-46 (2001).

176. Reed, A.M., Collins, E.J., Shock, L.P., Klapper, D.G. & Frelinger, J.A. Diminished class II-associated Ii peptide binding to the juvenile dermatomyositis HLA-DQ alpha 1*0501/DQ beta 1*0301 molecule. *J Immunol* 159, 6260-5 (1997).

177. Patil, N.S. et al. Rheumatoid arthritis (RA)-associated HLA-DR alleles form less stable complexes with class II-associated invariant chain peptide than non-RA-associated HLA-DR alleles. *J Immunol* 167, 7157-68 (2001).

178. Jasanoff, A., Wagner, G. & Wiley, D.C. Structure of a trimeric domain of the MHC class II-associated chaperonin and targeting protein Ii. *EMBO J* 17, 6812-8 (1998).

179. Castellino, F., Han, R. & Germain, R.N. The transmembrane segment of invariant chain mediates binding to MHC class II molecules in a CLIP-independent manner. *Eur J Immunol* 31, 841-50 (2001).

180. Hsing, L.C. & Rudensky, A.Y. The lysosomal cysteine proteases in MHC class II antigen presentation. *Immunol Rev* 207, 229-41 (2005).

181. Bakke, O. & Dobberstein, B. MHC class II-associated invariant chain contains a sorting signal for endosomal compartments. *Cell* 63, 707-16 (1990).

182. Lovitch, S.B. & Unanue, E.R. Conformational isomers of a peptide-class II major histocompatibility complex. *Immunol Rev* 207, 293-313 (2005).

183. Stadinski, B.D. et al. Diabetogenic T cells recognize insulin bound to IAg7 in an unexpected, weakly binding register. *Proc Natl Acad Sci U S A* 107, 10978-83 (2010).

184. Stadinski, B.D. et al. Chromogranin A is an autoantigen in type 1 diabetes. *Nat Immunol* 11, 225-31 (2010).

185. Mohan, J.F. et al. Unique autoreactive T cells recognize insulin peptides generated within the islets of Langerhans in autoimmune diabetes. *Nat Immunol* 11, 350-4 (2010).

186. Wiesner, M. et al. Dominance of an alternative CLIP sequence in the celiac disease associated HLA-DQ2 molecule. *Immunogenetics* 60, 551-5 (2008).

187. Landais, E. et al. New design of MHC class II tetramers to accommodate fundamental principles of antigen presentation. *J Immunol* 183, 7949-57 (2009).

188. Driver, J.P., Serreze, D.V. & Chen, Y.G. Mouse models for the study of autoimmune type 1 diabetes: a NOD to similarities and differences to human disease. *Semin Immunopathol* 33, 67-87 (2011).

189. Gold, R., Linington, C. & Lassmann, H. Understanding pathogenesis and therapy of multiple sclerosis via animal models: 70 years of merits and culprits in experimental autoimmune encephalomyelitis research. *Brain* 129, 1953-71 (2006).

190. Baker, N.A., Sept, D., Joseph, S., Holst, M.J. & McCammon, J.A. Electrostatics of nanosystems: application to microtubules and the ribosome. *Proc Natl Acad Sci U S A* 98, 10037-41 (2001).

191. Romagnoli, P. & Germain, R.N. The CLIP region of invariant chain plays a critical role in regulating major histocompatibility complex class II folding, transport, and peptide occupancy. *J Exp Med* 180, 1107-13 (1994).

192. Sette, A., Southwood, S., Miller, J. & Appella, E. Binding of major histocompatibility complex class II to the invariant chain-derived peptide, CLIP, is regulated by allelic polymorphism in class II. *J Exp Med* 181, 677-83 (1995).

193. Mukherjee, R., Chaturvedi, P., Lee-Chan, E. & Singh, B. Exogenous CLIP localizes into endocytic compartment of cells upon internalization: implications for antigen presentation by MHC class II molecules. *Mol Immunol* 45, 2166-76 (2008).

194. Villadangos, J.A., Schnorrer, P. & Wilson, N.S. Control of MHC class II antigen presentation in dendritic cells: a balance between creative and destructive forces. *Immunol Rev* 207, 191-205 (2005).

195. Bonnerot, C. et al. Association with BiP and aggregation of class II MHC molecules synthesized in the absence of invariant chain. *EMBO J* 13, 934-44 (1994).

196. Sievers, E. et al. Glycoprotein B from strain 17 of herpes simplex virus type I contains an invariant chain homologous sequence that binds to MHC class II molecules. *Immunology* 107, 129-35 (2002).

197. Lamb, C.A. & Cresswell, P. Assembly and transport properties of invariant chain trimers and HLA-DR-invariant chain complexes. *J Immunol* 148, 3478-82 (1992).

198. Neumann, J. & Koch, N. Assembly of major histocompatibility complex class II subunits with invariant chain. *FEBS Lett* 579, 6055-9 (2005).

199. Busch, R., Cloutier, I., Sekaly, R.P. & Hammerling, G.J. Invariant chain protects class II histocompatibility antigens from binding intact polypeptides in the endoplasmic reticulum. *EMBO J* 15, 418-28 (1996).

200. Dani, A. et al. The pathway for MHCII-mediated presentation of endogenous proteins involves peptide transport to the endo-lysosomal compartment. *J Cell Sci* 117, 4219-30 (2004).

201. ten Broeke, T. et al. Trafficking of MHC class II in dendritic cells is dependent on but not regulated by degradation of its associated invariant chain. *Traffic* 11, 324-31 (2010).

202. Munz, C. et al. Peptide analysis, stability studies, and structural modeling explain contradictory peptide motifs and unique properties of the NOD mouse MHC class II molecule H2-A(g7). *Eur J Immunol* 32, 2105-16 (2002).

203. Wang, P. et al. Peptide binding predictions for HLA DR, DP and DQ molecules. *BMC Bioinformatics* 11, 568 (2010).

204. Nielsen, M. et al. Quantitative predictions of peptide binding to any HLA-DR molecule of known sequence: NetMHCIIpan. *PLoS Comput Biol* 4, e1000107 (2008).

205. Forsgren, N., Lamont, R.J. & Persson, K. A crystallizable form of the Streptococcus gordonii surface antigen SspB C-domain obtained by limited proteolysis. *Acta Crystallogr Sect F Struct Biol Cryst Commun* 65, 712-4 (2009).

206. Ferrante, A. & Gorski, J. Cutting edge: HLA-DM-mediated peptide exchange functions normally on MHC class II-peptide complexes that have been weakened by elimination of a conserved hydrogen bond. *J Immunol* 184, 1153-8 (2010).

207. Dai, S. et al. Crystal structure of HLA-DP2 and implications for chronic beryllium disease. *Proc Natl Acad Sci U S A* 107, 7425-30 (2010).

208. Crawford, F., Huseby, E., White, J., Marrack, P. & Kappler, J.W. Mimotopes for alloreactive and conventional T cells in a peptide-MHC display library. *PLoS Biol* 2, E90 (2004).

209. Kauer, J.C., Erickson-Viitanen, S., Wolfe, H.R., Jr. & DeGrado, W.F. p-Benzoyl-L-phenylalanine, a new photoreactive amino acid. Photolabeling of calmodulin with a synthetic calmodulin-binding peptide. *J Biol Chem* 261, 10695-700 (1986).

210. Insaidoo, F.K., Zajicek, J. & Baker, B.M. A general and efficient approach for NMR studies of peptide dynamics in class I MHC peptide binding grooves. *Biochemistry* 48, 9708-10 (2009).

211. Selenko, P. & Wagner, G. NMR mapping of protein interactions in living cells. *Nat Methods* 3, 80-1 (2006).

212. Shcherbo, D. et al. Bright far-red fluorescent protein for whole-body imaging. *Nat Methods* 4, 741-6 (2007).

213. Shcherbo, D. et al. Near-infrared fluorescent proteins. *Nat Methods* 7, 827-9 (2010).

214. Makowski, M.R., Wiethoff, A.J., Jansen, C.H. & Botnar, R.M. Molecular imaging with targeted contrast agents. *Top Magn Reson Imaging* 20, 247-59 (2009).

215. Weissleder, R. et al. Ultrasmall superparamagnetic iron oxide: characterization of a new class of contrast agents for MR imaging. *Radiology* 175, 489-93 (1990).

216. Hultman, K.L. et al. Magnetic resonance imaging of major histocompatibility class II expression in the renal medulla using immunotargeted superparamagnetic iron oxide nanoparticles. *ACS Nano* 2, 477-84 (2008).

217. Chambers, J.M. et al. Cryptophane xenon-129 nuclear magnetic resonance biosensors targeting human carbonic anhydrase. *J Am Chem Soc* 131, 563-9 (2009).

218. Fairchild, R.M. et al. A water-soluble Xe@cryptophane-111 complex exhibits very high thermodynamic stability and a peculiar (129)Xe NMR chemical shift. *J Am Chem Soc* 132, 15505-7 (2010).

219. Lowery, T.J. et al. Optimization of xenon biosensors for detection of protein interactions. *Chembiochem* 7, 65-73 (2006).

220. Fogarty, H.A. et al. A cryptophane core optimized for xenon encapsulation. *J Am Chem Soc* 129, 10332-3 (2007).

221. Garcia, S. et al. Sensitivity enhancement by exchange mediated magnetization transfer of the xenon biosensor signal. *J Magn Reson* 184, 72-7 (2007).

222. Allen, M.J., MacRenaris, K.W., Venkatasubramanian, P.N. & Meade, T.J. Cellular delivery of MRI contrast agents. *Chem Biol* 11, 301-7 (2004).

223. Endres, P.J., Macrenaris, K.W., Vogt, S., Allen, M.J. & Meade, T.J. Quantitative imaging of cell-permeable magnetic resonance contrast agents using x-ray fluorescence. *Mol Imaging* 5, 485-97 (2006).

224. Dirksen, A. et al. Design and synthesis of a bimodal target-specific contrast agent for angiogenesis. *Org Lett* 6, 4857-60 (2004).

225. Mulder, W.J. et al. MR molecular imaging and fluorescence microscopy for identification of activated tumor endothelium using a bimodal lipidic nanoparticle. *FASEB J* 19, 2008-10 (2005).

226. Seward, G.K., Wei, Q. & Dmochowski, I.J. Peptide-mediated cellular uptake of cryptophane. *Bioconjug Chem* 19, 2129-35 (2008).

227. Boutin, C. et al. Cell uptake of a biosensor detected by hyperpolarized 129Xe NMR: the transferrin case. *Bioorg Med Chem* 19, 4135-43 (2011).

228. Wolber, J., Cherubini, A., Dzik-Jurasz, A.S., Leach, M.O. & Bifone, A. Spin-lattice relaxation of laser-polarized xenon in human blood. *Proc Natl Acad Sci U S A* 96, 3664-9 (1999).

229. Cleveland, Z.I., Moller, H.E., Hedlund, L.W. & Driehuys, B. Continuously infusing hyperpolarized 129Xe into flowing aqueous solutions using hydrophobic gas exchange membranes. *J Phys Chem B* 113, 12489-99 (2009).

230. Driehuys, B., Pollaro, J. & Cofer, G.P. In vivo MRI using real-time production of hyperpolarized 129Xe. *Magn Reson Med* 60, 14-20 (2008).

231. Bourne, R., Kurniawan, N., Cowin, G., Sved, P. & Watson, G. 16 T Diffusion microimaging of fixed prostate tissue: Preliminary findings. *Magn Reson Med* 66, 244-7 (2011).

232. Ruset, I.C., Ketel, S. & Hersman, F.W. Optical pumping system design for large production of hyperpolarized. *Phys Rev Lett* 96, 053002 (2006).

233. Zhou, X., Graziani, D. & Pines, A. Hyperpolarized xenon NMR and MRI signal amplification by gas extraction. *Proc Natl Acad Sci U S A* 106, 16903-6 (2009).

234. Mynar, J.L., Lowery, T.J., Wemmer, D.E., Pines, A. & Frechet, J.M. Xenon biosensor amplification via dendrimer-cage supramolecular constructs. *J Am Chem Soc* 128, 6334-5 (2006).

Appendix

Table X: Sequences of SPOT membrane in section 3.4.8 of main text (see figure 3.35)

index number	MW in g/mol	sequence N to C	notes	source of epitope
1	2224.9	K-I-T-Y-G-A-S-P-K-Y-V-K-Q-N-T-L-K-L-A-T	++ctrl	HA299-316, N-terminally extended wild-type HA sequence
2	1812.4	K-I-T-Y-G-A-S-A-A-Y-A-A-Q-A-A-A-A-A-A-A	+ctrl	HA299-316, N-terminally extended HA sequence with only P1 and P4 anchors left
3	1663.3	K-I-T-Y-G-A-S-A-A-A-A-A-A-A-A-A-A-A-A-A	--ctrl	HA299-316, N-terminally extended HA sequence with no pocket anchors left
4	2224.9	K-I-T-Y-G-A-S-P-K-Y-V-K-Q-N-T-L-K-L-A-T	++ctrl	HA299-316, N-terminally extended wild-type HA sequence
5	1503.9	P-K-Y-V-K-Q-N-T-L-K-L-A-T	HA WT	Influenza A Hemagglutinin 306-318
6	1503.9	T-A-L-K-L-T-N-Q-K-V-Y-K-P		
7	1732.4	K-M-R-M-A-T-P-L-L-M-Q-A-L-P-M	$CLIP_{106-102}$	Human Invariant chain 106-120
8	1732.4	M-P-L-A-Q-M-L-L-P-T-A-M-R-M-K		
9	2143.9	K-P-V-S-K-M-R-M-A-T-P-L-L-M-Q-A-L-P-M	$CLIP_{102-120}$	Human Invariant chain 102-120
10	2143.9	M-P-L-A-Q-M-L-L-P-T-A-M-R-M-K-S-V-P-K		
11	1582.2	G-D-N-Q-I-M-P-K-A-G-L-L-I-I-V		MAGA3_HUMAN Melanoma-associated antigen 3
12	1582.2	V-I-I-L-L-G-A-K-P-M-I-Q-N-D-G		
13	1008.4	S-I-L-G-G-V-A-T-Y-G-A		Putative uncharacterized protein [SMU_616] [Streptococcus mutans]
14	1008.4	A-G-Y-T-A-V-G-G-L-I-S		
15	1390.8	D-T-I-I-F-E-A-N-G-N-L-I-A		HEMA_I96A3 Hemagglutinin precursor, Influenza A
16	1390.8	A-I-L-N-G-N-A-E-F-I-I-T-D		
17	1509.9	E-L-I-H-V-L-H-G-L-Y-G-M-Q		CLOTE Tetanus toxin (Fragment) [Clostridium tetani]
18	1509.9	Q-M-G-Y-L-G-H-L-V-H-I-L-E		
19	1423.6	V-N-L-V-D-T-L-N-S-G-Q-Y-T		MP70_MYCTU Immunogenic protein MPT70 precursor [mpt70], Mycobacterium tuberculosis
20	1423.6	T-Y-Q-G-S-N-L-T-D-V-L-N-V		
21	1612.1	Q-Y-I-K-A-N-S-K-F-I-G-I-T-E		CLOTE Tetanus toxin (Fragment) [Clostridium tetani]
22	1612.1	E-T-I-G-I-F-K-S-N-A-K-I-Y-Q		
23	1646.1	A-V-L-E-D-P-Y-I-L-L-V-S-S-K-V		CH602_MYCUA 60 kDa chaperonin 2, Mycobacterium ulcerans
24	1646.1	V-K-S-S-V-L-L-I-Y-P-D-E-L-V-A		
25	1563.9	E-H-R-V-K-R-G-L-T-V-A-V-A-G-A		MYCTK 19 kDa lipoprotein antigen lpqH, Mycobacterium tuberculosis
26	1563.9	A-G-A-V-A-V-T-L-G-R-K-V-R-H-E		
27	1702.1	E-T-L-L-R-A-V-E-S-Y-L-L-A-H-S		BEV1L_BETVE Major pollen allergen Bet v 1-L, white birch
28	1702.1	S-H-A-L-L-Y-S-E-V-A-R-L-L-T-E		
29	1755.1	G-R-E-T-V-I-E-Y-L-V-S-F-G-V-W		HBEAG_HBVD7 External core antigen precursor (HBeAg), hepatitis B
30	1755.1	W-V-G-F-S-V-L-Y-E-I-V-T-E-R-G		
31	1548.9	I-A-F-N-S-G-M-E-P-G-V-V-A-E-K		CH602_MYCLE 60 kDa chaperonin 2 (Protein Cpn60 2), Mycobacterium leprae
32	1548.9	K-E-A-V-V-G-P-E-M-G-S-N-F-A-I		
33	1301.6	A-G-F-K-G-E-Q-G-P-K-G-E-P		CO2A1_HUMAN Collagen alpha-1(II) chain precursor
34	1301.6	P-E-G-K-P-G-Q-E-G-K-F-G-A		
35	1599.1	L-L-V-S-S-K-V-S-T-V-K-D-L-L-P		CH602_MYCUA 60 kDa chaperonin 2 (Protein Cpn60 2), Mycobacterium ulcerans
36	1599.1	P-L-L-D-K-V-T-S-V-K-S-S-V-L-L		
37	1776.2	P-L-K-M-L-N-I-P-S-I-N-V-H-H-Y		PP65_HCMVT 65 kDa phosphoprotein (pp65), 64 kDa matrix., human cytomegalovirus
38	1776.2	Y-H-H-V-N-I-S-P-I-N-L-M-K-L-P		
39	1886.4	S-M-R-Y-Q-S-L-I-P-R-L-V-E-F-F		CAMPM Putative virion core protein P4a [Camelpox virus]
40	1886.4	F-F-E-V-L-R-P-I-L-S-Q-Y-R-M-S		

41	1673	S-Q-W-A-R-E-A-L-Q-T-G-I-T-L-V		ENV_HTL1N Envelope glycoprotein gp62 precursor, Human Tcell leukemia virus
42	1673	V-L-T-I-G-T-Q-L-A-E-R-A-W-Q-S		
43	1956	T-R-Q-Q-N-Q-W-K-E-P-D-V-Y-Y-T		PP65_HCMVT 65 kDa phosphoprotein (pp65), 64 kDa matrix human cytomegalovirus
44	1956	T-Y-Y-V-D-P-E-K-W-Q-N-Q-Q-R-T		
45	1974.3	E-L-L-V-L-M-E-N-E-R-T-L-D-F-H-D		HEMA_I97A1 Hemagglutinin precursor, Influenza A virus
46	1974.3	D-H-F-D-L-T-R-E-N-E-M-L-V-L-L-E		
47	1556.3	I-G-L-S-M-A-G-S-S-A-M-I-L-A-A-Y		A85B_MYCTU Antigen 85-B precursor, Antigen 85 complex, Mycobacterium tuberculosis
48	1556.3	Y-A-A-L-I-M-A-S-S-G-A-M-S-L-G-I		
49	2224.9	K-I-T-Y-G-A-S-P-K-Y-V-K-Q-N-T-L-K-L-A-T	++ctrl	HA299-316, N-terminally extended wild-type HA sequence
50	1812.4	K-I-T-Y-G-A-S-A-A-Y-A-A-Q-A-A-A-A-A-A-A	+ctrl	HA299-316, N-terminally extended HA sequence with only P1 and P4 anchors left
51	1663.3	K-I-T-Y-G-A-S-A-A-A-A-A-A-A-A-A-A-A-A	--ctrl	HA299-316, N-terminally extended HA sequence with no pocket anchors left
52	2224.9	K-I-T-Y-G-A-S-P-K-Y-V-K-Q-N-T-L-K-L-A-T	++ctrl	HA299-316, N-terminally extended wild-type HA sequence
53	1696.3	K-G-F-K-G-V-D-A-Q-G-T-L-S-K-I-F		MBP_HUMAN Myelin basic protein (MBP) (Myelin A1 protein)
54	1696.3	F-I-K-S-L-T-G-Q-A-D-V-G-K-F-G-K		
55	1888.3	P-A-F-E-W-Y-Y-Q-S-G-L-S-I-V-M-P		A85B_MYCTU Antigen 85-B precursor (Antigen 85 complex), Mycobacterium tuberculosis
56	1888.3	P-M-V-I-S-L-G-S-Q-Y-Y-W-E-F-A-P		
57	1805.4	Q-A-G-F-F-L-L-T-R-I-L-T-I-P-Q-S		HBSAG_HBVG3 Large envelope protein (Large surface protein, Hepatitis B virus genotype G
58	1805.4	S-Q-P-I-T-L-I-R-T-L-L-F-F-G-A-Q		
59	1695.9	Q-D-A-Y-N-A-A-G-G-H-N-A-V-F-N-F		85B_MYCTU Antigen 85-B precursor (Antigen 85 complex), Mycobacterium tuberculosis
60	1695.9	F-N-F-V-A-N-H-G-G-A-A-N-Y-A-D-Q		
61	1905.6	R-G-Y-F-K-M-R-T-G-K-S-S-I-M-R-S		HEMA_I85A2 Hemagglutinin precursor, Influenza A virus
62	1905.6	S-R-M-I-S-S-K-G-T-R-M-K-F-Y-G-R		
63	1805.2	S-P-S-L-W-E-I-E-F-A-K-Q-L-A-S-V		RT31_MOUSE 28S ribosomal protein S31, mitochondrial protein, mus musculus
64	1805.2	V-S-A-L-Q-K-A-F-E-I-E-W-L-S-P-S		
65	1743.1	Y-D-V-P-D-Y-A-S-L-R-S-L-V-A-S-S		HEMA_I89A2 Hemagglutinin precursor, Influenza A virus
66	1743.1	S-S-A-V-L-S-R-L-S-A-Y-D-P-V-D-Y		
67	1458.9	T-G-S-G-A-G-I-A-Q-A-A-A-G-T-V-N-I	only derived from IEDB*, modified	Phosphate-binding protein pstS 1 precursor, Mycobacterium tuberculosis
68	1458.9	I-N-V-T-G-A-A-A-Q-A-I-G-A-G-S-G-T		
69	1922.5	G-F-A-T-Q-R-L-T-S-L-F-A-L-G-P-S-Q-K		Core protein p21 (Capsid protein C), Hepatitis virus
70	1922.5	K-Q-S-P-G-L-A-F-L-S-T-L-R-Q-T-A-F-G		
71	1997.2	V-L-E-K-N-V-T-V-T-H-S-V-N-L-L-E-D-S		HEMA_I96A3 Hemagglutinin precursor, Influenza A virus
72	1997.2	S-D-E-L-L-N-V-S-H-T-V-T-V-N-K-E-L-V		
73	2067.4	A-S-D-V-E-T-A-E-G-G-E-I-H-E-L-L-R-L-Q		V_MEASY Non-structural protein V [P/V], Measles virus
74	2067.4	Q-L-R-L-L-E-H-I-E-G-G-E-A-T-E-V-D-S-A		
75	1978.5	D-K-F-K-T-F-E-A-A-F-T-S-S-S-K-A-A-A-A	only 7 first amino acids comprise Ag with regard to *EXPASY*[#]	Pollen allergen Phl p 5b precursor, Phleum pratense
76	1978.5	A-A-A-A-K-S-S-S-T-F-A-A-E-F-T-K-F-K-D		
77	1966.4	G-V-S-T-A-N-A-T-V-Y-M-I-D-S-V-L-M-P-P		MP70_MYCTU Immunogenic protein MPT70 precursor [mpt70], Mycobacterium tuberculosis
78	1966.4	P-P-M-L-V-S-D-I-M-Y-V-T-A-N-A-T-S-V-G		

79	2026.6	Q-Q-F-I-Y-A-G-S-L-S-A-L-L-D-P-S-Q-G-M		A85B_MYCTU Antigen 85-B precursor, Antigen 85 complex, Mycobacterium tuberculosis
80	2026.6	M-G-Q-S-P-D-L-L-A-S-L-S-G-A-Y-I-F-Q-Q		
81	2143.8	V-P-R-I-S-Y-A-H-G-F-D-L-I-E-R-G-K-K-G		OMPA2_NEIMC Major outer membrane protein P.IA precursor, Neisseria meningitidis serogroup C
82	2143.8	G-K-K-G-R-E-I-L-D-F-G-H-A-Y-S-I-R-P-V		
83	2212.8	E-T-T-G-V-V-L-L-L-E-Y-I-P-E-I-T-L-P-V-I		TETX_CLOTE Tetanus toxin precursor (EC 3.4.24.68), Clostridium tetani
84	2212.8	I-V-P-L-T-I-E-P-I-Y-E-L-L-L-V-V-G-T-T-E		
85	2246.8	I-D-E-L-K-T-N-S-S-L-L-T-S-I-L-T-Y-H-V-V		MP70_MYCTU Immunogenic protein MPT70 precursor [mpt70], Mycobacterium tuberculosis
86	2246.8	V-V-H-Y-T-L-I-S-T-L-L-S-S-N-T-K-L-E-D-I		
87	2041.9	I-R-L-H-T-L-L-A-V-L-T-A-A-P-L-L-L-A-A-A	only derived from IEDB*, modified	Phosphate-binding protein pstS 1 precursor, Mycobacterium tuberculosis
88	2041.9	A-A-A-L-L-L-P-A-A-T-L-V-A-L-L-T-H-L-R-I		
89	2049.9	M-K-K-I-S-S-V-I-A-I-A-L-F-G-T-I-A-T-A-N		CAF1_YERPE F1 capsule antigen precursor [caf1], Yersinia pestis
90	2049.9	N-A-T-A-I-T-G-F-L-A-I-A-I-V-S-S-I-K-K-M		
91	2352.8	R-T-E-I-I-R-M-M-E-S-A-R-P-E-D-V-S-F-Q-G		NCAP_I97A1 Nucleoprotein (Nucleocapsid protein), Influenza A virus strain H5N1
92	2352.8	G-Q-F-S-V-D-E-P-R-A-S-E-M-M-R-I-I-E-T-R		
93	2135.8	V-D-A-Q-G-T-L-S-K-I-F-K-L-G-G-R-D-S-R-S		MBP_HUMAN Myelin basic protein (MBP) (Myelin A1 protein)
94	2135.8	S-R-S-D-R-G-G-L-K-F-I-K-S-L-T-G-Q-A-D-V		
95	1988.4	V-S-D-L-K-S-S-T-A-V-I-P-G-Y-P-V-A-G-Q-V		MP63_MYCTU Immunogenic protein MPT63 precursor, Myco-bacterium tuberculosis
96	1988.4	V-Q-G-A-V-P-Y-G-P-I-V-A-T-S-S-K-L-D-S-V		

*ImmuneEpitopeDataBase: http://www.immuneepitope.org/[96]
#http://www.expasy.org/

Figure X1:

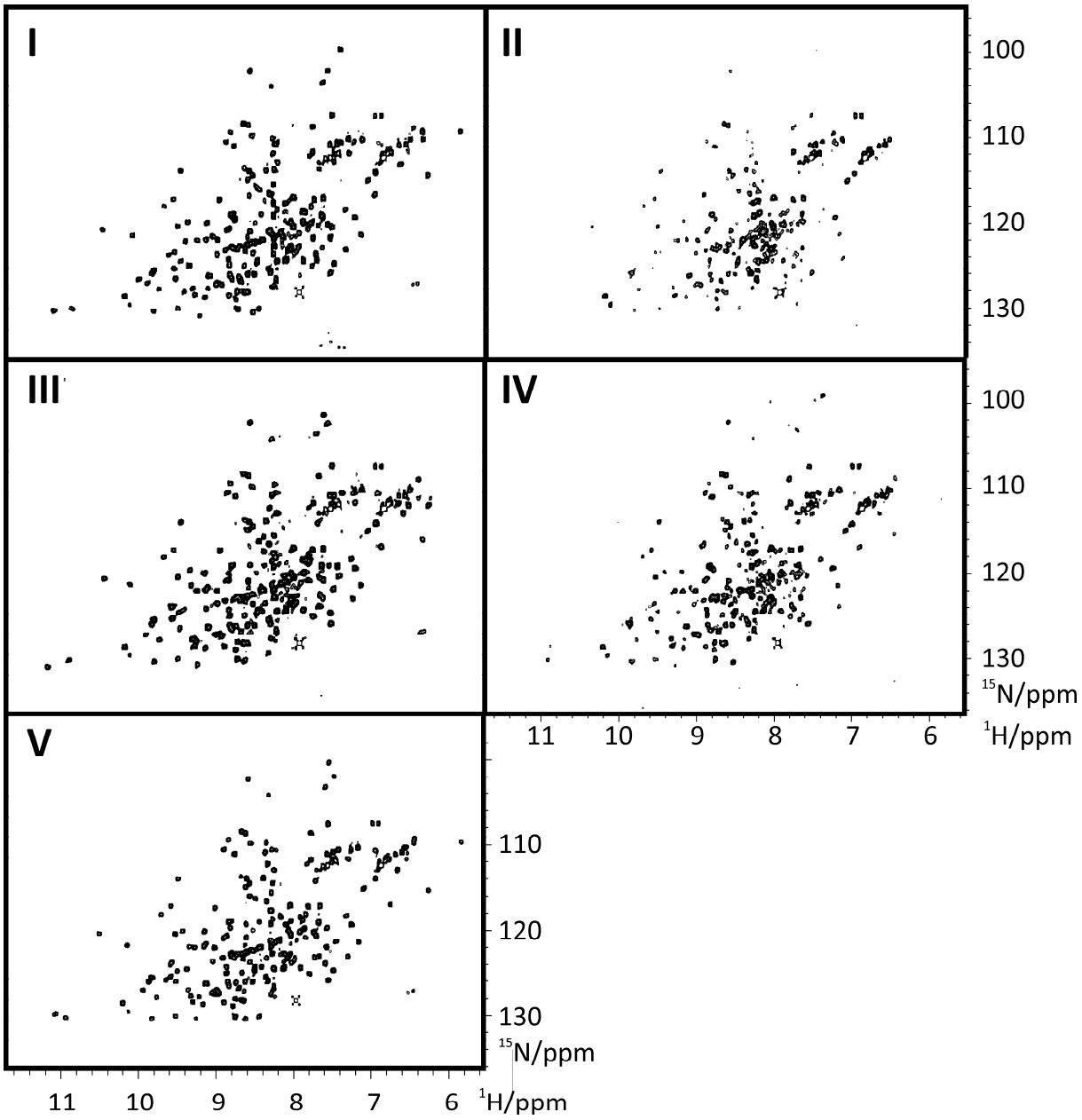

Figure X1: ^{1}H-^{15}N-HSQC spectra of HLA-DR1, ^{15}N-labeled in DRβ, after overnight loading with one of the peptides I-V in presence of the MLE FR.

Figure X2:

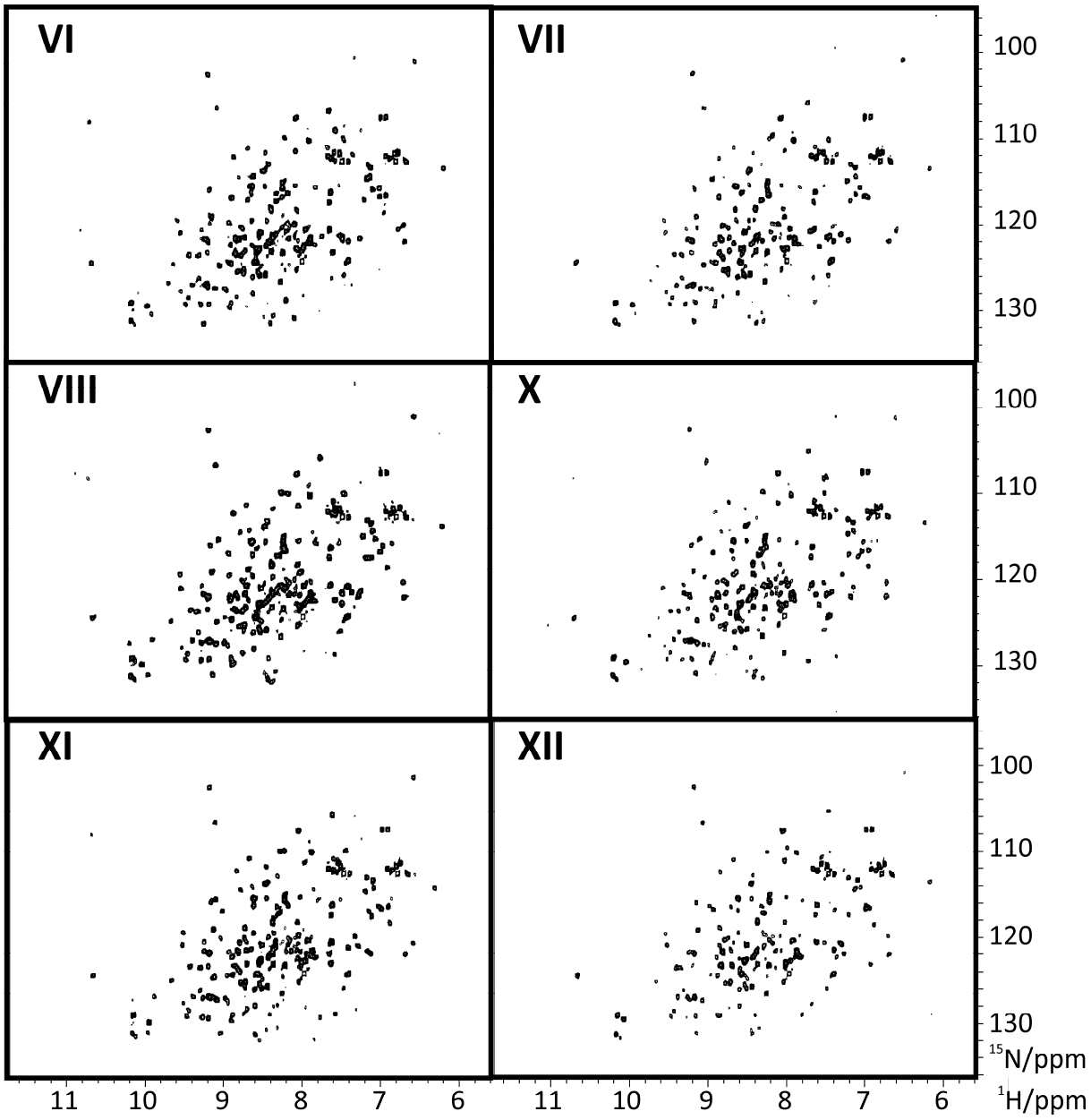

Figure X2: ^{1}H-^{15}N-HSQC spectra of HLA-DR1, ^{15}N-labeled in DRα, after overnight loading with one of the peptides VI-XII in presence of the MLE FR. No spectrum was obtained from the sample with peptide IX.

List of abbreviations

A	alanine
Abl	Abelson murine leukemia (viral oncogene homolog kinase)
approx.	approximately
APBS	Adaptive Poisson-Boltzmann Solver
AU	absorption unit
β-Me	β-mercaptoethanol
bp	basepair
C	cysteine
°C	degree Celsius
CD	cluster of differentiation
“cage”	Cryptophane A, CryptA
CEST	chemical exchange saturation transfer
CLIP	class II associated invariant chain peptide
CS(P)	chemical shift (perturbation)
CTL	cytotoxic lymphocytes
D	aspartic acid
1D/2D	one-dimensional/two-dimensional
D_2O	deuterated water
Da	Dalton
DAPA	diamino-propionic acid
DC	dendritic cell
DLS	dynamic light scattering
DMEM	Dulbecco’s modified eagle medium
DMSO	dimethylsulfoxide
DTT	dithiothreitol
E	glutamic acid
E.coli	Escherichia coli
EDTA	ethylenediaminetetraacetic acid
e.g.	*exempli gratia,* for example
ELISA	enzyme-linked immunosorbent assay
Elispot	enzyme-linked immuno-SPOT
F	phenylalanine
F	Faraday
FCS	fetal calf serum
FID	free induction decay
FT	Fourier transformation
G	glycine
g	gravitational accelaration
GF	gel-filtration

GSH	reduced glutathion
GSSG	oxidized glutathion
H	histidine
H/D	hydrogen/deuteron
HA	hemagglutinin
HLA	human leukocyte antigen
HSQC	heteronuclear single quantum correlation
Hz	Hertz
I	isoleucine
i.e.	*id est,* that is
Ii	invariant chain
Ig	immunoglobulin
IL	interleukine
INEPT	insensitive nucleus enhanced polarization transfer
IPTG	isopropyl-beta-thio-galactosid
K	lysine
K	degree Kelvin
K_d	dissociation constant
Kod	Thermococcus kodakaraensis
L	leucine
l	liter
LB	Luria Bertani
M	methionine
M	mol
m	meter
M9	minimal medium
MHC	Major histocompatibility complex
MIIC	MHC class II-containing compartment
min	minute
MLE	MHC loading enhancer
MRI	magnetic resonance imaging
MW	molecular weight
N	asparagine
(N)MR	(nuclear) magnetic resonance
NOESY	nuclear Overhauser effect spectroscopy
Ω	Ohm
OD	optical density
P	proline
PAGE	polyacrylamide-gelectrophoresis
PBS	phosphate-buffered saline
PCR	polymerase chain reaction
pH	$-\log_{10} [H^+]$
pdb	protein data bank

PEG	polyethyleneglycol
pMHC(II)	MHC(II)-peptide
ppm	parts per million
PRE	paramagnetic relaxation enhancement
Q	glutamine
R	ariginine
RMSD	root mean square deviation
rpm	returns per minute
RPMI	*Roswell Park Memorial Institute* medium
S	serine
s	second
S2	Schneider cells
SDS	sodium dodecylsulfate
Sf21	Spodoptera frugiperda cells
S/N	signal to noise (ratio)
T	threonine
T	tesla
Taq	Thermus aquaticus
TBS	Tris-buffered saline
TEMPO	2,2,6,6-tetramethylpiperidine-1-oxyl
Tris	tris(hydroxymethyl)aminomethane
TROSY	transverse relaxation optimized spectroscopy
U	unit
V	valine
V	Volt
v/v	volume per volume
W	tryptophan
w/v	weight per volume
WT, wt	wild-type

Acknowledgement

First of all I thank my supervisor Prof. Christian Freund for providing me with an exciting and challenging project, for many helpful hints, discussions and the support in developing my scientific personality. Thanks also to Prof. Volker Haucke for being available as second referee.

Gratitude is expressed to all collaborators in the house, Wolfgang and Lorenz at the PTB and people at the MDC for providing insights into new techniques, allowing alternative perspectives and the common pursuit of finding answers. Special thanks go to Sebastian Günther for many fruitful years of cooperative research on MHCII, for constant willingness to perform yet one more control experiment and for enthusiasm in discussing results as much as his know-how in MHC alleles, peptides, registers, pockets and structures. I am grateful to Jana Sticht for significantly shaping this thesis, reliable professional support with NMR, in particular the assignments, for excellent theoretical work on our and other's data and countless helpful contributions and ideas. With this, I also have to acknowledge people from the FMP NMR facility, especially Peter Schmieder, for their patience and for raising my comprehension for the method of NMR including commendable hands-on help at the spectrometer.

Many thanks to all of my lab colleagues for great scientific collaboration and enlightening discussions, in particular Bernhard for selfless sharing one bench with me and Daniela for joining me in endless ways of commuting, guaranteed fresh-coffee-supply and an excellent, varied lunch service. A good atmosphere, much fun in between, and well-dosed, extended beer sessions have not only once helped to overcome phases of frustration. Thanks to Katharina Thiemke and Kathrin Motzny for excellently and reliably organizing the lab.

I am thankful to the students Sophia Koch and Katharina Gröger for their effort to support my work, which they certainly did.

Most of all, I can only try to express deepest gratefulness to my little family for accepting my permanent absence. Particularly, I have to address Lenka's ability to convince me that there is much more to enjoy in life than work could ever provide. At the same time, Anne's confidence in me and her way to approve me in doing the right thing were the biggest form of help considerable over the past five years. *Dějkuji vám za všechno, moji nejmilejší!*

Publications/Posters/Awards

Manuscripts

Published manuscripts related to the presented study:

1) Rupp B, Gunther S, Makhmoor T, **Schlundt A**, Dickhaut K, Gupta S et al.: Characterization of Structural Features Controlling the Receptiveness of Empty Class II MHC Molecules. ***Plos One*** 2011, 6.

2) Gunther S*, **Schlundt A***, Sticht J, Roske Y, Heinemann U, Wiesmuller KH et al.: Bidirectional binding of invariant chain peptides to an MHC class II molecule. ***Proceedings of the National Academy of Sciences of the United States of America*** 2010, 107: 22219-22224.

*equal contribution

3) Schlundt A, Kilian W, Beyermann M, Sticht J, Gunther S, Hopner S et al.: A Xenon-129 Biosensor for Monitoring MHC-Peptide Interactions. ***Angewandte Chemie-International Edition*** 2009, 48: 4142-4145.

Published manuscripts related to other studies performed during the time of this thesis:

4) Kofler M, Schuemann M, Merz C, Kosslick D, **Schlundt A**, Tannert A et al.: Proline-rich Sequence Recognition - I. Marking GYF and WW Domain Assembly Sites in Early Spliceosomal Complexes. ***Molecular & Cellular Proteomics*** 2009, 8: 2461-2473.

5) Schlundt A, Sticht J, Piotukh K, Kosslick D, Jahnke N, Keller S et al.: Proline-rich Sequence Recognition – II. Proteomics Analysis of Tsg101 Ubiquitin-E2-Like Variant (UEV) Interactions. ***Molecular & Cellular Proteomics*** 2009, 8: 2474-2486.

Other manuscripts published during the time of this thesis:

6) Baur T, Ramadan K, **Schlundt A**, Kartenbeck J, Meyer HH: NSF- and SNARE-Mediated Membrane Fusion is Required for Nuclear Envelope Formation and Completion of Nuclear Pore Complex Assembly in Xenopus Laevis Egg Extracts. ***Journal of Cell Science*** 2007, 120: 2895-2903.

Poster contributions

Posters related to the presented study:

1) Schlundt *et al.*

"Modulation of MHC-peptide interactions by MHC Loading Enhancers (MLE)"

Joint PhD Retreat of MDC/FMP Berlin, Joachimsthal, September 2007

2) Schlundt *et al.*

"A Novel Binding Mode For MHCII Complexed Peptide Revealed At Atomic Resolution"

Campus Buch PhD Retreat MDC/FMP Berlin, Berlin-Buch, May 2010

3) Schlundt *et al.*

"Bidirectional Binding of a Self-antigen to an MHC Class II Molecule"

Keystone Symposium on *Frontiers in Biological NMR*, Big Sky, MT, USA, January 2011

Talk contributions to the presented study

1) ***"Bidirectional Binding of a Self-antigen to an MHC Class II Molecule"***

Keystone Symposium on *Frontiers in Biological NMR*, Big Sky, MT, USA, January 2011
(Poster Preview Talk)

2) ***"MHC loading enhancement at the molecular level"***

Oberjochseminar organized by University of Tübingen and EMC Microcollections, Oberjoch/Allgäu, February 2010

3) ***"Structural insights into the catalyzed exchange of peptides bound to MHC Class II molecules"***

Joint PhD Retreat of MDC/FMP Berlin, Kremmen, September 2009 (Selected Talk)

Awards

1) Winner of the Director's Fund Scholarship for attending the Keystone Symposium on *Frontiers in Biological NMR*, Big Sky, MT, USA, January 2011

Finances provided by: National Institutes of General Medical Science, Grant #1R13GM095021-01.

2) 2nd Place Poster Awards on the Campus Buch PhD Retreat MDC/FMP Berlin, Berlin-Buch, May 2010

Finances provided by: MDC/FMP Berlin.

Curriculum vitae

Der Lebenslauf ist in der Online-Version aus Gründen des Datenschutzes nicht enthalten.

For reasons of privacy protection the CV is excluded from the online version of this document.